The Journal of
Gemmology

Volume 30 No. 7/8
July/October 2007

The Gemmological Association of Great Britain

The Gemmological Association of Great Britain

Registered Charity No. 1109555

27 Greville Street, London EC1N 8TN
Tel: +44 (0)20 7404 3334 | Fax: +44 (0)20 7404 8843
e-mail: information@gem-a.com | Website: www.gem-a.com

The Journal of Gemmology

A description of pearl farming with Pinctada maxima in South East Asia

Professor H.A. Hänni
SSEF Swiss Gemmological Institute, Basel, Switzerland

Abstract: *This reports on a modern pearl farm in South East Asia which uses* Pinctada maxima *oysters. Marine biologists and geneticists supervise the pearling process. Culturing oysters from fertilized eggs has generally replaced wild oyster collection. In hatcheries larvae and spat are reared under scientifically controlled conditions. After around two years the oysters are about 12 cm in size and ready for the operation. Careful selection of donor oysters for the tissue graft and of host oysters to grow the pearls ensures optimum conditions for pearl formation. Excellent environmental conditions are sought to grow pearls of superior quality. High standards of working hygiene, X-ray checks and regular and frequent cleaning of the oysters and the holding nets are further steps to ensure high quality. Almost four years from the hatching of the larvae, the oysters are ready for a first pearl harvest. Most of the oysters are not re-beaded, and their muscle flesh is processed as seafood and the shells utilized for their nacre. The pearls are graded for quality and marketed mainly in Australia.*

Keywords: *pearl culturing process, pearl farming,* Pinctada maxima*, South Sea cultured pearls*

Introduction

In February 2006 the author had the opportunity to visit a pearl farm belonging to North Bali Pearls in Penyabangan, which is part of PT Cendana Indopearls, a company in the Atlas South Sea Pearls (Australia) group (*Figure 1*). In December 2006 a second trip was undertaken, this time to the West Papua area, for purposes of familiarization with the main pearl farming centre there. In both places, the author was afforded facilities at a state-of-the-art pearl farm to study the preparatory work that results eventually in the prized South Sea cultured pearls. The volume of scientific, technical and financial investment that has to go into a modern pearl farm is very impressive. The shares of these pearl forms are bought and sold on the stock exchange, and the success or otherwise of a harvest has a direct bearing on the share price.

The literature on oysters and cultured pearls is voluminous, and only a small selection can be listed here. On the biology of the *Pinctada maxima* oyster, see Dix, 1973 and Lowenstam and Weiner, 1989. On the farming of pearl oysters, see Jobbins and Scarratt, 1990; James, 1991; Müller, 1997. The microstructure of pearls is dealt with in Wise, 1970; Gauthier and Ajaques, 1989; Gutmannsbauer, 1993; Gutmannsbauer and Hänni, 1994. On issues of nomenclature, CIBJO, 1997, 2006,

ISSN: 1355-4565

Figure 1: *The pearl farm in North Bali, an aquacultural business with an ultra-modern approach to oyster production and pearl culturing in Penyabangan. Photo © H.A. Hänni.*

and Hänni, 2006a,b, are useful. For general information on pearls, see Hänni, 1995 and 1997; Schoeffel, 1996; Matlins, 1999; Hänni, 2001; Strack, 2006. Methods of identifying pearls are covered in Wada, 1981; Komatsu, 1987; Lorenz and Schmetzer, 1985.

Oysters used in cultured pearl production serve one of two distinct purposes. Some are used as mantle tissue donors, while others serve as host animals for the cultured pearls. Both halves of an oyster's shell have a layer of soft skin. This tissue, known as mantle tissue (or mantle epithelium), lines the whole shell and has produced both wings of the oyster.

A tiny piece of the outer surface of this mantle tissue is essential for transference of the nacre-forming ability to a different site for the purpose of growing a cultured pearl. The body of an oyster selected as a host animal has two sites where the transplanted mantle tissue can be accepted and will form a cultured pearl. One is the host's mantle tissue and the other is its gonad (reproductive organ). Pearls may be referred to accordingly as mantle-grown or gonad-grown. Located deep within the oyster shell, the gonad affords the room for one or two beads to be implanted in order to produce one or two beaded cultured pearls. In general, cultured pearls with beads will be the familiar saltwater-grown Akoya, South Sea and Tahiti varieties.

Cultured pearls without a bead usually derive from transplanted mantle tissue placed in the mantle of freshwater mussels, producing well-known varieties such as the Biwa or Chinese freshwater cultured pearls. Thus cultured pearls are always formed by the transfer of mantle tissue, regardless of whether the graft is into freshwater mussels or saltwater oysters, and regardless of the presence or absence of a bead. *Figure 2* provides an overview, illustrating sectioned cultured pearls of all types.

Pearl farmers who use *Pinctada maxima*,

Figure 2: *Cross-sections through different kinds of cultured pearls. Upper part: beadless pearls, e.g. South Sea 'keshi', Chinese freshwater cultured pearls. Lower part: cultured pearls with beads, e.g. Akoya, Tahiti and South Sea, and freshwater. Photo © H.A. Hänni.*

the large silver or gold lipped oyster (South Sea pearl oyster), insert a bead of nacre along with the mantle tissue (Japanese term: *saibo*). This is the practice followed at the farm in North Bali. Some of the grafted oysters expel this bead; however, the mantle tissue remains and forms a pouch inside which it produces a beadless cultured pearl, a variety marketed as a keshi cultured pearl (Hänni, 2006). But the great majority will retain the bead, form a pearl-sac round it and envelop the bead and deposit a good thick layer of nacre. This results in the classical South Sea cultured pearl.

Back in the 1960s, trading in cultured pearls was centred on Broome and Darwin in north-western Australia. Problems persisted over a long period in the rearing of oysters artificially from fertilized eggs, and therefore the animals required were harvested from the seabed by divers. They were then grafted and transported to warmer waters. As the harvesting of wild oysters in Australia is subject to quota, the production of cultured pearls is correspondingly limited.

The pearl farm in North Bali

The North Bali pearl farm is linked to other pearl farms in West Papua (Irian Jaya, Indonesia). The brief account provided here will indicate the complexity of modern production processes for cultured pearls with bead, and will refer for comparison to the production of beadless freshwater pearls. Thus, for example, a pearl oyster will produce a single cultured pearl, while as many as fifty may develop simultaneously inside freshwater mussels. The formation of beadless freshwater cultured pearls, however, may take several years when larger sizes are required.

In North Bali (Penyabangan) the author visited a farm which rears young oysters from fertilized eggs in a breeding facility. Carefully selected individuals are used to found a line of vigorous, handsome oysters, and the broodstock and subsequent generations will remain under genetic monitoring by scientists. With a view to minimizing disease and parasite infestation, the initial breeding and rearing stages take place in filtered seawater. The fertilized eggs and larvae are given the best possible conditions in which to grow into baby oysters (*Figure 3*).
The purified water is enriched by food in the form of specially cultivated micro algae. Once the juveniles reach a certain size, they lodge on special jute strings and continue to grow. At one month old they are transferred to ordinary seawater adjacent to the farm premises. By now they have grown to 1.5 or 2 mm in size. One net frame will accommodate up to 500 juvenile animals, and the hatchery as a whole has a population of several millions of larvae. Of these, about 20 per cent survive the transition from larva to oyster. When the young pearl oysters are 10 mm across, they are separated, and each tiny shell is re-housed in a net frame with

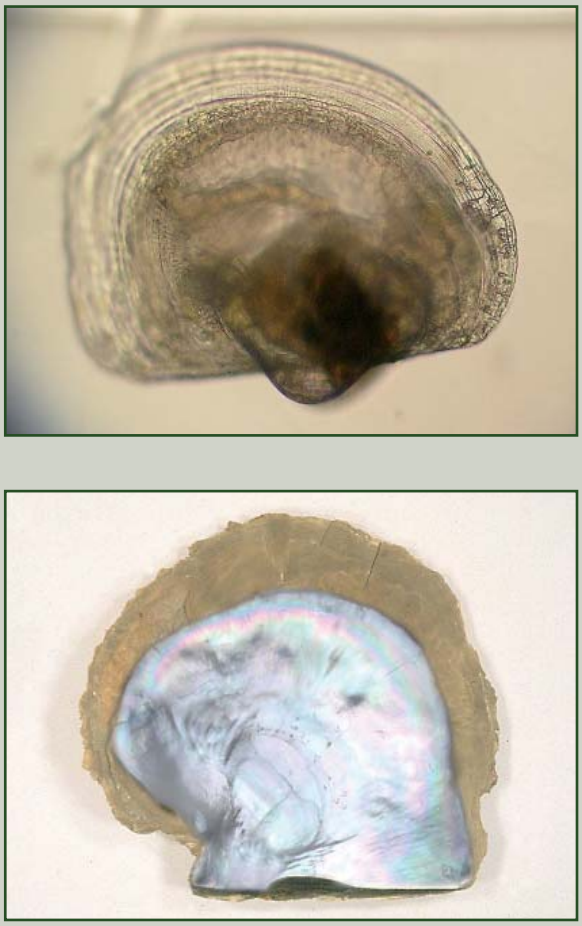

Figure 3: *A three-week-old* Pinctada maxima *oyster 2 mm across, photographed through the microscope, and a five-year-old shell half of the same species (18 cm). Photo © H.A. Hänni.*

64 others. These nets are suspended from horizontal longlines so that they hang at a depth of between 5 and 10 metres below the sea surface. From the shore the distinctive spherical black buoys supporting the hundreds of metres of line are clearly visible. The main activities involved in this phase of pearl oyster farming are regular removal of algae and also fouling organisms from nets and shells and monitoring of the growth rate of operated shells that have received their bead using X-rays (*Figure 4*). The work is carried out partly from ships or on shore.

The whole process of pearl formation could take place in Bali, but with a view to improving product quality, the North Bali Pearls management chose to ship most of the juvenile oysters at about eighteen months old to West Papua for depositing the nacre. In generous-sized ship-borne seawater tanks (*Figure 5*), as many as 40,000 *Pinctada maxima* at a time are freighted to clean waters remote from all civilization, and here they have almost two years to benefit from the ideal local growing conditions.

Figure 4: *X-ray monitoring after a cleaning process shows whether the bead has been retained in the oyster. Photo © H.A. Hänni*

Figure 5: *Workers handling nets with oysters ready for the tanks in the ship which will take them to Alyui Bay in West Papua (Irian Jaya). Photo © H.A. Hänni*

The ship takes a week to reach West Papua, the Indonesian part of New Guinea, also known as Irian Jaya. Ideal conditions are found in the Alyui Bay area (approximately 0 12'S, 130 14'E) where the coves between the islets are sheltered, and the water contains suitable minerals and plankton at the right temperature around 27 C.

The pearl farm in West Papua

The Alyui Bay base is not accessible overland but can be reached by sea from Sorong, a journey of 12 hours. Berthing facilities, office premises, production sheds, workshops, canteen and staff quarters are all on the shoreline and back directly onto jungle. The diving base essential for coping with the many and varied underwater tasks is also located by the pier. The company's board of management is Australian, the technical staff Indonesian. The pearling operations base and surrounding bays are under military guard as a precaution against theft of oysters.

Preparing the oysters for grafting

On reaching approximately 11-12 cm in size, the oysters undergo the surgery which enables production of the cultured pearls. They have to be conditioned for this operation, either by sinking the nets to the seafloor for 4-6 weeks or by covering

the nets for 4 weeks with fabric which has 1mm diameter holes. Either way the oysters are prevented from feeding and thus from producing gametes, which would cause problems during the surgical procedure (Taylor and Knauer, 2002). The food withdrawal slows down bodily processes and ensures empty gonads.

The operating table

The author's earlier visits to other pearl farms – in China, Australia and French Polynesia – had invariably made for extremely interesting observations with regard to work routines, technical provision and equipment. In contrast to some working conditions seen elsewhere by the author, the graft surgery conditions at PT Cendana Indopearls and Atlas South Sea Pearls in Indonesia (Bali and Irian Jaya) proved exemplary. The two most important innovations, in the author's assessment, have been the self-rinsing operating table with integral oyster-clamp and the cold-light fibre-optic lighting for the surgical procedures (*Figure 6*). The work-surface is continuously swilled clean by filtered seawater, and a spray device washes the instruments automatically as they are returned to their holders. The lighting used – from either a low-voltage lamp or a light pipe – affords the transplant technician a clear view of the operation site deep inside the barely opened oyster. This contrasts with some other farms visited in the past where the entire production shed had been lit by a small number of fluorescent tubes high in the ceiling.

Donor oysters and host oysters

The next step is to select which oysters will be tissue donors and which will be those that host the cultured pearls. Tissue donors provide pieces of mantle tissue for the graft. They must have nacre of the desired quality in terms of colour, lustre and 'orient' (iridescence). Young oysters are opened so that the quality of their nacre can be assessed.

Figure 6: *A clean workplace with good lighting for the operation site, hygienic surroundings and an instrument rack which is rinsed continuously characterizes the high standards at Atlas South Sea Pearls farms. Photo © H.A. Hänni*

Figure 7: *Two strips cut from the mantle tissue of a donor oyster are divided into tissue grafts (*saibo*) for transplantation. Photo © H.A. Hänni*

If the mantle tissue has grown on silvery, highly iridescent shell surfaces, the oyster is selected for tissue donation.

The remainder become potential host oysters which need to be large, vigorous specimens capable of providing optimal nurture for the transplant (Knauer and Taylor, 2002).

The mantle tissue graft

During subsequent preparation of the tissue pieces it is important not to lose track of which side had lain next to the shell, as only this outer mantle tissue is capable of secreting nacre. Two strips are cut out with scissors from the mantle tissue on each half of the shell and then cut into tiny grafting pieces (*Figure 7*). One tissue-donor oyster sacrificed for this purpose will yield about 30 *saibo*, each approximately 2.5 x 2.5 mm square. Next, these slivers of flesh containing

the complete genetic programme for the production of nacre are implanted one at a time in host oysters by a grafting technician. To make the transplant readily visible in the body of the oyster and ensure accurate positioning, the practice in many farms is to stain it red with eosin.

The bead

In Alyui, as also elsewhere, beads for the cultured pearls are derived from mussel-shell beads cut and shaped from thick-walled Pigtoe river mussels (Strack, 2006). These beads have a more or less parallel-layered structure. Even though the *Pinctada maxima* at Alyui deposit good thick coatings over the bead, care is taken to use beads that are white in colour. In Tahiti, where *Pinctada margaritifera* oysters produce dark-hued shells, it is possible to use nuclei that may be pale brown. Where snow-white beads are particularly important is for Akoya pearls, which have characteristically thin coatings. Here any brownish marbling of the beads would show conspicuously through the deposited nacre. The synthetic 'Bironite' type beads (Snow, 1999) and those made from the shell of the giant mussel *Tridacna maxima*, are not used at Alyui. The traditional Pigtoe beads are usually coated with the antibiotic tetracyclin as a prophylactic measure against disease and implant rejection.

The operation

The selected host oysters will still be young (11-12 cm), so the implanted beads must not exceed about 5.8-7.6 mm in diameter. Host oysters have to be vigorous, fast-growing specimens. Their own nacre does not need to be particularly fine, as the cultured pearl will acquire the quality characteristics introduced by the transplanted donor grafted tissue. The thickness of the deposit and the rate of growth, however, depend principally on the nurture, i.e. on the host oyster. Once the host has been slightly opened and secured in the operation clamp, the grafting technician makes a precisely performed incision in the gonad. The antibiotic-treated beads are then inserted and the tissue transplants added (*Figure 8*).

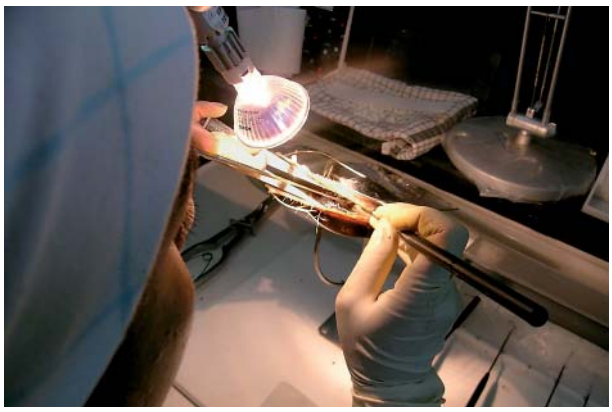

Figure 8: *A technician introduces a bead and a tissue graft into the gonad of a* Pinctada maxima. *On the excellently equipped workstation further tissue grafts and shell beads are waiting for transplantation. Photo © H.A. Hänni.*

The donor mantle tissue is accepted by the host oyster's gonad tissue, grows on in its new environment, and receives blood and minerals via the circulatory system.

The growth phase

Following the operation, the oyster is returned to seawater and allowed some time to recover. During this time, the mantle tissue graft in the gonad begins to fuse into its surroundings and also increases in size, growing concentrically around the bead and forming a closed sac. On its inner side, it gradually begins to secrete calcium carbonate in the form of aragonite platelets: the bead is acquiring its coating of mother-of-pearl. These thin aragonite platelets are what gives mother-of-pearl its unique characteristic orient.

Further checks carried out alongside routine cleaning permit the monitoring of growth and removal of casualties. Oysters that have rejected their bead are not re-seeded: they produce beadless cultured pearls, as the pearl-sac that has been formed fills up without a bead (Hänni, 2006). Oysters identified as bead-rejectors by X-ray are kept around three years in the water in order to produce substantial beadless cultured pearls, so-called South Sea keshi pearls.

It is during this growth phase that the quality of the cultured pearl will be determined. A number of factors are decisive. One important factor is the genetic makeup of the oyster concerned. This determines

its vigour and its growth rate. A second set of factors are the environmental conditions during the growth phase: light, available food, water temperature and salinity, etc. Other factors again are of human origin: hygiene during surgery, selection and condition of the transplant, and keeping feeding conditions at an optimum by regular net-cleaning (*Figure 9*).

When allowance is made for the condition of the mantle tissue, the formation of the pearl-sac follows a more or less routine course. Cleanly cut edges to the epithelium wound amply guarantee the formation of a fully functional pearl-sac. However, frayed edges will give rise to unsightly scar tissue which cannot produce problem-free nacre. Irregular shapes, dimples or rings may result.

As a rule, oysters that have undergone surgery at Alyui Bay will remain in the water for at least 18 months, sufficient time for an impressively thick coating of nacre to be secreted over the bead. Interestingly, pearl size is subject to major variation even when the maturing period inside the oyster is the same. Individual oysters will have nurtured their pearl-sacs to varying degrees, reflecting differences in their respective physical resources. 'Lazy' tissue or insufficient nourishment from the host will result in pearls that are smaller than those produced when all parts of the system have been working at their optimum. Where a nacre deposition period 'pregnancy' lasting nearly two years is involved, differences in the products from individual pearl-sacs will be more conspicuous than they would in thinly coated cultured pearls that have had only a short maturing period.

Figure 9: *Frequent cleaning with water jets and by hand is necessary to keep the nets and oyster shells free of parasitic animals and plants. A large number of boats are at work every day servicing the longlines. Photo © H.A. Hänni*

The harvest

The quality of day-to-day nacre deposition is affected by environmental influences, water temperature in particular. The shape of the cultured pearl is broadly speaking the product of the accumulated layers surrounding the bead. Irregularities may perpetuate themselves and lead to non-rounded shapes. However, surface characteristics such as colour, sheen and lustre are largely the outcome of the deposition of material over the few weeks preceding the harvest. Nacre formed at cooler temperatures is known to be made up of thinner platelets, which means that as nacre it is of finer quality. That in turn suggests that harvesting should take place just after a period during which thin platelets were being formed. Accordingly, the harvest proper is preceded by a number of oysters opened as small sample harvests. These give insight into the general condition and quality of the nacre formed up to that point. When the pearl is to be removed, the slightly opened oyster is held firmly in the clamp. A precisely executed incision opens up the gonad, and the cultured pearl can be lifted out with a specially designed tool (*Figure 10*). It is striking that a harvest of cultured pearls of uniform age yields a wide range of sizes and some variations in shape. Beadless (bead rejected) keshi pearls of the first generation are identified early on by X-ray checks when the shells undergo routine cleaning. These shells are separated and stay in separate nets, being allowed to grow for 12 months longer than the beaded cultured pearls in order to attain a marketable size. *Figure 11* shows a number of cultured pearls, all of the same age, from a sample harvest. However, the colours do not vary greatly, most of these pearls having either a clean silvery white colour or a gold tone. Half-tones are uncommon, as are pearls with constrictions (so-called 'circled' pearls).

Figure 10: *Removal of a cultured pearl from the gonad of a* Pinctada maxima. *The white part in the shell (to the left) is the powerful adductor muscle. Photo © H.A.Hänni.*

Figure 11: *A small trial harvest provides data on the present quality of the pearl surfaces. The picture shows a bead (yellow, width 6.5 mm) in comparison with pearls produced after 18 months in the shell. The mean diameter is about 12.5 mm. Photo © H.A.Hänni.*

Only those oysters that have formed top-quality pearls are beaded a second time; large beads are now used as the quality of the nacre that can be obtained diminishes as the pearl-sac grows older.

At Alyui Bay, the annual harvest in 2007 took place February. Most of the oysters were not re-beaded. Pearls from a first-harvest oyster range in size from 9 to 16 mm, with frequency peaking at 10 to 12 mm diameter (*Figure 12*). Pearls from re-beaded oysters yielded diameters of from 12 to 20 mm, with maximum frequency at 14 - 16 mm. Atlas South Sea Pearls open approximately 240,000 oysters annually. Oysters identified through X-ray monitoring during cleaning as having lost the implanted bead (10%) have been separated from the main population at an earlier stage. These oysters will have formed

Figure 12: *These beaded South Sea cultured pearls from Alyui Bay, West Papua (Irian Jaya) were harvested in February 2007. The diameters vary between 9 and 16 mm. Photo © H.A.Hänni.*

a beadless cultured pearl or keshi in their pearl-sac, and are allowed to grow for three years. About 15,000 keshi cultured pearls are produced annually in this way; they range from 5-15 mm in diameter with a mean of 8-9 mm.

About 90 per cent of the cultured pearls produced at Alyui Bay are put on the market in Australia, through the Pearlautore International Company. Eighty per cent are offered for purchase as loose pearls. The others, after being drilled through and graded for size, are traded as strings, along with pearls from other farms, and bought up in lots by wholesalers. A small number of pearls from the harvest go into jewellery manufactured in Atlas South Sea Pearls' own boutiques in Bali.

Acknowledgements

The author wishes to thank Dr Joseph Taylor for arranging access to North Bali Pearls und Atlas South Sea Pearls. The extremely interesting information provided by Dr Taylor was the stimulus for this paper. The author also had many absorbing discussions with Dr Taylor and Dr Jens Knauer. Warm thanks are also due to the

personnel of Atlas South Sea Pearls (Alyui Bay), in particular Mark Pieper and Kevin Smith. My gratitude is also expressed to Andy Müller of Hinata Trading, Kobe, Japan, for his many years of support for the SSEF in the form of information and materials for research and training in the field of cultured pearls and for introductions which greatly helped this study. My thanks finally go to Dr T. Gensheimer and Dr J. Knauer for their comments on the manuscript.

References

CIBJO, 1997. *Diamonds, Gemstones, Pearls*. International Confederation of Jewellery, Silverware, Diamonds, Pearls and Stones, 78A Luke Street, London EC2A 4PY

CIBJO, 2006. *The Pearl Book*. The World Jewellery Confederation, Milan, Italy www.cibjo.us/pearl.pdf

Dix, T.G., 1973. Histology of mantle and pearl sac of the pearl oyster Pinctada maxima(Lamellibranchia). *J. Malacological soc. Australia*, 2, 365-75

Gauthier, J.P., and Ajaques, J.M., 1989. La perle au microscope électronique. *Rev. Gemm. a.f.g.*, 99, 12-17

Gutmannsbauer, W., 1993. AFM provides new insight into biomineralization processes. *Topometrix Applications Newsletter*, 93(2), 5

Gutmannsbauer, W., and Hänni, H.A., 1994. Structural and chemical investigations on shells and pearls of nacre forming salt- and freshwater bivalve molluscs. *J.Gemm*., 24(4), 241-52

Hänni, H.A., 1995. A short synopsis of pearls: Natural, cultured, imitation. *J. Gemm. Assoc. Hong Kong*, XVIII, 43-6

Hänni, H.A., 1997. Über die Bildung von Perlmutter und Perlen. *Z. Dt.Gemmol.Ges*., 46(4), 183-96

Hänni, H.A., 2001. *Pearls: the formation of shell and pearls*. SSEF tutorial CD Rom 1, Edited by SSEF Swiss Gemmological Institute, Basel, Switzerland

Hänni, H.A., 2006a. A short review of the use of 'keshi' as a term to describe pearls. *J. Gemm*., 30 (1/2), 51-8

Hänni, H.A., 2006b. Keshi Perlen - ein erklärungsbedürftiger Begriff. *Z. Dt. Gemmol. Ges*., 55(1/2), 39

James, P.S.B.R., 1991. *Pearl oyster farming and pearl culture*. CMFRI Tuticorin, India

Jobbins; E.A., and Scarratt, K., 1990. Some aspects of pearl production with particular reference to cultivations at Yangxin, China. *J. Gemm*., 22(1), 3-15

Komatsu, H., 1987. *Introduction to pearl testing*. Zenkoku hôsekigaku kyôkai shuppanbu, Tokyo 1-24 (in Japanese)

Knauer, J., and Taylor, J.J.U., 2002. Production of silver-nacred *'saibo* oysters' of the silver- or goldlip *Pinctada maxima* in Indonesia. Abstract from Annual Meeting of World Aquaculture Society, Beijing

Lorenz, R.I., and Schmetzer, K., 1985. Möglichkeiten und Grenzen der röntgenographischen Untersuchung von Perlen. *Z. Dt. Gemm. Ges*., 34(1/2), 57-68

Lowenstam, H.A., and Weiner, S., 1989. *On Biomineralization*, University Press, Oxford

Müller, A., 1997. *Cultured Pearls, the first hundred years*. Andy Müller & Golay Buchel, Lausanne, Switzerland. ISBN 4-9900624-1-8

Matlins, A., 1999. *The Pearl Book. How to select, care for and enjoy pearls*. GemStone Press, Woodstock, Vermont, USA

Schoeffel, H., 1996. *Perlen, von den Mythen zu den modernen Zuchtperlen*. Schoeffel Pearl Culture, Schoeffel-Dumont, Köln, ISBN 3-7701-3638-1

Snow, M., 1999. Bironite: a new source of nuclei. www.spc.int/coastfish/News/POIB/13/POIB13-6.htm Biron Corp. Perth, Western Australia

Strack, E., 2006. *Pearls*. Rühle-Diebener-Verlag, Stuttgart

Taylor, J.J.U., and Knauer, J., 2002. *Inducing pre-operative condition in silver- or goldlip pearl oysters* Pinctada maxima *for pearl grafting*. Abstract from Annual Meeting of World Aquaculture Society, Beijing

Wada, K.,1981. Pearls. *J. Gemmol. Soc. Japan*, 8, 151-8

Wise, S.W.,1970. Microarchitecture and mode of formation of nacre (mother-of-pearl) in Pelecypods, Gastropods and Cephalopods. *Eclogae Geol. Helvetiae*, 63, 775-97

One hundred years 1908 2008

OF GEMMOLOGICAL EDUCATION

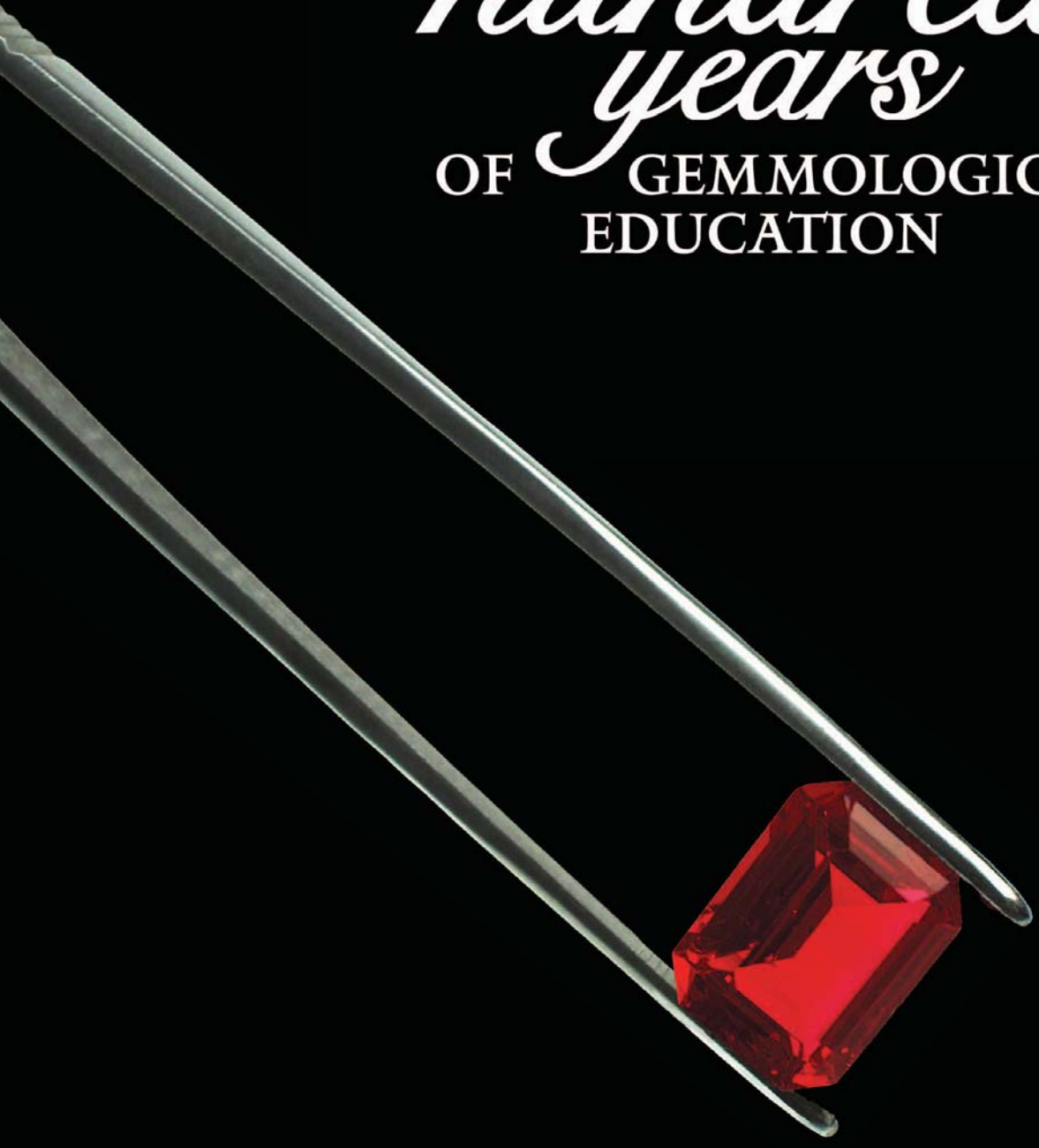

Gem-A

THE GEMMOLOGICAL ASSOCIATION
OF GREAT BRITAIN

Gem-quality taaffeites and musgravites from Africa

Dr Karl Schmetzer[1], Dr Michael S. Krzemnicki[2], Prof. Dr Henry A. Hänni[2], Dr Heinz-Jürgen Bernhardt[3] and Prof. Dr Thomas Pettke[4]

1. Taubenweg 16, D-85238 Petershausen, Germany
2. SSEF Swiss Gemmological Institute, Falknerstr. 9, CH 4001 Basel, Switzerland
3. ZEM, Institut für Geologie, Mineralogie und Geophysik, Ruhr-University, D-44780 Bochum, Germany
4. Institute of Geological Sciences, University of Bern, CH-3012 Bern, Switzerland

Abstract: *Gemmological, microscopic, chemical and spectroscopic properties of a parcel of 30 taaffeites and ten musgravites of African origin, most probably all from Tunduru, Tanzania, are presented. The faceted gemstones were identified by a combination of laser Raman microspectroscopy, quantitative electron microprobe analyses and LA-ICP mass spectroscopy. The variation of gemmological properties such as specific gravity and refractive indices is correlated with transition metal contents of the samples. Absorption bands in the UV-Vis range are assigned to iron in different valence states. Typical inclusions are primary apatite and magnesite crystals and healed feathers consisting of cavities that contain fluids and tiny secondary magnesite crystals. Gemmological and microscopic properties of these African stones are compared with characteristic features of taaffeites and musgravites from Sri Lanka. Most gem-quality taaffeites and musgravites from Sri Lanka and Africa originate from magnesian skarns or from calc-silicate rocks of metasomatic origin.*

Introduction

The taaffeite group consists of three independent mineral species, taaffeite, musgravite and pehrmanite (Armbruster, 2002). That the formulae and crystal structures of taaffeite and musgravite are distinct was established in the 1980s (Schmetzer, 1983 a,b; Nuber and Schmetzer, 1983). Only taaffeite and musgravite are known in gem quality, especially from Sri Lanka. Taaffeite, $BeMg_3Al_8O_{16}$, is a rare collector's stone, and musgravite, $BeMg_2Al_6O_{12}$, is considered as one of the rarest gem species known to date (McClure, 2001).

Since the 1980s, faceted taaffeites have continued to appear in parcels of cut and rough stones from Sri Lanka. Additionally, a gem-quality taaffeite from Myanmar has been reported by Spengler (1983) and recently, several samples from the Tunduru area in Tanzania have been described (anonymous, 1996; Burford, 1998). The first faceted musgravites, probably from Sri Lanka, were identified by Demartin *et al.* (1993).

Although the chemical formulae for the two Be-Mg-Al-oxides, taaffeite and musgravite, are no longer in dispute, the special physical and

ISSN: 1355-4565

chemical properties of chromium-, iron- and zinc-bearing, gem-quality taaffeites from Sri Lanka have come to light only within the last decade revealing more detailed knowledge of these gem materials (Schmetzer *et al*., 2000, 2005 a,b). The first quantitative chemical analyses of gem-quality musgravites from Sri Lanka were also reported recently (Schmetzer *et al*., 2005 c,d).

Taaffeites from Sri Lanka, in general, contain minor amounts of transition metals, especially iron and zinc, and in red to purplish red or intense purple specimens traces of chromium are also present. Some samples with extraordinarily high values of refractive indices (RI) and specific gravity (SG) contain extremely high zinc and/or iron values up to 8.87 wt.% ZnO and up to 5.62 wt.% FeO. Quantitative chemical analyses of gem-quality musgravites from Sri Lanka mostly revealed minor percentages of iron and zinc, but one sample contained a high amount of iron (4.91 wt.% FeO). Gemmological properties of taaffeites and musgravites such as SG and RI were found to be correlated with trace element contents of individual samples (Schmetzer, 2005; Schmetzer *et al*., 2006). In both minerals, taaffeite and musgravite, zinc and iron predominantly replace magnesium in the crystal structure.

In contrast to the detailed knowledge of the gemmological, physical and chemical properties of gem-quality taaffeites and musgravites from Sri Lanka established so far (see references cited above), only one chemical analysis of a gem taaffeite from Myanmar is known to the authors (Schmetzer *et al*., 2000), and quantitative chemical data of material from Tanzania are unknown.

Due to the similar chemical composition and crystal structure of taaffeite and musgravite, the gemmological properties of these independent species overlap. Consequently, for an unequivocal determination of faceted gems of this group a combination of special physical techniques such as X-ray diffraction and/or quantitative chemical analysis and/or micro-Raman spectroscopy is needed (Kiefert and Schmetzer, 1998). Because all specimens from Tunduru have so far been determined only by traditional gemmological methods, it is not known whether the samples described from Tanzania as taaffeites (anonymous, 1996; Burford, 1998) also contained some musgravites.

Consequently, the authors accepted the generous offer of W. Spaltenstein of Multi Colour Gems, Chantaburi, Thailand, to lend us 40 faceted specimens of taaffeite or musgravite of African origin for detailed gemmological, chemical and spectroscopic examination.

Materials and methods

The present study is based on 40 faceted stones ranging in weight from 0.35 to 3.97 ct (*Figures 1* and *2*). The rough gem material used for cutting these stones originated from the Tunduru mining area in Tanzania and consisted of mixed parcels containing the various gem species recovered in that particular area (see, for example, Johnson and Koivula, 1996, 1997; Henn and Milisenda, 1997, Burford, 1998). After cutting large lots of heavily water-worn rough pebbles in Thailand, the different gem materials found within the mixed parcels were sorted and taaffeites or musgravites were selected by gemmological methods, especially by the determination of optical properties.

In the cutting and sorting processes in Thailand, material from Tunduru is commonly mixed with imported rough from Ilakaka, Madagascar. However, at the time of writing (March 2007) gems of the taaffeite group have neither been reported from Ilakaka (see, for example, Schmetzer, 2000; Milisenda *et al*., 2001) nor identified in the laboratory of the Institut de Gemmologie de Madagascar in Antananarivo (T. Ramerison, pers. comm., 2006). Therefore, we assume that at least the majority of specimens examined in this study originate from Tanzania although we cannot completely exclude the possibility that a few stones could come from Madagascar. We are sure that none of the stones comes from Sri Lanka or Myanmar.

Standard gemmological methods were

used to determine the RI, optical character, SG and fluorescence under long- and short-wave ultraviolet radiation for all samples. Standard microscopic techniques were used to examine internal features of the stones under different lighting conditions, both with and without immersion liquids.

Subsequently we examined all 40 samples by laser Raman microspectroscopy using a Renishaw 1000 system equipped with a 514 nm argon laser. For each Raman spectum, 20 scans (10 seconds/scan) were accumulated. As a result, the lot could be subdivided into 30 taaffeites and 10 musgravites (for the distinction of taaffeites and musgravites using Raman spectra see Kiefert and Schmetzer, 1998). In addition, we analysed the solid inclusions of the samples using the laser Raman system mentioned.

To further characterize the samples we selected 15 taaffeites and all 10 musgravites for chemical analysis. To determine the quantitative chemical composition a Cameca Camebax SX 50 electron microprobe was used to obtain 10 point analyses from traverses across the table facets of all 25 gemstones. For the examination of beryllium contents (which cannot be determined by electron microprobe) and further trace element analysis we selected two taaffeites and three musgravites for laser ablation-inductively coupled plasma-mass spectroscopy (LA-ICP-MS) using a pulsed Excimer ArF laser with a characteristic wavelength of 193 nm, combined with special optics to homogenize the energy distribution across the laser beam combined with the Perkin Elmer ELAN 6100 ICPMS quadrupole instrument. Non-polarized UV-Vis (300-800 nm) absorption spectra were recorded using a Cary 500 Scan spectrophotometer.

Results

Identification of mineral species

The physical properties and chemical compositions of ten taaffeite and ten musgravite samples from Africa are summarized in *Tables I* and *II*. The data for the remaining 20 taaffeites more or less duplicated the properties of the taaffeites given in the table and would not supply any additional information of significance. The identification of our samples by laser Raman microspectroscopy as described by Kiefert and Schmetzer (1998) and recently by Okano *et al.* (2006) was conclusive for most but not all of the faceted taaffeites and musgravites. All specimens showed a high to extremely high background fluorescence in their Raman spectra, and in some this was sufficient to swamp the critical lines for the minerals and prevent unequivocal identification. With a combination of quantitative chemical analysis by electron microprobe and Raman microspectroscopy, however, all 30 taaffeites and ten musgravites were identified.

Figure 1: *These three violet, bluish grey and light purple taaffeites show the variation of colour seen in samples from Africa. The violet sample of 2.68 ct measures 9.0 mm in width.*

Figure 2: *The 10 studied musgravites from Africa show a wide range of colour from intense purple and light purple to violetish grey, bluish grey and bluish greenish grey. The largest sample of 3.97 ct measures 8.2 × 11.6 mm.*

Visual appearance and gemmological properties

The colours of the taaffeites vary between light purple, purplish violet, violet, greyish violet, bluish violet, greyish blue and bluish grey *(Figure 1)*. The musgravites show a similar colour variation, except that one is an intense purple and two have a bluish greenish grey colour *(Figure 2)*. Pleochroism in all stones is very weak or absent. All taaffeites and musgravites are inert to long- and short-wave ultraviolet radiation.

RIs and SGs of the taaffeites vary between 1.719 and 1.729 for ω and 1.715 and 1.723 for ε, and between 3.60 and 3.69 for SG. The musgravites have almost identical values in the same range, but with a smaller variation: their RIs vary between 1.719 and 1.725 for ω and between 1.715 and 1.720 for ε, and their SGs between 3.61 and 3.64. Thus, both groups of samples show overlapping ranges for these diagnostic gemmological properties. Consequently, for an unequivocal determination of a faceted gem of this mineral group a combination of sophisticated techniques such as X-ray diffraction (powder or single crystal techniques) and/or quantitative chemical analysis (for example, by electron microprobe) and/or micro-Raman spectroscopy is needed.

Microscopic observations

In some of the *taaffeites* we were able to identify rounded apatite grains or magnesite crystals. These closely resemble the internal features seen in taaffeites from Sri Lanka (see, for example, Schmetzer *et al*., 2000, 2005a,b, 2006).

In the *musgravites* we identified several small, somewhat rounded apatite crystals *(Figures 3* and *4)*, and a few larger magnesite inclusions, some of which are located in the centre of a rosette of tiny fluid (?) particles *(Figure 5)*. Healed fractures usually consisting of numerous small negative crystals with multiphase fillings are also present *(Figures 6* and *7)*. With Raman analysis, it was confirmed that the birefringent crystals within these cavities are also small magnesites. In one sample we observed a cluster of brownish tabular crystals (*Figure 8*), and the Raman spectrum indicated that it was probably mica. In another musgravite we observed a tiny black crystal surrounded by a tension crack, but the Raman spectrum could not be matched with that of a known mineral.

None of the examined taaffeites or musgravites revealed significant growth patterns or colour zoning. Also many were either completely free of or had inclusions that were too small for laser Raman microspectroscopy.

In summary, there was neither any characteristic inclusion that could be used for a distinction of taaffeites from musgravites, nor was any characteristic internal feature observed that would enable separation of African taaffeites and musgravites from stones originating from Sri Lanka.

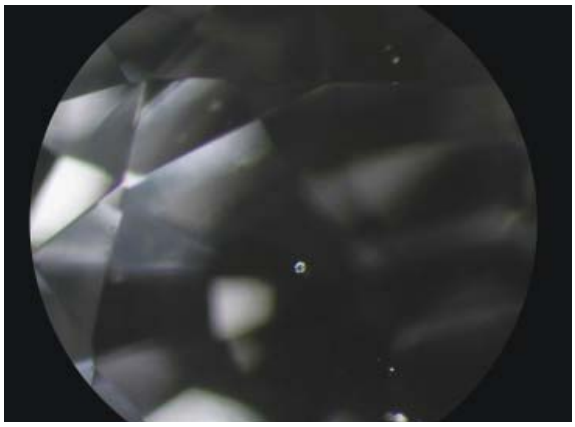

Figure 3: *Small somewhat rounded crystals of apatite are typical inclusions in musgravites from Africa. Magnified 20×.*

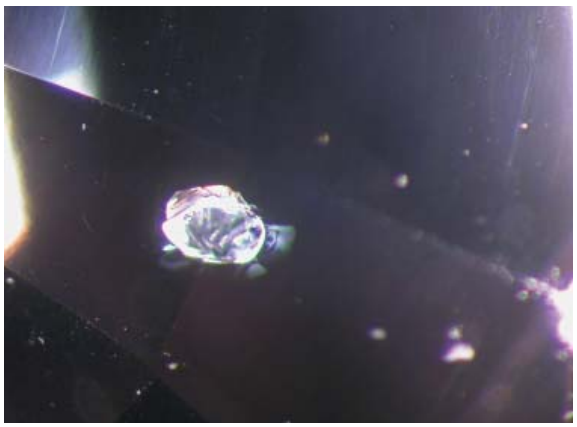

Figure 4: *Rounded apatite inclusion in musgravite from Africa, magnified 80×.*

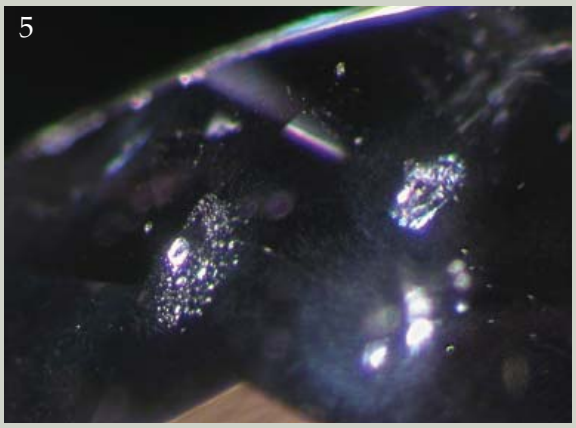

Figure 5: *Primary magnesite crystals occasionally with fluid (?) rosettes are also characteristic for musgravites from Africa. Magnified 70×.*

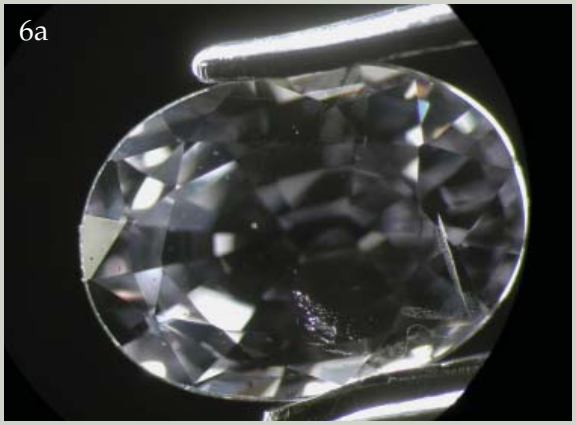

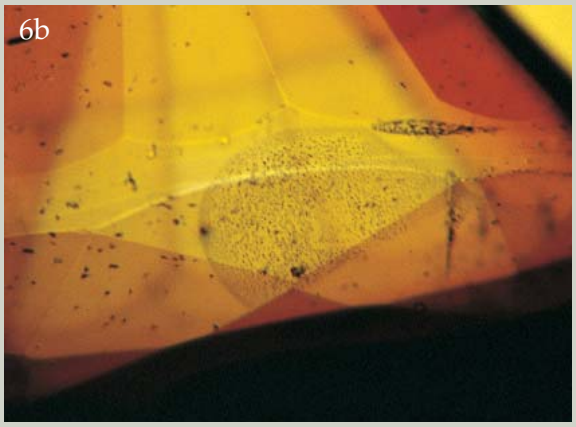

Figure 6: *Healed feathers consisting of small cavities with multiphase filling (fluid with tiny magnesite crystals) are common in musgravites from Africa. (a) overview, the stone measures 5.5 × 7.5 mm; (b) in immersion, only tiny particles are common; (c) with crossed polarizers, the birefringent crystals are clearly visible. (b) and (c) magnified 70×.*

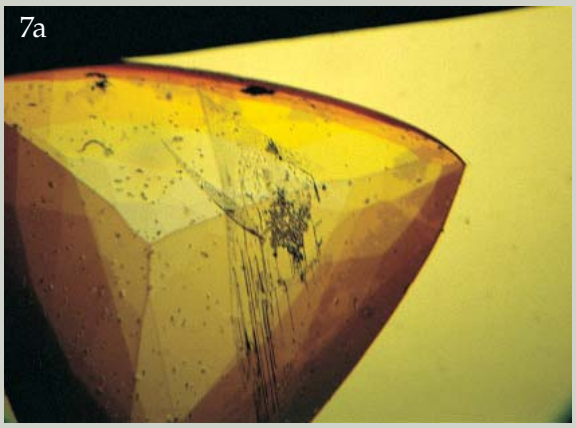

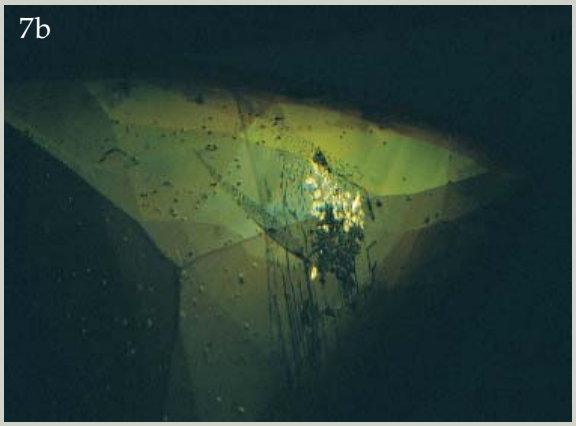

Figure 7: *Musgravite with a healed fracture with two-phase filling (fluid and solid). The fluid channels are clearly visible in plane polarized light in immersion (a) and the birefingent crystals become visible using crossed polarizers (b). Magnified 70×.*

Figure 8: *A cluster of brownish yellow platelets, probably mica, is an inclusion in a musgravite from Africa. Magnified 80×.*

Table I: *Physical properties and chemical compositions of taaffeites from Africa.*

Physical properties

Specimen	A	B	C	D	E	F	G	H	I	J
Weight (ct)	1.10	0.90	2.30	0.63	1.42	1.47	0.35	0.53	0.48	3.51
SG	3.60	3.61	3.60	3.62	3.61	3.63	3.64	3.64	3.66	3.69
RI ω	1.719	1.719	1.719	1.721	1.722	1.723	1.725	1.725	1.726	1.729
ε	1.715	1.715	1.715	1.717	1.718	1.719	1.720	1.720	1.721	1.723
Birefringence	0.004	0.004	0.004	0.004	0.004	0.004	0.005	0.005	0.005	0.006

Chemical composition (microprobe analysis, average of 10 analysis points each, wt.%)

Al_2O_3	73.56	73.41	73.63	73.39	73.28	72.98	73.01	72.52	72.52	71.89
V_2O_3	bdl	0.01	bdl	0.01	bdl	0.01	bdl	bdl	0.01	bdl
Cr_2O_3	0.01	0.01	0.01	bdl	0.01	0.02	0.01	0.01	0.01	0.01
TiO_2	0.01	0.01	0.01	0.01	0.01	0.01	0.01	0.01	0.01	0.01
MgO	21.16	20.98	20.91	20.67	20.41	20.01	19.99	19.68	19.09	18.19
FeO[a]	0.31	0.53	0.67	1.08	1.70	2.33	2.45	2.79	0.86	1.03
ZnO	0.17	0.17	0.12	0.11	0.15	0.08	0.08	0.04	3.34	4.78
MnO	0.01	0.02	0.02	0.02	0.03	0.04	0.05	0.05	0.05	0.02
BeO[b]	4.50	4.49	4.50	4.48	4.48	4.47	4.47	4.44	4.44	4.40
Sum	99.73	99.63	99.87	99.77	100.07	99.95	100.07	99.54	100.33	100.33
sum of transition metal contents (wt.%)[c]	0.51	0.75	0.83	1.23	1.90	2.49	2.60	2.90	4.26	5.85

Cation proportions based on 16 oxygens

Al	8.027	8.027	8.033	8.030	8.019	8.017	8.014	8.013	8.016	8.011
V	-	0.001	-	0.001	-	0.001	-	-	0.001	-
Cr	0.001	0.001	0.001	-	0.001	0.001	0.001	0.001	0.001	0.001
Ti	0.001	0.001	0.001	0.001	0.001	0.001	0.001	0.001	0.001	0.001
Sum trivalent cations	8.029	8.030	8.035	8.032	8.021	8.020	8.016	8.015	8.019	8.013
Mg	2.920	2.902	2.886	2.860	2.825	2.781	2.775	2.751	2.670	2.565
Fe	0.025	0.041	0.052	0.084	0.132	0.182	0.191	0.219	0.068	0.081
Zn	0.011	0.012	0.008	0.008	0.010	0.005	0.005	0.003	0.231	0.334
Mn	0.001	0.001	0.001	0.001	0.002	0.003	0.004	0.004	0.004	0.001
Sum divalent cations	2.957	2.956	2.947	2.953	2.969	2.971	2.975	2.977	2.973	2.981
Be[d]	1.000	1.000	1.000	1.000	1.000	1.000	1.000	1.000	1.000	1.000

bdl = below detection limit.

[a] Total iron as FeO. [b]Since beryllium is not detectable by microprobe analysis, the BeO content has been calculated for 1 Be per formula unit; for the theoretical composition of taaffeite ($BeMg_3Al_8O_{16}$) an amount of 4.52 wt.% BeO is required. [c]Calculated as (V_2O_3 + Cr_2O_3 + TiO_2 + FeO + ZnO + MnO). [d]Calculated on the basis of 16 oxygens assuming Be = 1.000.

Table II: *Physical properties and chemical compositions of musgravites from Africa.*

Physical properties

Specimen	A	B	C	D	E	F	G	H	I	J
Weight (ct)	1.18	0.44	3.97	0.36	0.46	0.61	0.35	0.86	0.65	0.60
SG	3.61	3.61	3.62	3.61	3.62	3.62	3.62	3.62	3.63	3.64
RI ω	1.719	1.720	1.721	1.721	1.722	1.722	1.722	1.723	1.724	1.725
ε	1.715	1.716	1.717	1.717	1.718	1.718	1.718	1.719	1.719	1.720
Birefringence	0.004	0.004	0.004	0.004	0.004	0.004	0.004	0.004	0.005	0.005

Chemical composition (microprobe analysis, average of 10 analysis points each, wt.%)

Al_2O_3	73.98	74.30	74.32	73.96	74.00	73.75	73.78	74.05	73.63	73.19
V_2O_3	bdl	0.01	bdl	bdl	bdl	bdl	0.01	bdl	0.01	bdl
Cr_2O_3	0.01	0.08	0.01	bdl	0.01	0.01	0.01	0.01	0.01	0.01
TiO_2	bdl	0.02	0.01	0.01	0.01	0.01	0.01	0.01	0.01	0.01
MgO	18.99	18.90	18.58	18.45	18.57	18.36	18.32	18.69	18.19	17.99
FeO[a]	0.61	1.09	1.20	1.23	1.45	1.59	1.56	1.51	1.84	2.00
ZnO	0.12	0.06	0.11	0.14	0.15	0.04	0.18	0.36	0.18	0.10
MnO	0.02	0.02	0.06	0.05	0.02	0.03	0.04	0.06	0.12	0.09
BeO[b]	6.04	6.08	6.06	6.03	6.05	6.02	6.03	6.07	6.02	5.98
Sum	99.77	100.56	100.35	99.87	100.26	99.81	99.94	100.76	100.01	99.37
sum of transition metal contents (wt.%)[c]	0.76	1.26	1.39	1.43	1.64	1.68	1.81	1.95	2.17	2.21

Cation proportions based on 12 oxygens

Al	6.004	5.997	6.013	6.013	6.001	6.007	6.007	5.986	6.002	6.003
V	-	0.001	-	-	-	-	-	-	0.001	-
Cr	0.001	0.004	0.001	-	0.001	0.001	0.001	0.001	0.001	0.001
Ti	-	0.001	0.001	0.001	0.001	0.001	0.001	0.001	-	0.001
Sum trivalent cations	6.005	6.003	6.015	6.014	6.003	6.009	6.009	5.988	6.004	6.005
Mg	1.950	1.930	1.901	1.898	1.905	1.891	1.886	1.911	1.875	1.866
Fe	0.035	0.063	0.069	0.071	0.083	0.092	0.090	0.087	0.106	0.117
Zn	0.006	0.003	0.006	0.007	0.008	0.002	0.009	0.018	0.009	0.005
Mn	0.001	0.001	0.003	0.003	0.001	0.002	0.002	0.003	0.007	0.005
Sum divalent cations	1.992	1.997	1.979	1.979	1.997	1.987	1.987	2.019	1.997	1.993
Be[d]	1.000	1.000	1.000	1.000	1.000	1.000	1.000	1.000	1.000	1.000

bdl = below detection limit.
[a]Total iron as FeO. [b]Since beryllium is not detectable by microprobe analysis, the BeO content has been calculated for 1 Be per formula unit; for the theoretical composition of musgravite ($BeMg_2Al_6O_{12}$) an amount of 6.08 wt.% BeO is required. [c]Calculated as (V_2O_3 + Cr_2O_3 + TiO_2 + FeO + ZnO + MnO).
[d]Calculated on the basis of 12 oxygens assuming Be = 1.000.

Table III: *Trace element contents in taaffeites and musgravites from Africa.*

Specimen	Taaffeite A	Taaffeite G	Musgravite A	Musgravite H	Musgravite I
Weight (ct)	1.10	0.35	1.18	0.86	0.65
Li	22	3	8	7	127
B	50	24	346	688	220
Ga	610	172	296	259	107
Sn	9	1	11	2	23

N.B. LA-ICP mass spectrometry was used. Results are in ppm and are means of three analysis points for each stone.

Chemical composition

The results of electron microprobe analysis are presented in *Tables I* and *II*. No distinct chemical zoning was observed in the traverses across the table facets of the samples. In addition to the principal components of taaffeite and musgravite, Al_2O_3, MgO and BeO (which is not detectable directly by electron microprobe), the samples contain distinct amounts of iron and zinc. The ranges of iron contents in both minerals (from 0.31 to 2.79 wt.% FeO in taaffeites and from 0.61 to 2.00 wt.% FeO in musgravites) are broadly similar.

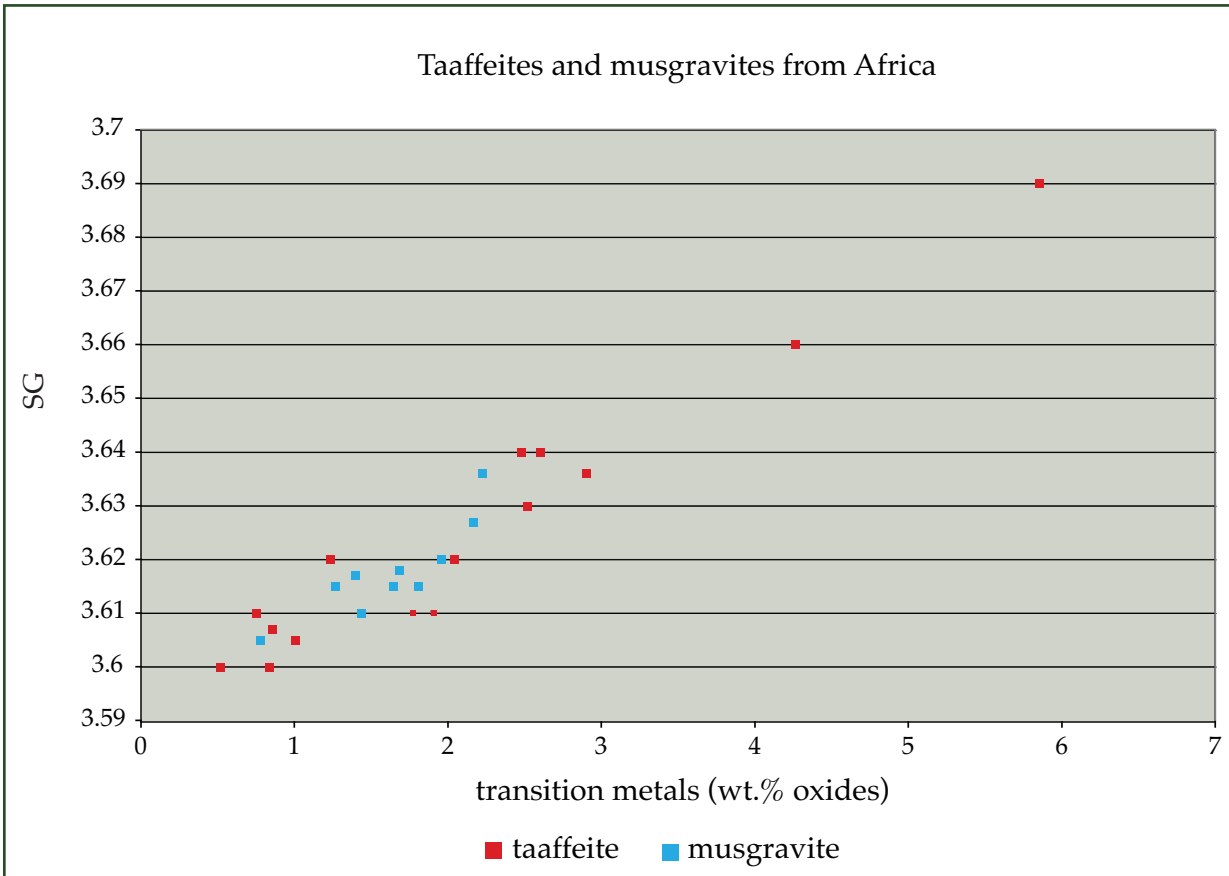

Figure 9a: *A correlation of the sum of transition metal contents with SG indicates the influence of chemical composition on gemmological properties of taaffeite and musgravite samples from Africa (for data see* Tables I *and* II*). 'Normal' samples have transition metal contents of up to 2.90 wt.%; two zinc-rich taaffeites with trace element contents of 4.26 and 5.85 wt.% are shown on the right of the diagram; the overlap of physical properties for samples of both minerals with similar transition metal contents is evident.*

There is, however, a distinct difference in the variation of zinc contents: the range observed for taaffeites is from 0.04 to 4.78 wt.% ZnO and for musgravites only from 0.04 to 0.36 wt.% ZnO. In one sample only (musgravite B) was there a significant chromium content of 0.08 wt.% Cr_2O_3. In addition, there are smaller traces of other transition metals present such as titanium and manganese.

Further trace element analyses for two taaffeites and three musgravites are given in *Table III*. Apart from the main constituents Be, Mg and Al, distinct contents of lithium, boron, gallium and tin were found. Na, Si, P, Ti, V, Cr, Mn, Fe, Co, Ni and Zn were also found as minor to trace elements in these samples, but at or below the detection limit were K, Ca, Sc, Ge, Rb, Sr, Y, Zr, Nb, Cs, La, Ce, Dy, Lu, Hf, Ta, W, Pb, Bi, Th and U. The taaffeites A and G show distinctly lower concentrations of boron than the three musgravites (samples A, H and I), but the other trace elements show overlapping concentration ranges.

The main difference in chemical composition between taeffeite and musgravite is their different beryllium contents, and since these cannot be measured by electron microprobe, the difference was proven directly by mass spectroscopy. Using the analytical results obtained for taaffeite A measured with this technique as an internal standard for the theoretical beryllium content of taaffeite (4.52 wt.% BeO), the value for taaffeite G was calculated to 4.51 wt.% BeO, and the analytical data for the three musgravites A, H and I gave BeO values of 6.03, 5.98 and 5.97 wt.%. These data confirm the generally accepted formulae for both mineral species, which requires an amount of 4.52 wt.% BeO for pure taaffeite (without iron and zinc contents) and an amount

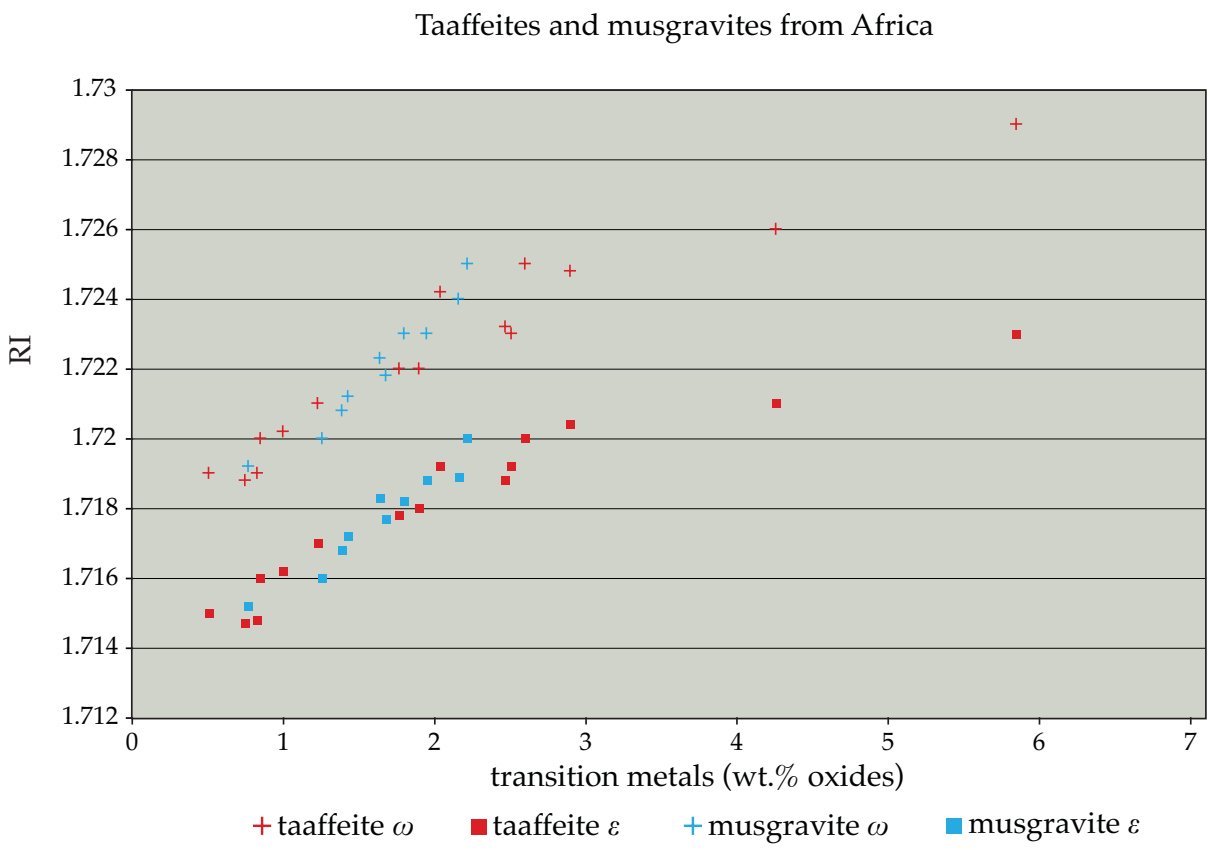

Figure 9b: *A correlation of the sum of transition metal contents with RIs ω and ε indicates the influence of chemical composition on gemmological properties of taaffeite and musgravite samples from Africa (for data see* Table I *and* II*). 'Normal' samples have transition metal contents up to 2.90 wt.%; two zinc-rich taaffeites with trace element contents of 4.26 and 5.85 wt.% are shown on the right of the diagram; the overlap of physical properties for samples of both minerals with similar transition metal contents is evident.*

of 6.08 wt.% BeO for pure musgravite (without iron and zinc contents).

The chemical compositions calculated according to the chemical formula of taaffeite for 16 oxygen atoms and 1 beryllium atom per formula unit is close to ideal cation proportions *(Table I).* The sum of trivalent cations is close to the theoretical value of 8.000 and the sum of bivalent cations is close to the ideal value of 3.000. These data indicate that only a small fraction of total iron may be present as Fe^{3+} with the majority of iron replacing magnesium as Fe^{2+}. The same applies for musgravite *(Table II):* the sum of trivalent cations is close to the theoretical value of 6.000 and the sum of bivalent cations is close to the ideal value of 2.000.

From this study, there is no evidence of any intermediate phase with a composition and formula between the two established mineral species, taaffeite and musgravite. The range of chemical composition shown by the 25 samples analysed in the present study is smaller than the range reported by Okano *et al.* (2006) for taaffeite and musgravite samples from Sri Lanka although this is based on semi-quantitative EDXRF analyses.

SGs and RIs of taaffeites and musgravites from Africa are compared with their individual sums of transition metal contents (V_2O_3 + Cr_2O_3 + TiO_2 + FeO + ZnO + MnO) in *Figures 9a* and *b*. In addition to iron, there is a strong correlation between higher zinc contents and increase in RI and SG of both species (Schmetzer *et al.,* 2000, 2006; Schmetzer 2005).

Spectroscopic properties and cause of colour

UV-Visible absorption spectra of the light purple, violet, greyish violet, greyish blue and bluish grey African taaffeite samples are similar to the spectra of iron-bearing taaffeites from Sri Lanka as already described by Schmetzer (1983b) and Schmetzer *et al.* (2005a), with the most prominent absorption bands at 629, 581, 557, 472, 458, 385 and 370 nm.

These absorption bands, mostly of low to moderate intensity, are assigned to iron, mostly to Fe^{2+} in tetrahedral coordination, with only the usually low-intensity 629 nm band, assigned to an Fe^{2+}/Fe^{3+} intervalence charge transfer absorption.

The spectra of the light purple, violet and greyish violet musgravites described in this paper *(Figure 10)* show the same absorption maxima and intensity relations for different absorption bands *(Figure 10,* sample H). The spectrum of the intense purple chromium-bearing stone shows a distinct absorption maximum at 557 nm which is assigned to an overlap of the iron-related absorption band at 557 nm with a chromium absorption located in the same spectral range *(Figure 10,* sample B). Chromium-bearing taaffeites from Sri Lanka with a similar absorption maximum at about 550 nm due to chromium have already been described by Schmetzer *et al.* (2000, 2006).

The absorption spectra of bluish grey or greyish blue African musgravites are similar to those of violet samples. Most absorption bands are of low to moderate intensity, but the 629 nm absorption band is more intense *(Figure 10,* sample F). The two bluish greenish grey musgravites (chemical properties see *Table II,* samples I and J) show the same type of spectrum although the 629 nm absorption band is even stronger and there is an additional maximum at 600 nm *(Figure 10,* sample I). Very similar spectra (Schmetzer, unpublished data) with an intense 629 nm absorption have been observed in two yellowish greenish grey and blue-green musgravites from Sri Lanka described recently (Schmetzer *et al*., 2005d).

This kind of spectrum with an intense 629 nm absorption has so far not been found in taaffeites. In bluish green spinels from Sri Lanka, however, a similar absorption feature has already been described (Schmetzer *et al*., 1989), where a similar intense absorption band at 645 nm was assigned to an Fe^{2+}/Fe^{3+} intervalence charge transfer absorption. The same cause could also explain the 629 nm absorption band in musgravite, where in addition to ferrous iron (Fe^{2+}), it also contains low concentrations of ferric iron (Fe^{3+}).

A more detailed interpretation of colours, absorption spectra and especially a more complete discussion of the assignment of absorption bands is beyond the scope of the present article.

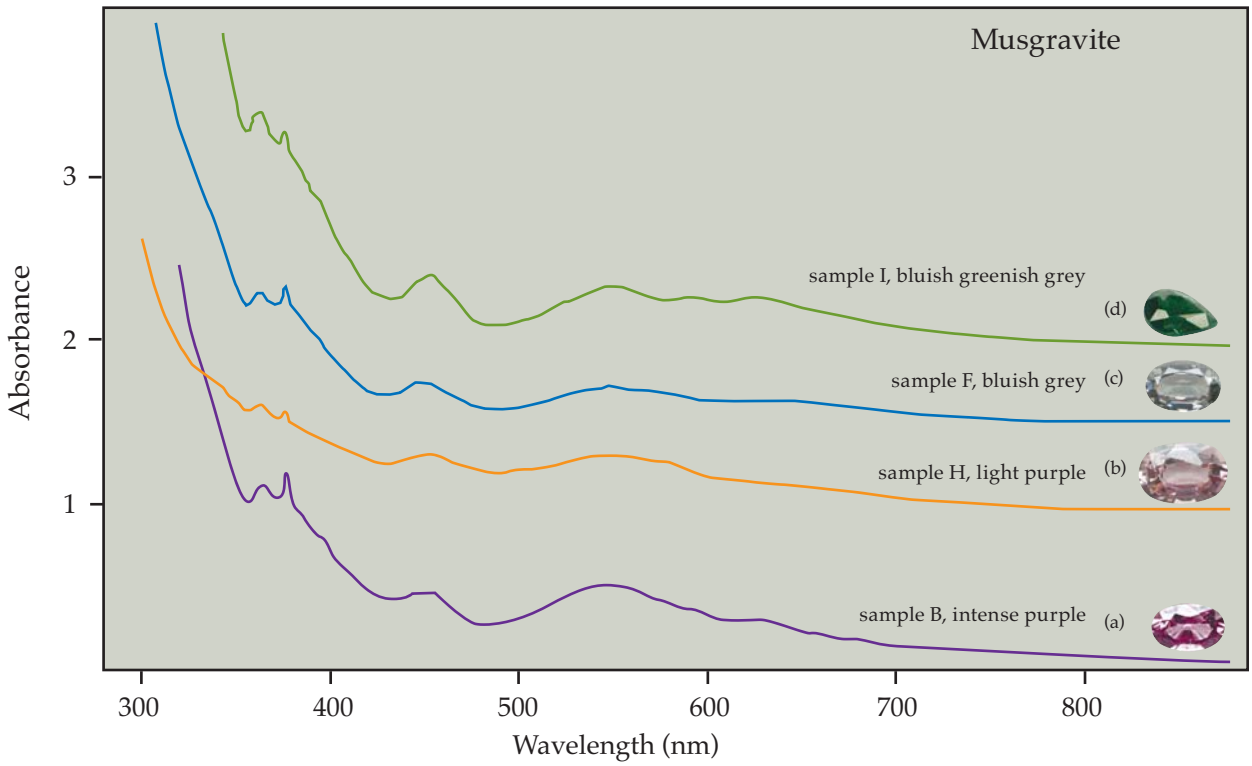

Figure 10: *Absorption spectra of iron- and chromium-bearing musgravites from Africa; from bottom to top: (a) iron- and chromium-bearing musgravite, sample B of* Table II*, intense purple; (b) iron-bearing musgravite, sample H, light purple; (c) iron-bearing musgravite, sample F, bluish grey; (d) iron-bearing musgravite, sample I, bluish greenish grey. The most characteristic iron-related absorption maxima are located at 629, 600, 581, 557, 472, 458, 385 and 370 nm; a chromium absorption band in spectrum (a) is located at about 550 nm; spectra of samples H, F, and I are vertically displaced for clarity. Sample H measures 4.9 x 7.1 mm.*

Discussion

Properties of taaffeites and musgravites from Africa

The taaffeites and musgravites from Africa are characterized by low to moderate iron contents. Two taaffeite samples only show distinct zinc contents of 3.34 and 4.78 wt.% ZnO, but no zinc-rich musgravites have been found. Only one musgravite showed unusual chromium contents of 0.08 wt.% Cr_2O_3.

The variations of RIs and SGs within taaffeites and musgravites are related to their contents of transition metals, i.e. these physical properties mainly increase with increasing iron and zinc contents (see again *Tables I* and *II, Figures 9a* and *b*). However, African taaffeites and musgravites with relatively low transition metal contents have overlapping ranges for these diagnostic gemmological properties. In addition, no significant inclusions or spectroscopic properties have been found which could be usefully combined with standard gemmological methods for a quick distinction of taaffeites from musgravites. Only the bluish greenish grey musgravites show a specific colour and related spectroscopic absorption features which have, so far, not been observed in taaffeites.

Consequently, for an unequivocal determination of faceted gems of the taaffeite group originating from Africa, a combination of sophisticated techniques such as X-ray diffraction (powder or single crystal techniques) and/or quantitative chemical analysis (for example by electron microprobe or LA-ICP-MS) and/or Raman microspectroscopy is needed. This fact is already common knowledge for stones from Sri Lanka.

Comparison of properties of taaffeites and musgravites from Africa and Sri Lanka

The gemmological, chemical and spectroscopic properties of most gem materials belonging to the taaffeite group from both Africa and Sri Lanka have so far shown no significant differences. Apart from some extraordinary taaffeites with extremely high iron and zinc contents reported from Sri Lanka (Schmetzer, 2005; Schmetzer *et al.*, 2006), the properties of normal taaffeites and musgravites from both sources overlap, especially their SGs and RIs (*Table IV*, *Figures 11a* and *b*). At present, gem-quality musgravites with high zinc contents are unknown from both occurrences. So far, all samples from both sources with a bluish greenish grey, yellowish-green or blue-green colour and an intense 629 nm absorption band have been identified as musgravites. Gem-quality taaffeites with that particular colour are unknown to the authors.

Considering the musgravite from Sri Lanka with lamellar spinel inclusions (Schmetzer *et al.*, 2005c) as a unique stone, taaffeites and musgravites from both sources show some common inclusions such as somewhat rounded apatite grains, isolated magnesite crystals and healed fractures consisting of negative crystals with multiphase fillings (magnesite and fluid). Other inclusions such as feldspar, graphite and mica have been reported only in a few stones and cannot be considered as characteristic for one mineral species or one locality. The only

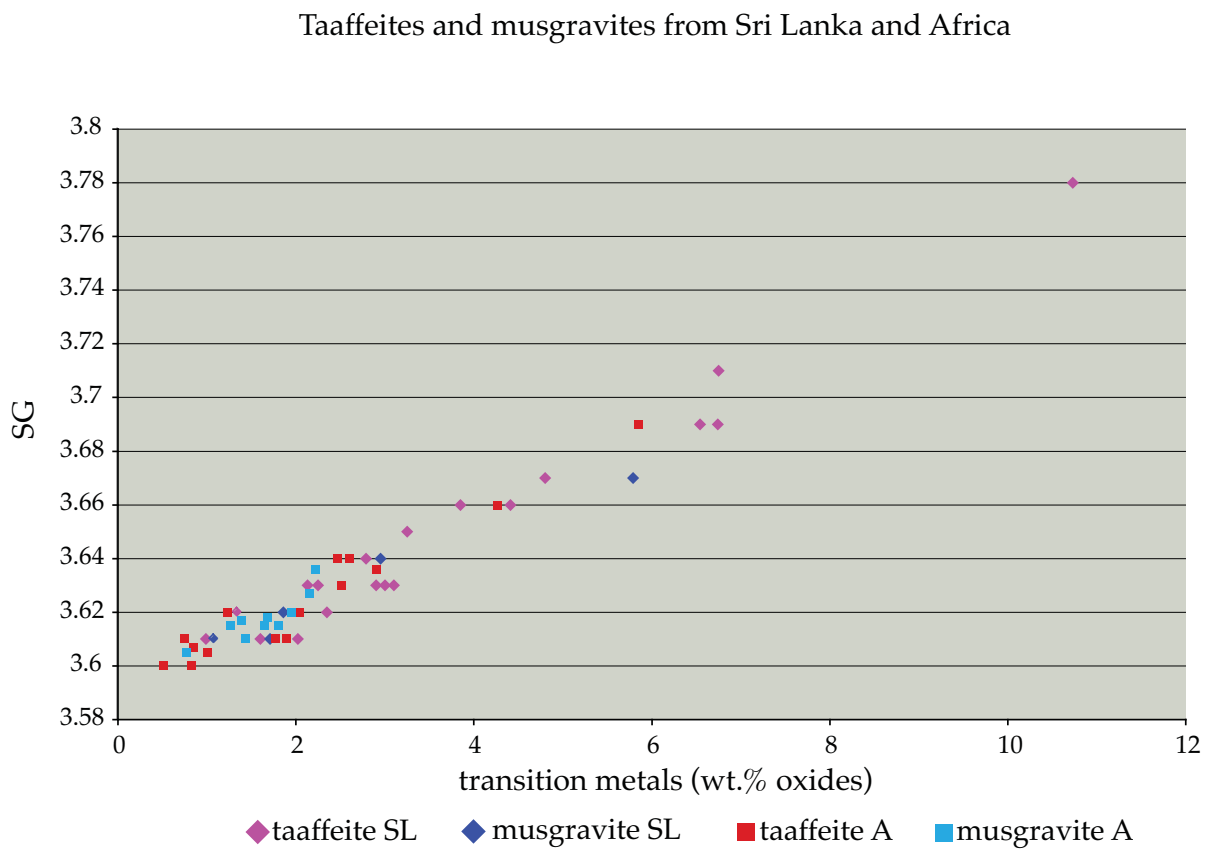

Figure 11a: *A correlation of the sum of transition metal contents with SG indicates the influence of chemical composition on gemmological properties of taaffeite and musgravite samples from Africa (data see* Tables I *and* II*) and Sri Lanka (data see* Table IV*). 'Normal' samples have transition metal contents up to 3.25 wt.%; zinc- and iron-rich specimens have transition metal contents between 3.85 and 10.73 wt.%. The overlap of physical properties for samples of both minerals from both sources with similar transition metal contents is evident. A = Africa, SL = Sri Lanka.*

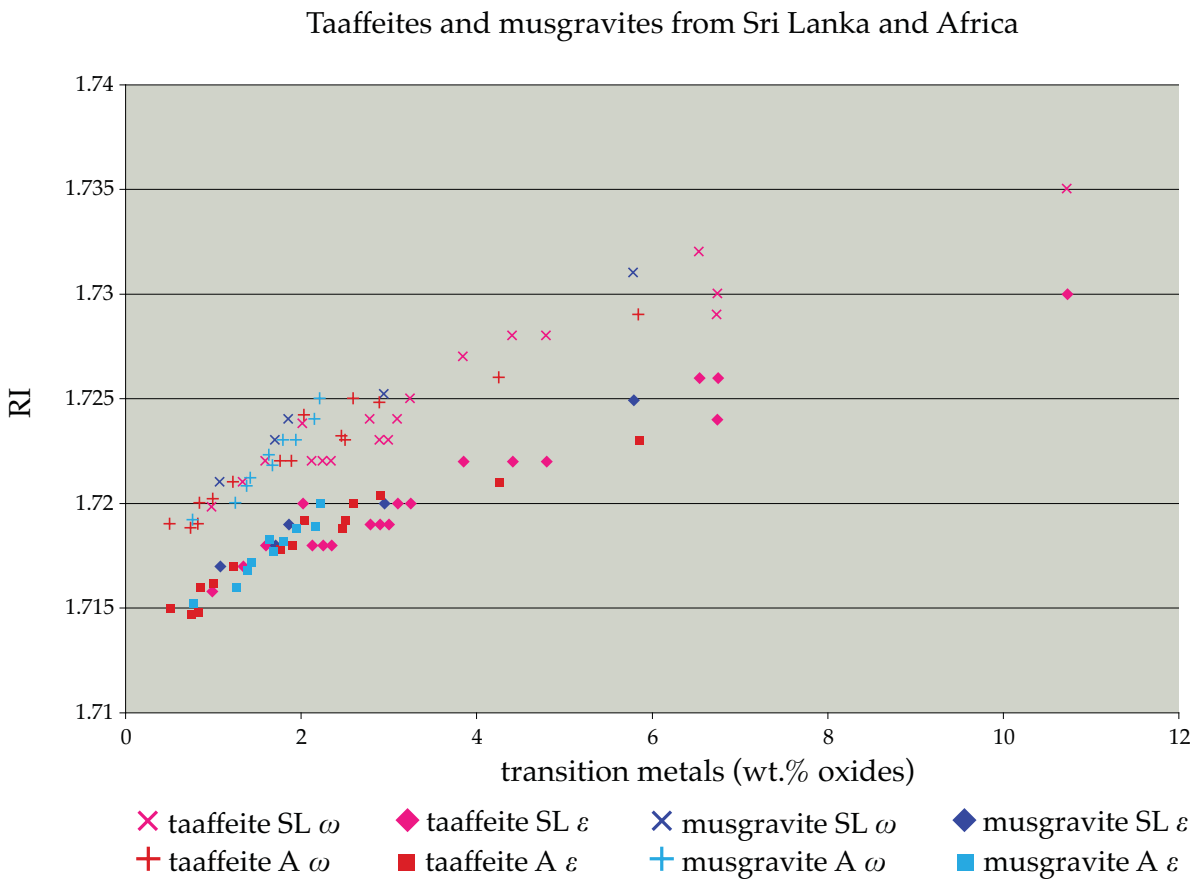

Figure 11b: *A correlation of the sum of transition metal contents with RIs* ω and ε *indicates the influence of chemical composition on gemmological properties of taaffeite and musgravite samples from Africa (data see* Tables I *and* II*) and Sri Lanka (data see* Table IV*). 'Normal' samples have transition metal contents up to 3.25 wt.%; zinc- and iron-rich specimens have transition metal contents between 3.85 and 10.73 wt.%. The overlap of physical properties for samples of both minerals from both sources with similar transition metal contents is evident. A = Africa, SL = Sri Lanka.*

inclusions which are relatively common in both taaffeite and musgravite from Sri Lanka are numerous tiny zircons with tension cracks; these have not so far been found in any of the African stones.

Origin of taaffeites and musgravites from Africa and Sri Lanka

General overviews of taaffeite and musgravite occurrences in different host rocks have been given by Grew (2002), Aleksandrov and Senin (2002) and Schmetzer *et al.* (2005d). Phase relationships in the BeO-MgO-Al_2O_3 system, especially of the pseudobinary system chrysoberyl ($BeAl_2O_4$) - spinel ($MgAl_2O_4$), are given by Franz and Morteani (2002). Both minerals are found in various environments, but typical host rocks are magnesian skarns and calc-silicates of metasomatic origin. Up to now only one primary source for taaffeite group minerals is known from Sri Lanka. The material from Bakamuna is described by Fernando and Hofmeister (2000) as taaffeite, but their chemical data (electron microprobe analysis) are a closer fit to musgravite. The material was found in the metasomatic contact zone of a marble with a high-grade metamorphic pelitic gneiss.

The presence of primary magnesite crystals and tiny magnesites in healed feathers within taaffeites and musgravites from Sri Lanka, suggests that their origin may lie in a magnesian skarn or metasomatic calc-silicate host rock (Schmetzer *et al.*, 2005d). A similar

Table IV: *Range of physical properties and chemical compositions of gem-quality taaffeites and musgravites from Sri Lanka[a] and Africa[b].*

Physical properties

	'Normal' taaffeites Sri Lanka	Iron- and zinc-rich taaffeites Sri Lanka	'Normal' musgravites Sri Lanka	Iron-rich musgravite Sri Lanka	'Normal' taaffeites Africa	Zinc-rich taaffeites Africa	'Normal' musgravites Africa
SG	3.61 – 3.65	3.66 - 3.78	3.61 - 3.64	3.67	3.60 - 3.64	3.66 - 3.69	3.61 - 3.61
RI ω	1.720 – 1.725	1.727 – 1.735	1.721 – 1.725	1.731	1.719 – 1.725	1.726 – 1.729	1.719 – 1.725
ε	1.716 – 1.720	1.722 – 1.730	1.717 – 1.720	1.725	1.715 – 1.720	1.721 – 1.723	1.715 – 1.720

Chemical composition (wt.%)

Cr_2O_3	0.01 – 0.21	0.01 – 0.15	0.01 – 0.02	0.01	0.01 – 0.02	0.01	0.01 – 0.08
FeO[c]	0.80 – 2.59	1.40 – 5.62	0.90 – 2.50	4.91	0.31 – 2.79	0.86 – 1.03	0.61 – 2.00
ZnO	0.05 – 1.18	0.07 – 8.87	0.04 – 0.43	0.70	0.04 – 0.17	3.34 – 4.78	0.04 – 0.36
Sum of transition metal contents[d]	0.99 – 3.25	3.85 – 10.73	1.05 – 2.99	5.79	0.51 – 2.90	4.26 – 5.85	0.77 – 2.22

Structural properties and inclusions

	Sri Lanka	Africa
Common	apatites, magnesite crystals, healed feathers with multiphase fillings (fluid and magnesite), zircons with tension cracks	apatites, magnesite crystals, healed feathers with multiphase fillings (fluid and magnesite)
Rare	growth structures and colour zoning, spinel lamellae, graphite, feldspar, mica	mica, black grain with tension cracks

[a]All data from: Schmetzer and Bank (1985), Bank and Henn (1989), Schmetzer *et al.* (2000), Schmetzer *et al.* (2005 a,b,c,d, 2006).
[b]This paper. [c]Total iron calculated as FeO. [d]Calculated as (Ga_2O_3 + V_2O_3 + Cr_2O_3 + TiO_2 + FeO + ZnO + MnO).

metasomatic origin has already been suggested for Sri Lankan taaffeite by Kampf (1991). A primary source of taaffeite or musgravite in Tanzania is unknown. The similarity of the inclusion patterns of these gem materials from Sri Lanka and Africa, especially the presence of primary magnesite crystals and magnesite as a component of multiphase inclusions in healed feathers, however suggests similar geological conditions in their formation.

Acknowledgements

We are grateful to Mr W. Spaltenstein of Multi Colour Gems, Chantaburi, Thailand, for the loan of the research material for the present study. We also thank Prof. E.S. Grew, University of Maine, Maine, U.S.A., for a critical review of the manuscript.

References

Aleksandrov, S.M., and Senin, V.G., 2002. Genesis and composition of spinellide and related mineral assemblages in greisenized magnesian skarn and dolomite at the Hsianghualing deposit, the People's Republic of China. *Geochemistry International*, 40(9), 860-73

Anonymous, 1996. Taaffeite found in Tunduru. *Jewellery News Asia*, No. 142, June, 58.

Armbruster, T., 2002. Revised nomenclature of högbomite, nigerite and taaffeite minerals. *European Journal of Mineralogy*, 14(2), 389-95

Bank, H., and Henn, U., 1989. Changierender Taaffeit aus Sri Lanka. *Zeitschrift der Deutschen Gemmologischen Gesellschaft*, 38(2/3) 89-94

Burford, M., 1998. Gemstones from Tunduru, Tanzania. *Canadian Gemmologist,* 19(4), 105-10

Demartin, F., Pilati, T., Gramaccioli, C.M., and de Michele, V., 1993. The first occurrence of musgravite as a faceted gemstone. *Journal of Gemmology,* 23(8), 482-5

Fernando, G.W.A. Rohan, and Hofmeister, W., 2000. Origin of some gem minerals in Sri Lanka: evidence from corundum-spinel-scheelite-taaffeite-bearing rocks. In: Rammlmair, D. et al. (Eds), *Applied mineralogy in research, economy, technology, ecology and culture.* 1, 293-96. A.A. Balkema publishers, Rotterdam, The Netherlands

Franz, G., and Morteani, G., 2002. Be-minerals: synthesis, stability, and occurrence in metamorphic rocks. In: Grew, E.S. (Ed.), *Beryllium: mineralogy, petrology, and geochemistry.* Min. Soc. of America, Washington. Reviews in Mineralogy & Geochemistry, 50, 551-89

Grew, E.S.,2002. Beryllium in metamorphic environments (emphasis on aluminous compositions). In: Grew, E.S. (Ed.), B*eryllium: mineralogy, petrology, and geochemistry.* Min. Soc. of America, Washington. Reviews in Mineralogy & Geochemistry, 50, 487-549

Henn, U., and Milisenda, C.C., 1997. Die Edelsteinvorkommen in Tansania: Die Region Tunduru-Songea. *Zeitschrift der Deutschen Gemmologischen Gesellschaft*, 46(1), 29-43

Johnson, M.L., and Koivula, J.I. (Eds), 1996. Gem News. Gem materials from the new locality at Tunduru, Tanzania. *Gems & Gemology,* 32(1), 58-9

Johnson, M.L., and Koivula, J.I. (Eds), 1997. Gem News. Tunduru-Songea gem fields in southern Tanzania. *Gems & Gemology,* 33(4), 305

Kampf, A.R., 1991. Taaffeite crystals. *Mineralogical Record,* 22(5), 343-7

Kiefert, L., and Schmetzer, K., 1998. Distinction of taaffeite and musgravite. *Journal of Gemmology,* 26(3), 165-7

McClure, S.F., 2001. Another musgravite. *Gems & Gemology,* 37(1), 60-2

Milisenda, C.C., Henn, U., and Henn, J., 2001. New gemstone occurrences in the south-west of Madagascar. *Journal of Gemmology,* 27(7), 385-94

Nuber, B., and Schmetzer, K., 1983. Crystal structure of ternary Be-Mg-Al oxides: taaffeite, $BeMg_3Al_8O_{16}$, and musgravite, $BeMg_2Al_6O_{12}$. *Neues Jahrbuch für Mineralogie Monatshefte,* 1983(9), 393-402

Okano, M., Kitawaki, H., and Abduriyim, A., 2006. Taaffeite and Musgravite. Website of the Gemmological Association of All Japan http://www.gaaj-zenhokyo.co.jp/researchroom/2006/2006_10a-01en.html

Schmetzer, K., 1983a. Taaffeite or taprobanite – a problem of mineralogical nomenclature. *Journal of Gemmology,* 18(7), 623-34

Schmetzer, K., 1983b. Crystal chemistry of natural Be-Mg-A1-oxides: taaffeite, taprobanite, musgravite. *Neues Jahrbuch für Mineralogie Abhandlungen,* 146(1), 15-28

Schmetzer, K., 2000. Spinel from Ilakaka, Madagascar. *Gems & Gemology,* 36(2), 169-71

Schmetzer, K., 2005. Rare gemstones from Sri Lanka: some extraordinary taaffeites and musgravites. *GEMMOBASEL 2005, Festschrift in honour of Prof. Dr. Henry A. Hänni.* Rühle-Diebener-Verlag, Stuttgart, pp. 34-7

Schmetzer, K., and Bank, H., 1985. Zincian taaffeite from Sri Lanka. *Journal of Gemmology,* 19(6), 494-7

Schmetzer, K., Haxel, C., and Amthauer, G., 1989. Colour of natural spinels, gahnospinels and gahnites. *Neues Jahrbuch für Mineralogie Abhandlungen,* 160(2), 159-80

Schmetzer, K., Kiefert, L., and Bernhardt, H.-J., 2000. Purple to purplish red chromium- bearing taaffeites. *Gems & Gemology,* 36(1), 50-9

Schmetzer, K., Kiefert, L., Bernhardt, H.-J., Burford, M., and Gunasekara, D.P., 2005a. Iron- and zinc-rich gem-quality taaffeites from Sri Lanka. *Journal of Gemmology*, 29(5/6), 290-8

Schmetzer, K., Kiefert, L., Bernhardt, H.-J., and Burford, M., 2005b. Two remarkable taaffeite crystals from Sri Lanka. *Journal of Gemmology,* 29(7/8), 461-6

Schmetzer, K., Kiefert, L., Bernhardt, H.-J., and Burford, M., 2005c. Gem-quality musgravite from Sri Lanka. *Journal of Gemmology*, 29(5/6), 281-9

Schmetzer, K., Kiefert, L., Bernhardt, H.-J., and Burford, M., 2005d. Musgravites from Sri Lanka. *Neues Jahrbuch für Mineralogie Abhandlungen*, 181(3), 265-70

Schmetzer, K., Kiefert, L., Bernhardt, H.-J., and Burford, M., 2006. The variation of gemmological properties and chemical composition of gem-quality taaffeites and musgravites from Sri Lanka. *Australian Gemmologist*, 22(11), 485-92

Spengler, W., 1983. Burmese parcel reveals rare find. *Jewellery News Asia*, 1(1), 39

Some observations on the composition and origin of opals from Java

H.C. Einfalt

Friedenstr. 46, D 75015 Bretten, Germany. email: hcv.einfalt@gmx.de

Abstract: *The precious opal from Rangkasbitung, Banten Province in West Java occurs in a decomposed tuff layer as a component of the paragenesis montmorillonite – zeolite (clinoptilolite) – opal which formed in an open fresh water system at low temperatures. White, water, brown and black precious opals and non-precious opals from this area have been investigated by various methods. The gemmological characteristics are described. Internal features consist of flow texture, microcrystalline granular quartz/chalcedony, and inclusions of zeolites. Several opals show indications of stress (micro-fractures, glide planes, deformed fields of play-of-colour) which is discussed as a possible reason for the poor stability of some Indonesian opals during processing and wear.*

Though all opals are optically isotropic, X-ray diffraction data indicate that three structural types are present: opal-A, opal-CT and a structurally intermediate opal-'C'. All opals are composed basically of small granules (nanograins) of 30 to 50 nm diameter. Spherical, regularly arranged aggregates of these granules are visible only in opal-A samples, whereas opal-CT and opal-'C' types appear relatively non-structured. Hydrofluoric acid-etched samples render visible in a SEM a very regular pattern of spheres of about 290 nm diameter in opal-A, but similar treatment of opal-'C' showed complete dissolution of spheres leaving a framework of pore cement. HF treatment of opal-CT left a massive cement and a hardly visible regular arrangement of only a few non-spherical voids.

Analyses of the main elements in five representative opals indicate a wide range of concentrations for Al (4200-10100 ppm), Ti (3-5700 ppm), Ca (1480-6370 ppm), Na (700-2450 ppm) and K (390-1630 ppm) as the main impurities. Iron (6-403 ppm) is relatively low and is unlikely as the sole cause of dark brown and black body colours. Major trace elements of tens of ppm are Ba, Zr, Y and Rb. With the exception of unusual high values of Ti, Ca and Mg in one opal and the low Ba content, the chemistry does not provide a direct genetic link to the tuffaceous host rock.

Keywords: *composition, deformation, inclusions, Indonesian opal, LA-ICP-MS, structure, XRD*

 ISSN: 1355-4565

Introduction

Precious opals of mainly brown to black body colour are produced in West Java/Indonesia, about 150 km southwest of Jakarta near the town of Rangkasbitung in the Banten province, by small scale miners (Lambert and Brown, 1994; Sujatmiko *et al*., 2004). The opals occur as irregularly-shaped nodules up to a few centimetres in diameter in a zone of decomposed tuff, up to 2 m thick, in the Pliocene Genteng Formation, a 700 m thick volcaniclastic sequence of tuff, pumice, breccia, claystone, conglomerates and polymict sandstones. The opal-bearing zone consists of clay (montmorillonite with minor kaolin), partially devitrified tuff particles, abundant small, water-clear plagioclase crystals of andesine composition, a few xenolithic rock fragments, and opal. Similar occurrences of precious brown opal in volcaniclastic sediments (welded tuffs) have been reported from Ethiopia (Johnson *et al*., 1996) and Somaliland (Kinnaird and Jackson, 2000; Kinnaird, 2002).

Since the physical properties of these opals are not well documented in the gemmological literature, the results of the investigation on several opal varieties from this location are reported here.

Gemmological characteristics

Body colour

Of the eleven precious opals, three are water-opals of colourless, water-white appearance (*Figure 1a*); three are so-called 'tea-opals' (Lambert and Brown, 1994) with a light brown to dark brown body colour (*Figure 2*); and one has an apparent grey body colour, caused by abundant thin white lines on the surface in a light brown and slightly

Sample material and methods of investigation

Thirteen opal samples with variable body colour were available for investigation using a binocular, polarizing microscope, X-ray diffraction, laser ablation ICPMS and a scanning electron microscope. Cutting and polishing of eight stones had been discontinued because of their low quality - they had opaque areas without play-of-colour, inclusions, small fractures or had been damaged during cutting. The weight of the cabochons ranged from 0.8 to 6.5 ct. Three samples consisted of rough gem material with a weight between 3.3 and 9.0 ct.

A stereo microscope with a maximum magnification of 45x was used for study of the opals in air and immersed in water, and under transmitted and oblique incident light. Thin sections of eight opals were examined using a standard polarizing microscope.

For viewing the samples under short- and long-wave UV light, a viewing cabinet was used.

Twelve samples were examined by XRD with a Siemens D500 diffractometer, Cu Kα radiation at 1.5405 Å, (delta lambda 0.0038 Å) and a graphite monochromator. Measurements were taken between 15.0 and 40.0 2θ at a scanning speed of 0.5 /min (standard parameter), followed by measurements on 7 samples with a low scanning speed of 0.06 /min between 18 and 27 2θ using corundum as internal standard.

Untreated and HF-etched surfaces of seven opals were investigated by SEM using a LEO 1530 GEMINI scanning electron microscope at 10 kV and a 5 nanometre Pt-coating of the samples.

Five opal samples with body colours ranging from water clear to brown and black were investigated for main and trace elements by laser ablation ICPMS using a New Wave Research UP 213 laser ablation unit and an Agilent 7500ce ICPMS with Ar as carrier gas, Si as internal standard (determined with microprobe) and NIST 610 as external standard. Each sample was measured at three sample points.

Figure 1: *Examples of opals from Indonesia with different body colours.* 1a*: This transparent water opal (IO 12, 4 ct) shows play-of-colour in comparatively large patches of red, blue and green.* 1b*: The apparent grey body colour of this turbid light brown 'tea-opal' (IO 8, 1.5 ct) is caused by traces of multiple parallel planar features which dissect the colour fields in two main directions (only one set is clearly visible). The fracture on the left side marks the direction of the second set. These are interpreted as latent microfractures.* 1c*: This typical black opal (IO 3, 2 ct) with red, green and blue play-of-colour developed surface fractures when exposed to strong heat from a 500 W photo lamp.* 1d*: This is a good example of spot-like red and green colour fields in a black opal (IO 2, 3.5 ct) which needs strong illumination to show its full colours.*

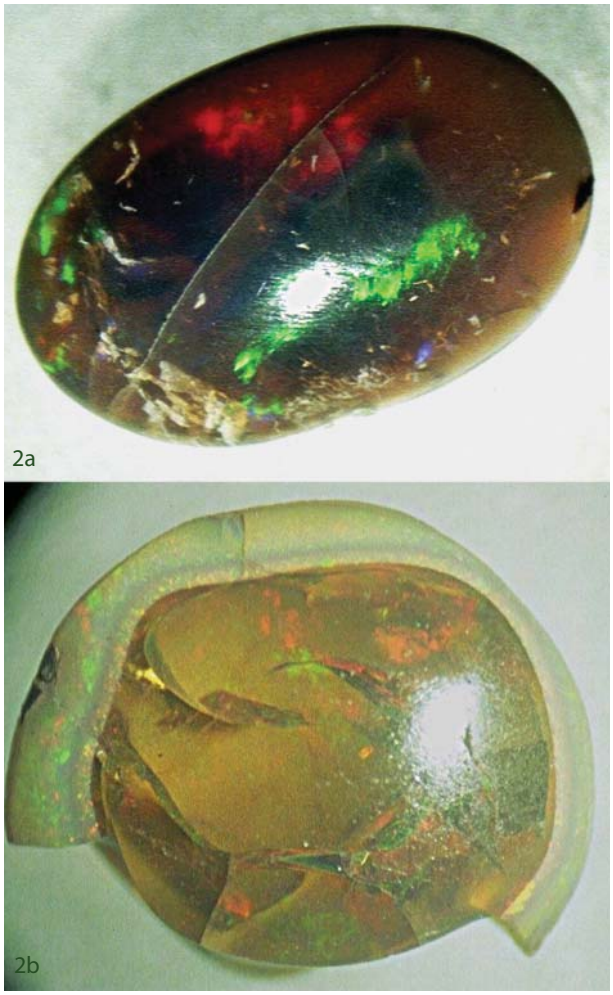

Figure 2: *'Tea opals' from Indonesia;* 2a: *The slightly translucent dark brown specimen IO 5 of 1.5 ct contains abundant white flaky inclusions, possibly the zeolite mordenite.* 2b: *A core of brown opal is surrounded by pin-fire white opal in this sample (IO 15, 1.5 ct) and is interpreted as two stages of crystallization. The pattern could be explained if one imagines replacement of a plant root (cross section), where firstly the 'tea opal' fills the inner part and then the white opal only develops after the outer more resistant layer of the root has decomposed.*

turbid groundmass (*Figure 1b*). The body colours of another three opals are black to the unaided eye (*Figures 1c* and *1d*), but when viewed under strong illumination at thin edges their body colour is a very deep brown. One white opal was also studied.

Of the two non-precious opals, one is pale yellow brown, while the other is dark brown with a reddish tinge, similar to fire-opal though of a not very attractive colour.

Diaphaneity

Of the three water opals, one is absolutely water-clear and the others are slightly turbid, though still transparent. The brown opals ('tea-opals') are translucent when light-coloured but only transmit light at their edges in the darker stones. The white and the three black opals are opaque. Of the non-precious opals, the pale yellow opal is nearly transparent, while the dark brown is only slightly translucent.

Play-of-colour

The play-of-colour is dominated by red, orange and green in most of the investigated samples, a common feature in Indonesian opals (Sujatmiko *et al.*, 2004). However, a close inspection with hand lens/binocular microscope and a stronger illumination also reveals the presence of subordinate patches of very deep blue. A similar preference for major reds and greens with minor royal blue patches has been reported from chocolate brown opals from Somaliland (Kinnaird, 2002). The play-of-colour is not always developed

throughout a cabochon: two brown opals had clearly visible colour fields next to areas of apparently non-precious opal. Strong illumination is needed for black opals to show their full play-of-colour. In the two non-precious opals, a very faint, spot-like play-of-colour appeared fleetingly when strong illumination was moved along their sides.

The fields or patches with play-of-colour are usually small (<1-2 mm, but in a few samples up to 5 mm), and a typical spot-like pattern is shown in *Figures 1c* and *d*. Their shape ranges from polygonal to somewhat elongated, commonly with serrated or blurred boundaries. The white opal has very small, densely packed colour fields, which give a sparkling impression ('pin fire') in red and blue. In cross-section, these colour fields are columnar and arranged in a parallel array perpendicular to the original surface of the rough gem. A dominantly green 'pin fire' is present in a white opal rim around a core of 'tea opal' in an unusual two-colour cabochon (*Figure 2b*).

Pseudo-birefringence

With the exception of one 'tea-opal' with faint play-of-colour, and the two non-precious opals, the other 5 opals examined in thin section (water opal, 'tea-opal' and black opal) showed pseudo-birefringence under crossed polarizers in strong blues to

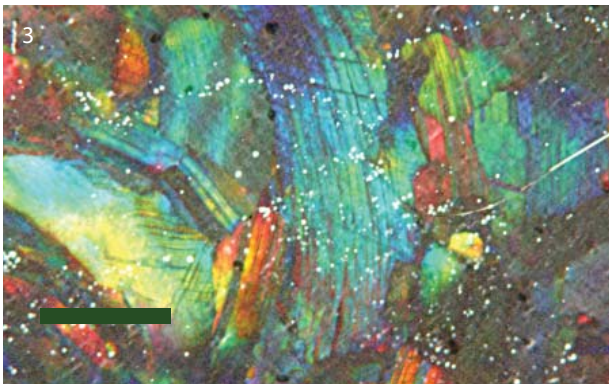

Figure 3: *Colour fields in this opal sample (IO 1) viewed under crossed nicols contain abundant dark lines from stacking faults and glide planes. Colour bands are slightly curvilinear which may indicate deformation due to external stress. Note also the variable and often small size of colour fields. (White spots are due to sample preparation). Thin section micrograph, length of bar: 0.5 mm.*

Figure 4: *Fields with play-of-colour (viewed as pseudo-birefringence colours) in this water opal (IO 9) are extremely elongated probably as a result of deformation. Thin section, crossed polarizers, length of bar: 0.5 mm.*

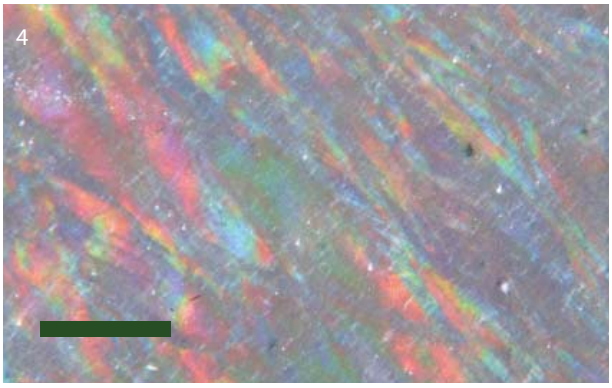

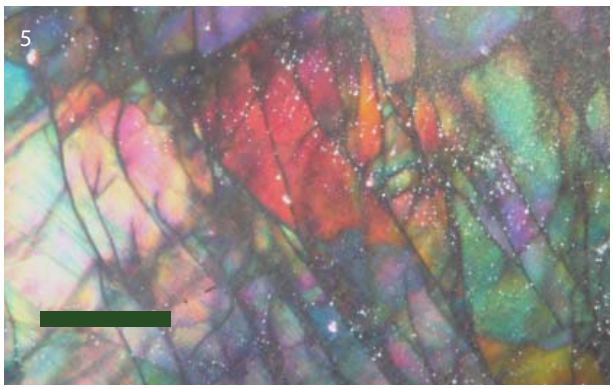

Figure 5: *Pseudo-birefringence in this dark brown opal (IO 1) reveals abundant cross cutting dark lines as traces of microfractures in three sets. (White spots are from thin section preparation). Thin section, crossed polarizers, length of bar: 0.5 mm.*

Figure 6: *The colour fields in this black opal (IO 6) are dissected and offset by three sets of microfractures, although the opal as a whole is still coherent. The light area in the lower right corner is a photographically overexposed aggregate of clinoptilolite with pale brown discoloration and a thin zone of microcrystalline quartz (?) at the contact with the opal. (Opal is broken off from the thin section in the angular grey area in the lower part of the picture). Thin section, crossed polarizers, length of bar: 0.5 mm.*

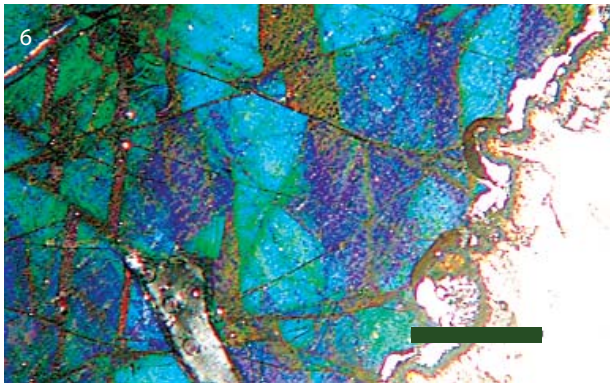

blue-greens, yellows and, less commonly, in reds. Dark striations inside the individual colour fields are caused by stacking faults (Graetsch, 1994) and probably also by glide planes and are common in several samples (*Figure 3*). A slight bending of these lamellae is present in the stone shown in *Figure 3* and the colour fields in the water opal shown in *Figure 4* indicate strong shearing. Abundant microfractures in two to three sets are visible in two samples under crossed polarizers, but this feature is hardly discernible or invisible in plane polarized light (*Figure 5*). In one sample, a displacement of fractured parts of colour fields is present (*Figure 6*).

Specific gravity and refractive index

The specific gravity (SG) range of 1.98 to 2.06 and the refractive index (RI) range of 1.435 to 1.468 of these stones have been reported by Sujatmiko *et al*. (2004). The SG values are in the normal range for opals (1.98 to 2.20 according to Webster, 1994) as are the RI values (1.44 to 1.46; Webster, 1994) with the exception of the somewhat high value of 1.468. The colourless or paler coloured opals have the lower SG and RI values.

Fluorescence

Although fluorescence in opal has been described in Webster (1994) as white to pale blue, pale brown or green with most black opal being inert, no conspicuous fluorescence under short or long wave UV light has been observed in most of the samples from Indonesia. The exceptions are in one water opal and in the white opal, which both gave a weak pale blue fluorescence under short and long wave UV light. Both are opal-A according to XRD results.

Reaction to heat

Illumination with a 500W photo lamp at a distance of 30 cm for a few minutes resulted in a network of cracks (crazing) on the surface of a black opal (*Figure 1c*).

Similarly, fractures developed in thin section material during prolonged microscopic work due to heating from the light source.

Hydrophane opal

The 'pin fire' white opal rim of the 'eye' cabochon shown in *Figure 2b* consists of hydrophane opal; this shows unusual behaviour of *losing* its play-of-colour when immersed in water, and regaining it on drying. The same effect was also observed in an off-white part of a flow-textured opal (see below). Similar observations on opal from Indonesia have been reported previously by Milisenda and Wild (2004) and Koivula and Tannous (2001). In both cases, the RIs of the white schlieren and of the white opal are slightly lower than the brown opal, perhaps caused by higher water content.

Internal features

Rock and mineral inclusions

Only three opals (the two non-precious opals and one water opal) are free of any inclusions and other internal features as described below. Strongly decomposed pale yellow-brown soft tuff particles and plagioclase crystals are associated with the rough opal and may occur as inclusions. Precious opal matter fills the microfractures in the tuff particles.

A massive aggregate of platelets arranged in parallel (*Figure 6*) in a black opal-CT has the optical characteristics of a zeolite (with a birefringence of about 0.006, and an RI higher than opal but lower than the araldite resin (1.62)) and a hardness much lower than quartz. Its XRD data are identical with clinoptilolite ($(Na, K, Ca)_{2-3}Al_3(Al, Si)_2Si_{13}O_{36}.12H_2O$). At its contact with the opal, the aggregate is embayed and rimmed by a pale brown zone and a thin band of what appears to be microcrystalline quartz. A similar zone surrounds the tuff inclusions at their contacts with opal.

Small, distorted, fibrous and colourless aggregates are abundant in another 'tea-opal' (*Figure 2a*) and according to their fibrous nature and optical data, are probably composed of another zeolite, possibly mordenite.

Twisted tube-like features of unknown nature are present in this opal, similar to

Table I: *XRD data of twelve samples of Indonesian opals (IO), with comparisons.*

Sample No.	Body colour	Type	4.10 Å peak1	I_{max}	FWHM $\Delta°2h$ CuKα	4.3 Å peak	2.50 Å I_{max}	FWHM $\Delta°2h$ CuKα
IO 1	dark brown	opal-CT	4.113/4.103	795	1.247	+	130	0.764
IO 7	brown	opal-CT	4.101/4.107	795	0.876	+	102	0.592
IO 11	colourless	pal-CT	4.107	750	0.801	+	130	0.630
IO 12	colourless	opal-CT	4.115/4.113	730	1.146	+	132	0.778
Herdian.[2] Graetsch		opal-CT opal-CT			0.54-0.75 0.68-1.11			
IO 6	black	opal-'C'	4.100	570	1.212	–	67	0.857
IO 3	black	opal-'C'	4.115/4.107	600	1.318	–	62	0.859
IO 4	brown	opal-'C'	4.101/4.101	790	1.128	–	92	0.928
IO 8	pale brown	opal-'C'	4.094	750	1.123	–	97	1.248
IO 13	brown[3]	opal-'C'	4.118	560	1.289	–	52	0.973
IO 14	pale yellow[3]	opal-'C'	4.114/4.109	550	1.467	–	49	1.467
Herdian.[2] Graetsch		opal-C opal-C			0.15-0.25 0.09-0.95			
IO 9	colourless	opal-A_G	broad peak			–	–	
IO 10	white	opal-A_G	broad peak			–	–	

N.B.

1. First measurement at 0.5 /min; second measurement at 0.06 /min and internal standard
2. Comparisons are quoted from the works of Herdianita et al. (2000) and Graetsch et al. (1994). Note the higher values of FWHM for opal-'C' compared with opal-C, and also a tendency for higher FWHM values in opal-CT in Indonesian samples.
3. Non-precious opal.

those in brown opals from Ethiopia (Johnson *et al*., 1996) and in a fire opal from Opal Butte, Oregon, USA (Holzhey, 1997). In the Indonesian opal, these tubes start at the interface of the tuff inclusion or of the massive zeolite layer, and protrude into the opal.

Two opals (opal-CT) contain tiny spherulites of chalcedony. They are probably not inclusions incorporated during growth/deposition of the opal but may be re-crystallization products of the opal during its ageing.

Flow texture

Irregularly shaped volumes which are pale brown to off-white, milky-turbid and opaque were found in six opals (white, black and brown opal). These have flow textures similar to those described by Johnson *et al*. (1996) in Ethiopian brown opals, and even have cell-like features as shown in their figure 14. In one opal, the off-white part is distinguished in thin section from the surrounding brown (near-colourless in section) opal by patches of brown discoloration and a slightly lower RI. Interestingly, play-of-colour, pseudo-birefringence and the patchy brown tinge vanished in a few seconds when the thin section was immersed in water, and then reappeared during drying, thus behaving like an inverse hydrophane, in contrast to the surrounding opal which was not affected optically.

Structure of opals

In thin sections, non-precious opals are isotropic under crossed polarizers but pseudo-birefringence is shown by precious opals. Initially, this would suggest that they are non-crystalline opals, but, based on their diffraction patterns, three structurally different types can be distinguished (*Table I*) and examination under the scanning electron microscope indicates that they also have different nanostructures.

X-ray diffraction results

Four precious opals (two water opals, a brown and a black opal) have the opal-CT structure, i.e. an opal with an extensive stacking disorder of cristobalite and tridymite units (see IO 1, 7, 11 and 12 in *Table I*). They are characterized in their diffractogram by a well developed 4.10 Å-peak with a small spread between 4.101 Å and 4.118 Å, combined with the characteristic shoulder at 4.3 Å (caused by extensive stacking disorder due to intercalated structural elements of tridymite and low-cristobalite), and a small peak at 2.50 Å (*Figure 7*). The main peak is rather broad at FWHM (full width at half-maximum height of peak) compared with data for opal-CT (e.g. Graetsch *et al*., 1994; Herdianita *et al*., 2000), which indicates small crystallite sizes in the Indonesian samples. Variations among the opal-CT samples of the intensity of the shoulder on the main peak, and the slight shift of its maximum indicate variable proportions of tridymite domains and therefore various degrees of structural order.

Flörke *et al*. (1991) distinguished between opal-CT_{LS} with a fibrous-parabolic texture under the polarizing microscope ('LS' for the length-slow optical character of the fibres) and opal-CT_M ('M' for a massy, almost isotropic character due to random orientation of the crystallites and their structural disorder). Since the four Indonesian samples do not show any fibrous texture under the polarizing microscope, they belong to the opal-CT_M type.

Opals IO 3, 4, 6 and 8 and non-precious opals IO 13 and 14, have X-ray patterns different from the four discussed above in that there is no 4.3 Å peak as a shoulder to the main peak (*Figure 8*). Though the diffraction pattern resembles opal-C (an opal of disordered low-cristobalite with minor evidence of tridymite stacking and superstructure reflections of low-cristobalite; Graetsch, 1994), the maximum of the main diffraction line is on the tridymite side (between 4.10 and 4.11 Å) rather than on the cristobalite side (4.04 Å), and there are no superstructure reflections of low-cristobalite visible (H. Graetsch, pers. comm.). These differences support the notation opal-'C'. The pattern is similar to the one for high-cristobalite which, however, is not stable below about 270 C. Compared with the opal-CT data, the intensity of the peak at 4.10 Å tends to be smaller and the FWHM is generally broader. The latter feature contrasts especially with data from real opal-C (*Table I*), where the FWHM is much smaller (narrower) because of a better structural order (Graetsch *et al*., 1994). The difference in the FWHM between opal-CT and opal-'C' is even stronger in the 2.50 Å peak and proves a very small crystallite size in the opal-'C' samples. Probably, SiO_4 tetrahedrons are arranged in short range order similar to that of cristobalite, but long range order is not present. Structurally, these opals could be intermediate between amorphous SiO_2 and cristobalite (H. Graetsch, pers. comm.). A slight asymmetry in the main peak of two opal-'C' samples towards the 4.3 Å shoulder hints at the presence of some tridymite domains and a transition to opal-CT.

The remaining two opals (the white opal IO 10 and a slightly turbid water opal IO 9) are X-ray amorphous: the diffractogram shows only a characteristic broad hump (*Figure 9*) between 15 and 30 2θ Cu Kα with a maximum at around 22.5 2θ Cu Kα (equivalent to a d-spacing of about 3.95 Å and therefore slightly different from the main peak of opal-CT) and no additional peaks. These samples are of opal-A type, or more precisely, of opal-AG type (G for gel-like, after the classification by Flörke *et al*., 1991).

7

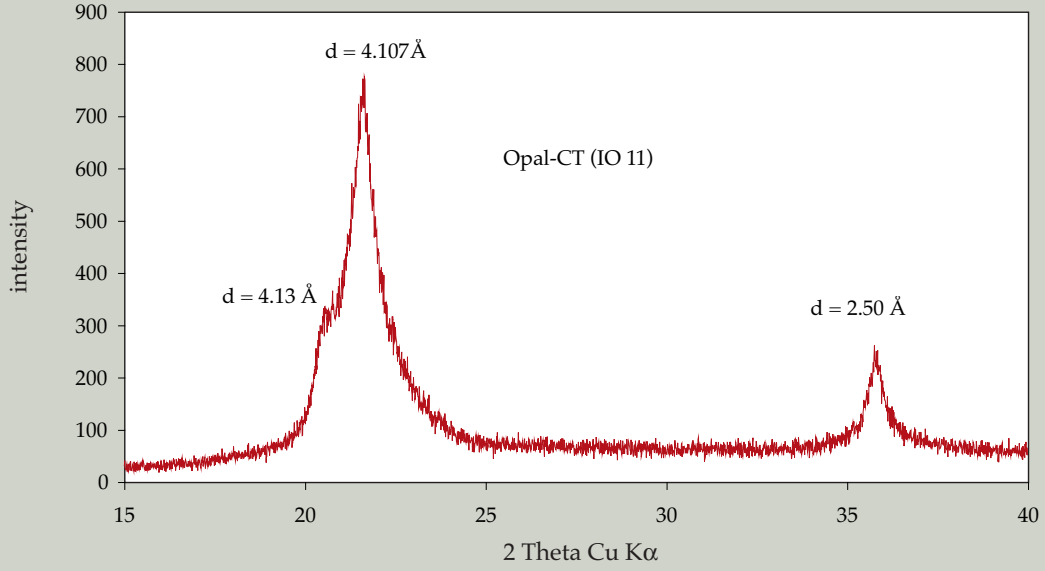

8

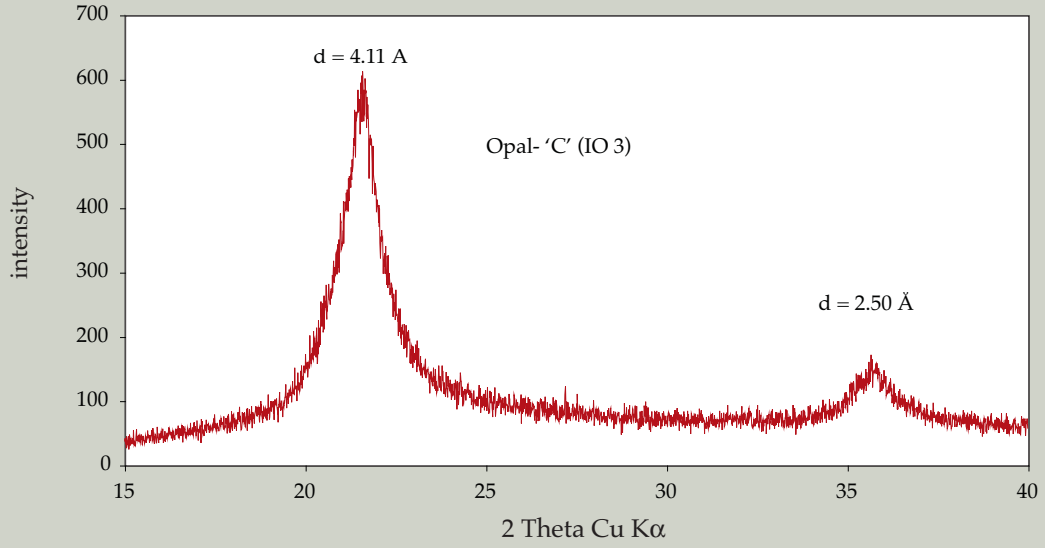

9

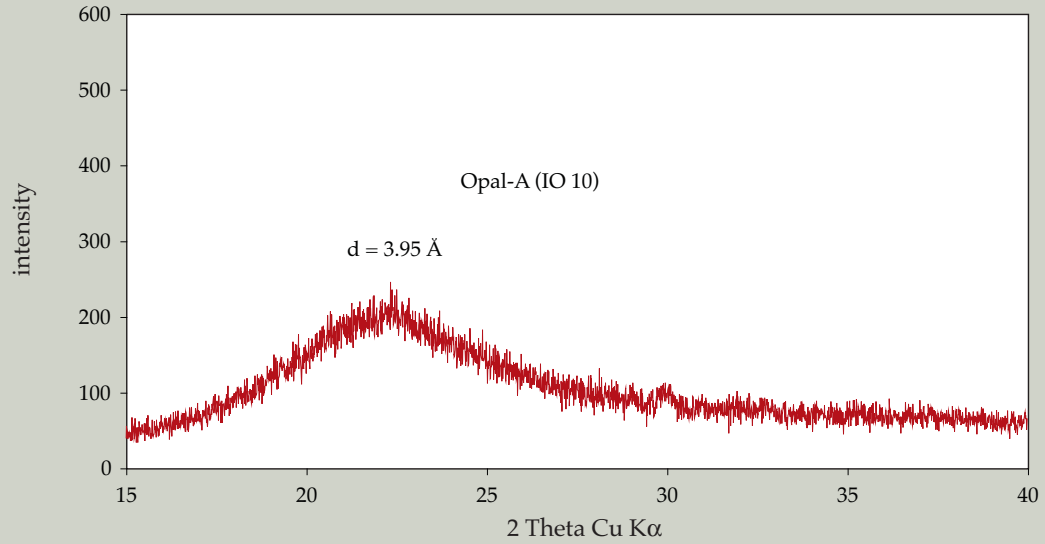

Figure 7: *The diffractogram of this opal-CT (water opal IO 11) displays a 'shoulder' at 4.13 Å next to the main peak (at 4.107 Å) which indicates domains of tridymite. Note the sharpness of the peak at 2.50 Å which results from better structural order than is present in opal-'C' (see* Figure 8*).*

Figure 8: *The diffractogram of opal-'C' (IO 3) shows a lower structural order than that of opal-CT: there is no shoulder at 4.13 Å on the main peak (which means an absence of tridymite domains) and the two reflections are broader than in opal-CT diffractograms.*

Figure 9: *This diffractogram of opal IO 10 shows the single and very broad reflection, characteristic for opal-A, around a d-value of 3.95 Å.*

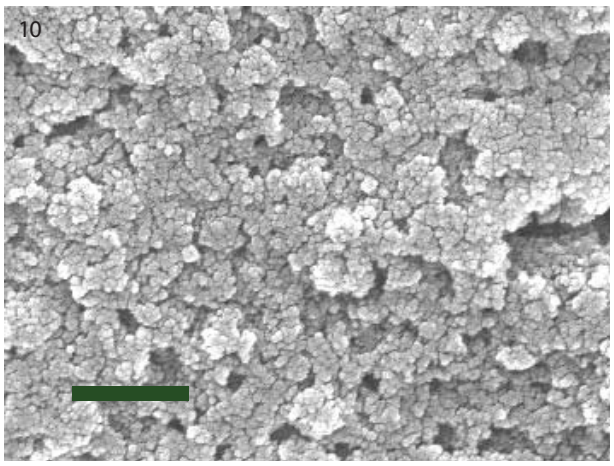

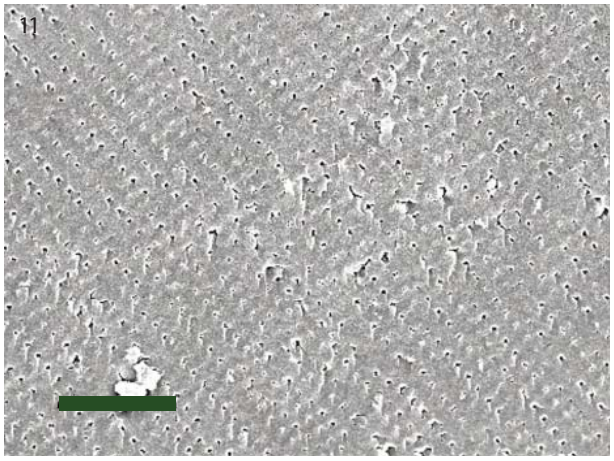

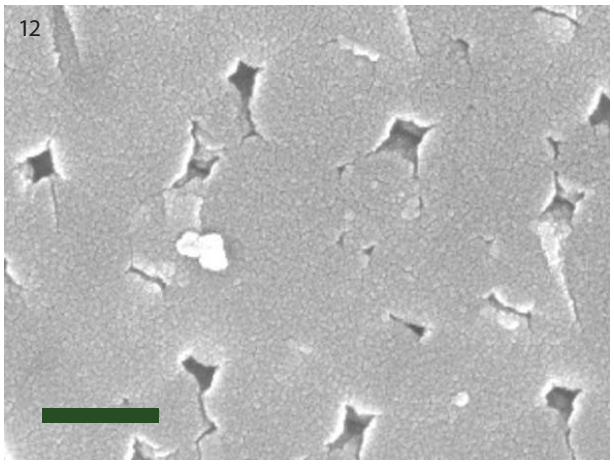

Figure.10: *This SEM image of sample IO 12, an opal-CT, shows the small particles (nanograins) making up the opals made visible by etching with hydrofluoric acid . Length of bar: 0.1 µm or 100 nm.*

Figure 11: *SEM image of opal-A (IO 9) showing the cuspate pore spaces marking the regular arrangement of spheres. Length of bar: 2 µm.*

Figure 12: *An enlarged part of the micrograph (Figure 11) reveals the densely packed spheres. Each sphere is composed of small granules (nanograins) of 30-50 nm in random packing. SEM image, length of bar: 300 nm.*

SEM investigation

Seven opals consisting of precious opal-A, -'C' and -CT and non-precious opal examined in a scanning electron microscope were all found to consist of a dense packing of small sub-rounded granules (nanograins) of 30 to 50 nm diameter (*Figure 10*) which themselves can be composed of a few still smaller particles. This grain-size is similar to that of the 50 nm diameter granules in fire opal from Mexico and the 10 to 40 nm in fire opal from Ethiopia and other localities (Fritsch *et al*., 1999, 2002). Thin platelets which form lepispheres in some opal-CT, for example as described by Flörke *et al*., (1975, 1991) and by Gaillou *et al*. (2006b), have not been found in Indonesian opal, whether or not acid-etched.

Whereas the granules in opal-'C', opal-CT and the non-precious opal do not show a systematic pattern, they appear fairly regularly arranged in the two opal-A samples into spherical aggregates. The white opal (IO 10) displays a weakly visible linear arrangement of spheres with a diameter of around 400 nm and very little pore space, and the water opal (IO 9) exhibits a well-developed array of small cusp-shaped, slightly distorted voids between densely packed and slightly deformed spheres of 320 to 410 nm diameter (*Figure 11*), with a frequency maximum at 360 to 380 nm. The large sizes and the variation in diameters may be due to the overgrowth of initially perfect spherical aggregates by additional nanograin deposition, indistinguishable from the nanograins in the spheres, into the voids between the spheres, but the pattern may be explained alternatively by strong compaction of large spheres. The remaining pore space is estimated from SEM micrographs at << 10 % only. Each sphere is composed of the above mentioned small granules without a visible regular internal arrangement (*Figure 12*), and their size is distinctly larger than in Australian precious opals where it is about 140 to 250 nm (Fritsch *et al*., 2002).

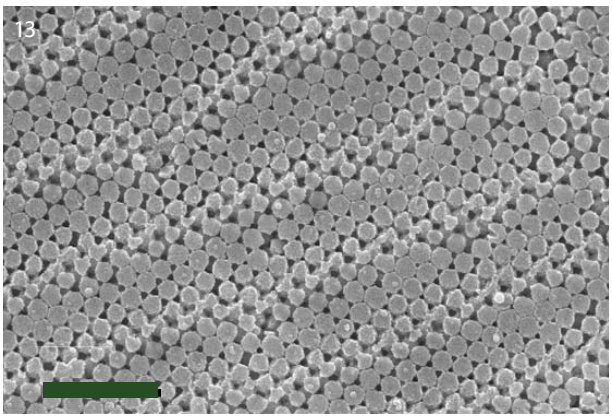

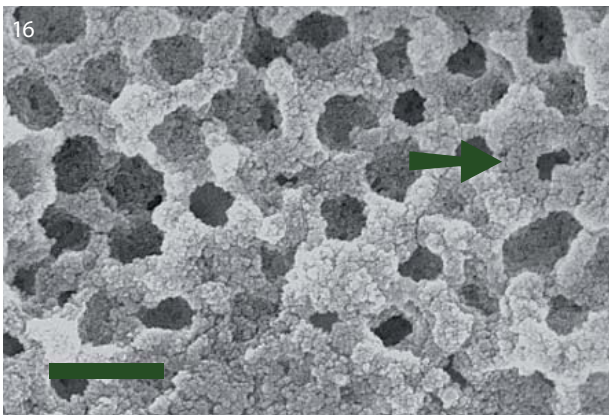

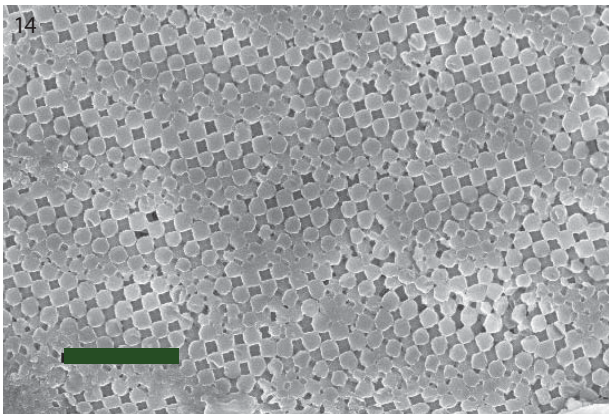

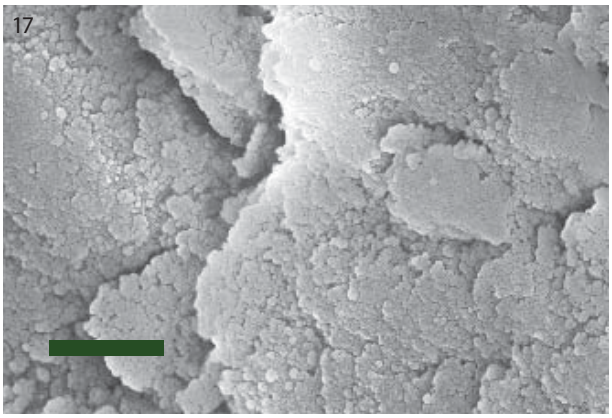

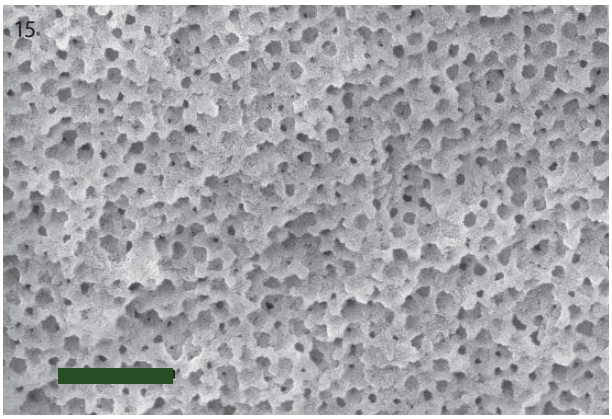

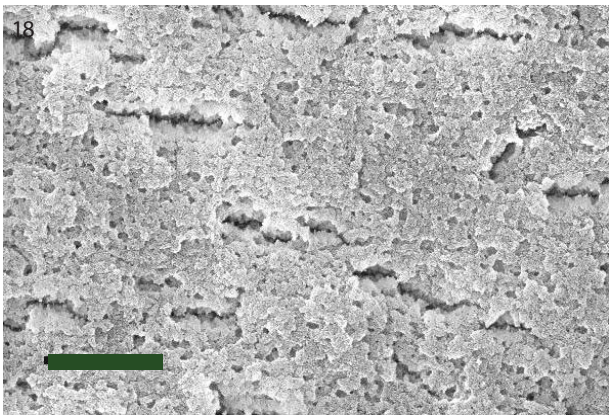

Figure 13: After etching with hydrofluoric acid, the regular internal structure of the opal-A sample (IO 9) becomes clearly visible as hexagonal close packed spheres (with a diameter of about 290 nm). Zones of square packed spheres mark subtle off-sets in the linear arrangement (stacking faults). The surface of the sample cuts obliquely through successive layers of spheres at a low angle, causing a periodic change in the size of the cross-sections of spheres on rows in a NW-SE direction. SEM micrograph, length of bar: 2 µm.

Figure 14: The regular arrangement of the spheres appears in some areas in square packing instead of the more common hexagonal close packing. Opal-A (IO 9), HF-etched. SEM micrograph, length of bar: 2 µm.

Figure 15: After HF-etching, opal-'C' (IO 3) shows a framework composed of small particles around sub-spherical holes. The holes represent former spheres and their systematic arrangement in rows is still visible despite a three-dimensional etching which exposes deeper (offset) layers. SEM micrograph, length of bar: 2 µm.

Figure 16: At higher magnification than in Figure 15, the nanograins of the framework cement are visible. These are usually without regular arrangement, but may show rarely a two-layer concentric shell around the dissolved sphere (right side of photo). Length of bar: 0.5 µm.

Figure 17: Planar, layer-like features in this HF-etched opal-CT (IO 1) are interpreted as stress-induced glide planes. SEM micrograph, length of bar: 2 µm.

Figure 18: This opal-CT (IO 12) is strongly cemented, original spheres are obscured and only indicated by unsystematically exposed, irregularly shaped holes. HF-etched specimen, SEM micrograph, length of bar: 2 µm.

Microstructures become much more visible after treatment of the opal surface with 10% hydrofluoric acid for 30 seconds (Fritsch *et al*. 2002). After etching, the water opal-A (IO 9) displayed a very regular arrangement of spheres, dominantly hexagonal close-packed (*Figure 13*) with patches of more open pattern with spheres occupying the corners of quadrangles (square-packed) shown in *Figure 14*. The etching was rather strong since the diameter of the spheres was reduced to about 290 nm at which point they were just in contact with surrounding spheres. Scanning over the sample revealed some areas of more or less equal-sized spheres showing no pattern of regular packing, and these coincide with the patches devoid of play-of-colour.

In contrast to the opal-A sample, the two investigated opal-'C' samples (a black precious (IO 3) and the brown non-precious opal (IO 13)) reacted to the HF treatment with dissolution of the cores (about 270 to 320 nm in diameter after dissolution) rather than the rims (*Figure 15*), leaving an acid-attacked framework of silica cement which is composed of randomly packed (rarely concentrically arranged) small granules or nanograins (*Figure 16*). In the non-precious opal, the etching behaviour was similar and the spherical holes also had fairly equal dimensions, but except over very short distances, were not systematically arranged. Fritsch *et al*. (2002) attribute the difference in solubility to probably better crystallized silica particles of the cement.

Of the two opal-CT samples, the dark brown opal IO 1 displayed a layered structure of flakes consisting of tiny granules in a dense, unsystematic arrangement (*Figure 17*). A weakly regular pattern of small holes in the massive cement is visible in the second opal-CT (water opal, IO 12) though not easily discernible due to variable intensity of etching (*Figure 18*).

The interesting questions concerning coagulation of the nanograins and why 'spheres' of certain sizes are formed can probably only be explained in terms of the physico-chemical processes operating in silica sols and gels, and are beyond the scope of this paper.

Chemical composition

Most opals are nearly pure SiO_2 with the total of other element concentrations (mainly Al, K, Na, Ca, Fe and not including H_2O) reaching approximately 1 to 2 weight % only. The total of these element oxides in five analysed Indonesian samples (*Table II*) ranges between 1.4 % and 3.7 % with a large variability in concentration ratios. In general, the element concentrations decrease in the order Al, Ca, Na, K, (Ti, Fe, Mg, Mn). The grey opal IO 8 has an unusually high Ti content (4900 ppm or 0.82 % TiO_2) and relatively high Ca, Mg and Fe which might reflect derivation from a tuffaceous host rock. Of the analysed trace elements, Rb, Sr, Zr and Ba may be dominant in different stones to the extent of several 10s of ppm. Other trace elements with concentrations above 1 ppm are Cr and Cs in all five opals, and V, Co, Ni and Nb in three of them.

Discussion and conclusions

One can draw several conclusions concerning genetic aspects and characteristics of the Indonesian opals from this short study.

The restricted occurrence of the opals as isolated nodules in a layer of clay-rich tuff, which extends laterally for several square km (Sujatmiko *et al*., 2004), points strongly to a direct genetic link to the host rock through an alteration process which decomposed the tuff particles. This is supported by the presence of zeolites (alkali-clinoptilolite, probably also mordenite) as inclusions in the opal or adhering to its surface. Both minerals have formed therefore under the same conditions. In the absence of metamorphic minerals from burial metamorphism or of external heat sources, the appropriate model for zeolite formation from a silicic tuff is an open system under fresh water conditions (Hay and Sheppard, 1981). Percolating ground water reacts with the glassy tuff particles to form montmorillonite (and opal, if a strong oversaturation in silica is already attained in this zone). In a somewhat deeper zone or

Table II: *Chemical compositions of five opals with different body colours from Indonesia.*

ppm	IO 1 dark brown	IO 3 black	IO 8 grey	IO 12 colourless	IO 13 brown
Si	440608	435233	430278	420929	420929
Al	5930 5660-6320	5936 5661-6219	9497 8846-10020	5445 5291-5639	4277 4248-4316
Ti	792 783-799	1029 1006-1053	4934 4543-5603	3.7 3.45-4.0	78 77.4-80.3
Fe	73 71.8-73.1	100 96.2-101.4	362 334.8-402.5	6.6 6.0-6.9	25 23.7-24.7
Mn	48 47.4-48.3	52 51.6-52.2	38 37.9-38.5	11 11.2-11.3	23 22.8-23.5
Mg	49 46.7-41.0	35 28.5-39.8	439 419.5-551.0	27 25.6-26.6	23 23.2-23.3
Ca	2640 2585-2767	2557 2520-2623	5952 5573-6361	1853 1844-1861	1489 1488-1490
Na	1273 1235-1299	2200 2122-2296	766 704-814	1782 1669-1888	2362 2317-2422
K	1184 1108-1276	599 552-658	939 895-996	1555 1480-1629	397 396-399
Total 1	96.2%	95.4%	95.8%	91.8%	91.5%
Total 2	1.9%	2.3%	3.7%	1.7%	1.4%
B	0.298-0.49	0.3-0.44	31.48-32.71	0.255-0.31	0.185-0.22
V	1.246-1.286	2.576-3.01	5.58-6.76	0.0043-0.01	0.23-0.251
Cr	2.083-2.4	2.78-4.01	3.71-4.77	1.2-1.558	1.22-1.19
Co	2.97-3.22	8.09-9.01	4.31-4.62	0.0155-0.0246	0.26-0.31
Ni	1.87-2.25	1.7-1.82	3.57-5.01	0.44-0.88	0.33-0.38
Rb	17.92-20.58	8.55-9.69	19.87-21.68	27.29-29.5	6.69-6.85
Sr	6.55-7.41	9.59-10.4	22.54-23.34	4.05-4.38	3.94-3.98
Y	30-30.32	30.54-32	31.55-34.53	0.0419-0.0456	7.98-8.67
Zr	11.26-11.67	25.92-28.94	51.06-55.52	2.55-2.82	8.14-8.72
Nb	1.763-1.852	2.04-2.144	9.8-10.77	0.0048-0.0059	0.154-0.163
Cs	2.18-3.03	1.87-2.009	3.65-4.15	5.52-5.86	1.632-1.701
Ba	14.57-15.09	58.11-60.65	40.54-43.11	8.51-9.19	12.73-13.48

N.B. Values obtained using LA-ICPMS; main elements are means of three sample points and minimum and maximum values are also given; ranges only are given for trace elements. Total 1 is the value for all oxides except water and Total 2 is the total of oxides minus silica and water.

under prolonged reaction between water and glassy tuff particles, its ionic strength and pH value increase with increasing amounts of dissolved Na^+, K^+, Ca^{2+} and $H_2SiO_4^{2-}$, from which zeolites (and opal) can precipitate with or without an intermediate gel stage, to form an assemblage of montmorillonite, opal and zeolite. Clinoptilolite and mordenite are the first zeolites to occur in such a system. The clinoptilolite in the Indonesian opal indicates a maximum temperature of opal formation of < 55 C (the upper stability of alkali-clinoptilolite; Hay, 1981) or, if the zeolite is Ca-rich, somewhat higher (up to about 90 C in case of a Ca-clinoptilolite).

Because of its wide range of element

concentrations and the lack of constant element ratios, the chemical composition of the five analysed opals does not seem to reflect directly the composition of the volcanic host rock from which they are derived. Variable degrees of tuff decomposition, locally and in time, with variable release of element concentrations into the groundwater can be expected during the process of silica precipitation as well as an effect of locally different composition of the tuff layer. The low Ba content (below 110 ppm) may be a direct indication of a volcanogenic as opposed to a sediment-hosted origin (Gaillou *et al*., 2006a), whereas the main element composition is well within the range of sediment-hosted opals, such as those from various Australian opal fields (Brown *et al*., 2004). Though the data base is still rather small, Indonesian opals show no signs of having a particularly distinctive composition.

The colour spectrum in a precious opal is a function of its refractive indices, the angle of incidence of light and, critically, the size of its silica spheres: the larger the diameter, the longer the wavelength of the diffracted light (e.g. Rossman, 1994; Sanders, 1968). The comparatively large size of the spheres in the Indonesian samples explains the dominance of red to green colours in these opals. According to calculations and a diagram by Wollaert *et al*. (1990), a minimum sphere diameter of about 260 nm is necessary to display red colours at a minimum angle of incident light (in addition to colours of shorter wavelength at larger angles), which is well satisfied by these samples. The main condition for the formation of larger spheres may be a comparatively low density of nucleation points in the silica sol which allows for larger masses of silica particles to agglomerate on each site compared with opals of dominantly blue play-of-colour.

For opal without play-of-colour, Rossman (1994) lists heterometric spheres, their random packing, their non spherical shape and complete filling of voids by silica cement as reasons for the absence of play-of-colour. In the one SEM-investigated non-precious Indonesian opal, the poorly ordered packing of equal-sized spheres is responsible for the absence of play-of-colour. Concerning the role of voids, their presence is not essential in producing play-of-colour (see Fritsch *et al*., 1999, 2002) and this is confirmed by the precious opal-CT and opal-'C' samples, which have no visible open voids in SEM micrographs. Rather, diffraction is caused by differences in refractive index between (hidden or visible) spheres and the silica between the spheres.

The body colour of precious and common opals has been a point of debate. Although many have thought that the iron and manganese contents can explain the colour of fire opals and of brown opals, Fritsch *et al*. (1999, 2002) have pointed strongly to mineral inclusions rather than elements in an ionic state and list examples of mineral inclusions as colouring agents in opal from various occurrences. They relate the colour of brown opals to nano-sized Fe-components (supposedly Fe-oxides or Fe oxy-hydroxides of 10-20 to 100-200 nm size) which they found in TEM images and by Raman spectroscopy, and the black zones in opals to traces of manganese. Similarly, Johnson *et al*. (1996) have reported iron pigmentation and tiny minerals (supposedly pyrite and iron oxide) in flow textured brown opals from Ethiopia. Gaillou *et al*. (2006 a) found higher Fe-contents correlated with increasing intensity of colour from yellow to brown (between 3000 and 13000 ppm in very dark brown opals; Gaillou, pers. comm.). However, Fe and Mn contents in the analysed Indonesian samples are very low (up to 362 and 53 ppm, respectively) and are therefore not expected to have a dominant effect on the body colour. Brown *et al*. (2004) found no systematic differences in Fe or Mn which could be related to dark and light coloured zones of banded Australian opal but there were significantly higher contents of other trace elements in the darker coloured bands. It is interesting in this respect, that the water-white precious opal IO 12 has lower concentrations of the transition elements Fe, Ti, V, Ni and Co by one to four orders of magnitude compared with the opals with brown to black body colour whereas the concentrations of the main elements Al, Na, K, Ca and Mg is well within the range shown by the other opals.

For black (non-precious) opal in silicic volcaniclastic sediments from Honduras, Banerjee and Wenzel (1999) relate the body colour to organic carbon compounds (probably porphyrins) which they confirmed using FTIR and UV-Vis measurements. This is a speculative but possible explanation for the black body colour in Indonesian opals: the origin of carbon could be either organic matter from the sediment layers in the Genteng Formation above the opal-bearing horizon or from more recent, decomposed plant roots which penetrated the tuff layer.

Opal from Indonesia often develops fractures during polishing or after it has been worn for some time. One cause for this poor stability lies in hidden, latent micro-fractures (*Figure 5*), which have been observed in thin sections of brown and black opal (see also Sujatmiko *et al*., 2004). There are also indications in the fields of play-of-colour, that several opals underwent some stress during their formation as indicated by glide planes, bent colour lamellae (*Figure 3*), crosscutting microfractures through several colour fields with a displacement of fragments against each other in a still coherent opal-CT mass (*Figure 6*), and a sub-parallel arrangement of elongated colour fields (*Figure 4*) in one opal-A cabochon which is interpreted as the result of shearing or squeezing. The deep linear or polygonal etching in HF-treated opal-CT, visible in SEM micrographs, may be also the result of mechanical weakness along micro fractures or stress-induced glide planes which allow for a more rapid and deeper acid attack.

Because there is no indication of tectonic impact on the host rock, a possible alternative cause of stress could have been increasing load of the overlying sediments brought about by the decomposition of tuff particles which weakens the internal stability of the tuff layer and results in its compaction and the deformation or collapse of cavities. Hence, opal in these voids will be deformed to various degrees, depending on the strength of the acting force and the rigidity of the opal. It seems possible that the observed flow texture also developed during this process: the layers of lighter and darker coloured bands which may have formed initially through undisturbed sedimentation of a coagulating silica sol (as proposed by Brown *et al*., 2004), could have been disturbed by internal flow as a reaction to compressive forces.

The conversion of initially amorphous opal matter (opal-A) to opal-CT/opal-C and finally to quartz has been known from early investigations of diagenetic processes in silica (e.g. Jones and Segnit, 1971; Kano, 1983), and has been more recently described as an ageing process of silica in sinters from hydrothermal fields in New Zealand (Herdianita *et al*., 2000). This process involves time since deposition, temperature changes, the chemical environment and the presence of other minerals as factors in these structural changes. In the Indonesian opal occurrence, opal-A, a structurally intermediate opal-'C', opal-CT and microcrystalline quartz/chalcedony are present in the same horizon. Therefore a multi-stage or a continuous process of opal formation over a prolonged period seems likely. More than one stage of opal formation is also indicated by the rim of white opal with a sharp contact against a core of 'tea opal' (*Figure 2b*, IO 15). According to this model, ageing has transformed the earliest precipitated opal-A into opal-CT, opal-'C' as a younger precipitate is in a transitional stage of transformation to opal-CT, and opal-A is the most recently formed of the three structural types.

However, Gaillou *et al*. (2006 b) state, that this ageing process is restricted to diatomite and sinter opal during their diagenesis and propose that the structural differences between opal-A and opal-CT are a primary feature from the silica precipitation stage and are due to variable growth rates and silica concentrations in the gel. They postulate that spheres in opal-CT are composed of nanograin aggregates as platelets or lepispheres which are not visible on freshly broken surfaces and are completely dissolved by HF-etching, therefore not directly detectable. This markedly different structure compared with opal-A would probably prohibit a transformation of opal-A to opal-CT unless future research indicates the possibility of a rearrangement of the randomly oriented nanograins of opal-A into the platelets of opal-CT during ageing of gem opal.

Acknowledgements

This paper was prepared during a teaching assignment in 2006/2007 at the Institute for Mineralogy and Geochemistry, University (TH) of Karlsruhe, Germany, and my thanks go to D. Stüben who made the laboratories of her institute available. For laboratory work I thank B. Oetzel for XRD-measurement and K. Nikoloski for thin section preparation, both at the Institute for Mineralogy and Geochemistry, and V. Zibat at the Laboratory for Electron Microscopy at the same University, for the SEM facilities. H. Graetsch from the Institute of Geology, Mineralogy and Geophysics at the Ruhr-University Bochum helped with control XRD-measurements for the problematic opal-'C' samples and the interpretation of data. T. Häger from the Institute of Geosciences/ Gemmological Section of the Johannes Gutenberg-University, Mainz, provided the Laser Ablation ICP-MS measurements on selected opals. I would like to thank especially my colleague Ir. H. Sujatmiko, Bandung/Indonesia, for providing the samples for this study.

References

Banerjee, A., and Wenzel, Th., 1999. Black opal from Honduras. *Eur. J. Mineral.*, 11, 401-8

Brown, L.D., Ray, A.S., and Thomas, P.S., 2004. Elemental analysis of Australian banded opals by laser-ablation ICP-MS. *N. Jb. Min. Monatsh.*, 2004, H 9, 411-24

Flörke, O.W., Graetsch, H., Martin, B., Röller, K., and Wirth, R., 1991. Nomenclature of micro- and non-crystalline silica minerals, based on structure and microstructure. *N. Jb. Miner.* Abh. 163,19-42

Flörke, O.W., Jones, J.B., and Segnit, E.R., 1975. Opal-CT crystals. *N. Jahrb. Mineral. Monatsh.*, H 8, 369-77

Fritsch, E., Ostrooumov, M., Rondeau, B., Barreau, A., Albertini, D., Marie, A.-M., Lasnier, B., and Wery, J., 2002. Mexican gem opals: nano and micro-structure, origin of colour, comparison with other common opals of gemmological significance. *Australian Gemm.*, 21, 230-3

Fritsch, E., Rondeau, B., Ostrooumov, M., Lasnier, B., Marie, A.-M., Barreau, A., Wery, J., Connoué, J., and Lefrant, S., 1999. Découvertes récentes sur l'opale. *Revue de Gemmologie*, 138/139, 34-40

Gaillou, E., 2006. *Relation entre nanostructure, propriétés physiques et mode de formation des opals A et CT.* Thèse de Doctorat, Université de Nantes, Faculté de Sciences et des Techniques, 312 p. http://www.gemnantes.fr/recherche/opale/index.html

Gaillou, E., Delauny, A., Fritsch, E., and Bouhnik-le-Coz, M., 2006a. Geologic origin of opals deduced from Geochemistry. *Gems & Gemology*, 42(3), (abstr. Gemological Research Conference 2006), 107

Gaillou, E., Fritsch, E., Aguilar-Reyes, B., Rondeau, B., Barreau, A., and Ostroumov, M., 2006b. Common gem opal : an investigation of micro- to nano-structure. Submitted to *American Mineralogist*. In: Gaillou, E., 2006. *Relation entre nanostructure, propriétés physiques et mode de formation des opals A et CT.* Thèse de Doctorat, Université de Nantes, Faculté de Sciences et des Techniques, 126–71. http://www.gemnantes.fr/recherche/opale/index.html

Graetsch, H., 1994. *Structural characteristics of opaline and microcrystalline silica minerals*. In: Heaney, P.J., Prewitt, C.T., and Gibbs, G.V. (Eds). *Silica: physical behaviour, geochemistry and materials application*. Washington D.C. Min. Soc. America, *Reviews in Mineralogy*, 29, 209-32

Graetsch, H., Gies, H., and Topalovi , I., 1994. NMR, XRD and IR study on microcrystalline opals. *Phys Chem Minerals*, 21, 166-75

Graetsch, H. Flörke, O.W., and Miehe, G., 1987. Structural defects in microcrystalline silica. *Phys. Chem. Minerals*, 14, 249-57

Hay, R.L., 1981. *Geology of zeolites in sedimentary rocks*. In: Mumpton, F.A. (Ed.), *Mineralogy and geology of natural zeolites.* Washington D.C. Min. Soc. America, *Reviews in Mineralogy*, 4, 53-64

Hay, R.L., and Sheppard, R.A. 1981. *Zeolites in open hydrological systems*. In: Mumpton, F.A. (ed.): Mineralogy and geology of natural zeolites. Washington D.C. Min. Soc. America, *Reviews in Mineralogy*, 4, 93-102

Heaney, P., 1994. *Structures and chemistry of low-pressure silica polymorphs*. - In: Heaney, P.J., Prewitt, C.T., and Gibbs, G.V. (Eds). *Silica: physical behaviour, geochemistry and materials application*. Washington D.C. Min. Soc. America, *Reviews in Mineralogy*, 29, 1-40

Herdianita, N.R., Browne, P.R.L., Rodgers, K.A., and Campbell, K.A., 2000. Mineralogical and textural changes accompanying ageing of silica sinter. *Mineralium Deposita*, 35, 48-62

Holzhey, G., 1997. Feueropal von Opal Butte, Oregon, USA. *Z. Dt. Gemmol. Ges.*, 46 (3), 161-8

Johnson, M.L., Kammerling, R.C., DeGhionno, D.G., and Koivula, J.I., 1996. Opal from Shewa province, Ethiopia. *Gems & Gemology*, 32(2), 112-20

Jones, J.B., and Segnit, E.R., 1971. The nature of opal. I. Nomenclature and constituent phases. *J. Geol. Soc. Australia*, 18, 57-68

Kano, K., 1983. Ordering of opal-CT in diagenesis. *Geochem. Journal*, 17, 87-93

Kinnaird, J.A., 2002. A note on chocolate brown opal associated with volcanic rocks in Somaliland. *Journal of Gemmology*, 28(2), 81-4

Kinnaird, J.A., and Jackson, B., 2000. Somaliland - a potential gem producer in the Mozambique Belt. *Journal of Gemmology*, 27(3), 139-54

Koivula, J.I., and Tannous, M., 2001. Gem news

international: new production of Indonesian opal. *Gems & Gemology*, 37(1), 70-1
Lambert, C., and Brown, G., 1994. A brief report on Indonesian opal. *The Australian Gemmologist*, 18, 359-61
Milisenda, C.C., and Wild, M., 2004. Hydrophanopal aus Indonesien. *Z. Dt. Gemmol. Ges*., 53 (4) 169-72
Rossman, G.R., 1994. *Colored varieties of the silica minerals*. - In: Heaney, P.J., Prewitt, C.T., and Gibbs, G.V. (Eds). *Silica: physical behaviour, geochemistry and materials application*. Washington D.C. Min. Soc. America, *Reviews in. Mineralogy*, 29, 433-65
Sanders, J.V., 1968. Diffraction of light by opals. *Acta Cryst*., A 24, 427-34
Sujatmiko, H., Einfalt, H.C., and Henn, U., 2004. Opal aus Java. *Z. Dt. Gemmol. Ges*., 53, 2/3, 105-12. English version: *The Australian Gemmologist*, 22(6), 254-59, 2005
Webster, R., 1994. *Gems - their sources, descriptions and identification. 5th edn*. Ed. P.G. Read. Butterworth-Heinemann, Oxford
Wollaert, E., Vochten, R., and Van Landuyt, J., 1990. Characterisation of gem opal and inferior opal qualities by means of electronmicroscopy. *Z. Dt. Gemmol*. Ges., 39, 4, 211-23

Vaterite in freshwater cultured pearls from China and Japan

U. Wehrmeister[1], D. E. Jacob[2]*, A. L. Soldati[2], T. Häger[1] and W. Hofmeister[1]

1. Centre of Gemstone Research, Johannes Gutenberg-Universität Mainz, D-55099 Mainz, FRG

*2. Department of Geosciences, Johannes Gutenberg-Universität, D-55099 Mainz, FRG, *Corresponding author, email: jacobd@uni-mainz.de*

Abstract: *Japanese and Chinese beaded and non-beaded cultured freshwater pearls of good quality were investigated with Raman spectroscopy and LA-ICP-MS. In 50% of the investigated non-beaded samples vaterite was identified by Raman spectrometry in polished cross-sections near the centre of the pearl as well as in small blemishes on the pearl surfaces. Continuous growth structures transect both vaterite and aragonite areas. Sodium and strontium concentrations are significantly lower in vaterite areas whereas the Mg concentration is up to two orders of magnitude higher and ratios of these elements allow distinction of the two phases using LA-ICP-MS. With the findings that vaterite is relatively common in the centres of high-quality freshwater cultured pearls and is the reason for lack of orient on some pearl surfaces, it is necessary to fully understand how it forms in order to optimize the quality of such pearls.*

Keywords: *aragonite, freshwater cultured pearls,* Hyriopsis, *LA-ICP-MS, Raman spectroscopy, trace elements, vaterite*

Introduction

Shells and pearls of molluscs are products of biomineralization, i.e. crystals formed by living organisms. The epithelial cells of the mollusc's mantle are responsible for the formation both of the shell (e.g. Addadi *et al*., 2006) and of pearls. They are composite materials composed of calcium carbonate crystals embedded in an organic matrix in a structure that is often referred to as a 'bricks and mortar' structure (e.g. Huang *et al*., 2004; Watabe, 1965; Snow *et al*., 2004). The organic matrix provides the framework in which the crystals form (e.g. Addadi *et al*., 2006) and contains macromolecules that have been found to play a key function in controlling the crystal growth process and the polymorph switch from calcite to aragonite during shell growth (Belcher *et al*., 1996; Sudo *et al*., 1997; Levi *et al*., 1998; Thompson *et al*., 2000; Feng *et al*., 2000; Addadi *et al*., 2006). In addition to the calcium carbonate polymorphs aragonite, calcite and vaterite, molluscs are able to produce amorphous calcium carbonate (ACC) which is believed to represent a precursor-product in the process of crystalline $CaCO_3$ formation in some organisms (Addadi *et al*., 2003, 2006; Beniash *et al*., 1999). The nacre of

 ISSN: 1355-4565

mollusc shells and pearls has been subject to numerous investigations to understand both its unique structural properties and the principles underlying the biomineralization processes (e.g. Watabe, 1965; Feng *et al*., 1999; Hou and Feng, 2003; Snow *et al*., 2004; Addadi *et al*., 2006). The mollusc's shell and pearls are both produced by epithelial tissue, and this is why it is used in pearl culturing (see next section). The continuous growth of a pearl can be clearly observed under the microscope by concentric rings of alternating fine dark organic material and thicker rings of calcium carbonate (e.g. Strack, 2001), as well as by rings of different colour intensity. Pearls are produced by a number of mollusc species in nature. The inner part of a marine pearl commonly consists of prismatic crystals of calcite and the outer layer of nacre is made up of aragonite platelets (e.g. Watabe, 1965), which are flat polygonal crystals with their *c*-axes perpendicular to the layer plane (e.g. Watabe, 1965; Song *et al*., 2003; Snow *et al*., 2004). Freshwater cultured pearls, however, have been shown to consist mostly of aragonite, with calcite only rarely reported. Instead, vaterite, a metastable $CaCO_3$ polymorph, has been found recently in the upper layers and at the surface of lacklustre freshwater cultured pearls (Ma and Dai, 2001; Ma and Lee, 2006; Qiao *et al*., 2006, Qiao and Feng, 2007).

The organisms secreting calcium carbonate control which polymorph is produced (Falini *et al*., 1996; Feng *et al*., 2000) and in some cases a switch from one polymorph to another has been observed (Thompson *et al*., 2000). However, although the aragonite calcite interface in molluscs and pearls has been investigated intensively (Belcher *et al*., 1996; Thompson *et al*., 2000; Dalbeck *et al*., 2006), very little is known about the vaterite - aragonite switch. Here, we present a systematic account of the occurrence of vaterite in good quality pearls from the mollusc genus *Hyriopsis* and show that vaterite is not restricted to lacklustre pearls and, thus, may represent an important factor in influencing the quality of pearls.

Freshwater cultured pearls

In general, freshwater pearls can be cultured with or without bead nuclei. In both cases it is necessary to implant a piece of epithelial tissue either in the gonad (usually with nucleus) or in the mantle tissue of the mussel. This tiny piece of tissue has the key function to stimulate the formation of a pearl sac (Landman *et al*., 2001). The newly formed pocket is lined by epithelial cells and becomes a biologically isolated compartment. Subsequently, the cells secrete the pearl material within this compartment, using a part of the implanted tissue as template. As the implanted cells are also responsible for the colour of the pearl, the section of the donor mussel's mantle epithelium from which the graft is taken is very important.

Chinese freshwater cultured pearls

A large number of rivers, lakes, waterways and natural and artificial ponds are available for pearl culturing in the southern, central and eastern regions of China (approximately 167000 km^2 (Strack, 2001)). Mussels most commonly used to culture freshwater pearls are *Hyriopsis cumingii* (also called the 'Triangle mussel' due to its shape). The tissue for implantation is usually taken from the mantle epithelium of a donor freshwater mussel of the same genus (Akamatsu *et al*., 2001). Earlier techniques used a 2 x 2 mm piece of mantle tissue cut from a two- to three-year-old mussel inserted into the mantle lobe. Nowadays larger pieces of mantle tissue of *c*. one-year-old mussels are used. The tissue of younger mussels is thinner and can be rolled more tightly before insertion (Akamatsu *et al*., 2001) yielding better round shapes of the pearls.

Freshwater cultured pearls in Japan: Lake Biwa and Lake Kasumigaura

Lake Biwa, the largest of Japan's lakes is situated on Honshu Island, 500 km west of Tokyo, close to Kyoto. The lake obtained its name from its form (a Biwa is a four-

stringed lute). Pearl culturing at Lake Biwa started in about 1914 (Landman *et al*., 2001), although the exact freshwater pearl mussel used originally is not known for certain. In the early 1920s, however, *Hyriopsis schlegeli*, MARTENS 1861 was already in use and the changeover from bead nucleation to beadless nucleation happened only ten years later. In Japan the Biwa pearl mussel is called 'Ikecho gai' because its form is similar to a butterfly (Ikecho, jap. butterfly and gai, jap. mussel). As a consequence of continuous environmental problems pearl culturing in Lake Biwa abruptly decreased in the early 1990s. Today, *Hyriopsis schlegeli* is nearly extinct at Lake Biwa. Only in small satellite lakes and ponds has pearl culturing survived. Pearl cultures there use a hybrid mussel species obtained by cross-breeding some of the remaining *Hyriopsis schlegeli* with their Chinese relative *Hyriopsis cumingii* (*Figure 1*). In February 2006 two of the authors (UW and DEJ) visited the pearl farms at Lake Biwa which produce high quality pearls, examples of which are shown in *Figure 2*.

Lake Kasumigaura, located approximately 60 km to the northeast of Tokyo, is Japan's second largest lake. The name 'Kasumigaura' includes the main river Nishiura and also the lakes Kitaura and Sotonasakaura and their connecting water courses. The first freshwater cultured pearls from Lake Kasumigaura were marketed in Europe around the mid-1990s. Already the first harvests yielded almost round pearls up to 20 mm in diameter. This meant that the pearls were comparable with the cultured pearls from the South Seas and Tahiti, both in size and in terms of price. Until the 1990s, not many details about pearl culturing companies in the region were available, but it can be assumed that pearls from harvests in the region were marketed together with pearls from Lake Biwa. Most Kasumigaura pearls contain bead nuclei made from American freshwater nacreous shell. A conspicuous feature of the bead is that it is drilled through to allow optimal handling during implantation into the mussel. Mr K. Yanase, one of the three farmers at Lake

1

2

3

Figure 1: *Pearl mussel from Lake Biwa (pearl culturer: K. Kawabata), a cross-breed of the Japanese Biwa pearl mussel* Hyriopsis schlegeli *with its Chinese relative* Hyriopsis cumingii.

Figure 2: *Freshwater cultured pearls of high quality from Lake Biwa. Mr Kawabata cultivates his pearls in the area of Omnihachiman City at the southern end of Lake Biwa.*

Figure 3: *Freshwater cultured pearls with bead nucleus from Lake Kasumigaura (pearl culturer K. Yanase). Photo: B. Dillenburger*

Kasumigaura who was visited by two of the authors (UW and DEJ) in February 2006, uses nuclei with diameters of 8 mm, 8.5 mm and 9 mm. The pearl farms of Mr K. Yanase are situated behind a dam in the southern region of the lake, in the connecting branches of the rivers and in artificial ponds that are fed with lake water. In each mussel only one pearl is cultured. The range of colour is broad and includes white, apricot, rosé, pink, mauve and violet tones. In a few pearls, their body tone may have an additional green, bronze or golden overtone, generally with a metallic lustre (*Figure 3*).

Material and experimental methods

Chinese freshwater cultured pearls without bead nucleus (*Hyriopsis cumingii*) of a wide colour range were bought from different pearl-dealers in Germany to obtain examples from different locations and which had been harvested at different times. Japanese freshwater cultured pearls of *Hyriopsis schlegeli* crossed with *Hyriopsis cumingii* from Lake Kasumigaura (bead-nucleated samples) and Lake Biwa (bead-nucleated and samples without beads) were obtained directly from the farmers.

Fifty pearl samples were chosen from over 200 and Raman spectra were obtained from their surfaces. Twelve (eleven from China, one from Lake Biwa) of these fifty samples (see *Figure 4*) were cut in half with a diamond-plated saw and polished with diamond paste on a copper plate to study the cross-sections by Raman spectroscopy.

Raman spectroscopy is a non-destructive method that allows clear identification of the different $CaCO_3$ polymorphs. For comparison, Raman spectra of inorganic aragonite, calcite and vaterite from the mineral collection of the Department of Geosciences, Johannes Gutenberg-University, Mainz were obtained (*Figure 5*).

The structures and Raman spectra of aragonite and calcite are well documented (e.g. Gabrielli *et al*., 2000; Anderson, 1996; Behrens *et al*., 1995; Urmos *et al*., 1991; Griffith, 1974; White, 1974). In contrast, the corresponding information for vaterite is still a matter of discussion. In the Raman spectrum of aragonite, three so-called internal modes (ν_1, ν_3 and ν_4) are Raman active and are reported to appear near 1085 cm^{-1} (ν_1) for the most intense band, near 1465 cm^{-1} (ν_3) and a doublet between 701 cm^{-1} and 705 cm^{-1} (ν_4). For

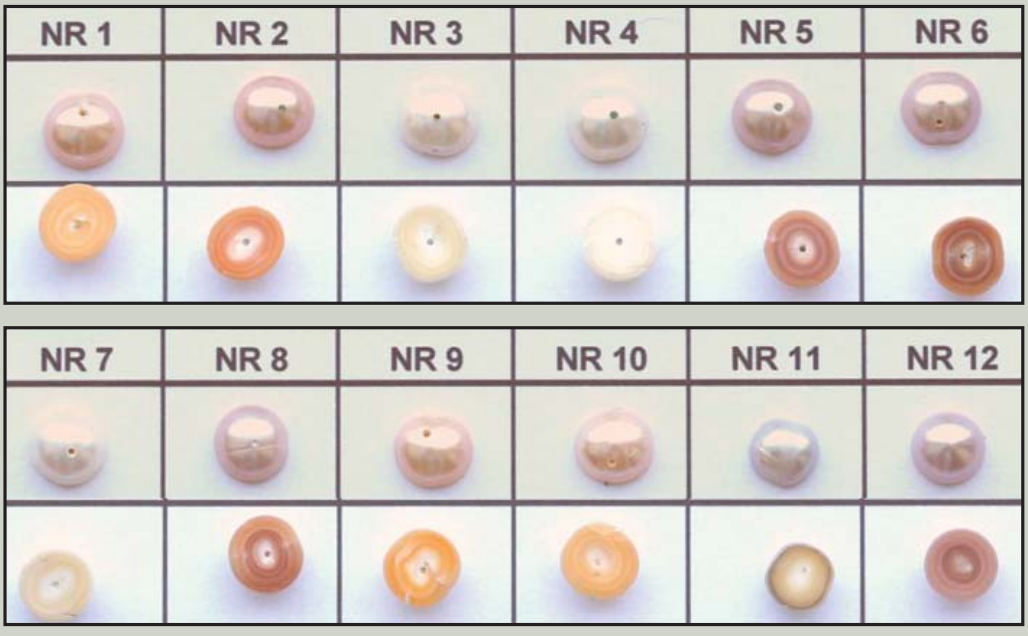

Figure 4: *Cross-sections of the beadless freshwater cultured pearls used in this study. Pearl numbers 1-10 and 12 are from China and number 11 is from Lake Biwa, Japan. All are between 7 and 9 mm in diameter.*

calcite the internal modes are given with 1086 cm^{-1} (ν_1) for the most intense band, near 1434 cm^{-1} (ν_3) and in the region of 711 cm^{-1} (ν_4). The Raman spectrum of vaterite shows a splitting of the most intense ν_1 band between 1074 cm^{-1} and 1090 cm^{-1}, and also a splitting of the ν_3 and ν_4 bands. Peak maxima are summarized in *Table I*.

While Gabrielli *et al*. (2000) observed two bands of the ν_1 vibration of vaterite, Gauldie *et al*. (1997) reported three bands. Behrens *et al*. (1995) attributed this spectral signal to a doublet at 1074 cm^{-1} and 1090 cm^{-1}, also referring to a third peak at 1080 cm^{-1} which was interpreted as a calcite impurity.

All Raman spectra were recorded at room temperature using a Horiba Jobin Yvon LabRAM HR spectrometer equipped with a Si-based CCD-detector (Peltier-cooled), an integrated Olympus BX41 optical microscope and an x-y-stage automatically controlled by software and a joystick. A 50x long-distance objective (numerical aperture 0.55) was selected. The reflected light and the Rayleigh light were reduced using the respective notch filters. The 514.5 nm line of an Ar^+-ion laser and the 632.8 nm He-Ne laser line were used for excitation. A grating with 1800 grooves per mm and a slit width of 100 µm were chosen and the laser power was 10 mW. Data acquisition and spectra treatment were carried out with the commercially available program LabSpec v4.02 (Jobin Yvon Horiba). For single point measurements, spectra were recorded twice. Peak analysis was performed with an Origin-lab® 7.5 professional software package. The peaks were fitted as the composition of either single or overlapping Lorentz curves.

For the mapping technique, a certain area of the cross section of the pearl was defined (for example 8.15 x 8.15 mm in the maps presented in *Figure 8*). Every 40 µm in x and y directions a spectrum was recorded twice for two seconds. Therefore the resulting numbers of spectra were *c*. 200 x 200 = 40000. With the LabSpec software the backgrounds of all 40000 spectra were subtracted and all spectra were decomposed into the respective subspectra with the implemented curve fitting procedure. The resulting intensity of every peak was converted to a colour code. Therefore, every pixel in the Raman-map represents one spectrum and every colour a certain intensity which, in turn, equals a certain amount of the respective phase. With this technique it is very easy to show clearly the distribution of the phases.

Trace elements in different $CaCO_3$ polymorphs were measured using LA ICP-MS (Laser Ablation Inductively Coupled Plasma Mass Spectrometry). This method uses a laser microscope as sampling device connected to an inductively coupled plasma-mass-spectrometer (ICP-MS) and material ablated by the laser from a specimen is swept directly into the mass spectrometer for analysis by a stream of argon or helium gas (Fryer *et al*., 1995). The instrument used in this study consists of a New Wave Research UP213 combined with an Agilent 7500ce quadrupole ICP-MS. The 213 nm wavelength (fifth harmonic wavelength of the Nd:YAG crystal) has the advantage over the older systems using 266 nm (fourth harmonic wavelength) that its absorbance in light-coloured or transparent material (e.g. aragonite, corundum, etc.) is higher, which is favourable for ablation and signal stability. In this way, up to *c*. 30 chemical trace elements (present in concentrations of less than 1 wt. %) can be determined simultaneously with minimal erosion on the specimen surface. Laser craters drilled in this way at our laboratory are typically 0.1 mm and can be further reduced to 0.05 mm (*Figure 10*). One analysis takes around 120 seconds on average, during which time-resolved signals for background (60 sec) and sample-signal (60 sec) are detected. The time-resolved detection of the signal also allows identification of material differences in the specimen (e.g. chemical zonation) which may either be natural or be caused by chemical treatment of pearls. Detection limits are generally significantly below one ppm (0.0001 wt.%). In this study, the laser was pulsed with 0.3 mJ per pulse at a frequency of 10 Hz. Laser spot sizes were 0.1 mm and argon was used as carrier gas. Data reduction was carried out using the commercially available software "Glitter" with ^{43}Ca as the internal and NIST SRM 612 glass as the external standards. All analyses were duplicated. In the case of high-quality samples, Raman investigations were carried out before laser ablation on the same spot.

Table I: *Raman peak maxima in cm^{-1} of the different $CaCO_3$ polymorphs*

$CaCO_3$-polymorph	reference	ν_1 symmetric stretching (CO_3^{2-})	ν_3 asymmetric stretching (CO_3^{2-})	ν_4 in-plane bending (CO_3^{2-})
Calcite	Bischoff *et al*., 1985	1085 (2.5)	1434 (2.0)	711 (3.6)
	Rutt & Nicola, 1974	1085	1435	711
	Urmos *et al*., 1991	1085 (2.5)		711 (4.5)
Aragonite	White, 1974	1087	1464 1466	703
	Urmos *et al*., 1991	1085 (2.1)	1462 (6.0)	701, 705
	Gabrielli *et al*., 2000	1085	1460, 1570	701, 705
	Urmos *et al*., 1991	1085 (2.2)	1462 (6.5)	701, 705
Vaterite	Gabrielli *et al*., 2000	1074 1090	1445, 1485 1550, 1595	668, 682, 740, 750
	Gauldie *et al*., 1997	1074 1081 1090		685, 740, 744, 751
	Behrens *et al*., 1995	1074 1090		740, 750

Results

Identification of $CaCO_3$ polymorphs

To distinguish aragonite and calcite from vaterite, the most intense band ν_1 (symmetric stretching) and the ν_4 (in- plane bending) signals in the Raman spectra of the three carbonate polymorphs can be used (*Table I* and *Figure 5*). In the Raman spectrum of synthetic vaterite (*Figure 5*) and in the vaterite areas of the freshwater cultured pearls a triplet at 1074 cm^{-1}, 1080 cm^{-1} and 1091 cm^{-1} for the ν_1 (CO_3^{2-}) signal is clearly visible. Raman signals in this wavenumber area for three pearl samples are shown in *Figure 6*. If calcite impurities were present, peaks in the ν_3 - and ν_4 - region would also have to be present, but were not found in our samples: this does not support the findings of Gabrielli *et al*. (2000). Our results clearly indicate that the observed Raman band at 1080 cm^{-1} should be attributed to vaterite and not to calcite impurities in vaterite (*Figure 6*, spectrum c). Nevertheless, vaterite areas in the pearls sometimes contain varying amounts of aragonite which was detected as an additional peak at 1085 cm^{-1} within the triplet of the ν_1 of vaterite (*Figure 6*, spectrum a). Depending on the amount of aragonite in the vaterite-aragonite mixture, this signal occurs as a shoulder (*Figure 6*, spectrum b) or as a separate peak (*Figure 6*, spectrum a) between the 1080 and 1091 cm^{-1} peaks of vaterite. The split of the ν_4 Raman band at 701 cm^{-1} and 705 cm^{-1} clearly indicates that this impurity is aragonite (*Table I* and *Figure 5*). In our samples the ν_4 Raman band of vaterite (*Figure 7*) gives rise to five peaks. Gauldie *et al*. (1997), Gabrielli *et al*. (2000) and Behrens *et al*. (1995) all reported fewer peaks for this Raman band (*Table I*), but the four peaks (685 cm^{-1}, 740 cm^{-1} , 744 cm^{-1} , and 751 cm^{-1}) observed by Gauldie *et al*. (1997), identified in fish earstones of the coho salmon, so-called otoliths, are in good agreement with four of our observed peaks (685 cm^{-1}, 739 cm^{-1}, 744 cm^{-1} , and 752 cm^{-1}). Gabrielli *et al*. (2000) also reported a peak with low intensity at 669 cm^{-1} but these authors did not detect the peak at 744 cm^{-1}, so, to the best of our knowledge, this is the first report to specify all five peaks for the ν_4 Raman band of vaterite.

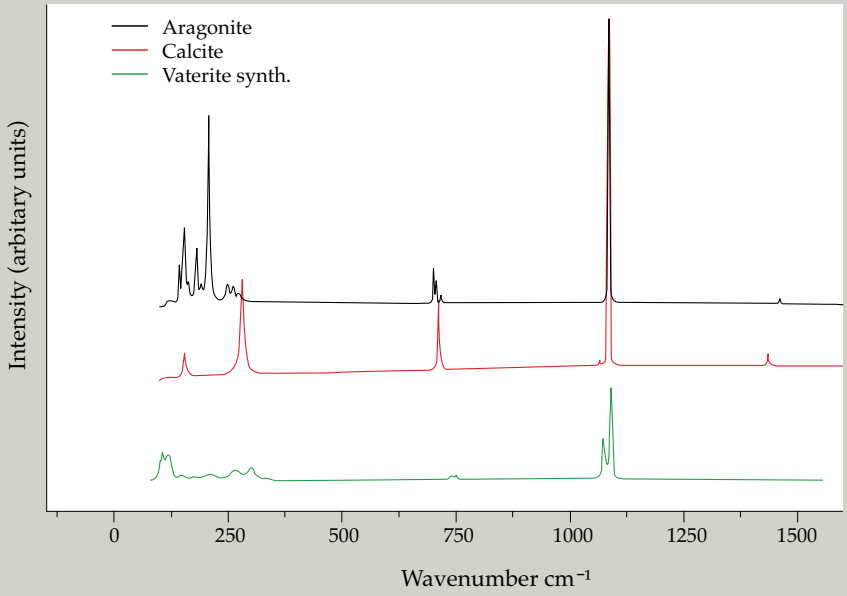

Figure 5: *Raman spectra of aragonite (black), calcite (red) and synthetic vaterite (green). Spectra were obtained from minerals in the collection of the Department of Geosciences, Johannes Gutenberg-University, Mainz. The spectra are vertically displaced for clarity.*

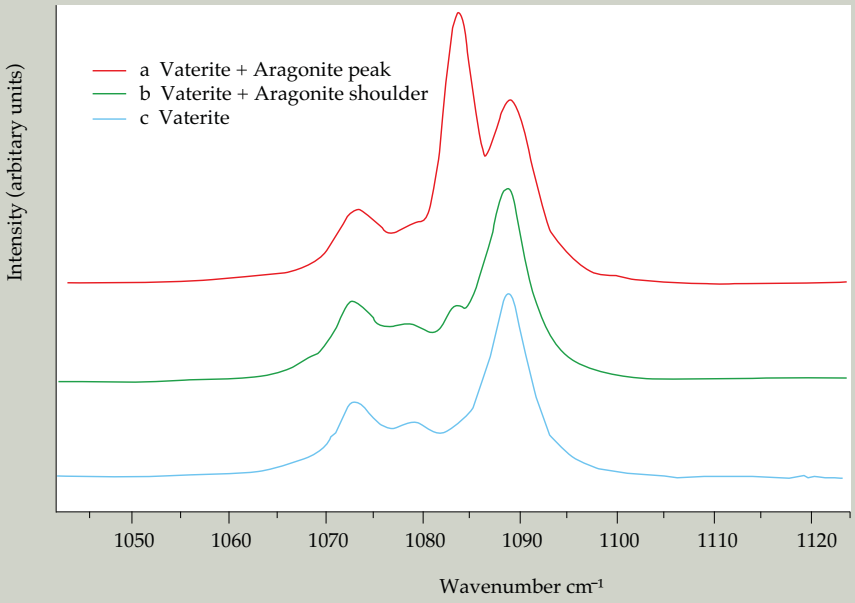

Figure 6: *Raman spectra of the pearl samples 4 (spectrum a), 11 (spectrum b) and 12 (spectrum c) show the triplet at 1074, 1080 and 1091 cm^{-1} of the ν_1 (CO_3^{2-}) Raman signal of vaterite clearly. A peak at 1085 cm^{-1} in spectrum a and a shoulder at this position in spectrum b indicate the presence of aragonite.*

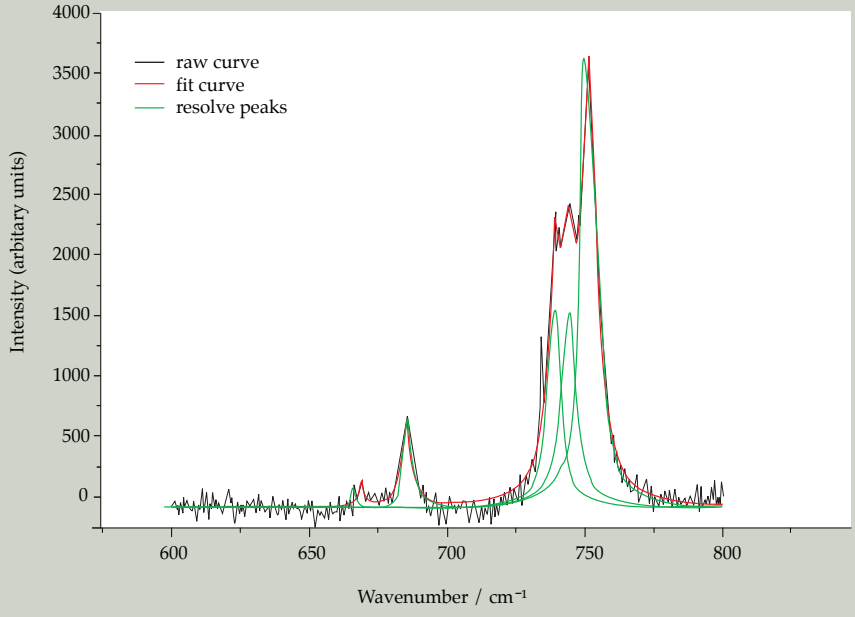

Figure 7: *Raman spectrum showing ν_4 (CO_3^{2-}) for the vaterite area in sample 12. The compound spectrum has been clearly resolved into five peaks at 669 cm^{-1}, 685 cm^{-1}, 739 cm^{-1}, 744 cm^{-1} and 752 cm^{-1} indicated by the green traces (see also* Table I*).*

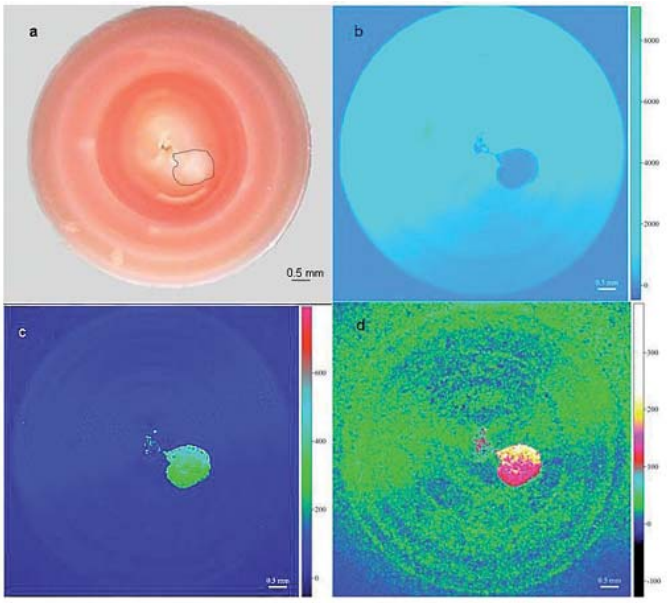

Figure 8: (a) *During cultivation, growth rings of different colours were formed in this Chinese freshwater cultured pearl (sample 12); the near-white vaterite area is outlined with a dotted line. Raman maps of this cross section are shown (*b, c *and* d*). The Raman map in (*b*) shows intensity variation at 1085 cm^{-1}. In the dark blue area in the centre of the pearl only low intensities were measured, whereas the turquoise areas clearly show aragonite intensities (i.e. high intensities for wavenumber 1085). Two Raman maps of vaterite peaks at 1091 cm^{-1} and 1074 cm^{-1} (*c *and* d *respectively) show high intensities in the roundish zone close to the centre and indicate that it consists of vaterite.*

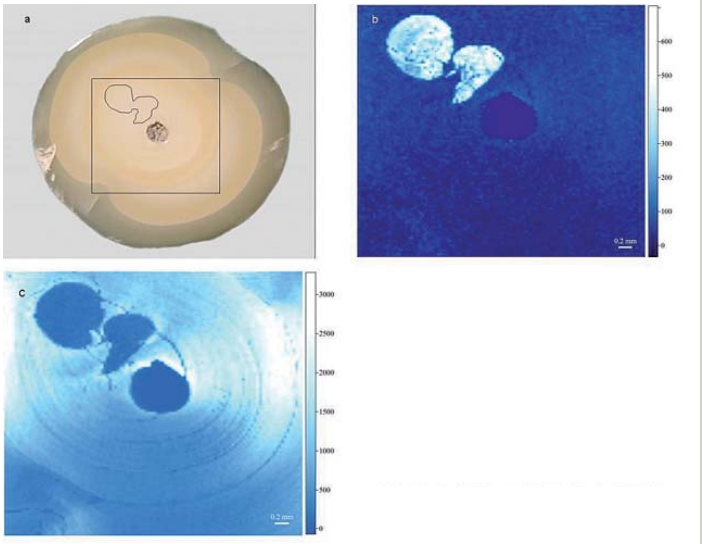

Figure 9: (a) *Polished cross-section of sample 4 (from China); the irregular shape of the vaterite area is outlined in black. The rectangular area was mapped by Raman spectroscopy and (*b*) shows the intensities at 1091 cm^{-1}, with the bright area indicating vaterite. (*c*) The pearl at 1085 cm^{-1}; the bright area indicates that it mostly consists of aragonite.*

Raman spectra from the surface of the freshwater cultured pearls exclusively showed the typical Raman shifts for aragonite. However, after sectioning of the pearls, vaterite areas could be identified by the Raman mapping technique in the inner parts of six samples, whose surfaces were previously found to consist of aragonite only.

Cross sections of two pearls typical of our sample are shown in *Figures 8a* and *9a* and their Raman maps are shown in *Figures 8b*, *c*, *d*, and *Figures 9b*, *c* respectively.

Within the Raman map pictured in *Figure 8b* the roundish area in the centre of the pearl shows low intensity responses at 1085 cm^{-1}, implying that this part consists neither of calcite nor of aragonite. The analysis of the complete Raman dataset shows that the major part of the pearl cross-section outside the roundish area close to the pearl's centre consists of aragonite (turquoise coloured area in *Figure 8b*). In *Figure 8c* the intensities at 1091 cm^{-1} - the most intense band of vaterite (*Table I*) are plotted, clearly indicating that this region (light green) consists of vaterite; this conclusion is supported by the map of intensities at 1074 cm^{-1} shown in *Figure 8d*.

Similarly, a Raman map of the intensities at 1091 cm^{-1} in the cross section of sample Nr. 4 (*Figure 9b*) shows an irregular area of high intensities indicating vaterite close to the centre of the pearl. The map in *Figure 9c* shows high intensities at 1085 cm^{-1} outside the vaterite area indicating aragonite.

In addition to its presence near the centres of good quality pearls, vaterite was also detected in small surface blemishes in a Kasumigaura pearl (*Figure 10*). This pearl is of high lustre, but shows a number of small pits on the surface that are pure white and lack the lustre of the surrounding pearl surface. Raman spectra clearly indicated that the white areas consisted of vaterite.

Ma and Lee (2006) reported on vaterite, aragonite and calcite in lustreless freshwater cultured pearls, and concluded that vaterite was rare or absent in high quality pearls, implying that if vaterite is present, it is one factor reducing the quality of pearls. Contrary to Ma and Lee (2006) our

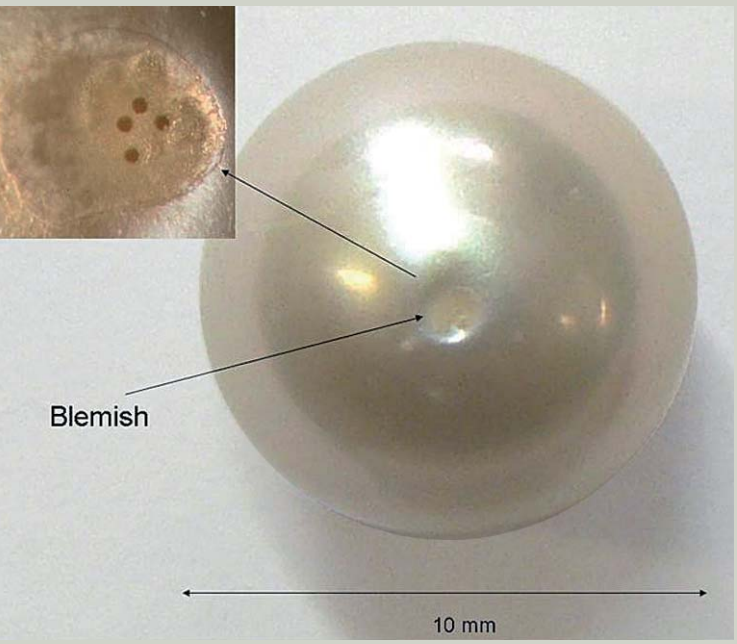

Figure 10: *Cultured Kasumigaura pearl of good quality with a little spot in which vaterite was determined by Raman investigations; laser ablation analyses were carried out after the Raman work and resulted in four tiny laser craters shown in the magnified inset.*

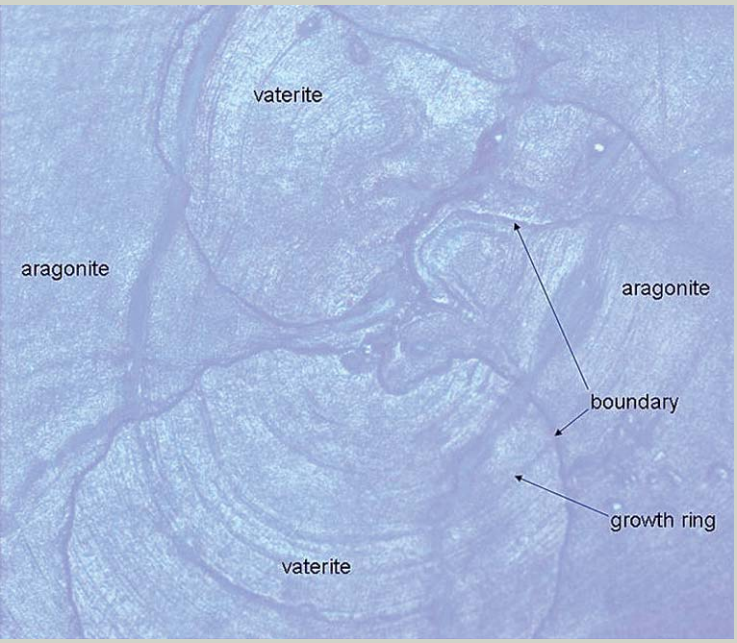

Figure 11: *Image of the inner part of the cross-section of pearl sample 4 (see* Figure 9*). The surface was etched and dyed with Mutvei's solution (Schoene* et al.*, 2000), which colours the pearl with different intensity depending on organic content. Thus, the boundaries between the vaterite and aragonite areas (arrows) and the growth rings which cross these boundaries without deviation are clearly visible.*

investigations show no evidence for the presence of calcite which is supported by the reports of Qiao *et al*. (2006).

Our results support the view that vaterite in the near-surface parts of the pearl (sub-surficial to surficial) is a major influence on quality. Additionally this study shows that vaterite is a common phase inside freshwater cultured pearls, both from China and Japan, and that these tiny regions are independent of vaterite occurrences at the surface of the pearl. In high-quality pearls, any vaterite is situated near the centre of the pearl and in close vicinity to the remnants of the tissue implant.

Microscopic observations

Under a binocular microscope, concentric growth rings of different colours in the sectioned samples are clearly visible whereas the vaterite areas are consistently and homogeneously of light colouring (nearly white), irrespective of the actual colour of the pearl. In *Figure 8a* the vaterite area (marked with dotted lines) is light coloured in contrast to the pink colour of the pearl, whereas in *Figure 9a* the vaterite area is not so distinct in an off-white sample. The morphology of any vaterite areas in the centre of a pearl varies from specimen to specimen, but it is almost always of a rounded shape and situated near the centre of the pearl (see *Figures 8*, *9* and *11*). To further study the micro-structure of the vaterite zones, cross-sections were treated with Mutvei's solution (Schoene *et al*., 2005). This etching method gently dissolves the calcium carbonate with acetic acid, while the organic matrix is stabilized with glutaraldehyde, and Alcian Blue colours the pearl with different intensity that highlights the organic regions (*Figure 11*). Under the microscope, the etched surfaces show a more intense blue at the boundaries between the different $CaCO_3$ polymorphs, implying that organic material is concentrated there. This chemical treatment also emphasizes organic growth rings and indicates that they traverse vaterite and aragonite areas alike.

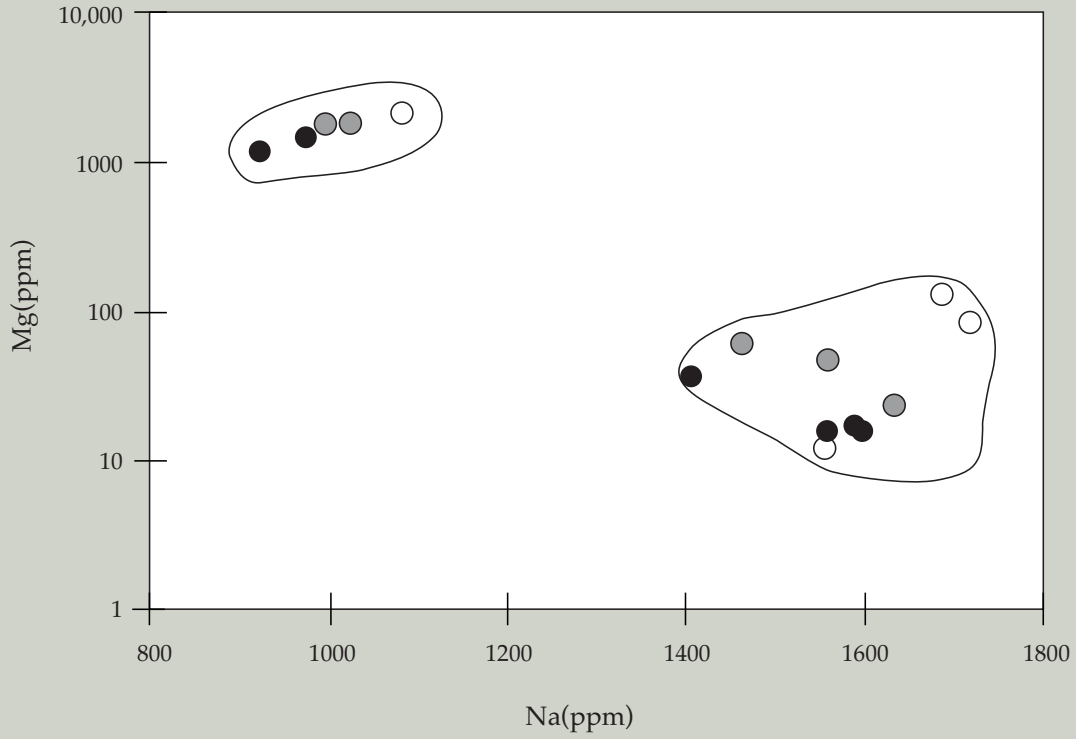

Figure 12: *A plot of Mg vs. Na concentrations (in ppm) from vaterite-bearing areas (left field) and aragonite-bearing areas (right field) in pearl samples 4 (solid symbols), 7 (open symbols) and 12 (grey symbols), indicates a Na/Mg ratio of 0.47 – 0.71 for vaterite and between 12 and 161 for aragonite.*

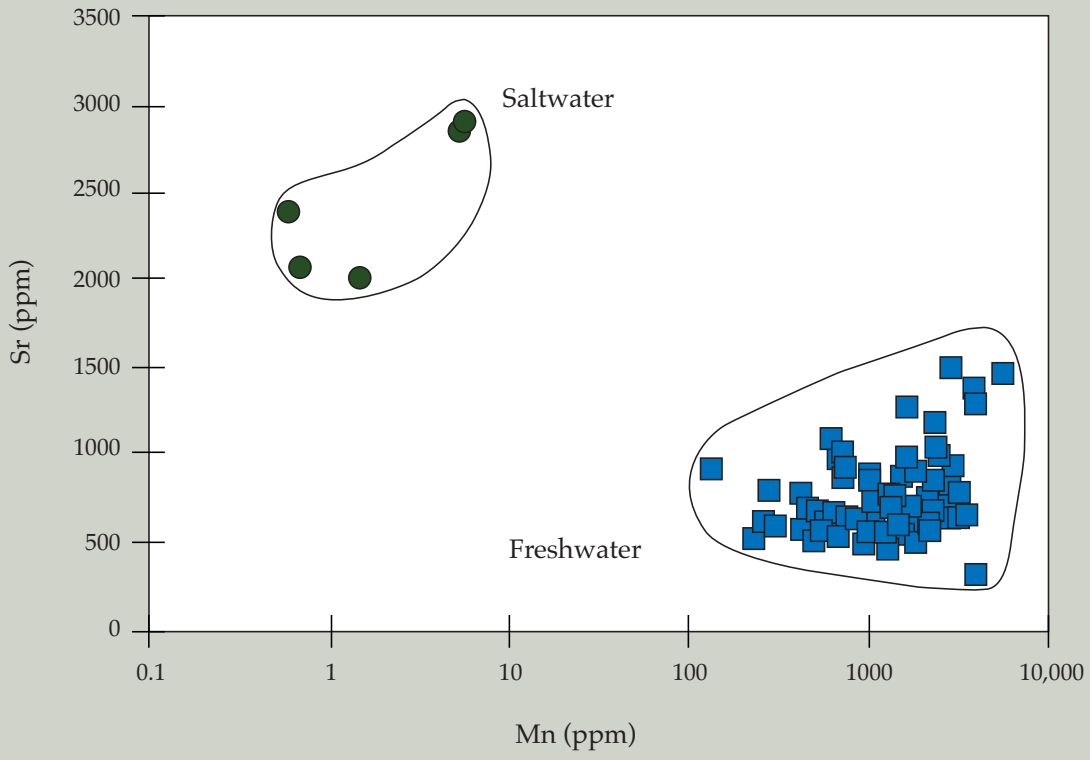

Figure 13: *A plot of strontium vs. manganese concentrations (in ppm) shows that this can be used to clearly distinguish between freshwater pearls and those grown in seawater.*

Chemical composition of vaterite and aragonite

In situ measurements of vaterite and aragonite areas by LA-ICP-MS show that magnesium concentrations are significantly higher in the vaterite (1121 – 2286 ppm) than in the aragonite areas (10.6 –140 ppm) (*Figure 12*).

Additionally, sodium and strontium concentrations are distinctly higher in the aragonite - (1409 – 1718 ppm and 323 – 923 ppm, respectively) than in vaterite-bearing areas (923 - 1083 ppm and 215 – 256 ppm, respectively). Thus, the measured Na/Mg ratios clearly distinguish vaterite (0.47-0.71) from aragonite (12-161). These results are supported by studies on vaterite and aragonite in fish otoliths. The concentrations of Mg in these biominerals were reported to be 30-fold higher in vaterite than in aragonite, whereas the concentrations of Sr were 10-fold higher in aragonite than in vaterite (e.g. Melancon *et al*., 2005). Brown and Severin (1999) examined the elemental distribution in otoliths of inconnu (*Stenodus leucichthys*) and identified regions depleted in Sr and Na. Further analyses of these regions revealed the presence of vaterite. The findings of Tomás and Geffen (2003), too, show lower sodium and strontium concentrations in the vaterite than in the aragonite areas of fish otoliths, whereas the concentrations of manganese are reported to be higher in the vaterite areas. In our study the Mn concentrations reveal no diagnostic difference between aragonite and vaterite implying that any difference due to structural or organic influence is disguised by the influence of water salinity on the Mn concentration in pearls (*Figure 13*; Jacob *et al*., 2006c).

In contrast to Melancon *et al*. (2005), who observed 20 fold higher Ba concentrations in aragonite than in vaterite, the Ba concentration in the aragonite areas (67 - 229 ppm) in our study show no significant difference from the Ba concentration in the vaterite areas (41 -283 ppm).

Discussion

Addadi *et al*. (2006) proposed that the nacre deposition process of molluscs occurs in a sequence of stages. The first stage is assembly of the organic matrix – the framework in which the minerals form. At the second stage, amorphous calcium carbonate (ACC) is deposited in this framework. In the following step the nucleation of individual aragonite crystals at the expense of the transient ACC phase takes place. It is possible that vaterite is also produced from ACC, either as a metastable precursor of aragonite (e.g. Hasse *et al*., 2000) or as an endproduct equivalent to aragonite. However, the mechanism of vaterite production *in vivo* has not been studied in detail. In their study, Marxen *et al*. (2003) discuss these questions and conclude that the transformation from ACC proceeds directly to aragonite without forming vaterite as a transient phase, which was supported by Hasse *et al*. (2000) in a study on snail shells.

Our observations indicate that aragonite and vaterite may grow simultaneously in the same growth ring but in different areas (*Figure 11*), corresponding well with the findings of Melancon *et al*. (2005), who reported on simultaneous growth of vaterite and aragonite in otoliths of lake trout. But textural evidence is still lacking to enable us to decide between two possible hypotheses: either vaterite acts as a precursor to the formation of aragonite but is stabilized by organic materials before this can take place, or vaterite and aragonite grow simultaneously.

While the crystal structure of vaterite is still a matter of discussion (see Kamhi, 1963; Meyer, 1969; Lippman, 1973) the detection of three peaks for ν_1 at 1074, 1080 and 1091 cm^{-1} (*Figure 6*) and the five components for ν_4 (e.g. in sample 12, *Figure 7*) in our study indicate that vaterite is hexagonal. This symmetry was proposed by Lippmann (1973) (see also Gabrielli *et al*., 2000), and was based on the high temperature modification of $YbBO_3$ (Bradley *et al*., 1966). Lippman (*op. cit*.) that in this crystal structure, substitution of strontium for calcium is less probable than in orthorhombic aragonite (Brown and Severin,

1999). This is supported in our study where Sr concentrations are significantly higher in aragonite than in vaterite. The lower concentration of Na in vaterite suggests that the crystal structure may restrict incorporation of ions larger than Ca (see Brown and Severin, 1999). But the substitution of smaller cations for Ca in vaterite is in good agreement with the significantly higher Mg concentrations in the vaterite areas. Noethig-Laslo and Brecevic (1998) have shown that the Mg^{2+} ion fits well into the vaterite structure, and Jiao *et al*. (2006) found that when Mg is present in adequate concentrations it is known to exert an important effect on aragonite precipitation.

Although the different elemental concentrations in aragonite and vaterite can be related to crystal structures, they may be overprinted by regional differences in trace element contents of the waters in which the pearl mussels were cultured. Firstly, Jacob *et al*. (2006c) showed that a clear distinction between freshwater cultured pearls from China and those from Lake Kasumigaura could be made on the basis of the Ba concentrations in the pearls. Secondly, Sr and Mn concentrations can vary according to the water salinity (see Banerjee and Rager, 2001; Banerjee and Habermann, 2000; Secor *et al*., 1995). And thirdly, some biological factors influence both elemental distribution and polymorph formation.

In vitro studies of molluscs have suggested that specific proteins and macromolecules have the ability to control growth and nucleation of the different polymorphs (see Belcher *et al*., 1996; Falini *et al*., 1996; Thompson *et al*., 2000; Gottliv *et al*., 2003; Matsushiro *et al*., 2003; Matsushiro and Miyashita, 2004).

Although the subject of study for a number of years now, the causes and the mechanisms for producing aragonite or vaterite in pearls have not yet been fully understood. However, most authors agree that the organic matrix plays a key role in controlling which $CaCO_3$ polymorph is formed: Qiao *et al*. (2006) consider that the controlling factors are some special soluble proteins; Ma and Lee (2006) assumed that organic material controls polymorph formation and stabilizes vaterite in pearls. One possible reason for the occurrence of vaterite in shell given by Hasse *et al*. (2000) is that it may simply be the sign of a disturbed mineralization process. This is consistent with the assumption that some vaterite formation in fish otoliths can be attributed to stress in the animal (Melancon *et al*., 2005; Brown and Severin, 1999). Sweeting *et al*. (2004) suggested that environmental stress may play an important role for the occurrence of vaterite in otoliths of coho salmons. Massou *et al*. (2004) also proposed that the main causes for interruptions in growth of fish otoliths can be attributed to external stress which still leaves the actual biochemical mechanisms that lead to vaterite formation largely unknown. Clearly, more detailed biochemical work is needed to reveal the underlying causes.

Conclusion

In this study we have shown that vaterite not only occurs at the surface, but also in the interior parts of freshwater cultured pearls from *Hyriopsis cumingii* and *Hyriopsis cumingii* hybridized with *Hyriopsis schlegeli*, independent of their quality, colour, cultivation method and provenance. To the best of our knowledge, this is the first time that vaterite has been identified in Japanese freshwater cultured pearls. Polished cross-sections revealed vaterite in 50% of the studied pearls. Thus, mineralization of vaterite is a common phenomenon in pearls from *Hyriopsis* mussels, but has not yet been observed in pearls from other mussel species. Strontium and sodium concentrations are significantly lower in vaterite compared with adjacent aragonite whereas the Mg concentration is up to two orders of magnitude higher. These large differences in Mg/Na ratios allow identification of these two polymorphs even without Raman spectroscopy.

The occurrence of the vaterite close to the centres of many pearls and commonly close to the remains of organic material derived possibly from implanted tissue, implies that vaterite has a significant role in the biomineralization process.

Acknowledgements

Support from the Johannes Gutenberg-University Research Fund for Young Scientists, from the Institute of Gemstone Research and the Geocycles Cluster have made this study possible. The authors are grateful for support from and for fruitful discussions with B. Dillenburger, Y. Demia, K. Yanase, M. Sakai, K. Kawabata and the brothers Ibuki. This is Geocycles Cluster contribution No. 117.

References

Addadi, L., Raz, S., and Weiner, S., 2003. Taking advantage of disorder. Amorphous calcium carbonate and its roles in biomaterialization. *Adv. Mater.,* 15(12), 959-70

Addadi, L., Joester, D., Nudelman, F., and Weiner, S., 2006. Mollusk shell formation: a source of new concepts for understanding biomineralization processes. *Chem. Eur. J.,* 12, 980-7

Akamatsu, S., Zansheng, I.T., Moses, T.M., and Scarratt, K., 2001. The current status of Chinese cultured pearls. *Gems & Gemology,* 37(2), 96-113

Anderson, A., 1996. Group theoretical analysis of the ν_1 (CO_3^{2-})- vibration in crystalline calcium carbonate. *Spectroscopy Letters,* 29, 5

Banerjee, A., and Habermann, D., 2000. Identification of Chinese freshwater pearls using Mn^{2+} activated cathodoluminescene. *Carbonates and Evaporites,* 15, 138-48

Banerjee, A., and Rager, H., 2001. Discrimination between sea-water and freshwater tissue-graft cultured pearls by EPR. *Canadian Gemmologist,* 22(3), 82-7

Behrens, G., Kuhn, L.T., Ubic, R., and Heuer, A.H., 1995. Raman spectra of vateritic calcium carbonate. *Spectroscopy Letters,* 28(6), 983-95

Belcher, A.M., Wu, X. H., Christensen, R.J., and Hansma, P.K., 1996. Control of crystal phase switching and orientation by soluble mollusc-shell proteins. *Nature,* 381, 56-8

Beniash, F., Addadi, L., and Weiner, S., 1999. Cellular control over spicule formation in sea urchin embryo structural approach. *J. Struct. Biol.,* 125(1), 50-62

Bischoff, W.D., Sharma, S.K., and MacKenzie, F.T., 1985. Carbonate ion disorder in synthetic and biogenic magnesian calcite: a Raman spectral study. *American Mineralogist,* 70, 581-9

Bradley, W.F., Graf, D.L., and Roth, R.S., 1966. The vaterite-type ABO_3 rare-earth borates. *Acta Cryst.,* 20, 283-7

Brown, R., and Severin, K.P., 1999. Elemental distribution within polymorphic inconnu (*Stenodus leucichthys*) otoliths is affected by crystal structure. *Canadian Journal of Fisheries and Aquatic Sciences,* 56(10), 1898

Dalbeck, P., England, J., Cusack, M., Lee, M.R., and Fallick, A.E., 2006. Crystallography and chemistry of the calcium carbonate polymorph switch in *M. edulis* shells. *Eur. J. Mineral.,* 18, 601-9

Falini, G., Albeck, S., Weiner, S., and Addadi, L., 1996. Control of aragonite or calcite polymorphism by mollusk shell macromolecules. *Science,* 271, 67-9

Feng, F.Q., Pu, G., Pei, Y., Cui, F.Z., Li, H.D., and Kim, T.N., 2000. Polymorph and morphology of calcium carbonate crystals induced by proteins extracted from mollusc shell. *Journal of Crystal Growth,* 216, 459-65

Feng, Q.L., Li, H.B., Cui, F.Z., and Li, H.D., 1999. Crystal orientation domains found in the single lamina in nacre of the *Mytilus edulis* shell. *Journal of Material Science Letters* 18(19), 1547-9

Fryer, B.J., Jackson, S.E. and Longerich, H.P., 1995. Design, operation and role of the laser-ablation microprobe coupled with an inductively-coupled plasma mass-spectrometer (LAM-ICP-MS) in the Earth-Sciences. *Canadian Mineralogist,* 33, 303-12, part 2

Gabrielli, C., Jaouhari, R., Joiret, S. and Maurin, G., 2000. *In situ* Raman spectroscopy applied to electrochemical scaling. Determination of the structure of vaterite. *J. Raman Spectrosc.,* 31, 497-501

Gauldie, R.W., Sharma, S.K., and Volk, E., 1997. Micro-Raman spectral study of vaterite and aragonite otoliths of the coho salmon *Oncorhynchus kisutch. Comp. Biochem. Physiol.,* 118 A(3), 753-7

Gottliv, B.-A., Addadi, L., and Weiner, S., 2003. Mollusk shell acidic proteins: in search of individual functions. *ChemBioChem.,* 4, 522-9

Griffith, W.P., 1974. Raman spectroscopy of minerals. *The infrared spectra of minerals.* V.C. Farmer (Ed.). Mineralogical Society, London. Monograph 4: 119-36

Hasse, B., Ehrenberg, H., Marxen, J.C., Becker, W., and Epple, M., 2000. Calcium carbonate modifications in the mineralized shell of the freshwater snail *Biomphalaria glabrata. Chem. Eur. J.,* 6(20), 3679-85

Hou, W.T., and Feng, Q.L., 2003. Crystal orientation preference and formation mechanism of nacreous layer in mussel. *Journal of Crystal Growth,* 258, 402-8

Huang, F., Chen, Z., Tong, H., Zhou, Y., Zhang, Z., and Yang, M., 2004. The microstructure of the shell and cultured blister pearls of *Pteria penguin* from Sanya, Hainan, China. *J. Gemm.,* 29(1), 25-36

Jacob, D.E., Wehrmeister, U., Häger, T., and Hofmeister, W., 2006a. Identifying Japanese Freshwater Cultured Pearls from Lake Kasumigaura. *The Australian Gemmologist,* 22, 539-41

Jacob, D.E., Wehrmeister, U., Häger, T., and Hofmeister, W., 2006b. Herkunftsbestimmung von Süßwasser-Zuchtperlen mit Laser Ablations ICP-MS. *Z. Dt. Gemmol. Ges.,* 55(1-2): 51-8 (in German)

Jacob, D.E., Wehrmeister, U., Häger, T., and Hofmeister, W., 2006c. Origin determination of freshwater cultured pearls from Lake Biwa (Japan), Kasumigaura (Japan) and China. First International Gem and Jewelry Conference GIT, Bangkok and Chantaburi, GIT

Jiao, Y., Feng, Q., and Li, X., 2006. The co-effect of collagen and magnesium ions on calcium carbonate biomineralization. *Materials Science and Engineering C,* 26, 648-52

Kamhi, S., 1963. On the structure of vaterite, $CaCO_3$. *Acta Cryst.,* 16, 770-2

Landman, N.H., Mikkelsen, P.M., Bieler, R., and Bronson, B., 2001. *Pearls: A Natural History*. Harry N Abrams, New York

Levi, Y.A.S., Brack, A., Weiner, S., and Addadi, L., 1998. Control over aragonite crystal nucleation and growth: An *in vitro* study of biomineralization. *Chem. Eur. J.,* 4(3), 389-96

Lippmann, F., 1973. *Sedimentary Carbonate Minerals.* Springer-Verlag, New York

Ma, H.Y., and Dai, T.G., 2001. The first discovery of vaterite in lustreless freshwater pearls of Leidan, Zhejiang. *Acta Mineral. Sin*., 21, 153-7

Ma, H.Y., and Lee, I.-S., 2006. Characterization of vaterite in low quality freshwater-cultured pearls. *Materials Science and Engineering C,* 26, 721-3

Marxen, J.C., Becker, W., Finke, D., Hasse, B., and Epple, M., 2003. Early mineralization in *biomphalaria glabrata:* Microscopic and Structural Results. *J. Moll. Stud.,* 69, 113-21

Massou, A.M., Le Bail, P.-Y., Panfili, J., Lae, R., Baroillers, J.F., Mikasolek, O., Fontanelle, G., and Auperin, B., 2004. Effects of confinement stress of variable duration on the growth and microincrement deposition in the otoliths of *Oreochromis niloticus* (Cichlidae). *Journal of Fish Biology,* 65, 1253-69

Matsushiro, A., and Miyashita, T., 2004. Evolution of hard-tissue mineralization: comparison of the inner skeletal system and the outer shell system. *J Bone Miner. Metab.,* 22, 163-9

Matsushiro, A., Miyashita, T., Miyamoto, H., Morimoto, K., Tonomura, B., Tanaka, A., and Sato, K., 2003. Presence of protein complex is prerequisite for aragonite crystallisation in the nacreous layer. *Mar. Biotechnol.,* 5, 37-44

Melancon, S., Fryer, B.J., Ludsin, S.A., Gagnon, J.E.,and Yang, Z., 2005. Effects of crystal structure on the uptake of metals by lake trout (*Salvelinus namaycush*) otoliths. *Canadian Journal of Fisheries and Aquatic Sciences,* 62(11), 2609-19

Meyer, H. J., 1969. Struktur und Fehlordnung des Vaterits. *Zeitschrift für Kristallographie,* 128, 183-212

Noethig-Laslo, V., and Brecevic, L., 1998. Mode and sites of incorporation of divalent cations in vaterite. *J.Chem. Soc., Faraday Trans.,* 94(12), 2005-9

Qiao, L., Feng, Q.-L., and Li, Z., 2006. Special vaterite found in freshwater lackluster pearls. *Crystal Growth and Design,* 7(2), 275-9

Qiao, L. and Feng, Q.-L., 2007. Study on twin stacking faults in vaterite tablets of freshwater lacklustre pearls. *Journal of crystal growth,* 304 (1), 253-6

Rutt, H.N., and Nicola, J.H., 1974. Raman spectra of carbonates of calcite structure. *J. Phys. C: Solid State Phys.,* 7, 4522-8

Schoene, B.R., Dunca, E., Fiebig, J., and Pfeiffer, M., 2005. Mutvei's solution: An ideal agent for resolving microgrowth structures of biogenic carbonates. *Palaeogeography, Palaeoclimatology, Palaeoecology,* 228, 149-66

Secor, D.H., Henderson-Arzapalo, A., and Piccoli, P.M., 1995. Can otolith microchemistry chart patterns of migration and habitat utilization in anadromous fishes? *Journal of Experimental Marine Biology and Ecology,* 192, 15-33

Snow, M.R., Pring, A., Self, P., Losnic, D., and Shapter, J., 2004. The origin of color of pearls in iridescence from nano-composite structure of the nacre. *American Mineralogist,* 89, 1353-8

Song, F., Soh, A.K., and Bai, Y.L., 2003. Structural and mechanical properties of the organic matrix layers of nacre. *Biomaterials,* 24, 3623-31

Strack, E., 2001. *Perlen*. Rühle-Diebener Verlag, Stuttgart

Sudo, S., Fujikawa, T., Nagakura, T., Ohkubo, T., Sakaguchi, K., Tanaka, M., and Nakashima, K., 1997. Structures of mollusc shell framework proteins. *Nature,* 387, 563-4

Sweeting, R.M., Beamish, R.J., and Neville, C.M., 2004. Crystalline otoliths in teleosts: Comparisons between hatchery and wild coho salmon (*Oncorhynchus kisutch*) in the Strait of Georgia. *Reviews in Fish Biology and Fisheries,* 14, 361-9

Thompson, J.B., Paloczi, G.T., Kindt, J.H., Michenfelder, M., Smith, B.L., Stucky, G., Morse, D.E., and Hansma, P.K., 2000. Direct observation of the transition from calcite to aragonite growth as induced by abalone shell proteins. *Biophysical Journal,* 79(6), 3307-12

Tomás, J., and Geffen, A.J., 2003. Morphometry and composition of aragonite and vaterite otoliths of deformed laboratory reared juvenile herring from two populations. *Journal of Fish Biology,* 63, 1383-1401

Urmos, J., Sharma, S.K., and MacKenzie, S.T., 1991. Characterization of some biogenic carbonates with Raman spectroscopy. *American Mineralogist,* 76, 641-6

Watabe, N., 1965. Studies on shell formation XI. Crystal-matrix relationships in the inner layers of mollusk shells. *J. Ultrastructure Research,* 12, 351-70

White, W.B., 1974. The Carbonate Minerals. *The Infrared Spectra of Minerals*. V.C. Farmer (Ed.). Mineralogical Society, London. Monograph 4

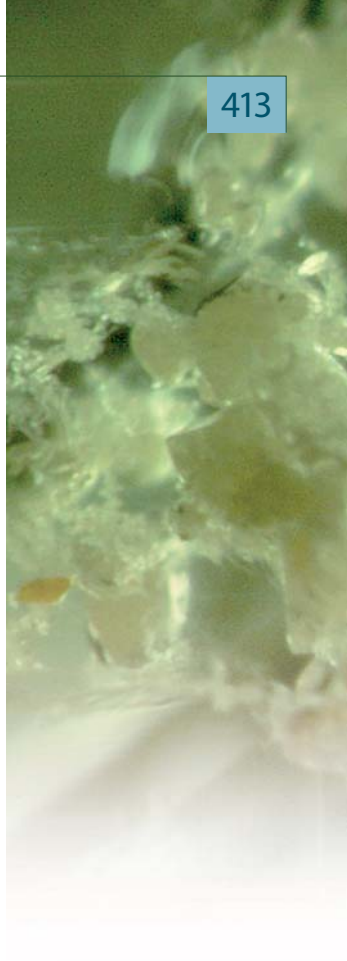

Vanadium-bearing gem-quality tourmalines from Madagascar

Dr Karl Schmetzer[1], Dr Heinz-Jürgen Bernhardt[2], Christian Dunaigre[3] and Dr Michael S. Krzemnicki[4]

1. Taubenweg 16, D-85238 Petershausen, Germany
2. ZEM, Institut für Geologie, Mineralogie und Geophysik, Ruhr-University, D-44780 Bochum, Germany
3. Gübelin Gem Lab, Maihofstr. 102, CH-6006 Lucerne, Switzerland
4. SSEF Swiss Gemmological Institute, Falknerstr. 9, CH-4001 Basel, Switzerland

Abstract: *Gemmological, microscopic, chemical and spectroscopic properties of green, vanadium-bearing gem-quality tourmalines from southern Madagascar are presented. The samples are iron- and lithium-free and are designated as calcic aluminous dravites. They reveal a small compositional variability for sodium, calcium, magnesium and aluminium. Positive correlations between Na and Al and between Ca and Mg are present, always with Al>6 atoms per formula unit and Mg<3 atoms per formula unit.*

Vanadium is the main transition metal present with smaller amounts of chromium and these cause the green coloration. Absorption bands in the UV-Vis range are assigned to V^{3+} on octahedral aluminium sites.

Mineral inclusions in the tourmalines were characterized by laser Raman microspectroscopy and quantitative microprobe analyses. The commonest are bytownite plagioclases, but quartzes and zircons are also present as well as cavities and healed fractures containing liquid and two-phase fillings (liquid/gas). Non-homogeneous irregularly shaped grains consist of a mixture of hydrous aluminium silicates and iron hydroxides.

The tourmalines from Madagascar are compared with iron-free or almost iron-free gem-quality tourmalines, mainly from East Africa. Correlation diagrams of Na, Ca, Mg and Al show two different population fields, a) with Al>6 and Mg<3 atoms per formula unit (aluminous dravites) and b) with Al<6 and Mg>3 atoms per formula unit (uvites). The main isomorphic replacement within this solid solution series occurs between the tourmaline end-members oxy-dravite, $Na(Mg_2Al)Al_6(BO_3)_3Si_6O_{18}(OH)_3O$, and uvite, $CaMg_3(MgAl_5)(BO_3)_3Si_6O_{18}(OH)_4$, and is represented by the substitutional scheme $Na^+ + 2Al^{3+} + O^{2-} \leftrightarrow Ca^{2+} + 2Mg^{2+} + (OH)^-$.

Keywords: *calcic aluminous dravite, electron microprobe analysis, isomorphic series, vanadian tourmaline, UV-visible absorption spectra*

 ISSN: 1355-4565

Introduction

Recently, a parcel of rough crystals and crystal fragments of a green mineral (*Figure 1*) were purchased as garnets from a German dealer in a local gem market in Madagascar. The transparent material of gem quality was indicated to originate from a new locality in southern Madagascar close to the occurrence of green, vanadium-bearing grossular (tsavorite) in the Gogogogo – Bekily area (see Mercier *et al.*, 1997). According to their crystal shape, their pleochroism and their optical properties (measured on rough crystal faces), the crystals were quickly identified as tourmaline.

Numerous tourmaline occurrences are known in Madagascar and the island is famous for multi-coloured and colour-zoned tourmalines, mostly elbaite and liddicoatite (Pezzotta, 2001; Dirlam *et al.*, 2002). A more detailed examination of the parcel of our tourmalines indicated that they are vanadium-bearing dravites, and since vanadium-bearing dravites of gem quality are, according to the knowledge of the present authors, not described in detail from Madagascar, the present study was undertaken to evaluate the properties of this new tourmaline material in detail.

Figure 1: *Rough crystal fragments and faceted vanadium-bearing tourmalines from southern Madagascar. The crystal showing striations on a prism face (lower right) measures about 8 x 13 mm; the faceted triangular stone weighs 0.23 ct and measures 4.2 x 4.1 mm.*

Vanadian tourmalines (dravites and uvites) from East Africa (Kenya and Tanzania) have been known in the gem trade since the end of the 1970s, and this light to intense green gem material has frequently been misnamed 'chromium-tourmaline' in the trade (see Schmetzer *et al.*, 1979; Schmetzer and Bank, 1979; Keller, 1992; Simonet, 2006). Just recently, vanadium-bearing gem-quality uvites from Zambia with a special trapiche inclusion pattern have been described by Hainschwang *et al.* (2007).

Materials and methods

From the original lot purchased in Madagascar containing several hundred tourmalines, about 30 rough crystal fragments were available for the present study. The larger part of the lot was faceted for commercial purposes and about 40 tourmalines were obtained from this part after cutting (*Figure 2*). Furthermore, a parcel of about 20 rough or sawn impure tourmaline fragments which had been rejected during the faceting process were available.

Standard gemmological methods were used to determine the refractive indices (RI), optical character, specific gravity (SG) and fluorescence under long- and short-wave ultraviolet radiation of 20 faceted stones. Standard microscopic techniques were used to examine the internal features under different lighting conditions for all rough, sawn and faceted samples, both with and without immersion liquids.

To determine the chemical composition of the tourmalines, we selected five samples for microprobe analysis using a Cameca Camebax SX 50 electron microprobe. For each tourmaline, we obtained 10 point analyses from traverses across the samples. To obtain qualitative data for water and lithium, two rough crystal fragments were powdered for wet chemical analysis. Lithium was determined by atomic absorption spectroscopy (AAS) and the water content was analysed by Karl-Fischer titration.

For the examination of boron contents (which, like lithium and water, cannot be determined routinely by electron microprobe)

and for trace element analysis we selected two faceted tourmalines for laser ablation-inductively coupled plasma-mass spectroscopy (LA-ICP-MS) using a pulsed Excimer ArF laser with a characteristic wavelength of 193 nm and special optics to homogenize the energy distribution across the laser beam combined with the Perkin Elmer ELAN 6100 ICPMS quadrupole instrument. As indicated above, further trace element analyses, e.g. for lithium, were also performed by mass spectroscopy.

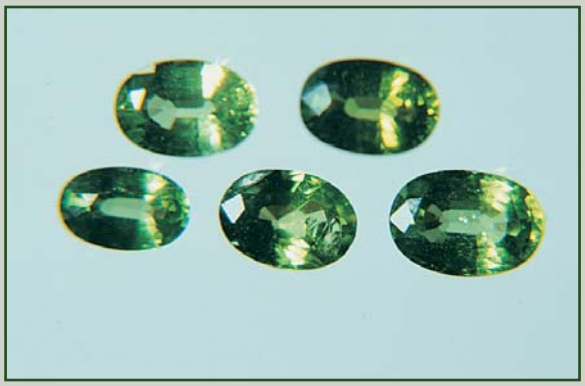

Figure 2: *Faceted vanadium-bearing tourmalines from southern Madagascar. Weights of samples between 0.33 ct and 0.60 ct, the largest tourmaline (lower right) measures 4.4 x 6.5 mm.*

Polarized UV-Vis-NIR (300-880 nm) absorption spectra were recorded for seven rough or faceted samples using a Perkin-Elmer Lambda 19 spectrophotometer. Unit cell dimensions were determined for one of the crystals analysed by electron microprobe using an automatic four-circle single crystal diffractometer and refined with powder data using $CuK_{\alpha 1}$ radiation with Si as internal standard.

To identify the inclusions present in the tourmalines, we examined 15 faceted samples by laser Raman microspectroscopy using a Renishaw 1000 system. In addition, we selected 12 heavily included crystal fragments which had been rejected for faceting. From these 12 tourmalines polished thin sections of 20-25 µm thickness were prepared to enable microscopic examination and quantitative microprobe analyses of mineral inclusions, and to carry out Raman microspectroscopy of selected inclusions which had already been measured by electron microprobe.

Results

Visual appearance and gemmological properties

The tourmaline crystals available for the present study mostly were irregular fragments without any crystal faces. Only a few samples showed prism faces, occasionally with striations parallel to the *c*-axis (*Figure 1*). All rough and faceted samples were homogeneously green without any distinct colour zoning (*Figures 1* and *2*).

Gemmological properties are summarized in *Table I*. Only small variations of refractive indices and specific gravity were observed. The pleochroism of all samples is distinct with a yellowish green coloration parallel to the *c*-axis and a more intense, slightly bluish green perpendicular to *c*. In short-wave ultraviolet light a weak to medium greenish yellow, slightly chalky fluorescence is present, but all samples are inert in long-wave UV.

Chemical composition

Chemical properties of five analysed samples are summarized in *Table II*. No compositional zoning of significance was detected within the single tourmaline crystals. All samples are sodium-, calcium- and magnesium-bearing aluminium tourmalines. Lithium is present only in trace amounts (average 0.004 wt.% Li_2O), and iron and manganese contents were at the detection limit of the electron microprobe. Distinct amounts of vanadium and chromium are present, with vanadium content always exceeding that of chromium.

The five tourmaline crystals examined by electron microprobe showed variation in their sodium, calcium, magnesium and aluminium contents. The compositional variability between different elements and especially a correlation between specific cations is, however, elucidated in more detail after calculation of the numbers of atoms per formula unit (apfu) according to the generally accepted structural formula of tourmaline on

Table I: *Physical and gemmological properties of V-bearing tourmalines from Madagascar.*

Colour	Green
Pleochroism parallel *c* perpendicular *c*	Yellowish green Bluish green
Refractive indices ω ε	1.638 – 1.640 1.618 – 1.620
Birefringence	0.020
Specific gravity	3.04 – 3.05
Unit cell dimensions[1] a_o (Å) c_o (Å)	15.9215 (1) 7.1867 (1)
Spectroscopic properties (nm) Absorption maxima ∥c Absorption maxima ⊥ c Intensity relations	 599, 441 610, 418, 370 (shoulder) 610 > 599 ; 441 > 418
UV fluorescence: short-wave long-wave	Weak to medium greenish yellow, slightly chalky Inert
Commonly-observed inclusions	Quartz, plagioclase (bytownite), zircon, solid multiphase inclusions consisting at least of hydrous aluminium silicates and iron hydroxides, cavities and healed fractures containing liquid and two-phase inclusions (liquid and gas)
Rarely-observed inclusions	Rutile, graphite, xenotime

[1] Refined powder data determined for sample D.

the basis of 31 anions (*Table II*).

According to the standard formula of magnesium-bearing aluminous tourmalines, $(Na,Ca,\square)(Mg,Al)_3(Mg,Al)_6(BO_3)_3Si_6O_{18}(O,OH,F)_4$, where the symbol □ represents a vacancy in the structure, we have to consider site occupancies of five cation-polyhedra, i.e. for Na,Ca,□ = X-site, Mg,Al = Y-site, Mg,Al = Z-site, B, and Si (see Tourmaline structure box). Various natural tourmalines with magnesium-aluminium disorder have been described, for which both cations, Al and Mg, are distributed within the two relevant octahedral Y- and Z-sites (Hawthorne *et al.*, 1993; Pieczka, 1999; Bloodaxe *et al.*, 1999; Da Fonseca-Zang *et al.*, 2001; Ertl *et al.*, 2003; Pertlik *et al.*, 2003; Marschall *et al.*, 2004; Novak *et al.*, 2004). This is more or less common and not an exceptional case (Grice and Ercit, 1993). For an exact determination of order/disorder and site occupancies of Mg and Al of our tourmaline crystals, which cannot be derived from analytical data, a crystal structure refinement would be necessary, but this is beyond the scope of the present paper. Thus, for simplicity of discussion of site populations in our samples, in which the amount of aluminium always exceeds 6 atoms per formula unit (Al > 6 apfu), we only consider the sums of magnesium and aluminium (Al + Mg) on the octahedrally coordinated Y- and Z-sites.

For all our samples, the sum of aluminium in Y- and Z-sites is >6 and the sum of magnesium in Y- and Z-sites is <3, with Al + Mg ~ 9, i.e. close to the theoretical value. The silicon tetrahedron is occupied mostly with Si but also a small almost constant substitution of about 0.1 atoms Al for Si is present. This feature has already been reported from vanadium-bearing gem-quality tourmalines from East Africa (MacDonald and Hawthorne, 1995), and is also common for iron-bearing members of the schorl-dravite series (Grice and Ercit, 1993). The boron content is almost equal to the theoretical value of 3, which indicates that no tetrahedral boron on Si-sites is present.

Table II: *Chemical composition of V-bearing tourmalines from Madagascar.*

Microprobe analyses (average of 10 point analyses each, wt.%)

Specimen	A	B	C	D	E
SiO_2	36.64	36.36	36.41	36.21	36.11
TiO_2	0.49	0.53	0.58	0.58	0.60
B_2O_3[1]	10.67	10.67	10.67	10.67	10.67
Al_2O_3	34.18	33.55	33.48	33.23	33.09
V_2O_3	0.17	0.19	0.19	0.19	0.20
Cr_2O_3	0.04	0.11	0.07	0.03	0.06
FeO[2]	0.01	0.02	0.01	0.02	0.01
MnO	0.01	0.02	0.01	0.01	0.02
MgO	10.63	10.75	10.96	10.99	10.96
CaO	1.58	1.75	1.93	2.36	2.43
Na_2O	1.56	1.49	1.48	1.37	1.36
K_2O	0.05	0.06	0.06	0.05	0.05
Li_2O[3]	0.00	0.00	0.00	0.00	0.00
F	0.48	0.50	0.51	0.40	0.38
H_2O[4]	3.00	3.00	3.00	3.00	3.00
-O=F	-0.20	-0.21	-0.21	-0.17	-0.16
Total	99.31	98.79	99.15	98.94	98.78

[1]Average analyses of two samples by LA-ICP-MS. [2]Total iron as FeO.
[3]Average analyses of two samples by wet chemical methods, LA-ICP-MS gave 0.004 Li_2O. [4]Average analyses of two samples by wet chemical methods.

Number of ions based on 31 (O, OH, F)

Specimen	A	B	C	D	E
Si	5.910	5.901	5.893	5.881	5.877
Al	0.090	0.099	0.107	0.119	0.123
Sum T site	6.000	6.000	6.000	6.000	6.000
B	2.970	2.988	2.980	2.990	2.997
Al	5.914	5.896	5.896	5.901	5.892
Ti	0.059	0.065	0.071	0.071	0.074
V	0.022	0.024	0.025	0.024	0.026
Cr	0.005	0.015	0.008	0.004	0.008
Sum Z site	6.000	6.000	6.000	6.000	6.000
Mg	2.557	2.600	2.645	2.661	2.658
Fe	0.002	0.003	0.002	0.002	0.001
Mn	0.002	0.003	0.003	0.002	0.003
Li	0.003	0.003	0.003	0.003	0.003
Al	0.493	0.421	0.384	0.340	0.333
Sum Y site	3.057	3.030	3.037	3.008	2.998
Na	0.487	0.468	0.465	0.433	0.429
K	0.010	0.012	0.012	0.010	0.011
Ca	0.273	0.305	0.335	0.411	0.424
Sum X site	0.770	0.785	0.812	0.854	0.864
OH	3.228	3.247	3.239	3.250	3.258
F	0.246	0.257	0.261	0.207	0.194

Approximate formula: $(Na_{0.4}Ca_{0.4}\square_{0.2})(Mg_{2.6}Al_{0.4})Al_6(BO_3)_3(Si_{5.9}Al_{0.1})O_{18}(OH_{3.25}F_{0.25}O_{0.5})$

Tourmaline structure

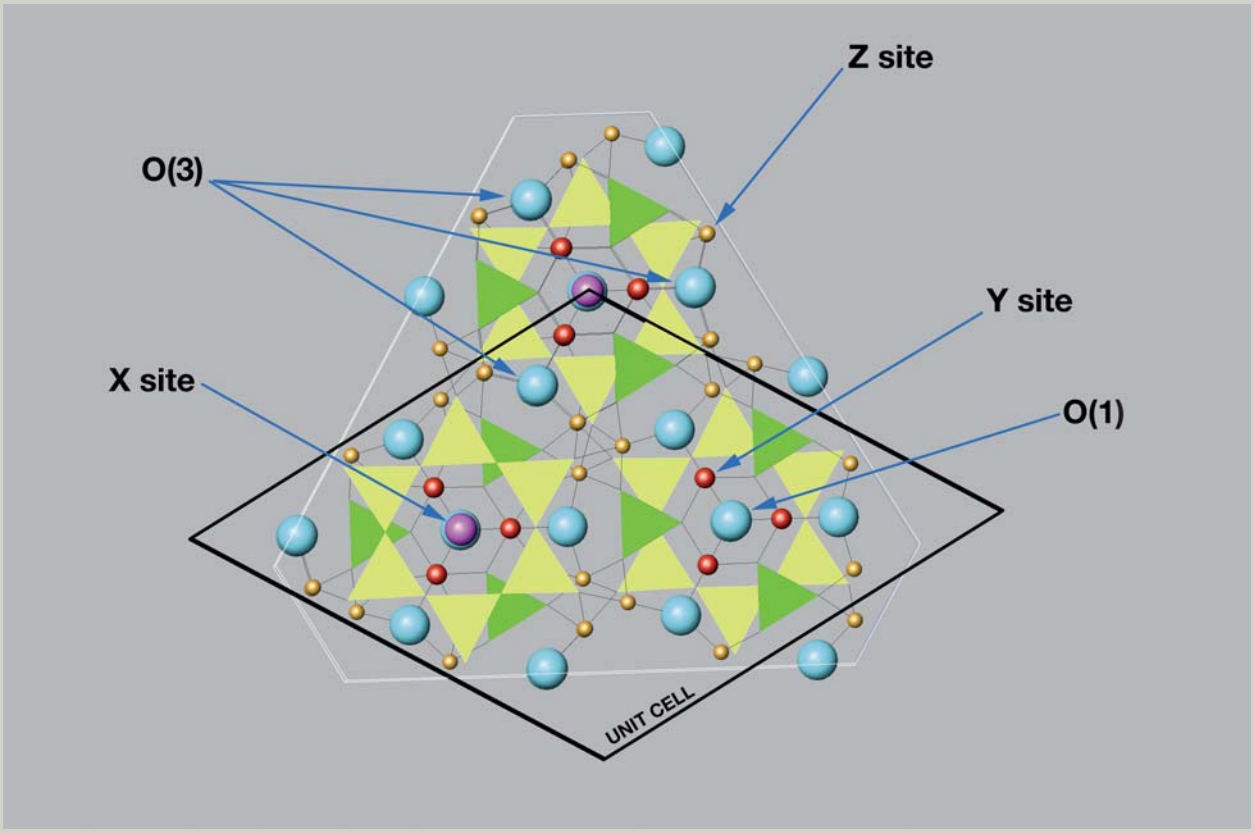

Tourmaline structure projected parallel to the (0001) plane; yellow: (SiO_4)-tetrahedra, green: planar (BO_3)-groups, purple: X-sites, red: Y-sites, orange: Z-sites, blue: V-and W-sites (representing O(3)- and O(1)-sites). From Simmons (2002), reproduced by permission of Litographie, LLC, East Hampton, CT, USA.

To understand the different schemes of isomorphic replacement within the oxydravite, dravite and uvite solid solution series discussed in this paper, it is helpful to consider the tourmaline structure in detail. A general summary is given in various textbooks and monographs (see, e.g., Dietrich, 1985; Deer *et al.*, 1986; Klein, 2002; Simmons, 2002).

The tourmaline structure (see above) consists of (Si_6O_{18})-rings of six edge-sharing (SiO_4)-tetrahedra, which are linked to planar (BO_3)-groups. These structural elements of silicon- and boron-polyhedra are linked to each other by different cations on X-, Y- and Z-sites of the tourmaline structure.

The X-site is coordinated by nine anions and the Y- and Z-sites are octahedrally coordinated. The Y-octahedron is somewhat larger than the Z-octahedron. In the present case, the X-site contains Na, Ca or vacancies, and the Y- and Z-sites are occupied by Mg and Al.

The formula unit of tourmaline contains 31 anions which are located at eight different lattice sites at the corners of the different coordination polyhedra of the tourmaline framework. Six of these eight different lattice sites contain only oxygen, and only two of these eight sites, designated O(1) and O(3), can also contain hydroxyl-groups and fluorine, (OH) and F.

The O(3)-sites, which are also designated as V-sites, can only contain oxygen and hydroxyl-groups, and the O(1)-sites, which are also designated W-sites, can contain oxygen, hydroxyl-groups and fluorine.

This is typical for members of the schorl-dravite series (see, e.g., Grice and Ercit, 1993; Bloodaxe *et al*., 1999). At the X-site, the sums of Na and Ca are consistently below the ideal maximum value of 1, which means that vacancies are present at this site.

As already mentioned, the main compositional variables in the five tourmalines are Na, Ca, Mg and Al.

For the X-site a negative correlation is found between the site occupancies of sodium and calcium (*Figure 3a*), and for the (Y+Z)-sites, a negative correlation is found between the site occupancies of magnesium and aluminium (*Figure 3b*). Comparing the site populations of cations between X and (Y+Z) polyhedra, positive correlations are observed between magnesium and calcium and between aluminium and sodium (*Figures 3c,d*), and there are negative correlations between magnesium and sodium and between aluminium and calcium. Vacancies on the X-site show a positive correlation with Al-contents and a negative correlation with Mg-contents (*Figures 3d* and *c*). These data indicate a coupled isomorphic replacement of four cations on X- and (Y+Z)-sites (*Figure 3e*) according to the scheme

$$(Na^{1+}+Al^{3+}) \leftrightarrow (Ca^{2+}+Mg^{2+}).$$

This heterovalent substitution scheme is similar to the known isomorphic replacement

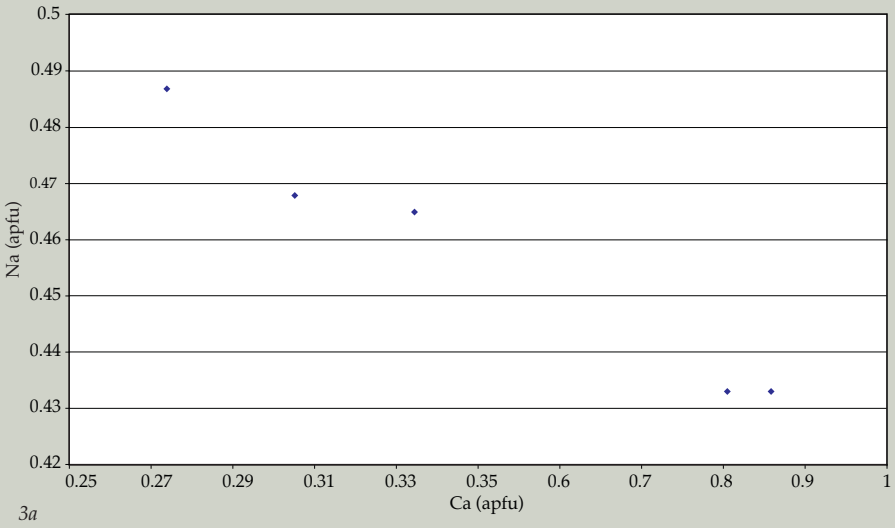

3a

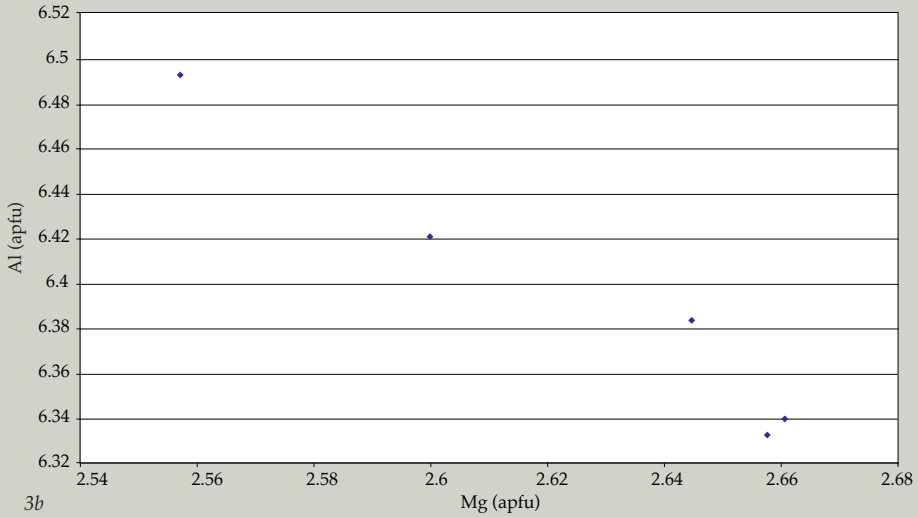

3b

Figure 3: *Correlation diagrams of site populations of various major components in X-, Y- and Z-sites of vanadium-bearing tourmalines from southern Madagascar.*

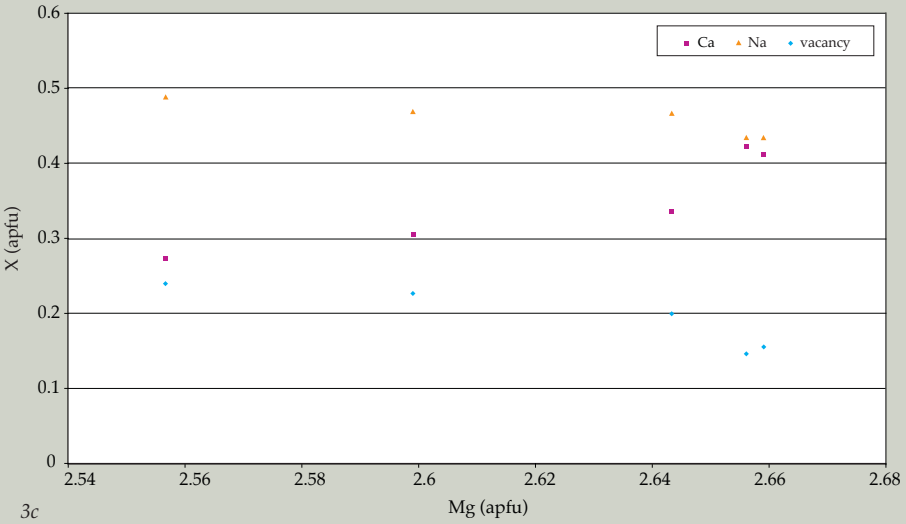
Ca
Na
vacancy
X (apfu)
Mg (apfu)
0.6
0.5
0.4
0.3
0.2
0.1
0
2.54
2.56
2.58
2.6
2.62
2.64
2.66
2.68

3c

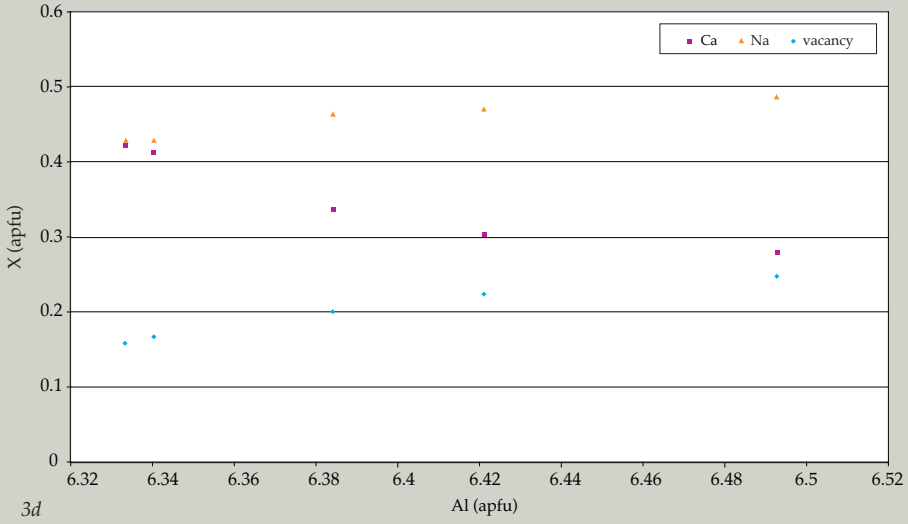
Ca
Na
vacancy
X (apfu)
Al (apfu)
0.6
0.5
0.4
0.3
0.2
0.1
0
6.32
6.34
6.36
6.38
6.4
6.42
6.44
6.46
6.48
6.5
6.52

3d

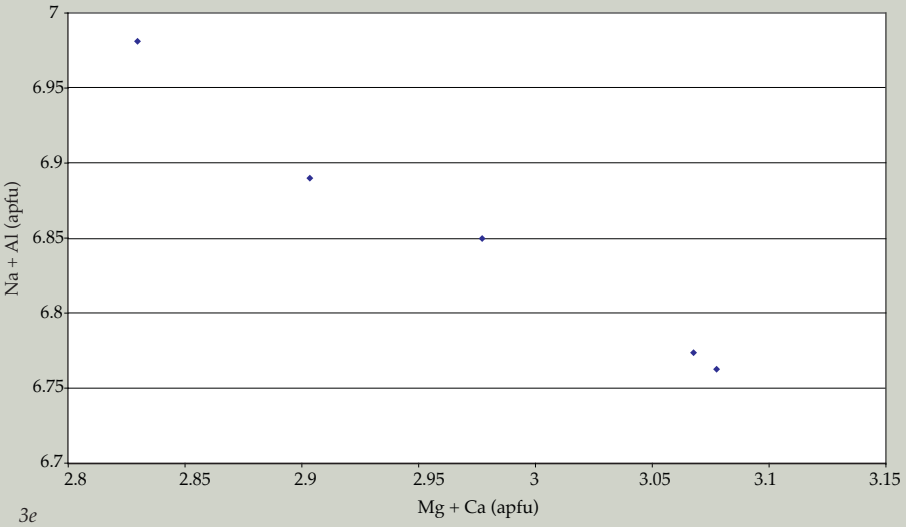
Na + Al (apfu)
Mg + Ca (apfu)
7
6.95
6.9
6.85
6.8
6.75
6.7
2.8
2.85
2.9
2.95
3
3.05
3.1
3.15

3e

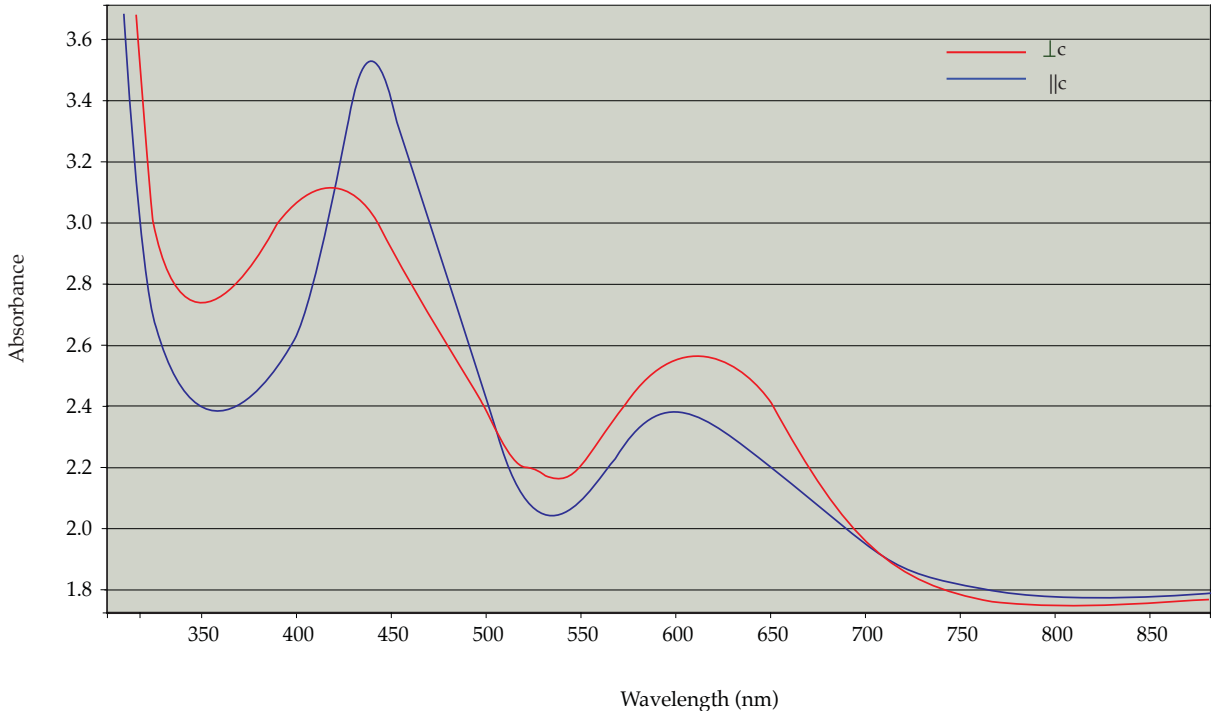

Figure 4: *Polarized UV-visible absorption spectrum of a vanadium-bearing, iron-free tourmaline from southern Madagascar.*

within the dravite – uvite solid solution series (for further details see Discussion and *Table V*).

An approximate, somewhat simplified formula (where traces of transition metals are omitted) for an average composition for the five analysed tourmaline crystals from Madagascar reads:

$$(Na_{0.4}Ca_{0.4}\square_{0.2})(Mg_{2.6}Al_{0.4})Al_6(BO_3)_3(Si_{5.9}Al_{0.1})O_{18}(OH_{3.25}F_{0.25}O_{0.5})$$

Spectroscopic properties and cause of colour

The absorption spectrum of the green vanadium-bearing tourmalines from Madagascar consists of two strong absorption bands with maxima at 599 and 441 nm in the spectrum parallel to *c* and maxima at 610 and 418 nm in the spectrum perpendicular to *c* (*Figure 4*). In some samples in addition to these major absorption bands, an additional shoulder is seen at 370 nm in the spectrum perpendicular to *c* (not shown in *Figure 4*).

This type of spectrum is consistent with the data reported in the literature for vanadium-bearing tourmaline from East Africa (Schmetzer, 1978, 1982); the stronger absorption bands were assigned to V^{3+} on octahedrally coordinated aluminium-sites (Z-sites) of the tourmaline structure.

The absorption bands of chromium in dravite occur at 588 and 417 nm, which are in the same spectral range as those of vanadium (Manning, 1969; Schmetzer, 1978; Nuber and Schmetzer, 1979; Halvorsen and Jensen, 1997; Simonet, 2000) and, thus, the two superimposed absorptions cannot be separated. Consequently, the colour of the green dravites from Madagascar is caused mainly by trivalent vanadium on aluminium sites, with some enhancement from the traces of chromium.

Features seen with the microscope, identification of inclusions

The tourmaline samples from Madagascar contain numerous, mostly irregularly shaped solid inclusions (*Figure 5*) as well as cavities with liquid and two-phase inclusions (liquid/gas). These two-phase inclusions were homogenized under microscopic illumination, i.e. the gas bubble disappeared after a slight increase of temperature. On cooling to room temperature, the gas bubbles reappeared and the inclusions were again two-phase. This type of reaction is characteristic for two-phase inclusions consisting of liquid and gaseous CO_2.

Table III: *Chemical composition of plagioclase inclusions in V-bearing tourmalines from Madagascar (data of samples A and C represent bytownite grains with high and low albite/anorthite contents, respectively; data of sample B represent a grain of intermediate composition).*

Microprobe analyses (wt.%)				Number of ions based on 8 O			
Inclusion	A	B	C	Inclusion	A	B	C
Na_2O	3.17	2.72	2.04	Na	0.283	0.242	0.183
K_2O	0.13	0.11	0.06	K	0.008	0.006	0.004
CaO	14.48	15.35	16.80	Ca	0.715	0.757	0.830
Al_2O_3	30.99	32.13	32.95	Al	1.683	1.743	1.790
SiO_2	49.98	48.92	47.59	Si	2.303	2.251	2.195
Total	98.75	99.23	99.44	Total	4.992	4.999	5.002

Table IV: *Chemical composition of fine-grained multiphase inclusions in V-bearing tourmalines from Madagascar (ranges, wt.%).*

	Hydrous aluminium silicates	Hydrous iron aluminium silicates[3]	Iron hydroxides
No. of analyses	4	5	5
SiO_2	46.34 – 60.03	43.96 – 63.73	1.38 – 2.81
TiO_2	0.01 – 0.07	0.02 – 0.04	0.09 – 0.19
Al_2O_3	26.21 – 35.95	9.21 – 23.06	2.67 – 3.20
Fe_2O_3[1]			76.39 – 77.21
FeO[2]	0.54 – 2.18	7.24 – 16.32	
MnO	0.01 – 0.11	0.01 – 0.16	0.02 – 0.10
MgO	0.29 – 0.72	1.35 – 3.58	0.30 – 0.37
CaO	0.09 – 0.40	0.28 – 0.78	0.33 – 0.47
Na_2O	0.09 – 0.41	0.16 – 0.29	0.10 – 0.15
K_2O	0.08 – 0.32	0.87 – 1.75	0.03 – 0.05

[1]Total iron as Fe_2O_3. [2]Total iron as FeO.
[3]Possibly a mixture of hydrous aluminium silicates and iron hydroxides.

For the identification of solid inclusions, Raman microspectroscopy of inclusions in faceted gems was combined with optical microscopy of polished thin sections and electron microprobe analyses of solids localized in these thin sections. In addition to optical microscopy in reflected and transmitted light, numerous back-scattered electron (BSE) images were obtained using the electron microprobe to evaluate homogeneity within included solids. This technique is very sensitive to compositional variations between the tourmaline host and its inclusions, and especially to compositional variations within non-homogeneous mineral grains. In addition, mineral grains in thin sections analysed by electron microprobe were also submitted to Raman microspectroscopy.

As a result, we were able to identify several minerals present as crystals with specific external forms or as single irregularly shaped mineral grains. In addition, non-homogenous inclusions consisting of several mineral phases within a single grain were also recorded.

a. Single mineral phases (Figures 5-8). Irregularly shaped plagioclase grains and euhedral quartz crystals are common inclusions. Numerous zircon crystals were also observed, frequently in close contact

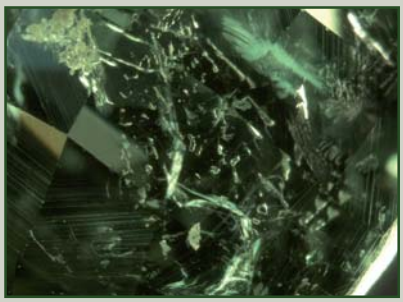

5a

5b

5c

5d

5e

5f

5g

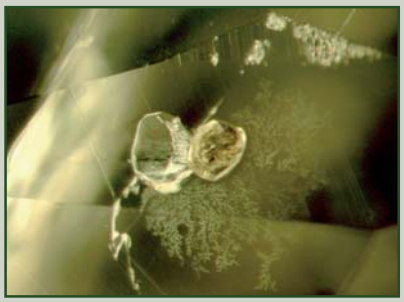

5h

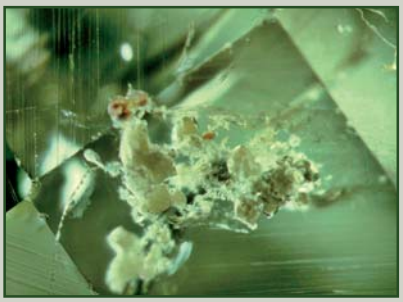

5i

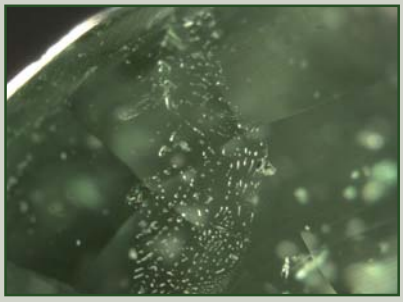

5j

5k

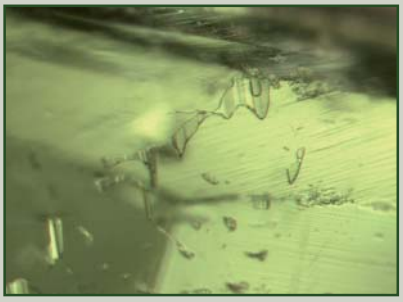

5l

Figure 5: *Inclusion patterns of vanadium-bearing tourmalines from Madagascar as seen with the gemmological microscope:* (a) *general overview with aggregate of irregularly shaped, non-homogeneous grains consisting of hydrous aluminium silicates and iron hydroxides (upper left), cavities with liquid and two-phase (liquid and gas) filling, 80×;* (b) *aggregate of irregularly shaped plagioclases, 40×;* (c) *aggregate of irregularly shaped plagioclases and black graphite platelet, 80×;* (d) *irregularly shaped plagioclase, 80×;* (e) *aggregate with quartzes, plagioclase and zircons with tension cracks, 60×;* (f) *euhedral zircon crystals with tension cracks, 80×;* (g) *euhedral quartz crystal (left) and black graphite (right), 80×;* (h) *quartz and xenotime (right), 80×;* (i) *aggregate of irregularly shaped, non-homogeneous grains consisting of hydrous aluminium silicates and iron hydroxides, 80×;* (j) *cavities with liquid and two-phase (liquid and gas) filling, 60×;* (k) *cavities with liquid and two-phase (liquid and gas) filling, 80×;* (l) *cavities with liquid and two-phase (liquid and gas) filling, 80×.*

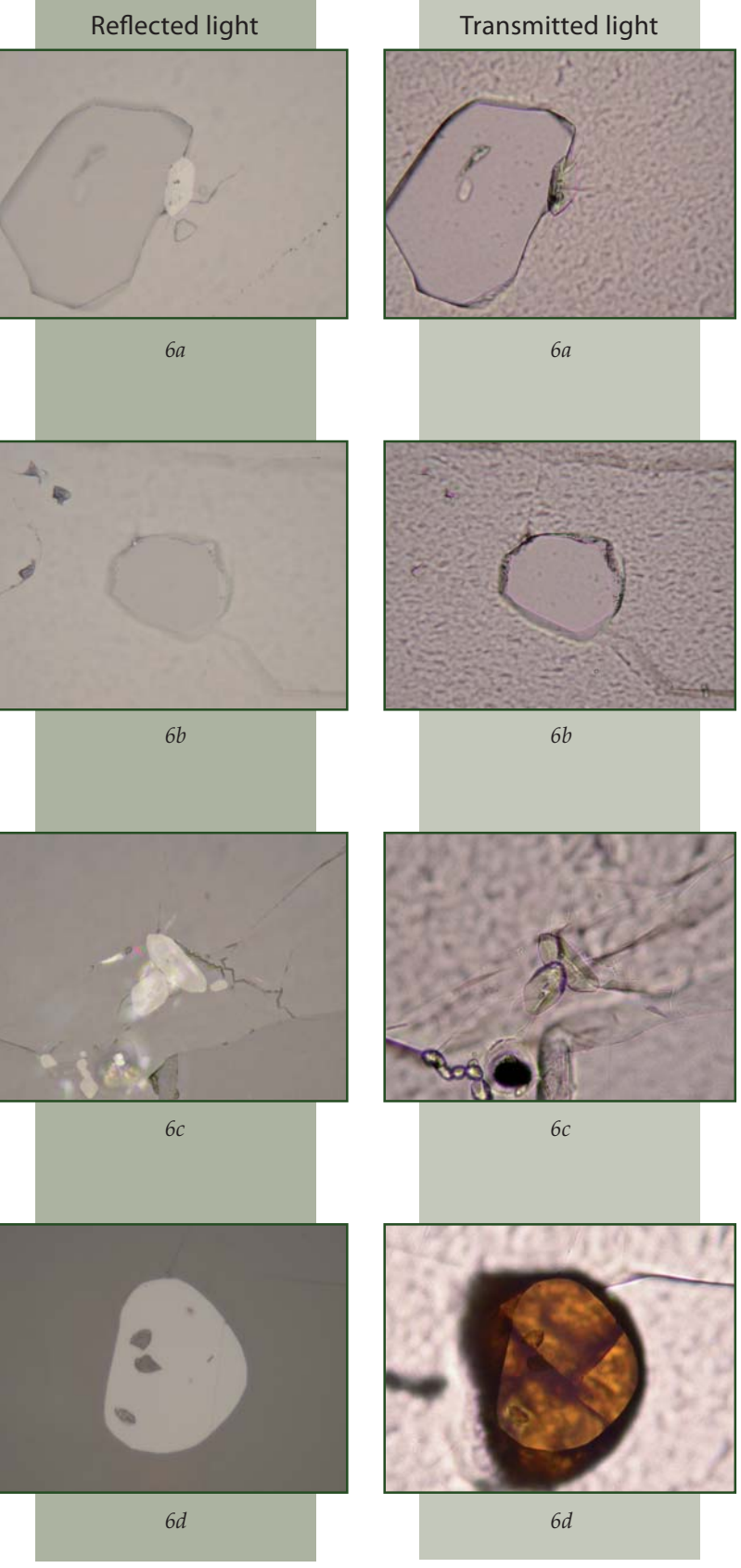

Figure 6: *Mineral inclusions in vanadium-bearing tourmalines from Madagascar as observed in polished thin sections in reflected (left column) and transmitted light (right column):* (a) *plagioclase and zircon, width of photo 0.35 mm;* (b) *quartz, width of photo 0.15 mm;* (c) *zircons, width of photo 0.15 mm;* (d) *rutile, width of photo 0.15 mm.*

with plagioclase or quartz grains. Less common are black graphite platelets, rutile and xenotime.

Quantitative analyses of 22 plagioclase grains in seven tourmaline host crystals were obtained and some representative analyses are given in *Table III.* All plagioclases represent a continuous compositional range from albite$_{28.4\%}$ anorthite$_{71.6\%}$ to albite$_{18.1\%}$anorthite$_{81.9\%}$, i.e. all analysed plagioclase grains are in the compositional range of bytownite.

b. *Non-homogeneous inclusions (Figures 5 and 9).* Fine-grained admixtures of several minerals are present in off-white to pale yellow, irregularly shaped grains in many tourmalines. In thin sections, they are visible as intensely intergrown colourless to off-white and reddish-brown phases (*Figure 9*), but were too small to identify unambiguously.

Quantitative microprobe analyses of several small to extremely small particles (*Table IV)* indicated that they are:

- hydrous Al-silicates, most probably clay minerals such as kaolinite (off-white to colourless component) and
- Fe-hydroxides with smaller amounts of Al and Si, most probably limonitic iron hydroxides (reddish-brown component)

Several grains or phases contain iron, aluminium, and silicon as major components, with smaller amounts of magnesium and potassium (*Table IV*). However, we were unable, even by a combination of quantitative electron microprobe analyses and Raman spectroscopy of the same grains to clarify if these inclusions represent

- hydrous Fe-Al-silicates which are admixtures of the two phases specified above, namely hydrous Al-silicates and Fe-hydroxides, or
- hydrous Fe-Al-silicates which are separate mineral species.

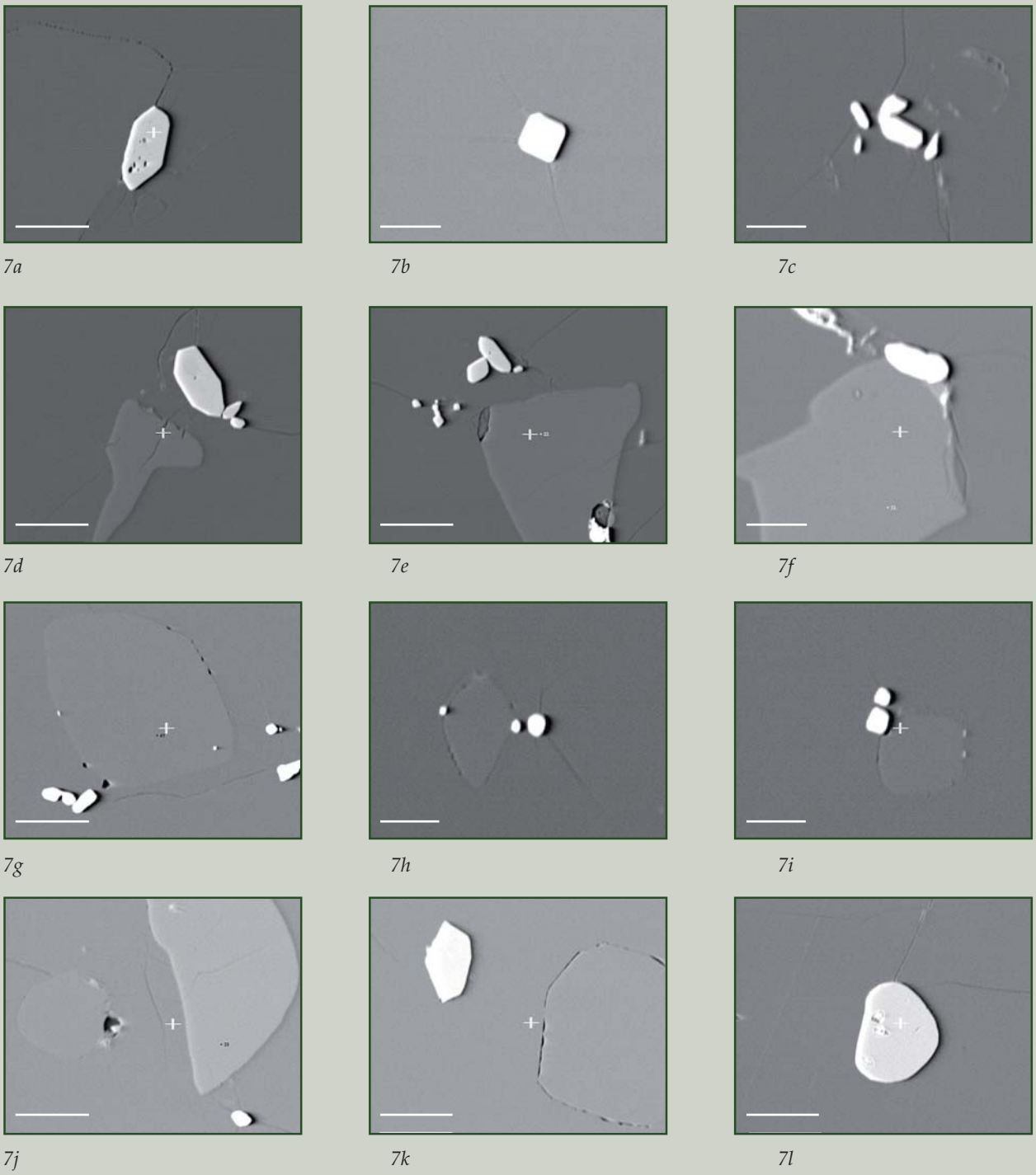

7a 7b 7c

7d 7e 7f

7g 7h 7i

7j 7k 7l

Figure 7: *Back-scattered electron (BSE) images of mineral inclusions in vanadium-bearing tourmalines from Madagascar as observed in polished thin sections: (upper row) zircons; (second row) plagioclases and zircons; (third row) quartzes and zircons; (lower row) plagioclase, quartz and zircon (left), quartz and rutile (centre), rutile (right). Zircons and rutiles show bright electron images. The bars at the bottom left of the images represent 50 µm in a, d, e, g, j, k and l, and 20 µm in b, c, f, h and i.*

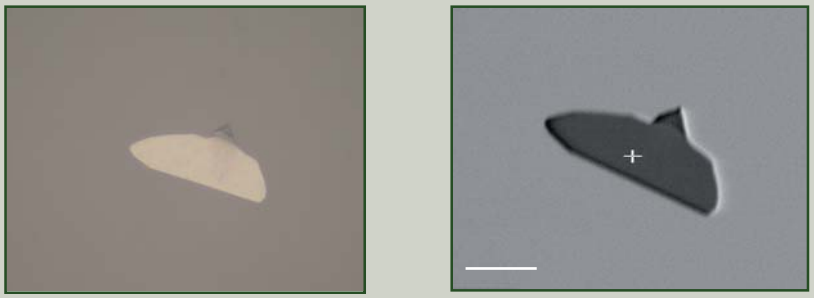

8a 8b

Figure 8: *Inclusion of graphite (bright) in reflected light (a, width of photo 0.15 mm) and back-scattered electron (BSE) image of graphite (dark) (b, the bar at the bottom left of the image represents 20 µm) in vanadium-bearing tourmaline from Madagascar.*

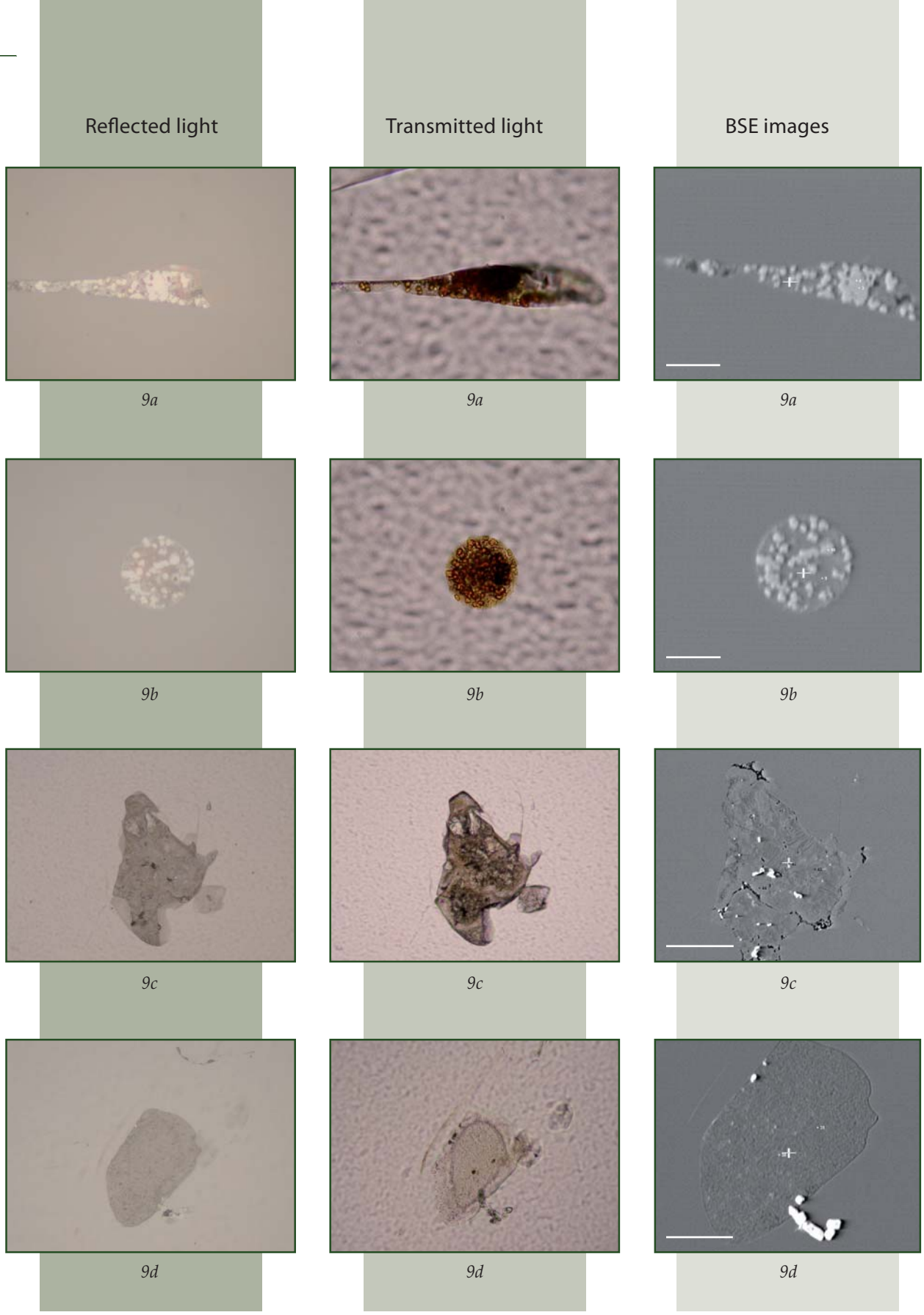

Figure 9: *Non-homogeneous mineral grains in vanadium-bearing tourmalines from Madagascar as observed in polished thin sections in reflected (left), in transmitted light (middle) and as back-scattered electron (BSE) images of the same grains (right). In the two grains pictured in 9a and 9b, iron hydroxides are dominant and hydrous aluminium silicates are subordinate mineral phases (width of all four photos 0.15 mm, the bars at the bottom left of the BSE images represent 20 µm). In the two grains pictured in 9c and 9d, hydrous aluminium silicates are dominant and iron hydroxides are subordinate mineral phases (width of all four photos 0.35 mm, the bars at the bottom left of the BSE images represent 100 µm in 9c and 50 µm in 9d).*

Table V: *Properties of some magnesium-bearing gem quality tourmalines from East Africa and Madagascar.*

Locality	Analysed samples	Colour	V_2O_3 (wt.%)	Cr_2O_3 (wt.%)	FeO[a] (wt.%)	Al (apfu)	Mg (apfu)	Designation
Landanai, Tanzania[1]	3	pale green to intense green	0.14 – 0.30	nd	nd	<6	>3	uvite
Gerevi Hills, Tanzania[1]	3	pale brown or green	0.11 – 0.36	nd	nd to 0.10	>6	<3	calcic aluminous dravite
Umba Valley, Tanzania[1]	1	green	0.44	0.15	nd	>6	<3	calcic aluminous dravite
Kwale District, Kenya[1]	4	green to intense green	1.78-4.03	nd to 0.55	nd	>6	<3	calcic aluminous dravite
Tsavo Park, Kenya[1]	1	green	0.08	0.53	0.02	>6	<3	calcic aluminous dravite
Lualenyi, Kenya[1]	1	brownish green	0.37	nd	0.17	>6	<3	calcic aluminous dravite
Voi-Taveta area, Kenya[2]	4	yellow	nd	nd	nd	>6	<3	calcic aluminous dravite
Lelatema (?), Tanzania[3]	2	green	0.04 – 0.06	0.36 – 0.64	nd	>6	<3	calcic aluminous dravite
East Africa[4]	9	pale green to intense green	0.18 – 1.54	0.03 – 0.17	nd	<6	>3	uvite
Umba Valley, Tanzania[5]	2	green	0.05	0.22 – 0.34	nd to 0.06	>6	<3	calcic aluminous dravite
Yellow Mine, Taita-Taveta District, Kenya[6]	4	yellow, green, blue green	nd to 0.03	0.01 – 0.43	nd to 0.03	>6 6	<3 3	calcic aluminous dravite calcic dravite
John Saul Mine, Taita-Taveta District, Kenya[6]	2	yellow green, yellow pink	0.01 – 0.14	0.06 – 0.09	0.07 – 0.92	>6	<3	calcic aluminous dravite
Mukongonyi, Taita-Taveta District, Kenya[6]	1	yellow brown	0.01	0.06	0.17	>6	<3	calcic aluminous dravite
Kavungu Mine, Jivunda, Zambia[7]	2	green	0.28 – 0.35	0.06 – 0.15	nd – 0.01	<6	>3	uvite
Southern Madagascar[8]	5	green	0.17 – 0.20	0.03 – 0.11	0. 01 – 0.02	>6	<3	calcic aluminous dravite

[a] Total iron as FeO. apfu = atoms per formula unit. nd = not detected.
[1] Schmetzer *et al*. (1979). [2] Hänni *et al*. (1981). [3] Bank and Henn (1988). [4] MacDonald and Hawthorne (1995).
[5] Halvorsen and Jensen (1997). [6] Simonet (2000). [7] Hainschwang *et al*. (2007). [8] this paper.

Discussion

Properties of magnesium-bearing tourmalines from East Africa, Zambia and Madagascar

Magnesium-bearing gem-quality tourmalines have been described from different localities in East Africa and recently also from Zambia (see *Table V*). On the basis of colour-causing trace elements, we can divide such tourmalines into three groups:

a. those samples with vanadium concentrations up to 4.03 wt.% V_2O_3, with distinctly smaller or no chromium content. According to our analytical results, the gem material from Madagascar belongs to this group.
b. a second group of localities supplied tourmalines with higher chromium than vanadium contents. The highest chromium content reported to date has been 0.64 wt.% Cr_2O_3.

The colour intensity of any tourmaline

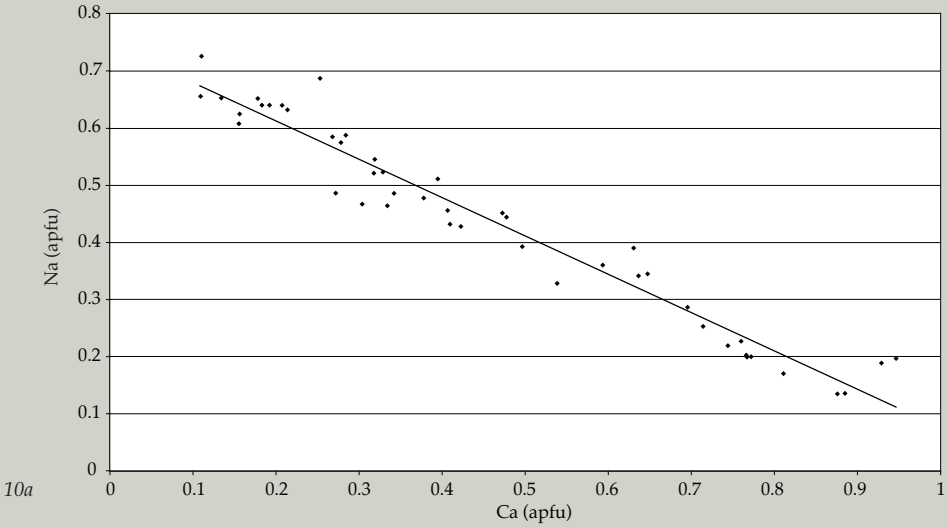

10a

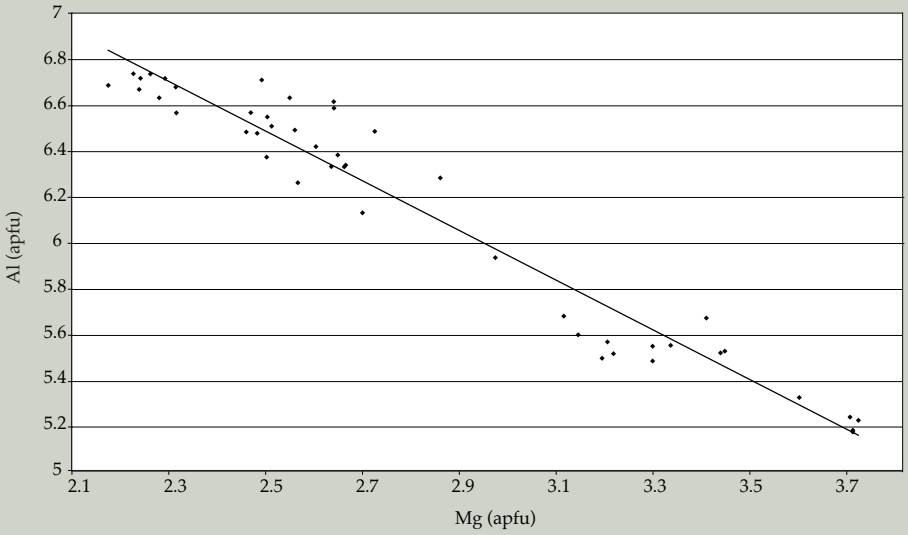

10b

Figure 10: *Correlation diagrams of site populations of various major components in X-, Y- and Z-sites of magnesium-bearing gem quality tourmalines from East Africa, Zambia and southern Madagascar; the diagrams are based on 37 analyses of tourmalines from East Africa, four analyses of tourmalines from Zambia and five analyses of tourmalines from southern Madagascar.*

10c

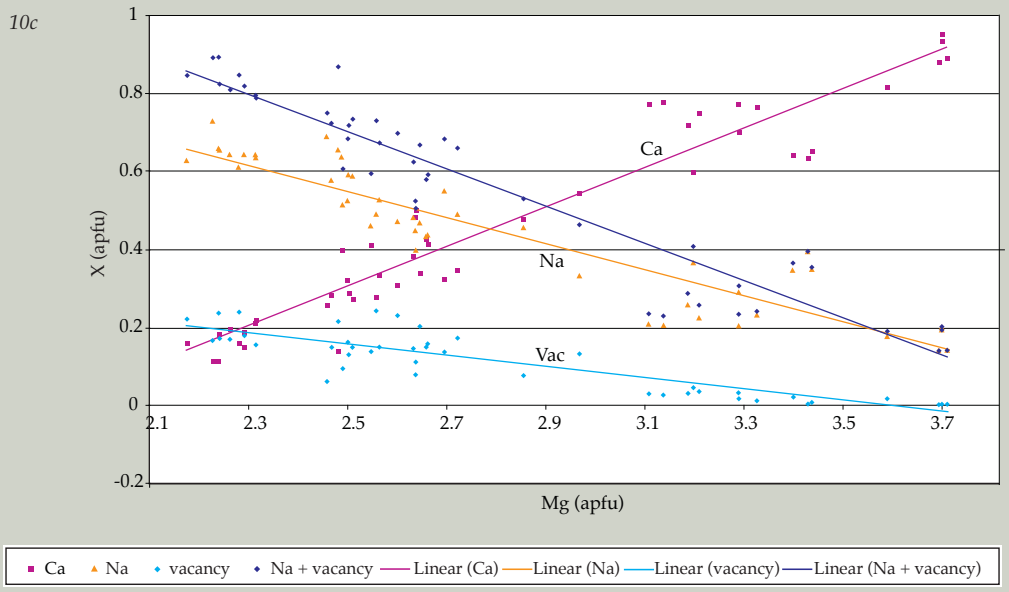
X (apfu)
Mg (apfu)
Ca
Na
Vac
Ca
Na
vacancy
Na + vacancy
Linear (Ca)
Linear (Na)
Linear (vacancy)
Linear (Na + vacancy)

10d

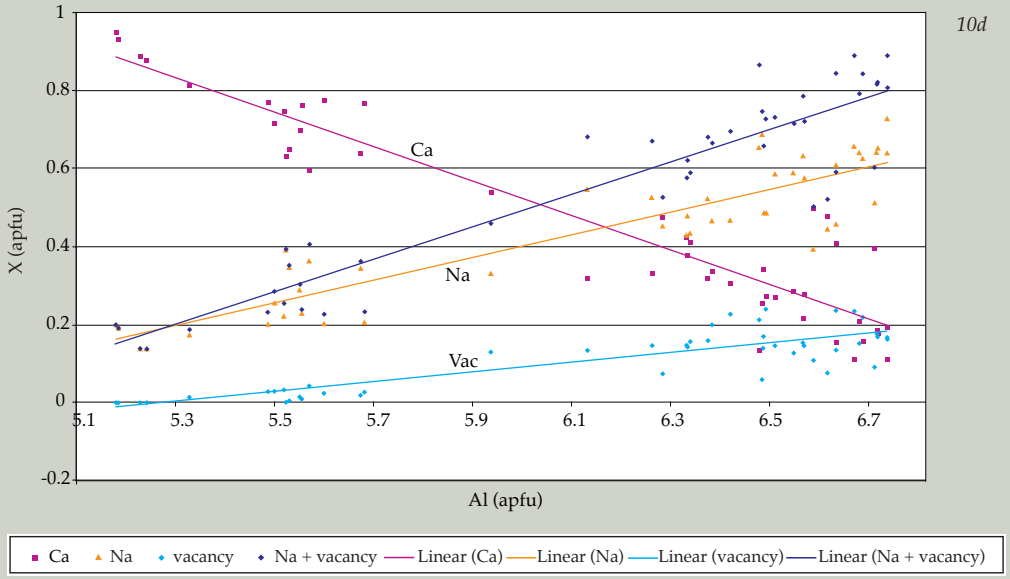
X (apfu)
Al (apfu)
Ca
Na
Vac
Ca
Na
vacancy
Na + vacancy
Linear (Ca)
Linear (Na)
Linear (vacancy)
Linear (Na + vacancy)

10e

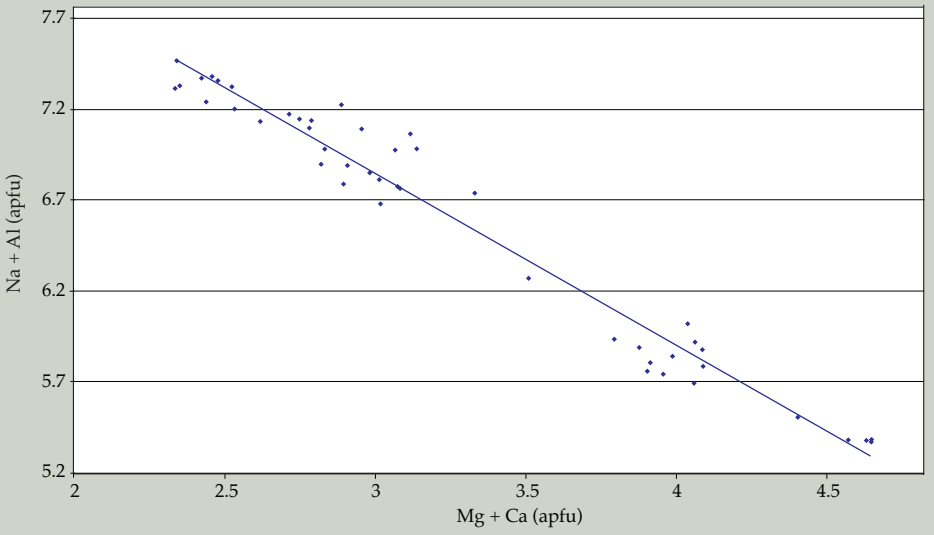
Na + Al (apfu)
Mg + Ca (apfu)

from either group is directly related to its vanadium or chromium contents.

c. In those tourmalines with vanadium or chromium and additional small iron and/or titanium contents, brownish green or brown colours may also be observed. Tourmalines with small iron and/or titanium contents, but without vanadium or chromium, are yellow, yellowish brown or brown.

The samples of all three groups with different coloration mentioned above, i.e. with V>Cr or with Cr>V or with Fe and/or Ti (without V or Cr), are sodium- and calcium-bearing, magnesium-rich aluminium tourmalines.

All these magnesium-bearing tourmalines show variation in their Na, Ca, Mg and Al contents and correlation diagrams have been plotted for the five samples from Madagascar, 37 analysed tourmalines from various literature references in East Africa and four samples from Zambia (see again *Table V*). In *Figure 10a*, there is a clear negative correlation between the site occupancies of sodium and calcium (X-site), and for the (Y+Z)-sites, there is also a negative correlation between the site occupancies of magnesium and aluminium (*Figure 10b*). Comparing the site populations of cations between X and (Y+Z) polyhedra, there are positive correlations between magnesium and calcium and between aluminium and sodium (*Figure 10 c,d*), and negative correlations between magnesium and sodium and between aluminium and calcium (*Figure 10 c,d*). Vacancies on the X-site show a positive correlation with Al-contents and a negative correlation with Mg-contents (*Figure 10 c,d*). These trends are also observed if we compare the sum of sodium and vacancies (Na + vacancy) with magnesium, calcium and aluminium (*Figure 10 c,d*). All these data indicate a coupled replacement of sodium or (sodium + vacancies) and aluminium by calcium and magnesium (*Figure 10e*).

This substitution is heterovalent and is the same as the known isomorphic replacement within the dravite $NaMg_3Al_6(BO_3)_3Si_6O_{18}(OH)_4$ – uvite $CaMg_3(MgAl_5)(BO_3)_3Si_6O_{18}(OH)_4$ solid solution series, which is represented by the scheme $(Na^{1+}+Al^{3+}) \leftrightarrow (Ca^{2+}+Mg^{2+})$.

The magnesium-bearing calcic tourmalines can be subdivided into two population fields. A first subgroup with Al<6 and Mg>3 apfu (atoms per formula unit), is consistent with the traditionally accepted composition and formula of uvite. A second subgroup consists of tourmalines, also with distinct calcium contents, but with Al>6 and Mg<3 apfu. The material from Madagascar belongs to this second subgroup, the samples of which can be designated as calcic aluminous dravites. Only one calcium-bearing sample (from the Yellow Mine, Kenya) had Mg-contents of 3 as well as Al-contents of 6 apfu and can be designated as calcic dravite. So far, no calcium-free dravites have been analysed from the different localities in East Africa, Zambia and Madagascar (see again *Table V*), neither within the bright green, vanadium- or chromium-bearing, nor within the yellow to brown, low-iron gem tourmalines. Vacancies on X-sites are more abundant in the group with Al>6 (aluminous dravites) than in the group with Al<6 (uvites) where they are fewer or almost negligible.

According to Henry and Guidotti (1985), tourmalines of the two subgroups mentioned above originate from two different types of host rocks:

a. tourmalines with Al<6 and Mg>3 apfu (uvites) originate from metacarbonates and meta-pyroxenites
b. tourmalines with Al>6 and Mg<3 (aluminous dravites) mainly originate from low-Ca meta-ultramafics and Cr,V-rich metasediments, but they also come from metapelites and metapsammites which may or may not coexist with an Al-saturating phase.

The different genetic origins of tourmalines of the two subgroups may well be the cause of their differences in composition.

Comparing the chemical compositions of gem-quality magnesium-bearing tourmalines from East Africa, Zambia and Madagascar with the formulae of different tourmaline end-members as proposed by Hawthorne and Henry (1999), we only have to consider the formulae and isomorphic replacement schemes of lithium- and iron-free members of the rather complex tourmaline solid solution series (*Table VI*). For a more detailed

Table VI: *Formulae of iron- and lithium-free tourmaline end-members and isomorphic replacement schemes.*

Formulae of tourmaline end-members[1]

Name (see box)	X-site	Y-site	Z-site	T	B	V	W
Dravite	Na	Mg_3	Al_6	Si_6O_{18}	$(BO_3)_3$	$(OH)_3$	(OH)
Oxy-dravite*	Na	Mg_2Al	Al_6	Si_6O_{18}	$(BO_3)_3$	$(OH)_3$	O
Olenite	Na	Al_3	Al_6	Si_6O_{18}	$(BO_3)_3$	O_3	(OH)
Uvite	Ca	Mg_3	$MgAl_5$	Si_6O_{18}	$(BO_3)_3$	$(OH)_3$	(OH)
Oxy-uvite*	Ca	Mg_3	Al_6	Si_6O_{18}	$(BO_3)_3$	$(OH)_3$	O
Calcic magnesium-foitite*	$Ca_{0.5}\,\square_{0.5}$	Mg_3	Al_6	Si_6O_{18}	$(BO_3)_3$	$(OH)_3$	(OH)
Magnesium-foitite*	$\square$	Mg_2Al	Al_6	Si_6O_{18}	$(BO_3)_3$	$(OH)_3$	(OH)

Isomorphic replacement schemes[1]

End-member	Dominant replacement scheme	End-member
Oxy-dravite*	$Al^{3+} + O^{2-} \leftrightarrow Mg^{2+} + (OH)^-$	Dravite
Oxy-uvite*	$Al^{3+} + O^{2-} \leftrightarrow Mg^{2+} + (OH)^-$	Uvite
Olenite	$Al^{3+} + O^{2-} \leftrightarrow Mg^{2+} + (OH)^-$	Dravite
Dravite	$Na^+ + Al^{3+} \leftrightarrow Ca^{2+} + Mg^{2+}$	Uvite
Oxy-dravite*	$Na^+ + Al^{3+} \leftrightarrow Ca^{2+} + Mg^{2+}$	Oxy-uvite*
Dravite	$Na^+ + (OH)^- \leftrightarrow Ca^{2+} + O^{2-}$	Oxy-uvite*
Dravite	$Na^+ \leftrightarrow 0.5\,Ca^{2+} + 0.5\,\square$	Calcic magnesium-foitite*
Oxy-dravite*	$Na^+ + O^{2-} \leftrightarrow \square + (OH)^-$	Magnesium-foitite*

* Hypothetical end-members. [1]The symbol $\square$ represents vacancies on X-sites.

discussion of possible Na,Ca substitution schemes in iron-bearing aluminium tourmalines, the reader is referred to the papers of Burt (1989), Henry and Dutrow (1990), Hawthorne (1996) as well as Hawthorne and Henry (1999).

It is evident that the tourmalines from East Africa, Zambia and southern Madagascar are sodium-calcium aluminium-magnesium tourmalines with the number of aluminium atoms per formula unit between 7 and 5 [7>Al(apfu)>5] and the number of magnesium atoms per formula unit between 2 and 4 [2<Mg(apfu)<4] . Sodium and calcium, on the other hand, both vary between 1 and 0 apfu. This is the known compositional range for Mg-bearing tourmalines, samples with Mg <2 apfu (compositional miscibility gap between oxy-dravite and olenite) or with Mg>4 apfu are extremely rare or unknown (see, e.g., Dunn, 1977; Dunn *et al*., 1977; Foit and Rosenberg, 1979). Consequently, the tourmalines are members of a solid solution series between the end-members oxy-dravite, $Na(Mg_2Al)Al_6(BO_3)_3Si_6O_{18}(OH)_3O$, and uvite, $CaMg_3(MgAl_5)(BO_3)_3Si_6O_{18}(OH)_4$. It is important to underline, that within the two end-members of this series, 1 Na apfu is replaced by 1 Ca apfu, and, in addition, 2 Al apfu are replaced by 2 Mg apfu. Charge balance within this series is maintained by dehydroxylation.

For this solid solution series the isomorphic replacement scheme does not correspond to any common replacement schemes between dravite and other magnesium-bearing tourmaline end-members given in *Table VI*. However, by a combination of the schemes oxy-dravite – dravite (identical with oxy-uvite – uvite): $Al^{3+} + O^{2-} \leftrightarrow Mg^{2+} + (OH)^-$ and dravite – uvite (identical with oxy-dravite – oxy-uvite): $Na^+ + Al^{3+} \leftrightarrow Ca^{2+} + Mg^{2+}$ we can derive an isomorphic replacement scheme between the

end-members oxy-dravite – uvite as follows:

$Na^{+} + 2Al^{3+} + O^{2-} \leftrightarrow Ca^{2+} + 2Mg^{2+} + (OH)^{-}$.

This scheme is dominant for the tourmaline solid solution series oxy-dravite – uvite and represents the compositional variability observed for the gem material from East Africa, Zambia and southern Madagascar.

In detail, to explain the average composition of our samples from Madagascar, $(Na_{0.4}Ca_{0.4}\square_{0.2})(Mg_{2.6}Al_{0.4})Al_6(BO_3)_3(Si_{5.9}Al_{0.1})O_{18}(OH_{3.25}F_{0.25}O_{0.5})$ and starting from a tourmaline end-member with oxy-dravite composition, the first substitution is in the oxy-dravite – uvite series: 0.3Na + 0.6Al + 0.3O → 0.3Ca + 0.6Mg + 0.3(OH) (*Table VI*, lower box, rows 5 and 2).

To derive the vacancies in the X-site, we have to add two further substitutions, which are formally represented by the series dravite – calcic magnesium-foitite and oxy-dravite – magnesium-foitite (*Table VI*, lower box, rows 7 and 8), which for the Madagascar tourmalines translates to:

0.2Na → 0.1Ca + 0.1□

and 0.1Na + 0.1 O → 0.1□ + 0.1(OH)

where the symbol □ indicates vacancies on X-sites. These three substitutions sum as follows:

0.6Na + 0.6Al + 0.4O → 0.4Ca + 0.2□ + 0.6Mg + 0.4(OH)

To complete the explanation of the composition of the Madagascar tourmalines, we have to consider the replacement of a small fraction of silicon by aluminium according to: $Si^{4+} + O^{2-} \rightarrow Al^{3+} + (OH)^{-}$, in the present case 0.1Si + 0.1O → 0.1Al + 0.1(OH).

Summary

The green gem-quality tourmalines from southern Madagascar are calcic aluminous dravites with limited compositional variability consisting mainly of coupled isomorphic replacement between (Na,Al) and (Ca,Mg), and vacancies on X-sites. The tourmalines are essentially iron- and lithium-free, but contain small amounts of vanadium and chromium, with $V_2O_3 > Cr_2O_3$ which is the cause of the green coloration.

Common solid inclusions are plagioclase (with a compositional variability within the bytownite field), quartz and zircon.

Irregularly shaped grains consist of a mixture of at least two minerals, namely hydrous aluminium silicates and iron hydroxide. We were unable to confirm whether more mineral phases – perhaps hydrous iron aluminium silicates – may be present within this admixture. Isolated cavities and healed fractures containing liquid and two-phase inclusions (liquid and gas) are also common.

Acknowledgements

The authors are grateful to Dr H. Graetsch, Ruhr-University Bochum, Germany, for the determination of the unit cell dimensions of sample D by X-ray diffraction. Prof. Dr Thomas Pettke, University of Bern, Switzerland, was helpful with the analysis of our samples by mass spectroscopy.

References

Bank, H., and Henn, U., 1988. Colour-changing chromiferous tourmalines from East Africa. *Journal of Gemmology*, 21 (2), 102-3

Bloodaxe, E.S., Hughes, J.M., Dyar, M.D., Grew, E.S., and Guidotti, C.V., 1999. Linking structure and chemistry in the schorl-dravite series. *American Mineralogist*, 84, 922-8

Burt, D.M., 1989. Vector representation of tourmaline compositions. *American Mineralogist*, 74, 826-39

Da Fonseca-Zang, W.A., Zang, J.W., and Hofmeister, W., 2001. Die Mg-Verteilung in der Turmalinstruktur. *Berichte der Deutschen Mineralogischen Gesellschaft, Beihefte zum European Journal of Mineralogy*, 13, No.1, 36

Deer, W.A., Howie, R.A., and Zussman, J., 1986. *Rock-forming minerals. Vol. 1B, 2nd Edition, Disilicates and Ring Silicates.* Longman Scientific & Technical, Harlow

Dietrich, R.V., 1985. *The tourmaline group.* Van Nostrand Reinhold Company Inc., New York

Dirlam, D.M., Laurs, B.M., Pezzotta, F., and Simmons, W.B., 2002. Liddicoatite tourmaline from Anjanabonoina, Madagascar. *Gems & Gemology*, 38 (1), 28-53

Dunn, P.J., 1977. Uvite, a newly classified gem tourmaline. *Journal of Gemmology*, 15 (6), 300-8

Dunn, P.J., Appleman, D., Nelen, J.A., and Norberg, J., 1977. Uvite, a new (old) common member of the tourmaline group and its implications for collections. *The Mineralogical Record*, 8(2), 100-8

Ertl, A., Hughes, J.M., Brandstätter, F., Dyar, M.D., and Prasad, P.S.R., 2003. Disordered Mg-bearing olenite from a granitic pegmatite at Gaslarn, Austria: a chemical, structural, and infrared spectroscopic

study. *Canadian Mineralogist*, 41, 1363-70
Foit, F.F. Jr., and Rosenberg, P.E., 1979. The structure of vanadium-bearing tourmaline and its implications regarding tourmaline solid solutions. *American Mineralogist*, 64, 788-98
Grice, J.D., and Ercit, T.S., 1993. Ordering of Fe and Mg in the tourmaline crystal structure: the correct formula. *Neues Jahrbuch für Mineralogie Abhandlungen*, 165 (3), 245-66
Hainschwang, T., Notari, F., and Anckar, B., 2007. Trapiche tourmaline from Zambia. *Gems & Gemology*, 43 (1), 36-46
Halvorsen, A., and Jensen, B.B., 1997. A new colour-change effect. *Journal of Gemmology*, 25 (5), 325-30
Hänni, H.A., Frank, E., and Bosshart, G., 1981. Golden yellow tourmaline of gem quality from Kenya. *Journal of Gemmology*, 17 (7), 437-42
Hawthorne, F.C., 1996. Structural mechanisms for light-element variations in tourmaline. *Canadian Mineralogist*, 34, 123-32
Hawthorne, F.C., and Henry, D.J., 1999. Classification of the minerals of the tourmaline group. *European Journal of Mineralogy*, 11, 201-15
Hawthorne, F.C., MacDonald, D.J., and Burns, P.C., 1993. Reassignment of cation site occupancies in tourmaline: Al-Mg disorder in the crystal structure of dravite. *American Mineralogist*, 78, 265-70
Henry, D.J., and Dutrow, B.L., 1990. Ca substitution in Li-poor aluminous tourmaline. *Canadian Mineralogist*, 28, 111-24
Henry, D.J., and Guidotti, C.V., 1985. Tourmaline as a petrogenetic indicator mineral: an example from the staurolite-grade metapelites of NW Maine. *American Mineralogist*, 70, 1-15
Keller, P.C., 1992. *Gemstones of East Africa*. Geoscience Press, Phoenix, Arizona
Klein, C., 2002. *Mineral Science. 22nd Edn.* John Wiley & Sons Inc., New York
MacDonald, D.J., and Hawthorne, F.C., 1995. The crystal chemistry of Si ↔ Al substitution in tourmaline. *Canadian Mineralogist*, 33, 849-58
Manning, P.G., 1969. Optical absorption spectra of chromium-bearing tourmaline, black tourmaline and buergerite. *Canadian Mineralogist*, 10, 57-70
Marschall, H.R., Ertl, A., Hughes, J.M., and McCammon, C., 2004. Metamorphic Na- and OH-rich disordered dravite with tetrahedral boron, associated with omphacite, from Syros, Greece: chemistry and structure. *European Journal of Mineralogy*, 16, 817-23
Mercier, A., Moine, B., Delorme, J., and Rakotondrazafy, M.A.F., 1997. A note on a new occurrence of vanadian grossular garnet from Madagascar. *Journal of Gemmology*, 25 (6), 391-3
Novák, M., Povondra, P., and Selway, J.B., 2004. Schorl-oxy-schorl to dravite-oxy-dravite tourmaline from granitic pegmatites; examples from the Moldanubicum, Czech Republic. *European Journal of Mineralogy*, 16, 323-33
Nuber, B., and Schmetzer, K., 1979. Die Gitterposition des Cr^{3+} im Turmalin: Strukturverfeinerung eines Cr-reichen Mg-Al-Turmalins. *Neues Jahrbuch für Mineralogie Abhandlungen*, 137 (2), 184-97
Pertlik, F., Ertl, A., Körner, W., Brandstätter, F., and Schuster, R., 2003. Na-rich dravite in the marbles from Friesach, Carinthia, Austria: chemistry and crystal structure. *Neues Jahrbuch für Mineralogie Monatshefte*, 2003 (6), 277-88
Pezzotta, F., 2001. *Madagascar. A mineral and gemstone paradise*. extraLapis English No. 1, Lapis International, LLC, East Hampton, CT
Pieczka, A., 1999. Statistical interpretation of structural parameters of tourmalines: the ordering of ions in the octahedral sites. *European Journal of Mineralogy*, 11, 243-51
Schmetzer, K., 1978. *Vanadium III als Farbträger bei natürlichen Silikaten und Oxiden – ein Beitrag zur Kristallchemie des Vanadiums*. Thesis, University of Heidelberg
Schmetzer, K., 1982. Absorptionsspektroskopie und Farbe von V^{3+}-haltigen natürlichen Oxiden und Silikaten – ein Beitrag zur Kristallchemie des Vanadiums. *Neues Jahrbuch für Mineralogie Abhandlungen*, 144 (1), 73-106
Schmetzer, K., Nuber, B., and Abraham, K., 1979. Zur Kristallchemie Magnesium-reicher Turmaline. *Neues Jahrbuch für Mineralogie Abhandlungen*, 136 (1), 93-112
Schmetzer, K., and Bank, H., 1979. East African tourmalines and their nomenclature. *Journal of Gemmology*, 16 (5), 310-11
Simmons, W.B., 2002. The tourmaline group. In: *Tourmaline. A gemstone spectrum*. extraLapis English No. 3, pp. 10-23. Lapis International, LLC, East Hampton, CT
Simonet, C., 2000. Geology of the Yellow Mine (Taita-Taveta District, Kenya) and other yellow tourmaline deposits in East Africa. *Journal of Gemmology*, 27 (1), 11-29
Simonet, C., 2006. Les tourmalines magnésiennes d'Afrique de l'Est. *Revue de Gemmologie*, No. 157, 4-7

Clarification of measurement of the RIs of biaxial gemstones on the refractometer

B. Darko Sturman
Curator Emeritus, Natural History Department,
Royal Ontario Museum, Ontario, Canada

Abstract: *All possible refractometer observations on biaxial gemstones can be represented by four patterns shown in diagrams where RIs are plotted on the vertical axis and rotation angles on the horizontal axis. New understanding of the behaviour of biaxial gemstones on the refractometer is based on calculated movements of shadow edges for many different orientations of the optical elements and the gem table or a gem facet.*

Keywords: *biaxial gemstones, gem identification, refractive index calculations, refractometer*

Introduction

The refractometer is one of the oldest and the most reliable gemmological instruments and it is still the central instrument of many gemmologists. Modern refractometers are an improvement over older instruments as they have better optics and a larger scale that allows more precise readings, but the most important improvement is the availability of monochromatic light in small, battery-operated units that can be taken anywhere.

The great majority of gem identifications are based on determination of the minimum and the maximum refractive indices (RIs) that can be easily and accurately determined on any gemstone with well polished facets regardless of its optical orientation. Additional tests or procedures in identification are required only for those gemstones that show an overlap in their RIs with other gemstones. In these cases, a determination of the optic character or the optic sign is needed and this may be accomplished with the help of the polarizing filter.

However, many gemmologists have been reluctant to learn and apply this method, and many alternative methods based on observations without using the polarizing filter have been proposed and are described in gemmological textbooks and teaching manuals. These methods could not be comprehensively tested because of the limited understanding of the behaviour of biaxial gemstones on the refractometer and some of them may be incomplete, confusing or may even lead to incorrect identifications.

There is no reason for this problem to continue. Today we can use two different

 ISSN: 1355-4565

methods to predict observations on any gemstone regardless of the orientation of its optical elements relative to the gem table or any other facet. Every statement and every procedure new or old can be tested.

In 1942 Burbage and Anderson used an algebraic method to calculate RIs and the movements of the shadow edges on a topaz whose optical elements were in a particular orientation to the gem table. Recently, computer-based calculations were made for many different orientations of a chrysolite in *The Journal of Gemmology* by Xinhua Song *et al*., 2005.

In the same issue of *The Journal of Gemmology*, Sturman (2005) used a different method to test procedures for use of the polarizing filter in identifications using the refractometer. A brief overview of this graphic method, based on the use of the stereographic projections, is presented in the Appendix.

In this article, all possible observations on biaxial gemstones on the refractometer are discussed. Diagrams are used to represent observations on the refractometer during the rotation of a gemstone, with rotation angles plotted on the horizontal axis and the corresponding RIs on the vertical axis. In routine work, it is not necessary to record rotation angles and RIs, or to construct diagrams. Any observation on the refractometer can be related to a pattern presented on a diagram if three simple rules are followed:

1. Observe whether the shadow edges are constant (do not change during the rotation) or variable (show different RIs – i.e. move up and down).
2. Observe if they touch (get together) during the rotation – a single shadow edge is observed at a time.
3. Always rotate a gemstone in a clockwise direction and:
   a. where two variable shadow edges are visible, start the observation where the maximum RI (γ) is observed, or
   b. where a constant and a variable shadow edge are visible, start the observation where shadow edges are separated the most.

Review of optical properties of biaxial gemstones related to identifications on the refractometer

Identification of a gemstone on the refractometer is a very different process from the identification of a mineral grain on the polarizing microscope. Terms and concepts such as indicatrix, acute or obtuse bisectrix, the normal to the optic axes plane or positions of the principal vibration directions are very important for mineralogists. In contrast, they are of no importance to gemmologists using the refractometer for identification.

All that a gemmologist really needs to know is the following simple rule. In general, light is divided into two rays as it moves through an anisotropic (uniaxial or biaxial) gemstone. These two rays:

- are polarized and have different vibration directions – detected using a polariscope
- have different RIs – observed on the refractometer
- may have different absorption (colours) – detected using a dichroscope
- may move in slightly different directions – observed as image doubling with a lens, microscope or even with the naked eye.

The phrase 'in general' is used to indicate that there are exceptions to this rule; when light moves in special directions called the optic axes, it is not divided into two rays and continues to move in the same way as it would through an isotropic gemstone. In any other direction, two rays are formed and their properties (vibration directions, RIs, colours or the slight difference in directions in which they move) depend on the direction of light passing through a gemstone.

In order to understand the behaviour of light in biaxial gemstones, RIs for every possible direction should be examined and then represented in some informative way. Mineralogists use the indicatrix, where RIs are plotted on the vibration directions of light rays. It is extremely useful to mineralogists working on the polarizing microscope but is

of very limited use to gemmologists working with the refractometer.

In this article, RIs are related to directions of light rays through a gemstone – directions that constantly change during the rotation of a gemstone on the refractometer. Studies of the behaviour of light moving in many different directions show that biaxial gemstones have three characteristic RIs – principal RIs α, β and γ. Principal RI α has the lowest value, γ has the highest and β is an intermediate RI between the two. In most directions, as light is split into two rays, the observed RIs of the two rays are not the minimum and maximum but something in between and are marked as α' (a ray with the lower RI) and γ' (a ray with the higher RI). Studies showed another important fact; α' is always between α and β, and γ' is always between γ and β. Therefore, β is an equally important characteristic constant as the minimum and maximum RIs (α and γ).

Figure 1 shows two gemstones (sinhalite and peridot) with exactly the same minimum and maximum RIs; α=1.668 and γ=1.707. However, there is an essential difference in the way the light travels through sinhalite and peridot. In both gemstones, in general, two rays are formed but in sinhalite, the ray with the lower RI (α') is always between 1.668 and 1.698 and the other ray, γ' is always between 1.698 and 1.707. In peridot, α' is always between 1.668 and 1.688 and the other ray γ' is always between 1.688 and 1.707. In sinhalite β=1.698 and in peridot β=1.688 (see *a* and *b* in *Figure 1*).

Peridot and sinhalite may show the same minimum and maximum RIs but there is an essential difference in the value of the principal RI β that can be used in identification.

Observations on the refractometer

In general, when a biaxial gemstone is set on the refractometer and is rotated, then different directions of light passing through a gemstone are examined and different RIs are observed. However, we do not observe every possible direction of light travelling through a gemstone but only directions that are parallel to the gem table or a facet. A rotation of 180° is all that is needed to bring every direction in the gem table (or a facet) to coincide with the elongation axis of the refractometer (direction of light through the refractometer).

In general, two rays formed in a biaxial gemstone are seen as two shadow edges in the refractometer eyepiece. As a gemstone is rotated and directions of light are changed, the positions of the shadow edges may also change; as seen in the eyepiece, they may move up or down, they may stay constant, or they may diverge, converge or even join together.

These movements of the shadow edges – the behaviour of the biaxial gemstones on the refractometer during the rotation of the gem through 180° – depend on the orientation of the optical elements and the gem table or a facet. Only a limited number of directions may be observed (directions parallel to the gem table) and, therefore, limited movements of the shadow edges are seen. The observations presented in *Figure 1* are seldom seen in practice. It requires a very special position of the optical elements and the gem table. This is the only orientation where the full movements of both shadow edges can be seen; from α to β on the α' shadow edge and from γ to β on the γ' shadow edge.

- In biaxial gemstones with other orientations of the gem table and optical elements, the full movement (from α to β and from γ to β) may be seen on only one shadow edge; the movement of the other shadow edge is limited.

All possible orientations of the optical elements of biaxial gemstones and the gem table can produce many possible observations, but all observations can be described by the patterns shown in *Figures 1, 2, 3* and *4*.

These patterns can be further divided into two groups:

1. Patterns with two variable shadow edges – moving up and down during the rotation.
   a. Two variable shadow edges – touching
   b. Two variable shadow edges – not touching, and
2. Patterns where one shadow edge is

constant – showing the same reading during the rotation of the gem.
a. A constant and a variable shadow edge – intersecting in two points
b. A constant and a variable shadow edge – not touching.

Two variable shadow edges – touching (Figure 1)

The patterns shown in *Figure 1* were discussed above. Two variable shadow edges meet at one point during the rotation and a single shadow edge is seen only at this point. This single shadow edge gives the reading of the principal RI β. Unfortunately, the pattern shown in *Figure 1* is seldom seen in practical work. It is observed only on gemstones that have a very special orientation of the gem table (or a facet) and the optical elements. Determination of α and γ is straightforward; α is the minimum reading on the α' shadow edge and γ is the maximum reading on the γ' shadow edge. Principal RIs α and γ are generally observed at different rotation positions.

Two variable shadow edges – not touching (Figure 2)

This is the most common pattern of observation on biaxial gemstones (*Figure 2*). The lowest and highest RI readings for a gem can always be found when testing any flat polished

a. Sinhalite

α=*1.668* α'=*1.668 – 1.698* β=*1.698*
γ=*1.707* γ'=*1.698 – 1.707*

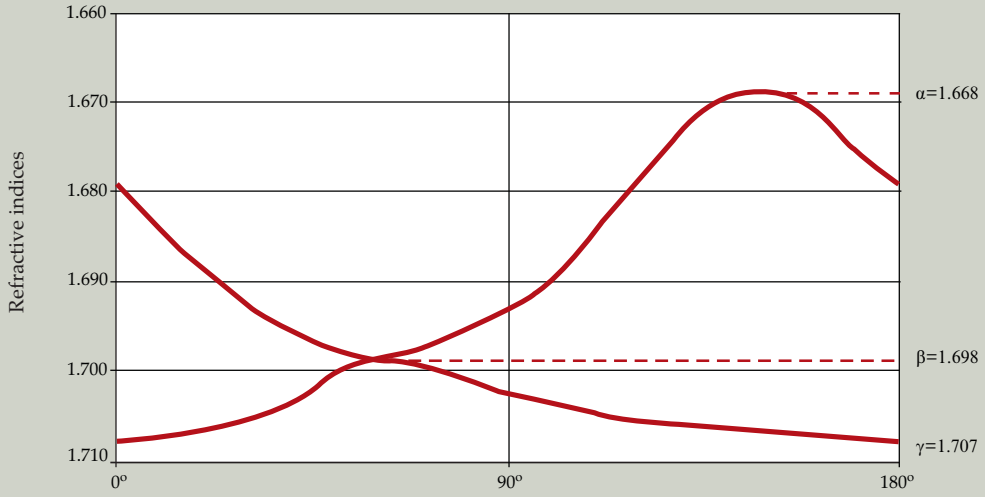

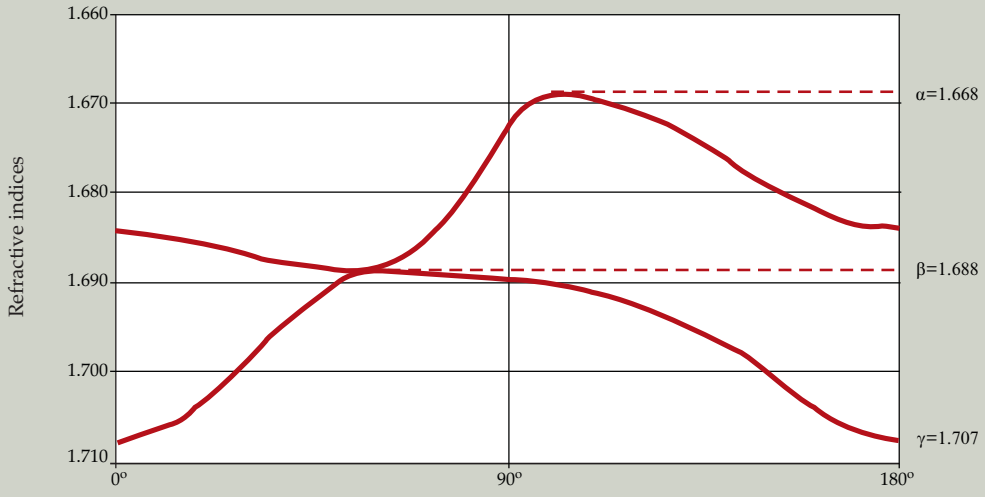

b. Peridot

α=*1.668* α'=*1.668 – 1.688* β=*1.688*
γ=*1.707* γ'=*1.688 – 1.707*

Figure 1: *Patterns of RI variation with rotation of biaxial gemstones on a refractometer: two variable shadow edges – touching. Two shadow edges (α' and γ') meet in one rotation position where a single shadow is seen, giving the value of the principal RI β.*

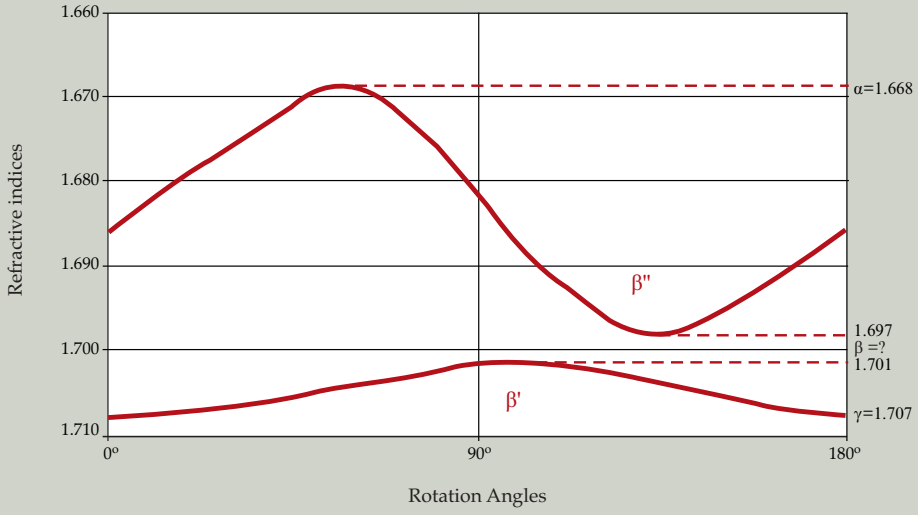

a. *Two possible* β *readings should be recorded as:*

From γ'	*From* α'
γ=*1.707*	α=*1.668*
β'=*1.701*	β"=*1.697*

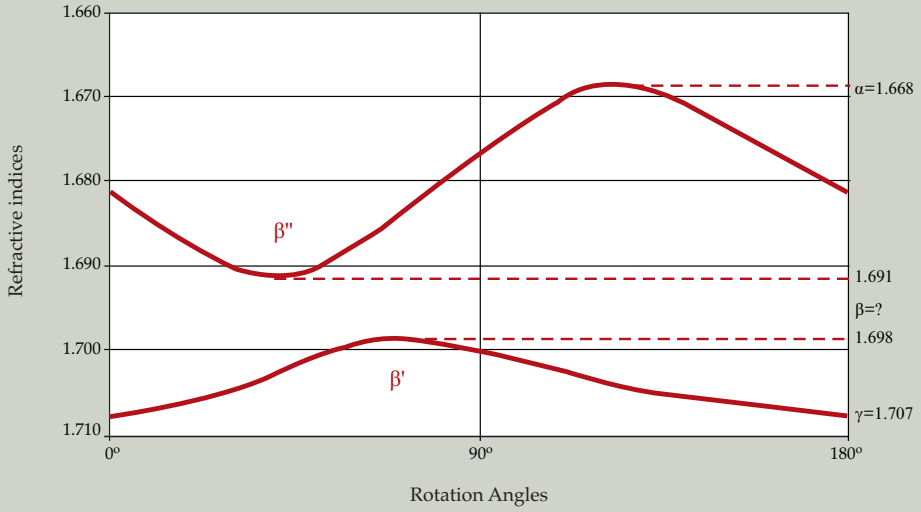

b. *Two possible* β *readings should be recorded as:*

From γ'	*From* α'
γ=*1.707*	α= *1.668*
β'=*1.698*	β"= *1.691*

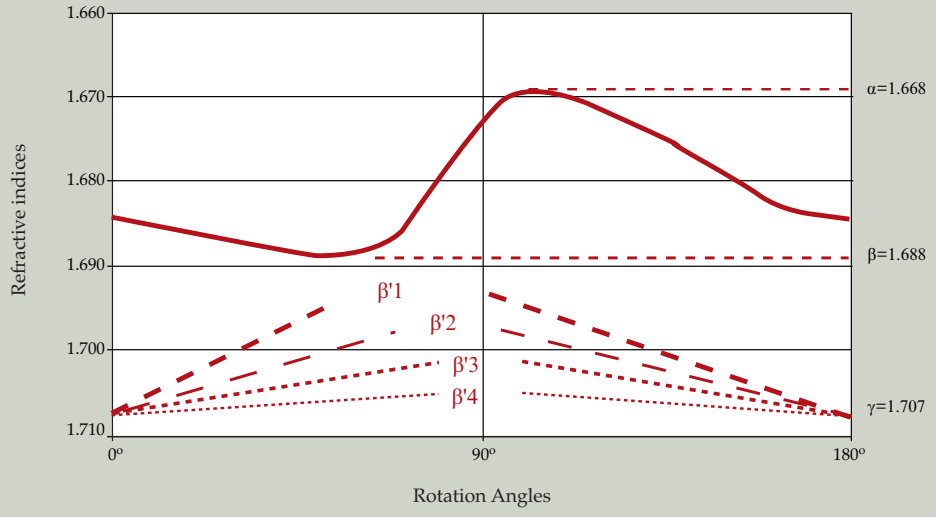

c. *Shadow edge* α' *moves all the way from* α *to* β.
Shadow edge γ' *may show many possible* β' *readings – they depend on the orientation of the gem table and optical elements.*

Figure 2: *Two variable shadow edges – not touching.*

surface on a gem. Thus, α is the minimum reading on the α' shadow edge and γ is the maximum reading on the γ' shadow edge. Principal RIs α and γ are generally observed at different rotation positions.

- While one shadow edge always moves from the minimum or maximum RI to β, the movement of the other shadow edge is limited – it does not move all the way to β.

Therefore, there are two positions observed during the rotation that may give the value of β (*Figure 2a* and *2b*):

- the lowest reading on γ' and
- the highest reading on α'.

A polarizing filter or additional procedures must be used to decide which β is correct and identify the true β.

It is important to remember that one shadow edge (either α' or γ') will always move to β – the true β – but that the value of false β seen on the other shadow edge depends on the orientation of the gem table (or facet) and the optical elements. In *Figure 2c* the pattern is shown where the α' shadow edge moves from α to β. The movement of the γ' shadow edge is limited and can change direction at any value. Several possible β' positions (β'1, β'2, etc) are shown to illustrate some of the many possible observations on gemstones with different orientations of the gem table and the optical elements.

The text comments in *a* and *b* of *Figure 2* show a simple way of keeping a record of observations that can be used later in interpretation of data – if needed. There is no need to construct a diagram, or to record rotation angles and corresponding readings of the RIs etc. All that is needed are four readings in rotation positions that can easily be identified. The main advantage of this method is that the original observation is easily repeated after a few hours or after several years – by the same observer or by a new one.

The γ' shadow edge is observed first and the maximum RI γ is recorded. This is the starting point of any future observation. The gemstone is then rotated and the γ' shadow edge is observed until the position of β' (the minimum reading on γ') is found and recorded. After this, the gemstone is rotated back to the starting position and then the α' shadow edge is observed. As a gemstone is rotated (always clockwise, for consistency) the readings on the α' shadow edge may either increase or decrease. *Figure 2a* shows an example where readings on α' first decrease to α (the lowest reading on the α' shadow edge) and then the readings increase to β'' (the highest reading on the α' shadow edge). In other gemstones with different orientations of the optical elements and the gem table (e.g. in *Figure 2b*), the readings on the α' shadow edge may first increase to β'' and then decrease to α.

A constant and a variable shadow edge – intersecting at two positions (Figure 3)

The pattern in *Figure 3a* is characterized by one shadow edge that gives a constant reading during the rotation. The other shadow edge is variable and moves up and down between the maximum RI γ and the minimum RI α. During the rotation of a gemstone on the refractometer, the distance between the constant and the variable shadow edges gets smaller and smaller until they meet in two rotation positions and only a single shadow edge is observed. These rotation positions give the value of β; α and γ are recorded as the minimum and the maximum RIs. The pattern shown in *Figure 3a* is rarely observed because it requires a very special orientation.

Much more commonly observed are patterns on gemstones where the alignment of the optical elements and the gem table (or a facet) is at a small angle to the special orientation of *Figure 3a*. *Figure 3b* shows such a pattern. It is still possible to get a close estimate of β because both shadow edges move to almost the same reading, but not at the same stage of the rotation. Although β' and β'' seem to be the same, they are not, but the difference is too small to be seen on the refractometer scale. This pattern is easily recognized as being similar to that in *Figure 3a*. Either one or the other shadow edge stays constant at the β reading during a long period of the rotation but when it moves it may be sudden and fast. Care must be taken to make sure that the minimum and the maximum RIs (α and γ) are accurately determined because of possible fast

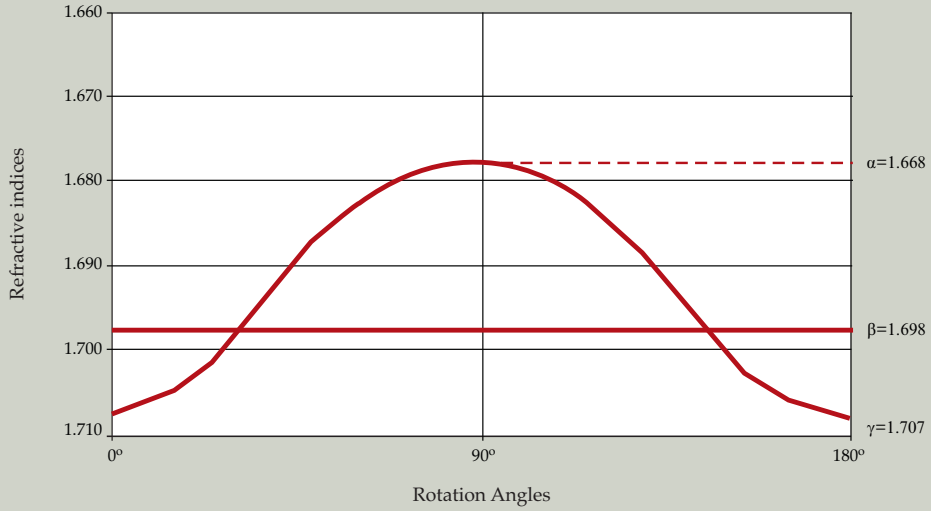

a. *A rarely observed pattern in biaxial gemstones, only seen when the principal vibration direction Y is precisely perpendicular to the gem table. During rotation of 180°, one shadow edge stays constant – giving β. At two rotation positions, the constant and the variable shadow edges join together – making a single shadow edge.*

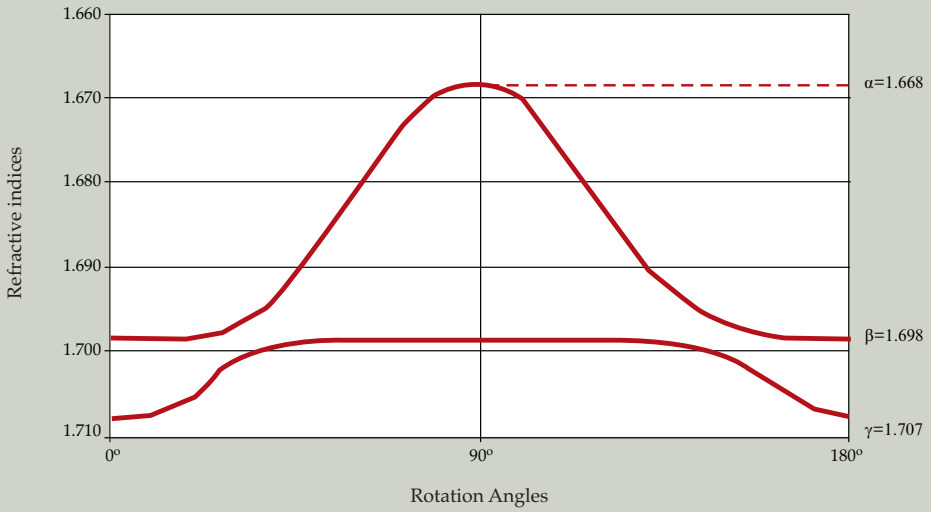

b. *This pattern is produced when the principal vibration direction Y is not quite perpendicular to the gem table. Two variable shadow edges stay separated at all times during rotation. On determining β, make sure that both shadow edges move to the same value. If not, go to c.*

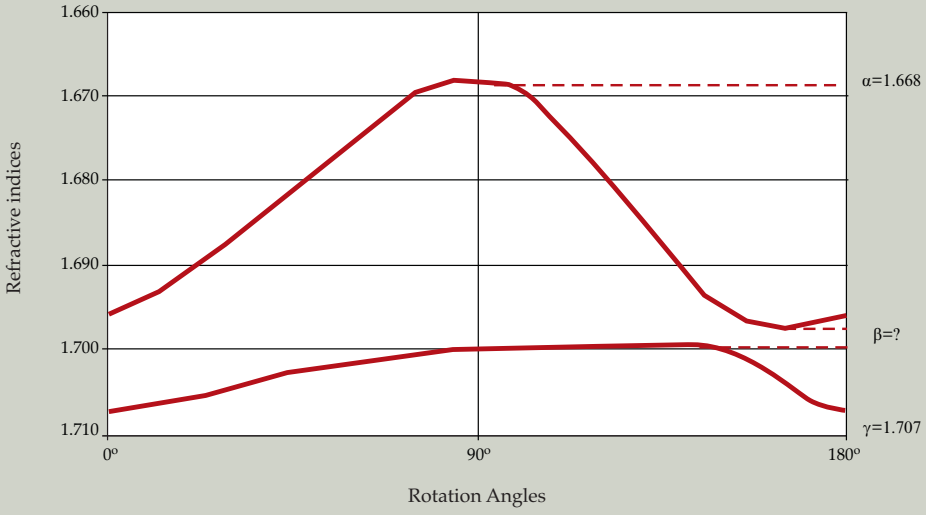

c. *When both shadow edges do not move to the same β, the polarizing filter must be used to identify the true β.*

Figure 3: *A variable and a constant shadow edge intersecting; and a variable and near-constant shadow edges almost touching.*

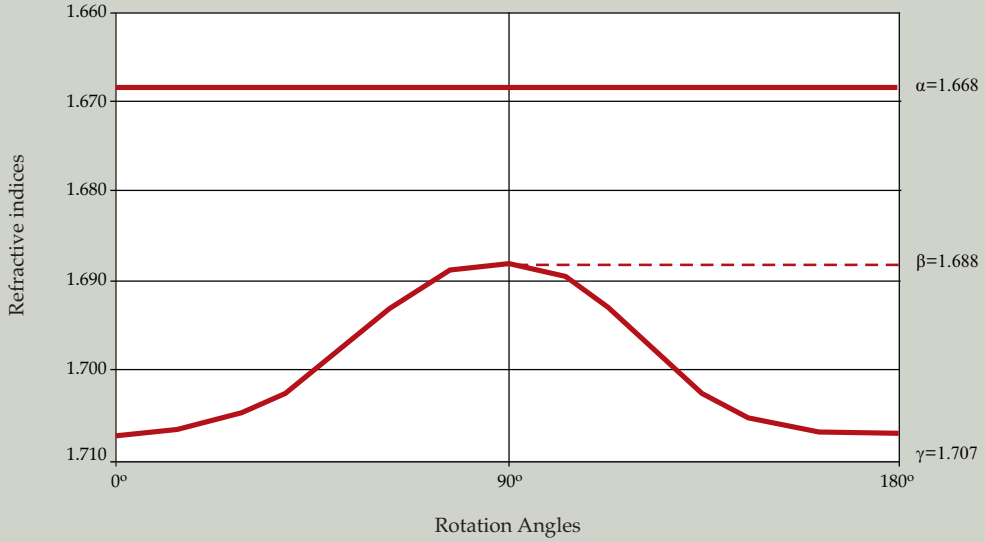

a. *A biaxial gemstone (peridot) in a special orientation of the gem table and optical elements.* α *is determined on the constant shadow edge and* β *and* γ *are determined on the variable shadow edge.*

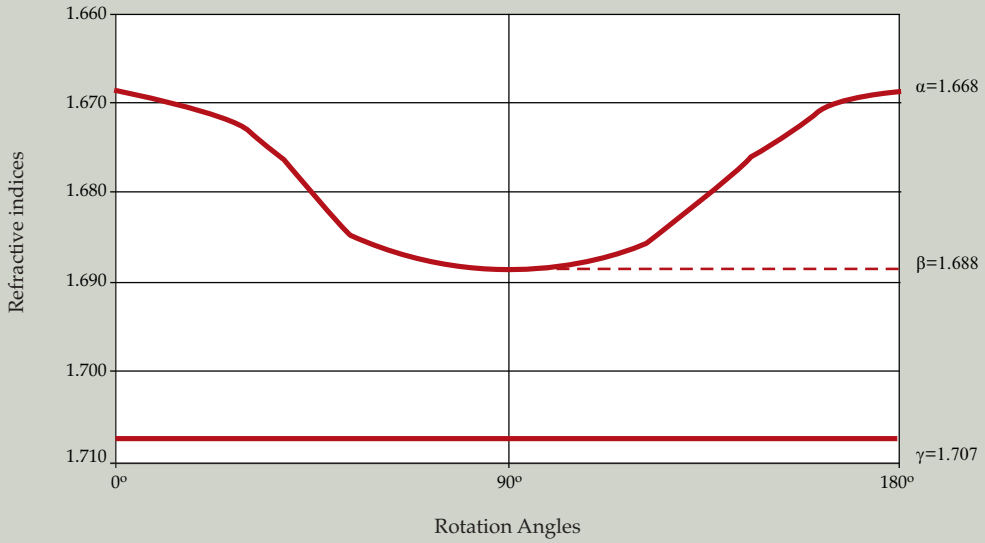

b. *A biaxial gemstone (peridot) in another special orientation of the gem table and optical elements.* γ *is determined on the constant shadow edge and* α *and* β *are determined on the variable shadow edge.*

Figure 4: *A constant and a variable shadow edge – not touching.*

movements of the shadow edges at the rotation positions where α and γ are determined.

Figure 3c shows a pattern where neither shadow edge moves to the same reading. The rotation patterns still show extensive ranges where either one or the other shadow edge stays close to the β reading but the polarizing filter or other procedures must be used to identify the true β.

A constant and a variable shadow edge – not touching (Figure 4)

The patterns shown in *Figures 4a* and *4b* can be observed both on uniaxial and on biaxial gemstones in special orientations of the optical elements and gem table. Either α or γ stays as a constant shadow edge during the rotation.

In *Figure 4a* the principal RI α is seen as a constant shadow edge while the variable shadow edge γ' moves from maximum separation at γ to β. In *Figure 4b* the principal RI γ is seen as a constant shadow edge, while the variable shadow edge moves from α to β.

- It is important to remember that other tests must be used to determine whether a gemstone is uniaxial or biaxial.

However, once a stone is identified as biaxial, its three principal RIs (α, β, γ) can easily be determined.

Conclusions

All possible movements of shadow edges observed on biaxial gemstones during rotation on the refractometer can be described by four sets of patterns shown in *Figures 1, 2, 3* and *4*. On some patterns the three principal RIs (α, β, γ), the optic character and the optic sign, can easily be determined; on other patterns additional tests are needed or the polarizing filter must be used.

- Determination of α and γ is straightforward – they are the minimum and the maximum RIs present in all patterns.
- Determination of β is straightforward in some patterns – see *Figure 1* and *Figure 3*.
- In rotation patterns like those in *Figure 4*, the polarizing filter must be used to identify the stone as uniaxial or biaxial. However, once it is identified as biaxial, all three RIs (α, β, γ) can be read directly during the rotation.
- In the most common pattern *(Figure 2)*, additional tests must be made or the polarizing filter must be used, in order to identify the true β.

The great majority of observations on biaxial gemstones are variations of a pattern described in *Figure 2* – two variable shadow edges not touching. The other patterns in *Figures 1, 3* and *4* require special orientations of the optical elements and the gem table (or a facet) and are only rarely observed. The reason that they are observed at all is that gem cutters sometimes use a large crystal face as the gem table. In many orthorhombic or monoclinic gemstones for example, optical elements are in special orientations with the large faces and these show the features explained in *Figures 1, 3* and *4*.

Acknowledgement

I thank Duncan Parker for many helpful discussions during the preparation of this manuscript. His extensive experience in identification and in the teaching of gemmology was most useful. Comments by the reviewers greatly improved the manuscript.

References

Burbage, E.J., and Anderson, B.W., 1942. An analysis of the movement of shadow-edges on the refractometer in the case of biaxial gemstones. *Mineralogical Magazine*, 26, 246-52

Sturman, B.D., 2005. Use of the polarizing filter on the refractometer. *J. Gemm.*, 29(5/6), 341-8

Xinhua Song, Ruihua Wu and Weizheng Wu, 2005. The variation of RI with rotation of a doubly refractive gemstone on the refractometer hemicylinder. *J. Gemm.*, 29(5/6), 331-40

Appendix

Calculation of the RIs of biaxial gemstones during rotation on the refractometer

First step

Determination of the vibration directions (x' and z') for selected positions during the rotation of a gemstone on the refractometer. Stereographic projection (with the plane of the projection set parallel to the gem table) and the modified Biot-Fresnel construction were used.

Second step

Determination of the positions of a particular vibration direction (x' or z') in relation to the principal vibration directions X, Y and Z. In order to make these measurements simpler, the stereographic projection was rotated so that principal vibration directions were in the standard position (Z vertical and X horizontal with phi=0°) and angles phi and rho were measured for each particular vibration direction (x' or z').

Third step

Equation of the indicatrix given in many textbooks (for example, Bloss: Optical Crystallography (1961), p.155, equation 9-2) was used to calculate RI for each vibration direction (x' or z'). These calculated RIs and the rotation angles were then plotted on diagrams in order to show movement patterns of the shadow edges.

Determination of the optic axial angle in biaxial gemstones and its use in gemmology

B. Darko Sturman
Curator Emeritus, Royal Ontario Museum, Canada

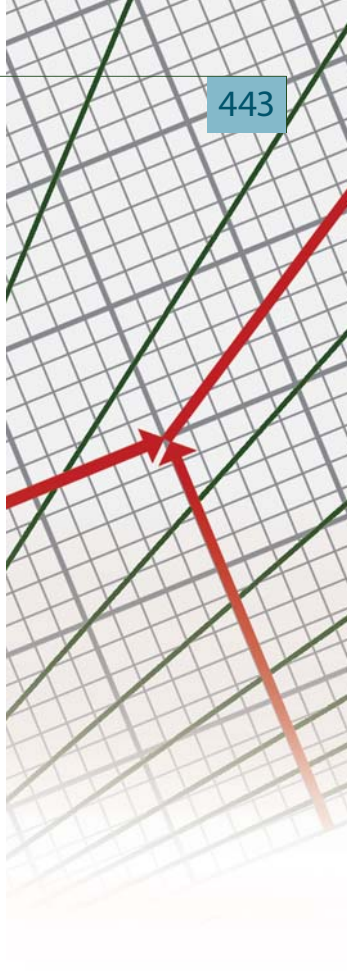

Abstract: *From the very beginning of the use of the refractometer in identification of gemstones, gemmologists faced two problems:*

- *how to differentiate between biaxial gemstones with similar or overlapping RIs*
- *how to distinguish a uniaxial and a biaxial stone in an orientation which produced one variable and one constant shadow edge.*

The use of the polarizing filter to solve these problems can be avoided in many cases by the use of the optic axial angle method. The most important feature of this method is that it is reliable. Also, whether or not the method can be applied is quick to determine.

Determination of an optic axial angle can be made on a simple diagram and the list of biaxial gemstones and their optic axial angles are shown. Determination of the optic axial angle requires the same data as determination of the optic sign but it is a much more discriminatory constant for use in identification of biaxial gemstones.

Keywords: *biaxial gemstones, optic axial angle diagram*

Introduction

Optical mineralogy has played a very important role in the development of our understanding of earth processes and earth materials. From the mid-nineteenth to the mid-twentieth century, many methods were developed and various accessories designed for the study of minerals and rocks with the polarizing microscope. A large amount of data on the optical properties of minerals was collected and used, not only to identify minerals in rocks but also to determine their chemical composition and structural state, thus giving important clues on the conditions under which rocks were formed and about the geological forces that affected them.

Optical gemmology uses many of the concepts, methods and data on the optical properties of minerals in the study of gems. There are, however, some concepts in optical mineralogy that have not been properly applied in gemmology. One such concept is the use of the optic axial angle in identification of biaxial gemstones.

ISSN: 1355-4565

The main reason for this is that very different procedures are used for its determination: in gemmology it is done on the refractometer, whereas in mineralogy the polarizing microscope is used.

The optic sign (positive or negative) and the optic axial angle (the angle between the optic axes) are very important constants in identification of biaxial mineral grains with the polarizing microscope. They are observed with a special lens on the polarizing microscope producing conoscopic light and these constants (optic sign and optic axial angle) are fully independent from other determinations. A mineralogist may make an error in estimates of refractive indices (RIs) or birefringence of some mineral grain but this does not in any way affect the determination of the optic sign and the optic axial angle.

The optic sign and the optic axial angle of biaxial gemstones are determined in a very different way in gemmology. They are calculated from the principal RIs α, β and γ, which are determined on the refractometer.

The rule for the optic sign is very simple:

$\beta-\alpha < \gamma-\beta$ - optic sign is positive

$\beta-\alpha > \gamma-\beta$ - optic sign is negative

Equally simple is determination of the optic axial angle on the diagram in *Figure 1* from differences β-α and γ-β.

Any error in the determination of the principal RIs (α, β and γ) can lead to a wrong determination of the optic sign or the optic axial angle and consequently to the incorrect identification of a gemstone.

Determination and the use of the optic angle in gemmology

Determination of the optic axial angle, the angle between the optic axes in biaxial gemstones, can be made quite straightforward, and requires similar data to those needed to determine the optic sign. All three RIs, α, β and γ, are determined on the refractometer and the differences β-α and γ-β are calculated and plotted on the optic axial angle diagram in *Figure 1*. An example of use of the diagram and the list of biaxial gemstones and their optic axial angles are also shown in this figure. The construction of the diagram is described in Appendix I.

The difference between the use of the optic sign and the optic axial angle can best be explained by a simple example. The optic sign divides gemstones into two groups, positive and negative, in the same way as, for example, gemstones can be divided into colourless and coloured. The optic axial angle divides biaxial gemstones into many small groups in the same way as the information on colour can be used to divide coloured gemstones into many smaller and well defined groups (blue, red, yellow, etc). Therefore, the use of the optic axial angle in gemmology is potentially of greater help in identification of gemstones on the refractometer.

Such use can be applied in three different sets of circumstances:

1. to differentiate between biaxial gemstones with overlapping RIs – if β can be observed directly (*Figure 2*);
2. to differentiate between biaxial gemstones with overlapping RIs – if two solutions for β are possible (*Figure 3*),
3. to differentiate between a uniaxial gemstone and a biaxial gemstone (with special orientation of the gem table and the optical elements) (*Figure 4*).

In the discussion, diagrams are used to show the movements of the shadow edges during the rotation of a gemstone on the refractometer (*Figures 2, 3* and *4*). The rotation angles are plotted on the horizontal axis of a diagram and the corresponding RIs on the vertical axis. Diagrams are also used to indicate rotation positions where α, β and γ are determined. In the routine work, there is no need to record and plot the rotation angles and corresponding RIs every 30° or 60° in order to make diagrams. All that is required is to recognize the special rotation positions at which α, β and γ can be determined and this can be mastered in a few minutes by comparing diagrams with observations on a particular gemstone.

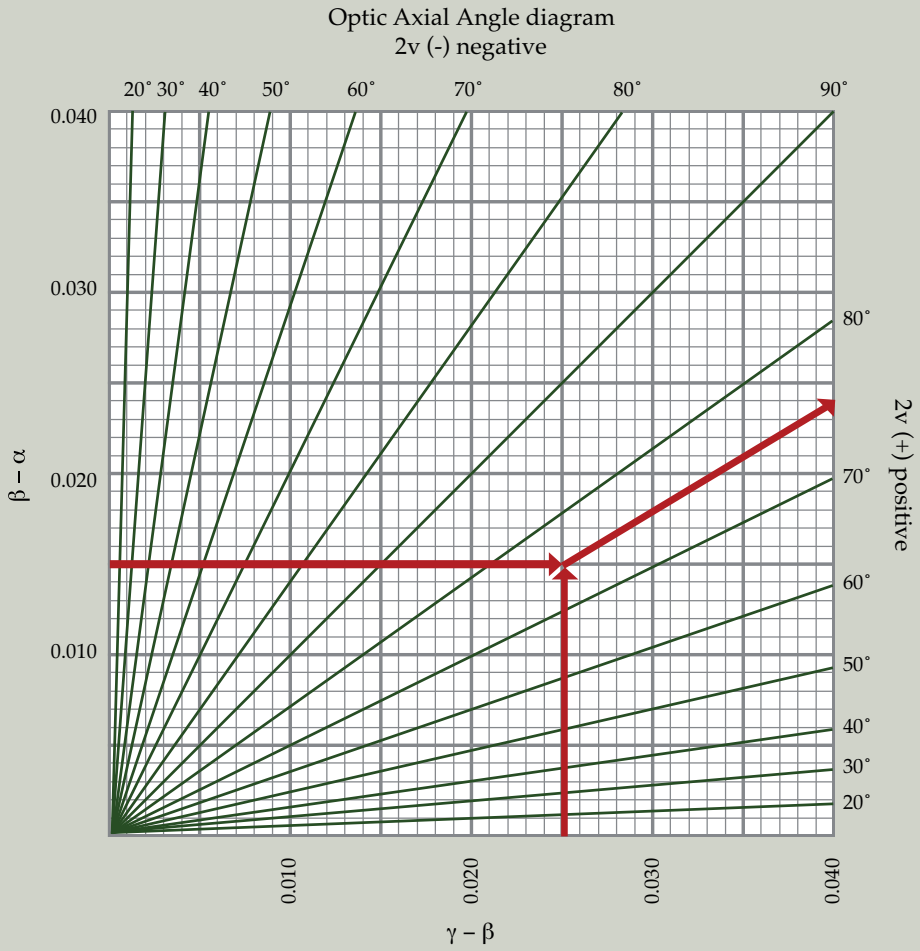

Figure 1: *Optic axial angle diagram with plotted example of gemstone with α 1.600, β 1.615, γ 1.640; so β - α = 0.015, γ - β = 0.025 and 2V is + 75°. List of biaxial gemstones with their optic axial angle and sign.*

Biaxial Gemstones

Name	2V (sign)	
Actinolite	80 -85	(-)
Albite	~90	
Amblygonite	70 -85	(+)
Andalusite	~90	
Aragonite	20	(-)
Augelite	50	(+)
Axinite	65 -85	(-)
Baryte	40	(+)
Beryllonite	70	(-)
Boracite	80 -90	(+)
Brazilianite	70 -75	(+)
Chrysoberyl	30 -70	(+)
Colemanite	55	(+)
Danburite	~90	
Datolite	75	(-)
Diaspore	85	(+)
Diopside	55 -60	(+)
Enstatite	45 -90	(+)
Epidote	~90	
Euclase	50	(+)

Name	2V (sign)	
Grandidierite	30	(-)
Hambergite	~90	
Herderite	70	(-)
Iolite	40 -90	(-)
Kornerupine	5 -50	(-)
Kyanite	80	(-)
Labradorite	~90	
Lazulite	65 -70	(-)
Legrandite	35 -50	(+)
Natrolite	60 -65	(+)
Orthoclase/Sanidine	20 -90	(-)
Peridot	~90	
Petalite	~90	
Rhodonite	60 -70	(+)
Sillimanite	20 -30	(+)
Sinhalite	55	(-)
Spodumene	50 -70	(+)
Tanzanite	40	(+)
Topaz	45 -70	(+)
Zoisite	30 -50	(+)

1. Biaxial gemstones with overlapping RIs – if β can be read directly

Figure 2 shows examples where all three principal RIs of a biaxial gemstone can be read directly during the rotation of that gemstone. Principal RI α is the smallest value on the diagram, γ is the largest and β is indicated in two different ways:

- For gemstones A and C in *Figure 2*, the principal RI β is read in the position where two variable shadow edges meet – a single shadow edge is observed.
- For gemstone B in *Figure 2*, the principal RI β is indicated by the value reached by both shadow edges. The shadow edges may or may not meet. However, on rotation, first one shadow edge and then the other move to the same reading giving β.

Three possible patterns of observations on peridot or sinhalite gemstones are presented in the *Figure 2*. RIs observed on gemstones A, B and C were used to determine three optic axial angles (2V) on the optic axial angle diagram in *Figure 1* and these are compared to the optic axial angles on the list. All three gemstones have RIs and birefringence in agreement with both peridot and sinhalite. However, the calculated optic axial angles make identification fast and reliable:

Gemstone A with 2V (-) = 88° indicates peridot
Gemstone B with 2V (-) = 88° indicates peridot
Gemstone C with 2V (-) = 53° indicates sinhalite

Many biaxial gemstones on the list in *Figure 1* show a range of values of optic axial angles rather than a single value. For example, the optic axial angle observed on actinolite gemstones can lie between 80° and 85° (depending upon its precise composition) with a negative optic sign. In some gemstones this range is in the 2V = 90° area and their optic sign can be either positive or negative. A small error in determination of the RIs of ±0.001 could easily therefore indicate an erroneous optic sign. For this reason, in dealing with a gem with an optic angle close to 90° it is better that gemmologists do not describe it as positive or negative, but say that it has an optic angle of '2V about 90°'.

Apart from measurement error, there can be real variation in the optic axial angle of some gemstones and the reason for this is the same as for the variation in their RIs. Their chemical composition can vary as two or more elements can replace each other and this, in turn, is reflected in the variation of optical properties. For example, variation in the Mg to Fe ratio in peridot crystals from different localities is reflected in variation of the maximum RI γ from 1.670 to about 1.720 (a difference of 0.050). The corresponding change in optic axial angle is about 15° (from 2V (+) = 80° to 2V (-) = 85°, shown as 2V ~ 90 on the list in *Figure 1*).

In the examples given in *Figure* 2, use of the optic axial angle gives fast, simple and reliable identifications of gemstones such as peridot or sinhalite. The same result can be obtained by simply using values of α, β and γ for peridot and sinhalite. However, values of β are seldom given in gemmological literature. Furthermore, many gemstones do not have a single value of β but show the range of values, similarly to ranges for α and γ. For any particular set of α and γ values, a corresponding β value must be given. This may involve a time consuming and, sometimes, fruitless search through the literature.

All this is avoided with the use of the optic axial angle in identification of gemstones. *Figure 1* gives everything needed for practical use: list of gemstones with their optic axial angles and a diagram for determination of optic axial angles from α, β and γ.

The special patterns of movements of shadow edges shown in *Figure 2* are unfortunately seldom observed in practice (see Sturman (2007) in this issue). RI β can be read directly only on gemstones with a favourable orientation of the gem table (or a facet) and its optic elements. Much more commonly encountered are the patterns shown in *Figure 3*, where two variable shadow edges remain separated during the rotation. This leads to two possible readings of the principal RI β.

2. Biaxial gemstones with overlapping RIs – if two solutions for β are possible

Identification of a peridot and sinhalite on the refractometer is an example given in many textbooks and its use is continued in this section.

Figure 3 shows observations on peridot or sinhalite gemstones where two variable

Gemstone A

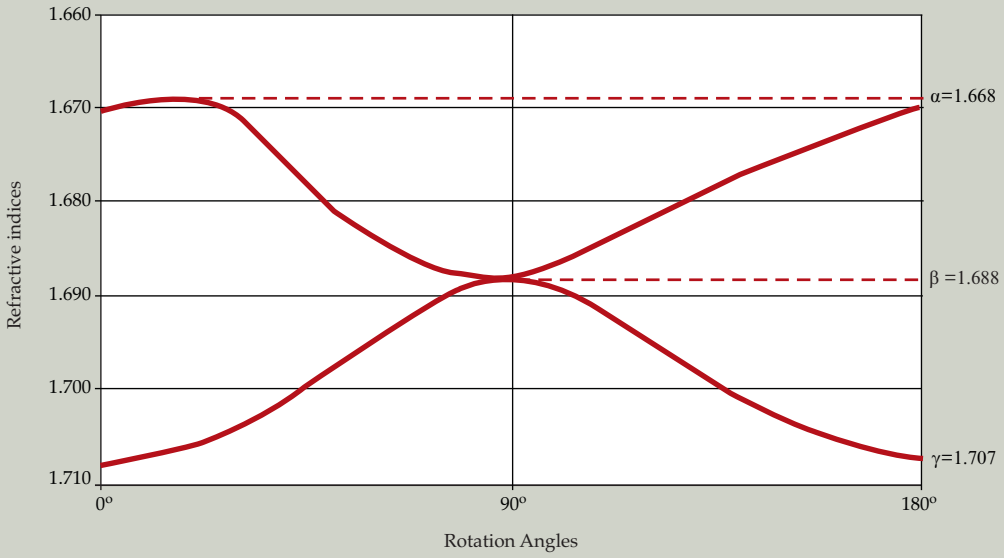

β - α = 0.020
γ - β = 0.019

optic axial angle
2V (-) = 88

Gemstone B

β - α = 0.020
γ - β = 0.019

optic axial angle
2V (-) = 88

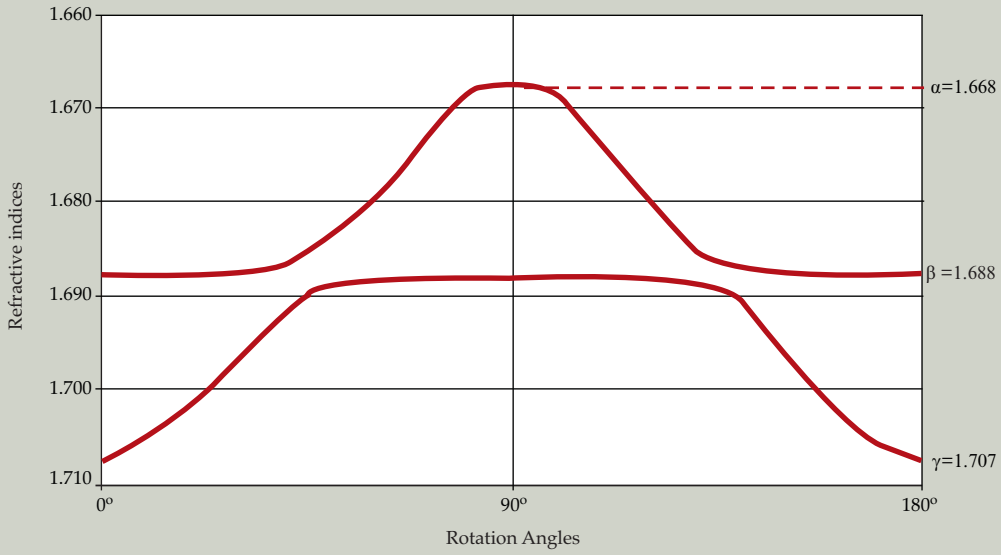

Gemstone C

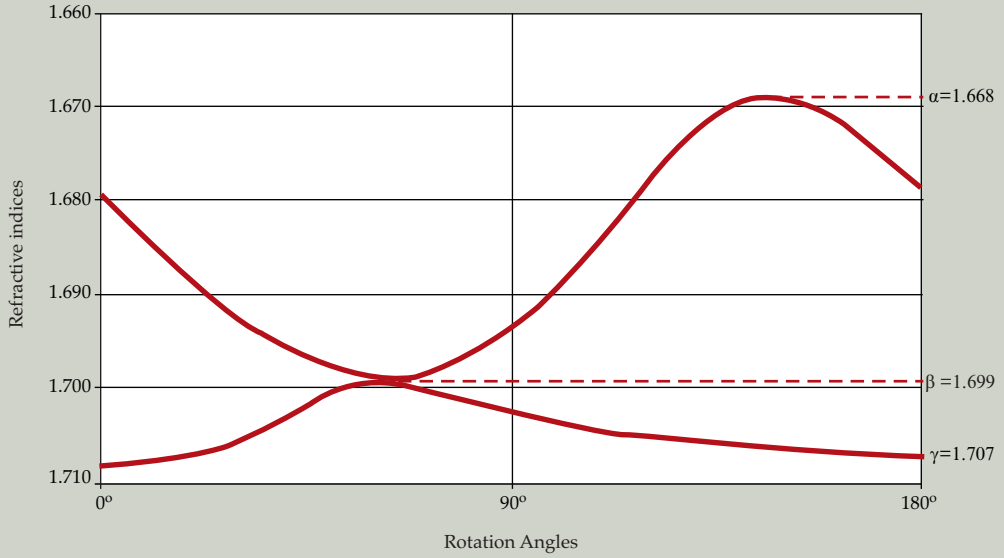

β - α = 0.031
γ - β = 0.008

optic axial angle
2V (-) = 53

Figure 2: *Diagrams showing relations of RIs with rotation angles on the refractometer in gemstones where β can be read directly. Examples of the derivation of the optic axial angle and its sign are given for three stones.*

Gemstone D

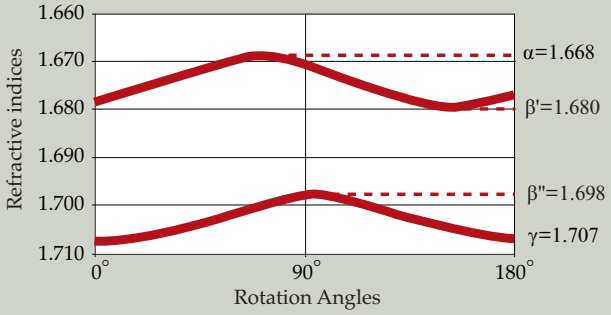

Solution I	Solution II
α = 1.668	α = 1.668
β" = 1.698	β' = 1.680
γ = 1.707	γ = 1.707
β" - α = 0.030	β' - α = 0.012
γ - β" = 0.009	γ - β' = 0.027
Optic axial angle 2V" (-) = 57	Optic axial angle 2V' (+) = 68
May be sinhalite	Cannot be peridot
Indicates sinhalite	

Gemstone E

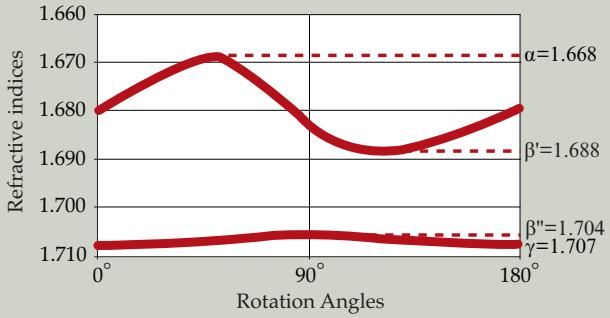

Solution I	Solution II
α = 1.668	α = 1.668
β' = 1.688	β" = 1.704
γ = 1.707	γ = 1.707
β' - α = 0.020	β"- α = 0.036
γ - β' = 0.019	γ - β" = 0.003
Optic axial angle 2V' (-) = 88	Optic axial angle 2V" (-) = 32
May be peridot	Cannot be sinhalite
Indicates peridot	

Gemstone F

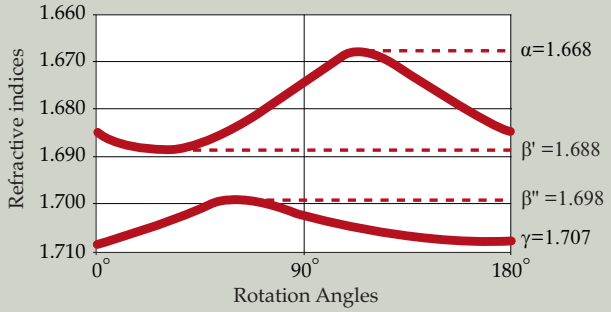

Solution I	Solution II
α = 1.668	α = 1.668
β' = 1.688	β" = 1.698
γ = 1.707	γ = 1.707
β'- α = 0.020	β"- α = 0.030
γ - β' = 0.019	γ - β" = 0.009
Optic axial angle 2V' (-) = 88	Optic axial angle 2V" (-) = 57
May be peridot	May be sinhalite
May be either peridot or sinhalite	

Figure 3: *Diagrams showing the relation of RIs with rotation angles on the refractometer in gemstones where the true value of* β *is not immediately apparent. Each variable shadow edge has one rotation position where a possible* β *can be observed, denoted by* β' *and* β". *Two possible optic axial angles 2V' and 2V" can be derived from* β' *and* β" *and these are compared with a standard list to reach a conclusion as indicated in examples D, E and F.*

shadow edges do not meet or reach the same reading. Each shadow edge has a position where a possible β can be observed. It is

- the highest reading on the shadow edge containing α and
- the lowest reading on the shadow edge containing γ.

Only one is the true β, the other is a false β. Instead of using the polarizing filter to identify the true β, the problem can be solved by determination of the optic axial angle for both possible β readings. One of these two optic axial angles must be in agreement with a particular gemstone. If it is not, then it cannot be this particular gemstone.

The procedure is as follows: during rotation of a gemstone to identify α and γ, both readings for possible β are also recorded. Then, both possible βs are used to determine the corresponding optic axial angles – there is no need at this stage to determine which is the true β and which is false. The role of the possible error in determination of the RIs is discussed in Appendix II.

The use of the optic axial angle in identification of biaxial gemstones with two possible β readings is best explained by examples shown in *Figure 3*. Observations on three gemstones, D, E and F, gave RIs and birefringence that agree with both sinhalite and peridot. Then determinations of the optic axial angles of D and E made their identification very simple, fast and reliable. But the movements of the shadow edges on the third gemstone (F) are consistent for either peridot or sinhalite. In this case, it is impossible to use this procedure in identification. The criteria are straightforward:

- If one optic axial angle agrees with sinhalite and the other does not agree with peridot then we have a reliable identification – the results indicate sinhalite (*Figure 3*, gemstone D).
- Similarly, if one optic axial angle agrees with peridot and the other does not agree with sinhalite then, again, we have a reliable identification – the results indicate peridot (gemstone E).
- However, if one agrees with peridot and the other agrees with sinhalite (gemstone F) then identification based on the use of the optic axial angle is not possible, because this particular pattern of movements of shadow edges can be observed on both sinhalite and peridot.

3. Identification of a gemstone as uniaxial or biaxial (in special orientations)

It is possible that a uniaxial and a biaxial gemstone may have similar RIs and give identical patterns when rotated on the refractometer. For example, observations on gemstone G in *Figure 4* gave the following data:

One variable and one constant shadow edge, not touching, with

RI maximum = 1.642 – observed on the constant shadow edge, and

RI minimum = 1.620 – observed on the variable shadow edge in the position where shadow edges are at maximum separation.

This pattern (a variable and a constant shadow edge) could be observed on a uniaxial gemstone (tourmaline) or on a biaxial gemstone (actinolite) with a special orientation of the gem table.

The solution to this problem is to interpret the observed data on the basis of two different assumptions; first, as if the gemstone were uniaxial and then as if it were biaxial. In uniaxial gemstones the shape (dip) of the variable shadow edge depends on the angle between the gem table (or a facet) and the optic axis. It depends on the cutter's choice of the gem table and it can be anything between the two extremes of

- two constant and parallel shadow edges and
- a constant and a variable shadow edge that meet.

A similar pattern (a constant and a variable shadow edge) can be observed on biaxial gemstones with special orientation of the gem table and optic elements. However, the shape (dip) of the variable shadow edge in biaxial gemstones depends on the value of β. If the dip of the variable shadow edge does not give the reading of β of actinolite, then this pattern cannot be produced by actinolite. Instead of the search for β values through the literature, a simple determination of the optic axial angle is all that is needed.

If the calculated optic axial angle does not agree with the values listed in *Figure 1* for a particular gemstone, then it cannot be this gemstone. Gemstone G in *Figure 4* is firmly indicated as tourmaline because the calculated optic axial angle is clearly outside the range for actinolite. Observed data on Gemstone G rule out the possibility that it may be actinolite.

In some situations the observed data may be in agreement with actinolite and with tourmaline, such as those for gemstone H in *Figure 4*. In this case, the method does not provide a solution and the polarizing filter must be used.

The role of the possible error in determination of the RIs is discussed in Appendix II.

Conclusion

The optic axial angle is a very useful constant in identification of biaxial gemstones on the refractometer. It requires the same observations as determination of the optic sign but it is much more useful. It is especially valuable in the following situations:

- in identification of biaxial gemstones with RIs which overlap those of other gem species,
- in differentiating between uniaxial and biaxial gemstones in special orientations.

These problems can be solved with the use of the polarizing filter. However, many gemmologists are reluctant to use it and many procedures without the use of the polarizing filter have been described in textbooks and teaching manuals. They may be very simple or very complex, but many of them have, unfortunately, one thing in common – they can lead to an incorrect identification.

The optic axial angle method described in this article is an alternative to these procedures. It offers simple, fast and very reliable solutions to two problems mentioned above. It cannot be applied in every situation but the observer knows right away if it can, or cannot, be used.

The optic axial angle method is a step between the initial observation (minimum and maximum RIs) and detailed observations with the polarizing filter (Sturman, 2005). It is not used every time a gemstone is set on the refractometer but only when needed. *Figures 1, 2, 3* and *4* contain all the guidance needed for confident and reliable use of the method. If anyone decides to use the method years after reading the article, all that is required is a quick look at the figures – hopefully kept close to the refractometer.

Acknowledgements

I wish to thank Duncan Parker for help in preparation of this manuscript and many useful discussions. Comments by the reviewers greatly improved the manuscript.

References

Sturman, B.D., 2005. Use of the polarizing filter on the refractometer. *J. Gemm.*, 29(5/6), 341-8

Sturman, B.D., 2007. Clarification of measurment of the RIs of biaxial gemstones on the refractometer. *J. Gemm.*, 30(7/8), 434-42

Appendix I

Optic axial angle diagram

The optic axial angle – the angle between the optic axes of biaxial gemstones - depends on the principal RIs α, β and γ according to the equation I-1. There are several diagrams that can be used in order to avoid the complex calculations. One such diagram is shown in the article on the use of the polarizing filter by Sturman (2005). It is not very complex but it may be made even simpler by the use of the approximate equation I – 2. This equation was used to prepare a simple optic axial angle diagram shown in *Figure 1* in this article.

$$\tan 2V_z = \frac{1/\alpha^2 - 1/\beta^2}{1/\beta^2 - 1/\gamma^2} \qquad \text{Equation I-1}$$

$$\tan 2V_z = \frac{\beta - \alpha}{\gamma - \beta} \qquad \text{Equation I-2}$$

The error introduced by the use of the approximate equation and the simpler diagram is much smaller than the error of (±0.001 or 0.002) that can be expected in the readings of the RIs in the routine work with the refractometer. Therefore, the optic axial angle diagram in *Figure 1* can be safely used in most routine determinations of the optic

Gemstone G
If uniaxial:

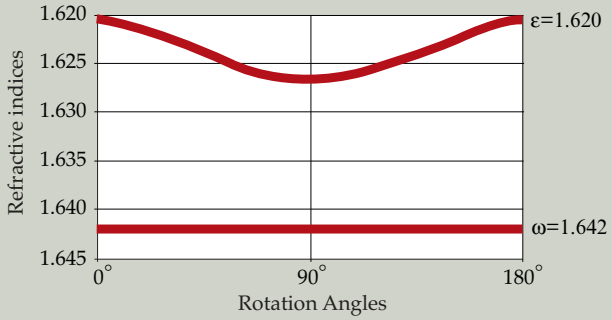

Gemstone G
If biaxial:

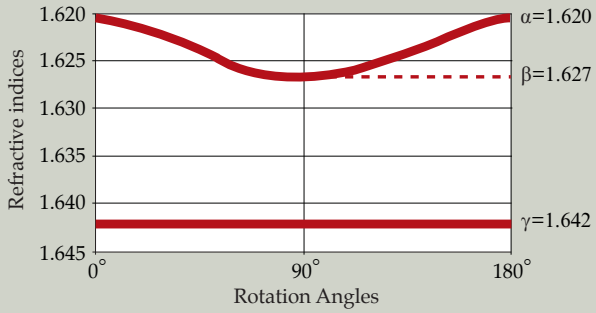

Solution I	Solution II
ε = 1.620	β - α = 0.007
ω = 1.642	γ - β = 0.015
Optic sign (-)	2V (+) = 70
RIs, birefringence and optic sign all agree with tourmaline	Optic axial angle does not agree with actinolite
Cannot be actinolite - indicates tourmaline	

Gemstone H
If uniaxial:

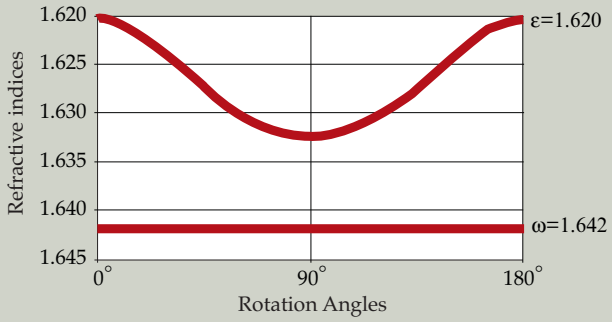

Gemstone H
If biaxial:

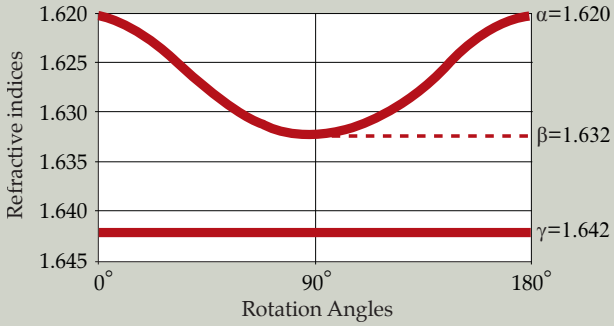

Solution I	Solution II
ε = 1.620	β - α = 0.012
ω = 1.642	γ - β = 0.010
Optic sign (-)	2V (-) = 84
RIs, birefringence and optic sign all agree with tourmaline	Optic axial angle agrees with actinolite
Can be either actinolite or tourmaline	

Figure 4: *Diagrams showing relations of RIs with rotation angles on the refractometer in gemstones where one shadow edge is constant. In uniaxial gemstones, the shape of the variable shadow edge (the dip of the variable line during the rotation) depends on the cutter's choice of the gem table. The variable line may be horizontal, almost horizontal, dip all the way to a constant line or it can come to any position in between – it depends only on the choice of the gem table. In biaxial gemstones – where shadow edges of either α or γ stay constant during the rotation), the dip of the variable line depends on the value of β. In gemstone G, the RIs and birefringence indicate that it can be tourmaline or actinolite, but the shadow edges patterns and calculation of the optic axial angle (2V) rule out actinolite. In gemstone H, the calculated optic axial angle agrees with actinolite - it may be either actinolite or tourmaline.*

axial angles.

Most gemstones have partial birefringences (β-α and γ-β) smaller than 0.040 and for them the optic axial angle can easily be determined on the diagram. For the very few gemstones with larger birefringence, the use of the diagram is also simple; both partial birefringences are divided by the same number (2, 3, etc) until they are smaller than 0.040 and the optic axial angle is then found on the simplified diagram. It must be mentioned, however, that in this case, the error caused by the use of the simplified diagram may be larger than 1° or 2°.

Appendix II

The effect of a possible error in determination of the RIs.

A possible error in determination of the RIs depends very much on the clarity with which shadow edges are seen. This in turn depends on many factors such as the quality of the polish of facets, quality of the monochromatic light, construction and the optics of the refractometer, etc. It is impossible to give a general set of values that can be applied to every observation.

The safest test for any observation is to make several repeated readings of the RIs. This would indicate the possible errors and give the extreme values that must be used in the interpretation of the results. In a great majority of observations this is not required because results will clearly indicate one way or the other. However, in borderline cases, a simple and fast test may be used to avoid repeated measurements. We named it a 'β +/- 0.002' test.

Figure 5 gives an example of the use of this test. Gemstone I gave a pattern (a constant and a variable shadow edge) that can be observed on uniaxial and biaxial gemstones. Maximum RI, minimum RI and birefringence indicate that it may be tourmaline or actinolite. The solution as biaxial gave an optic axial angle of 2V (+) = 86° – it is close to but not in the actinolite range given in *Figure 1*. The 'β +/- 0.002 test' (addition or subtraction of 0.002 from the observed β) gives two additional β values that can be used in calculations of the optic axial angles. One of these calculated optic axial angles (2V (-) = 84°) is within the range of actinolite. Therefore, the optic axial angle method does not give an identification in this case; Gemstone I can be either tourmaline or actinolite. Other procedures must be used in identification.

It must be pointed out that the safest procedure is to determine the possible error in measurements of the RIs for every determination. It is also important that an observer accepts the fact that in some situations the optic axial angle method cannot give a reliable result. Even more important is the fact that an observer at all times knows whether or not the method can be used.

Gemstone I

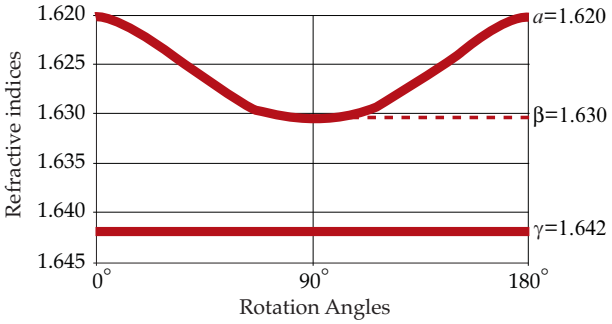

Solution as biaxial:	New solution based on the β +/- 0.002 Test	
β = 1.630	β = 1.632	β = 1.628
β - α = 0.010	β - α = 0.012	β - α = 0.008
γ - β = 0.012	γ - β = 0.010	γ - β = 0.014
2V (+) = 86	2V (-) = 84	2V (+) = 75
Cannot be Actinolite	May be Actinolite	Cannot be Actinolite

Figure 5: *The use of the* β +/- 0.002 *test. The observed* β=1.630 *gives 2V (+) = 86° - not in the range of 2V (-) = 80°-85° for actinolite (see list on* Figure 1*). The test (addition or subtraction of 0.002 to or from the observed* β*) gives two more values to be used in calculation of the optic axial angles. One of these gives the optic axial angle of 2V (-) = 84°- it is within the range given for actinolite. Therefore, the observed pattern can be expected on actinolite crystals with the usual error in determination of the RIs.*

Letter to the Editor

'Bright Line Technique' examples

In their article 'Better refractometer results with the Bright Line technique' (*The Journal of Gemmology*, 2007, 30(5/6), 287-96), Don Hoover and Cara Williams provided a most useful coverage of the refractometer by looking at the history of these unorthodox methods of illumination and explaining the resultant enhanced shadow edge phenomena.

I would like to expand a little on the information contained in their article.

A typical setup (*Figure 1a*) uses a fibre optic light source which is easily bent into variable positions for overhead lighting. Without further modification, the white light produces spectral shadow formations *(Figure 1b)*. Practice is required to distinguish the conclusive shadow information from the rogue shadows which are likely to form. The colour shadow in the 1.50 region is such a rogue. With a polarizer in position over the eyepiece, the quartz ordinary ray registers its universal RI 1.544.

Figure 1a.

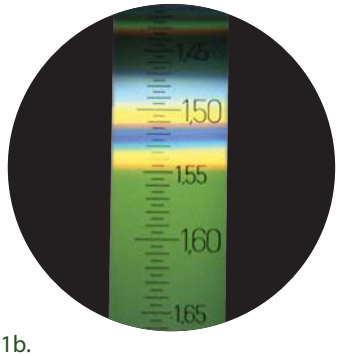

Figure 1b.

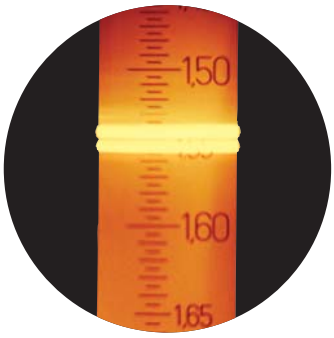

Figure 2b.

Figure 2a.

With a yellow filter held over the end of the fibre optic *(Figure 2a)*, the information is much clearer.

In this instance, there is no polarizer, and the two quartz shadow edges are seen simultaneously: 1.544, 1.553 (*Figure 2b*).

In their summary, the authors state: "This tool can significantly increase the confidence in measurement of refractive indices, especially for difficult cases." Small gemstones are a case in point, where there is no shadow formation by conventional illumination, as was the case with some 1.5 mm flux-grown synthetic emeralds *(Figure 3a)*.

In such an instance, apart from ensuring that initially the prism and gem are clean, a pencil-end is a useful accessory to gently press the stone into a full surface contact with the refractometer prism.

Figure 3a.

ISSN: 1355-4565

This is preferable with small stones, as to use an index finger would certainly result in refractometer liquid contacting the skin.

If there is still no shadow formation *(Figure 3b)*, introduce a fibre optic light above but also behind the stone. The optimum position can soon be found by manoeuvring the light until a horizontal bright line forms on the scale.

With practice, the observer learns how to interpret the RI reading to three places of decimals. Here the extraordinary ray registers at 1.560 *(Figure 3c)*, lower than that of any natural emerald, and in conjunction with the polarizer and rotation of the stone, the birefringence can be measured. Note how, with the top lighting method, the shadow column is inverted to spread down the scale.

Figure 3b.

Figure 3c.

An interesting refractometer behaviour was obtained with a painite *(Figure 4a)*. Such a gemstone was regarded with gemmological awe only a few years ago. Today there are painites in their thousands, principally from Myanmar. In appearance, they have a colour reminiscent of a red garnet. Such is the value of these previously rare gems, that £100 for a 2.5 x 2 mm gem requires that they be positively identified, and distinguished from a similar looking garnet which would have little or no value.

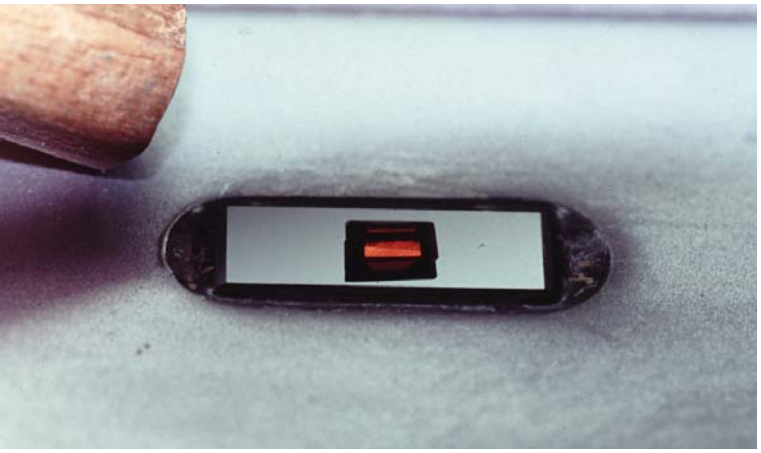

Figure 4a.

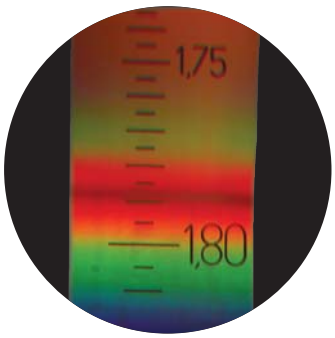

Figure 4b.

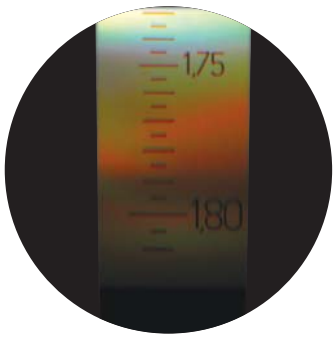

Figure 4c.

What is intriguing about the painite is that its two RIs span that of the contact liquid (RI 1.81), the extraordinary ray approximately RI 1.787 (*Figure 4b*) and the 'unseen' ordinary ray (Webster (1994, p.356): RI 1.8159). By rotation of the polarizer, the ordinary ray retains a total shadow column across the liquid boundary (*Figure 4c*).

Some idea of the ord-ray RI measurement can be gained by a loupe estimation of the facet doubling (Webster (op. cit.): birefringence 0.029), and adding on the estimated figure to the extraordinary ray RI 1.787.

The writer originally stumbled on this inverted lighting technique as an aid to the distant vision (spot) method for dealing with cabochon gems (Hodgkinson, 1988).

Subsequent experimentation revealed the interesting area of top light illumination for awkward faceted gems.

However, the Hoover/Williams article has laid bare the whole area, and must surely lead to a new dimension of interest in the humble refractometer.

Alan Hodgkinson FGA DGA
Portencross by West Kilbride
Ayrshire

Reference

Hodgkinson A., 1988. The refractometer - Distant Vision and awkward specimens. *J. Gemm.*, 21(1), 32-5

Webster, R., 1994. *Gems.* 5th edn. Ed. P.G. Read. Butterworth-Heinemann Ltd., Oxford

Abstracts

Diamonds

Global rough diamond production since 1870.

A.J.A. Bramse (archonespl@iinet.net.au). *Gems & Gemology*, 43(2), 2007, 98-119.

A compilation and analysis of data for the global production of rough diamonds (both by weight and by value) is presented, covering 27 countries, 24 major diamond mines and eight advanced projects. Production from Africa was dominant until the middle of the twentieth century. Not until the 1960s did production from non-African sources (first the Soviet Union, then Australia and now Canada) become important. Distinctions between carat weight and value affect relative importance significantly. The total global production from antiquity to 2005 is estimated at 4.5 billion carats valued at US$ 300 billion, with an average value per carat of $ 67. For the 1870-2005 period, South Africa ranks first in value and fourth in carat weight; Botswana ranks second in value and fifth in carat weight. Global production for 2001-2005 was approximately 840 million carats with a total value of $ 55 billion, for an average value of $ 65 per carat; for this period, USSR/Russia ranks first in weight and second in value, but Botswana is first in value and third in weight, just behind Australia. R.A.H.

The evolution of diamond morphology in the process of dissolution: experimental data.

A.F. Khokhryakov and Y.N. Pal'yanov (palyanov@uiggm.nsc.ru). *American Mineralogist*, 92(5-6), 2007, 909-17.

Experiments on the dissolution of octahedral, pseudo-dodecahedral and cubic natural diamond crystals in water-containing carbonate and silicate systems in high-*P*, high-*T* conditions in the diamond stability field are reported. The dissolution agents used included $CaCO_3$, $CaMg(CO_3)_2$. $CaMgSi_2O_6$ and kimberlite from the Udachnaya pipe, Yakutia, with the addition of distilled water. The experimental data show that diamonds change their morphology from octahedra, dodecahedra and cubes to tetrahexahedroids when the weight loss is 20-25%, to a cube when the loss is 50% and a pseudo-dodecahedron transforms into a tetrahexahedroid when the weight loss is as low as 10%. A comparison of crystal morphology surface features and goniometric data for diamond dissolution forms produced in water-bearing systems with rounded natural diamonds showed their complete identity. A scheme has been constructed for morphological evolution of natural diamond crystals during their dissolution. R.A.H.

Argyle in Western Australia, the world's richest diamondiferous pipe: its past and future.

V. Lorenz. *Gemmologie. Z. Dt. Gemmol. Ges.*, 2007, 56(1-2), 35-38.

First discovered in 1976 in the Ellendale area by the Kalumburu Joint Venture and its successor the Ashton Joint Venture, Argyle proved to be the richest pipe. The pipe is heavily deformed both horizontally and vertically, about 2 km long with a diameter varying between 10 and 500 m. Contents vary between 1 ct/t to 5 ct/t. Originally only about 5% were considered gem quality, but this has somewhat improved due to marketing of brown stones. With the whole pipe being extensively mined, it was expected that it would have to be closed by 2007/08, but life has now been extended for about another eight years. Only two of the Ellendale lamproite pipes are now being worked. E.S.

The south Tien Shan belt of diamondiferous alkaline basic rocks.

V.S. Lutkov and A.R. Faiziev. *Doklady Earth Sciences*, 413(2), 2007, 192-4.

Diamond crystals in the southern Tien Shan can be divided into three types: (1) fragments of transparent and translucent, colourless and grey, isotropic octahedral; (2) irregular grains composed of intergrowths of white and grey, transparent and translucent, octahedral faces; (3) light yellow and yellow grains of cubic crystals and combination of plane-faced cubes and octahedra. The western sector of the southern Tien Shan includes unique kimberlite pipes and dykes of K-silicate rocks and carbonatites. Major element and trace element analyses are presented for nine samples of Lower Mesozoic alkaline basic rocks. These rocks are characterized by the coexistence of two heterogeneous mineral associations. High contents of magnetite (3-15 kg/t) are associated with native metals, moissanite and diamonds. The concentrates of some large samples contain as much as 150-200 yellow-green diamond octahedra (0.05-0.2 mm in size). A.M.C.

ISSN: 1355-4565

Branded diamonds: their advantages and limitation: a literature review.

A. Lynch. *Australian Gemmologist*, 22(12), 2006, 542-55.

This paper discusses the marketing processes involved in branding diamonds, drawing on literature from mass psychology, market research and targeted marketing. The author considers how marketing techniques have been applied by diamond companies such as De Beers, Argyle Diamonds and BHP/Billiton (Ektai and Canadia brands). L.J.

Lab notes.

T.M. Moses and S.F. McClure (Eds). *Gems & Gemology*, 43(1), 2007, 47-55.

Notes are given on blue diamonds showing multiple phosphorescence colours, a known HPHT annealed yellow-orange diamond with a strong 480 nm absorption band, a 3.14 ct black diamond coloured by very dense clouds of micro-inclusions, and a vivid yellow 1.35 ct synthetic diamond apparently grown at a relatively high temperature of ~ 1700 C. R.A.H.

Maintaining consumer confidence in detecting synthetic and treated diamonds.

S. Quinn. *Gemmologie. Z. Dt. Gemmol. Ges.*, 2007, 56(1-2), 43-6.

The DTC is maintaining confidence by identifying synthetic and treated diamonds, and assessing their gemmological properties and their impact. Synthetic diamonds on the market are comparatively easy to detect. Techniques like HPHT treatment and multiple treatments including irradiation require more advanced instruments and knowledge. The main categories of concern are type I and fancy-coloured diamonds. E.S.

Serenity coated colored diamonds: detection and durability.

A.H. Shen (andy.shen@gia.edu), W. Wang, M.S. Hall, S. Novak, S.F. McClure, J.E. Shigley and T.M. Moses. *Gems & Gemology*, 43(1), 2007, 16-34.

The gemmological, spectroscopic and chemical properties of diamonds treated using the new 'Serenity Technologies' coating technique for inducing various 'fancy' colours are reported. This technique produces colours that include intense blue, green, yellow and orange to pink to purple-pink. The presence of a coating can be ascertained with magnification by observation of an interference-related coloured film (often with a bronze tint), scratches and colourless and/or dark areas on the surface of pavilion facets. Confirmation of the treatment can be provided by UV-Vis absorption spectra and chemical analysis. The latter has also revealed that the coating is a SiO_2 film doped with Au and/or Ag for blue, pink and yellow coloration, or with a surface film of Fe_2O_3 for orange. The colours produced by this treatment are stable to some standard jewellery repair and cleaning procedures, but they are not considered permanent. R.A.H.

The journey of light = freedom of expression.

G. Tolkowski. *Gemmologie. Z. Dt. Gemmol. Ges.*, 2007, 56(1-2), 65-6.

Expression, art, adornment equal beauty – this is carried by the journey of light. E.S.

[Zoning in diamonds from 'Mir' kimberlite pipe: FTIR data.]

E.A. Vasilyev and S.V. Sofroneev. *Proceedings of the Russian Mineralogical Society*, 136(1), 2007, 90-101. (Russian with English abstract.)

A study of plates prepared from diamonds of the 'Mir' kimberlite pipe by FTIR microspectroscopy showed that the formation of B1 defects occurred at annealing during crystal growth, but that the B2 centres were formed mainly after growth had been terminated. It is shown that development of the B2 defects in natural diamonds is a secondary process related to the aggregation of admixture nitrogen; that process had the kinetics of the decomposition of an oversaturated solid solution. There are thus possibilities for the determination of the temperature and duration of growth of natural diamonds. R.A.H.

Gems and Minerals

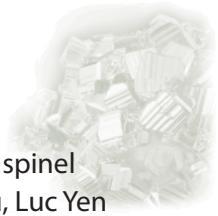

The sapphire and spinel deposit of An Phu, Luc Yen mining district, Yen Bai province, Vietnam.

D. Blauwet. *The Mineralogical Record*, 37, 2006, 224-38.

Account of a journey made to the Luc Yen mining district of Vietnam and of the ruby and spinel occurrences at the An Phu mine near the village of An Phu. Specimens recovered are described. M.O'D.

Gem corals: X-ray diffraction, solid state NMR, elemental analysis.

R. Bocchio, S. Bracco, A. Brajkovic, A. Comotti and V. Rolandi. *Australian Gemmologist*, 22(12), 2006, 524-32.

The crystallographic features and chemical composition of gem quality corals have been investigated by X-ray diffraction, NMR and laser ablation inductively coupled plasma mass spectrometry. The Octocorallia corals were found to be mainly calcitic while the Hexacorallia were mainly aragonitic in composition. Mg and Sr were considered to be the best discriminating elements, with the trace elements displaying much overlap between the two coral types. The calcitic corals have higher amounts of Mg while the aragonitic corals have more Sr. L.J.

[Mineralogy of fossil resins of Northern Eurasia.]

M.A. Bogdasarov. *Proceedings of the Russian Mineralogical Society*, 135(6), 2006, 66-78. (Russian with English abstract.)

An investigation is reported on the diagnostic properties and genesis of fossil resins from the Cretaceous, Tertiary and Quaternary sediments of N Eurasia on the basis of their physical and chemical characteristics, including their morphology, size, mass, density, optics, mechanical and thermal properties, elementary chemical compositions, etc. The constitution of amorphous organic minerals with a polymeric structure including fossil resins allows the use of IR spectrometry, e.p.r., DTA at

low heating rates, X-ray structural analysis, chemical analysis, emission spectrometry, etc. A summary of results from an investigation of the amber-bearing provinces of Baltic-Dnieper, N. Siberia and the Far East shows that resins of the Baltic-Dnieper province can be determined as amber (succinite). The amber-like resins of the N Siberian and Far Eastern provinces are mainly represented by the resins retinite and gedanite, too fragile to have any value in jewellery. Widespread viscous fossil resins on the Sakhalin coast, Far Eastern province, are rumanite and have a high potential for use. R.A.H.

Crocoite and associated minerals from Tasmania.

R.S. Bottrill, P.A. Williams, S. Dohnt, S. Sorrell and N.R. Kemp. *Australian Journal of Mineralogy,* 12, 2006, 59-90.

Magnificent crystals of orange crocoite from Tasmania are described and illustrated. Many are collector or even gem-quality. Associated minerals and geological details are given for all Tasmanian locations. M.O'D.

Stichtite from western Tasmania.

R.S. Bottrill (rbottill@mrt.tas.gov.au) and I.T. Graham. *Australian Journal of Mineralogy*, 12(2), 2006, 101-7.

The Dundas area of western Tasmania is the type locality for stichtite. This colourful but uncommon mineral (a magnesium-chromium hydroxycarbonate) is most plentiful on Stichtite Hill, near the Adelaide and Red Lead silver-lead-crocoite mines; several other localities are listed, all near Dundas. The host rocks are serpentinized dunite. The stichtite is pale pink to deep purple, fine grained and commonly contains disseminated chromite grains. It is hosted in massive, yellowish green to dark green serpentinite, yielding the material for attractive ornamental carvings. R.A.H

Blue and pink opals from Acari, Peru.

A. Brakovic, V. Rolandi, P. Vignola and R. Grizzetti. *Australian Gemmologist*, 23(1), 2007, 3-15.

Opals from Peru have been analysed by optical microscopy, X-ray powder diffraction, SEM-EDXA, Raman microscopy, FTIR (ATR) and ESR spectra and the results presented. The opals showed no play of colour. XRD detected cristobalite and tridymite in both varieties classifying them as opal-CT, as well as small amounts of chalcedony. Copper was found to be the colourant in the blue opals, and carotenoids, quinones and/or Fe(III) centres in the pink opals. The genesis of these opals has been attributed to volcanism and volcanic events. L.J.

Another imitation elephant pearl.

G. Brown. *Australian Gemmologist*, 22(12), 2006, 556-7.

Objects described as 'elephant pearls' or 'bamboo pearls' purchased in Angkor Wat, Cambodia have been examined and shown to be made from compact mammalian cortical bone. Traces of the bone structure are evident, such as Haversian and Volkmanns canals. L.J.

Madagascar tourmalines: new data and new localities.

E. Castaman, A. Donini, E. Gambini, A. Marzola, E. Pesota and M. Superchi. *Gemmologie. Z. Dt. Gemmol. Ges.*, 2007, 56(1-2), 61-4.

Multi-coloured tourmalines have been found in the pegmatites of Tsarafara (Sahatany area), in Andranomanelatra and in Ampanivan; these pegmatitic dykes are characterized by boron enrichment and concentrations of rare elements. Raman spectra were obtained. E.S.

Thermal treatment of Brazilian beryls.

G. de Oliveira Polli and H.M.P. Roeser. *Gemmologie. Z. Dt. Gemmol. Ges.*, 2007, 56(1-2), 47-50.

Commercially, thermal treatment is used mainly for blue and green aquamarines, morganite and heliodor to improve and modify their natural colour. This can usually be achieved by heating the stone for 1-2 hours at temperatures varying between 350–900 C. Ninety percent of aquamarines and morganites on the market are heat treated. For this research 383 yellow, blue, colourless, pink and green beryls from 19 Brazilian localities were used. Colour introduction by diffusion treatment could not be applied to colourless beryls as this mineral does not support the high temperatures and long exposure times necessary, but it was possible to produce a surface covering with a stable colour. E.S.

Euromineralexpo.

[Various authors.] *Rivista Mineralogica Italiana,* 31, 2007, 32-9.

Among gem-quality mineral specimens on display at Euromineralexpo, Torino, 6-8 October 2006, were trapiche emerald from Colombia, opal from Betroka, Madagascar, ruby from Luc Yen, Yan Bai province, Vietnam, danburite from Betafo, Madagascar (a yellow faceted stone of 13.28 ct), deep pink to red fluorite from Chumar Bakhoor, Pakistan, and an emerald crystal of 6.5 cm from Dafdar, Toshgorgan, Xinjiang, China. M.O'D.

Continuity and change in Chinese freshwater pearl culture.

D. Fiske (dfiske@gia.edu) and J. Shepherd. *Gems & Gemology*, 43(2), 2007, 138-45.

Most Chinese freshwater cultured pearls are produced by implanting tissue pieces in the mantle of *Hyriopsis cumingii* mussels. In the late 1990s *H. schlegelii* mussels were imported from Japan and were cross-bred with native *H. cumengii* mussels. Using the two pure species and the hybrid, Chinese farmers now produce tissue-implantation-only cultured pearls and have developed a method termed coin-bead/spherical-bead nucleation. This method has yielded significant quantities of jewellery-quality baroque shapes and lesser quantities of jewellery-quality rounds and near-rounds. R.A.H.

The changes in the Japanese jewellery market.

M. Furuya. *Gemmologie. Z. Dt. Gemmol. Ges.*, 2007, 56(1-2), 21-22.

The history of Japanese jewellery is about 2000 years old as shown by beads found in ancient tombs, but as a fashion industry it was not until 1970 that fine gold jewellery was first made. The fine jewellery industry

now accounts for many billions, and there is a growing market for wholesalers, retailers, mail orders and import of less expensive jewellery from China and India. E.S.

Trapiche tourmaline from Zambia.

T. Hainschwang (thainschwang@yahoo.com), F. Notari and B. Anckar. *Gems & Gemology*, 43(1), 2007, 36-46.

Well-formed crystals of green tourmaline from NW Zambia show a growth pattern reminiscent of trapiche emeralds when sliced perpendicular to the *c*-axis, and were originally encountered in parcels sold in Zambia as emeralds. The trapiche appearance may have originated from skeletal growth, the pattern being formed from a black carbonaceous substance (mostly graphite) partly filling growth tubes concentrated in three areas: (1) along the three edges of the trigonal pyramids, (2) at the interface between the trigonal pyramids and the prism faces and (3) between individual growth sectors of the prism. Spectroscopic and chemical analyses indicate that the tourmaline is uvite coloured green by a vanadium-related mechanism. Electron microprobe analyses are given for the green central region and the black trapiche ray for two slices of this trapiche tourmaline. R.A.H.

Recent developments in pearl testing.

H.A. Hänni. *Gemmologie. Z. Dt. Gemmol. Ges.*, 2007, 56(1-2), 23-4.

Trade rules require correct designation of natural, cultured and imitation pearls, the distinction of natural pearls from beaded or beadless cultured pearls being a major task in the gemmological lab. Identification of treatment is also required. X-ray shadow pictures are still used for first identification, ED-XRF analysis separates freshwater from saltwater products. Pearls stained black with silver nitrate can be detected; coating and polishing can be detected by SEM. X-ray luminescence differentiates between freshwater and seawater pearls based on manganese content. Raman spectroscopy can show up organic dyes. UV-VIS-NIR can identify some natural and treated colours. So-called 'chocolate' pearls are controversial as they may be bleached or stained. The latest technique is LA-ICPMS which can discriminate pearls on the basis of multi-element trace analysis. E.S.

Gemstone deposits in Vietnam and China.

W. Hofmeister. *Gemmologie. Z. Dt. Gemmol. Ges.*, 2007, 56(1-2), 25-28.

Due to overall tectonic regimes in the south-east Asia region, some geological settings in Vietnam and China have appropriate high pressure and temperature histories for gemstone formation. Ruby and sapphire are deposited in typical metamorphic and pseudo-magmatic environments. Rubies are found in the Day Nun-Con Voi region in the province Yen Bai in Northern Vietnam. Pseudo-magmatic sapphire occurs from Dac Lac in central Vietnam and Changle, Shandong Province, eastern China, showing the typical crystallographic, chemical and gemmological features of magmatic sapphires. Slightly changing chemistry of the rocks can produce gem spinels, sometimes being accompanied by emerald-green amphibole minerals. Gneissic rocks can produce good quality star rubies and sapphires. Around the city of Malipo, Yannan province in China and Ha Giang Province in Vietnam, there are granitic to granodioritic rocks cut by pegmatite veins, which give rise to the occurrence of beryl. The emerald colour is produced by small amounts of chromium and larger amounts of vanadium. E.S.

Identifying Japanese freshwater cultured pearls from Lake Kasumigaura.

D.E. Jacob, U. Wehrmeister, T. Häger and W. Hofmeister. *Australian Gemmologist*, 22(12), 2006, 539-41.

Laser ablation inductively coupled plasma mass spectrometry is used to show that Japanese Kasumigaura pearls have lower Ba/Sr and Ga/Sr ratios than Chinese pearls which have much higher and more variable ratios. L.J.

Durability testing of filled emeralds.

M.L. Johnson. *Gems & Gemology*, 43(2), 2007, 120-37.

Detailed reports are given of the treatment of 128 emeralds with nine emerald fillers (Araldite 6010, cedarwood oil, paraffin oil, unhardened and surface-hardened Opticon, a mixture of cedarwood oil and Canada Balsam, surface-hardened Norland Optical Adhesive 65, and the solid fillers Gematrat and Permasave). The emeralds were then exposed (along with 14 unfilled emeralds) to common conditions of wear and cleaning. After some six years, the emeralds were subjected to one of the following tests of durability: exposure to long-wave UV radiation, mild heat and incandescent light in a display case, five chill-thaw cycles, a desiccation environment, ultrasonic cleaning, cleaning with steam or mild chemical solvents. Changes were seen in 35% of the filled emeralds after the mild exposure tests; those with liquid fillers were especially susceptible. The desiccation environment made fissures visible in most emeralds. Hard fillers damaged their host emeralds by expanding cracks during durability testing, and chill-thaw cycling extended cracks in both filled and unfilled emeralds. Emeralds with liquid fillers were the most susceptible to changes in appearance due to ultrasonic cleaning. These results are discussed and some observations are made on the effectiveness of different fillers. A possible script for use by a jeweller to warn clients about filled emeralds and their maintenance and care is provided. R.A.H.

Emerald and alexandrite from the Malysheva Mine, Ural Mountains, Russia.

L. Kiefert. *Gemmologie. Z. Dt. Gemmol. Ges.*, 2007, 56(1-2), 29-30.

The first emeralds were found in 1831 in the Urals near the Takovaya river, 90 km north of Ekaterinburg. Today the emeralds come from the Malysheva mine in the old Takovaya river region. The mine also produced a small quantity of alexandrites. E.S.

Recent micro-observations of inclusions and related structures in gems.

J.I. Koivula. *Gemmologie. Z. Dt. Gemmol. Ges.*, 2007, 56(1-2), 31-4.

Identification of inclusions in gemstones is a very specialized skill. Destructive analysis is to be discouraged and the inclusion might add to the host gem by its rarity or beauty. Sometimes inclusions are exposed by breakage or during cutting, which makes identification easier. Gem materials used for research have usually been rejected by the trade. Modern microscopic techniques and current technologies may facilitate discovering and identifying new inclusions. E.S.

Gem news international 2007.

B. Laurs (Ed.) (blaurs@gia.edu). *Gems & Gemology*, 43(1), 2007, 56-80.

Items noted include a cat's-eye leifite from Mont Saint-Hilaire; play-of-colour opal from Piaui, Brazil; yellow prehnite from the Merelani tanzanite mine, Tanzania; green variscite with orange-brown veining containing tiny inclusions of native gold from central Western Australia; fine spodumene, morganite and tourmaline from weathered pegmatite at Tsarafara, Madagscar; small pink crystals of pezzottaite from Myanmar; and large cabochons and rough nodules of turquoise from a copper mine in Sonora, Mexico. R.A.H.

The origin of color in 'fire' obsidian.

C. Ma (chi@gps.caltech.edu), G.R. Rossman and J.A. Miller. *The Canadian Mineralogist*, 45(3), 2007, 551-7.

A variety of obsidian from Glass Buttes, Oregon, known as 'fire' obsidian for its thin layers showing various colours, was investigated with field-emission SEM, EPMA, electron back-scatter diffraction and optical spectroscopy methods. The thin layers, 300-700 nm thick, give rise to brilliant colours in reflection and mainly consist of concentrated nanometric crystals of magnetite. The colour is caused by thin-film optical interference, in which the thin layers have a higher calculated index of refraction ($1.496 < n < 1.519$) than that of the host glass (n 1.481). R.A.H.

What's new in minerals.

T. Moore. *The Mineralogical Record*, 38(3), 2007, 211-32.

Among gem minerals exhibited at the 2007 Tucson Gem and Mineral Show were aquamarine from the Shigar Valley, Northern Areas, Pakistan, and a turquoise pseudomorph after apatite from the La Caridad mine, Nacozari de Garcia, Sonora, Mexico. Chrome-green spodumene (hiddenite) has been recovered from a pocket at the Adams Farm, Alexander County, North Carolina, U.S.A. M.O'D.

The significance of new cuts in the 21st century.

B. Munsteiner. *Gemmologie. Z. Dt. Gemmol. Ges.*, 2007, 56(1-2), 39-40.

Facet cutting was developed by Ludwig von Berquem in 1476. From the 1960s there has been significant development of new gem cuts and these are discussed. E.S.

The Xianghuapu mines, Chenzhou Prefecture, Hunan Province, China.

B. Ottens. *The Mineralogical Record*, 38(1), 2007, 55-63.

Green crystals of fluorite are described from working quarries at Xianghuapu, Chenzhou Prefecture, Hunan Province, China. Crystals are found as cubes or as combinations of the cube and octahedron. Some material believed to be from these mines and offered for sale in the past may have been colour-enhanced by artificial irradiation. M.O'D.

Adventure rough stones – on the way to the mines.

E. Petsch. *Gemmologie. Z. Dt. Gemmol. Ges.*, 2007, 56(1-2), 41-42.

The author relates stories of early and present mining in far corners of the earth mainly by pioneers from Idar-Oberstein. E.S.

What's new in minerals.

J. Polityka. *The Mineralogical Record*, 37, 2006, 73-87.

Among gem-quality mineral specimens observed at the Springfield show of 2005 were deep red chondrodite from Badakhshan, Afghanistan, and a painite crystal of 6 mm from Mogok, Myanmar. M.O'D.

Marble-type ruby deposits.

D. Schwarz and D. Ohnenstetter. *Gemmologie. Z. Dt. Gemmol. Ges.*, 2007, 56(1-2), 51-2.

Marble hosted ruby deposits in central and south-east Asia, in the Urals in Russia and in Tanzania are the most important sources of gem-quality rubies. In Asia these deposits are located from Afghanistan to Vietnam. They are spatially related to major tectonic structures. Rubies from marble-hosted deposits show specific features compared with those found in other hosts. E.S.

Seventy-five years German Gemmological Association.

Gemmologie. Z. Dt. Gemmol. Ges., 2007, 56(1-2), 3-16.

Short overview of the history, development and present state of the German Gemmological Association which was founded by G.O. Wild in the Idar Gewerbehalle (trade hall), where a local gemmological exhibition had been housed since 1897. Wild was born in Idar, but had lived some time in the U.S.A., where he had come into contact with G.F. Kunz. In 1935 the association had 300 members and started training courses. After the war a Gemstone Research Institute was founded under the leadership of Prof. K. Schlossmacher. In 1953 the first exams were held and the first *Zeitschrift* was published, which is now in its 56th volume. Hans Caesar, Xaver Saller and Prof. H. Bank have been Presidents, a post filled at present by Dr Th. Lind. The Association works closely with various German universities and relevant international organizations. More than 30,000 have taken part in their educational programmes. E.S.

Observations on new coated gemstones.

J.E. Shigley. *Gemmologie. Z. Dt. Gemmol. Ges.*, 2007, 56(1-2), 53-6.

Historically inks, tints, dyes, paints and varnishes have been applied to surfaces of gemstones to improve, enhance or hide the underlying colour. Today many treatments are applied, such as irradiation, HPHT annealing or chemical diffusion. Multiple coatings may be applied. Commercial companies are advertising

improvements to diamond, corundum, topaz, beryl, opal, apatite, spinel, zoisite and possibly others. Coloured coatings are intended to enhance, hide or change the underlying body colour, while colourless coatings are intended to improve durability by sealing the surfaces of CZs or synthetic corundums. One coating substance is diamond-like carbon (DLC), an amorphous carbonaceous material with some physical properties similar to diamond. These coating materials present certain challenges to the jewellery trade, such as what are they, how thick are they, do they compromise identification, how durable are they and how much should the trade be concerned by them. E.S.

'New beryllium diffusion treatment' proves to be natural corundum surface-coated with cobalt.

C.P. Smith. *Gemmologie. Z. Dt. Gemmol. Ges.*, 2007, 56(1-2), 57-60.

Over the past year vivid blue sapphires have been on the market in Bangkok and New York; they were said to be produced in Chanthaburi, Thailand, by a 'new' beryllium treatment. The colour resembles Paraiba tourmaline. They were found to be natural corundum, surface-treated with cobalt, and were easily identified by their mottled surface and absorption spectrum of three bands at 550, 585 and 625. E.S.

Pink-to-red coral: a guide to determining origin of color.

C.P. Smith (chsmith@aglgemlab.com), S.F. McClure, S. Eaton-Magaña and D.M. Kondo. *Gems & Gemology*, 43(1), 2007, 4-15.

Due to a variety of environmental and legal factors, the supply of high-quality, natural-colour coral in the pink-to-red range has dramatically decreased in recent years and the quantity of dyed coral on the market has increased. From a study of more than 1000 natural- and treated-colour samples, the authors summarize the procedures that are useful in the identification of colour origin of pink-to-red coral. A variety of techniques, including magnification, exposure to acetone and Raman analysis, can determine if the colour of a piece of such coral is dyed. Although both magnification and the use of acetone have limitations, Raman spectroscopy can establish conclusively whether the specimen contains carotene and that the colour is natural. R.A.H.

Tormaline policrome in Vietnam.

F. Tamagnini. *Rivista Mineralogica Italiana*, 31, 2007, 104-7.

Deposits of multi-coloured tourmaline are described from Vietnam. Pink appears to be the predominating colour and some crystals appear to be of gem quality. M.O'D

From the Laboratory.

Tay Thye Sun. *Australian Gemmologist*, 23(1), 2007, 16-21.

This report includes comments on: a composite stone-plastic moulding of a Buddha statue; an imitation coconut pearl; a rare star ruby with red rays; B-Jade with blue surface sheen; a citrine displaying blue-green flashes; a large treated blue topaz for investment; a ruby paperweight; and an unusual Sri Lankan sapphire. L.J..

Ikons, classics and contemporary masterpieces of mineralogy.

W.A. Thompson. A supplement to *The Mineralogical Record*, 2007. The Mineralogical Record, Tucson, 192 pp.

About 175 beautiful mineral specimens are shown full-page in colour with facing descriptions and notes on mineral collecting. Though many specimens are of gem quality the crystals are unlikely to be fashioned. The photographs are well up to the *Record's* standard of excellence. M.O'D.

Gem corundums from Nan Khun-Nam Yuen, north-eastern Thailand.

P. Wathanakul, W. Atichat, V. Pisutha-Arnond, C. Sutthirat and D. Schwarz. *Gemmologie. Z. Dt. Gemmol. Ges.*, 2007, 56(1-2), 67-70.

The Nam Khun-Nam Yuen gem field is located in the Ubonratchathani province, in the north-east of Thailand bordering Cambodia. Blue-green-yellow sapphires and minor rubies have been found and the corundum population is bi-modal. Basaltic rocks are nearby. The stones are generally free from inclusions. Fine rutile needles and tiny zircons are rare, but secondary iron stains are common. Colour zoning is typical. Some light green-yellow sapphires with high transparency can be heat-treated to greenish-yellow or yellow under appropriate heating conditions. E.S.

Gallery reviews: Mineral museums update.

J.S. White. *The Mineralogical Record*, 37(4), 2006, 323-9.

Among the museums surveyed are the Natural History Museum, London, the Royal Museum, Edinburgh, the National Museum of Natural History, Smithsonian Institution, Washington DC, U.S.A., and the Royal Ontario Museum, Toronto, Canada. M.O'D.

Red wulfenite from the Kuruktag Mountains, Xinjiang Uygur, China.

W.E. Wilson and M.J. Origlieri. *The Mineralogical Record*, 38(1), 2007, 67-71.

Red crystals of wulfenite, some undoubtedly of ornamental quality, are described from a manganese deposit 300 kmx from the city of Hami and about 500 km from the Mongolian border, Xingjiang Uygur Autonomous Region, China. Crystals up to 4 cm on edge are reported. M.O'D.

Contrasts in gem corundum characteristics, eastern Australian basaltic fields: trace elements, fluid/melt inclusions and oxygen isotopes.

K. Zhaw (Khin.Zaw@utas.edu.au), F.L. Sutherland, F. Dellapasqua, C.G. Ryan, T.-F. Yui, P.T. Mernagh and D. Duncan. *Mineralogical Magazine*, 70(6), 2006, 669-87.

Corundum xenocrysts from alkaline basalt fields differ in their characteristics and hence in their lithospheric origins. Detailed comparisons are made between sapphires from Weldborough,

NE Tasmania, and those from Barrington, New South Wales. The Tasmanian sapphires are magmatic (high Ga, av. 200 ppm), and dominated by Fe (av. 3300 ppm) and variable Ti (av. 400 ppm) as chromophores. They contain Cl, Fe, Ga, Ti and CO_2-rich fluid inclusions and yield $\square^{18}O$ values (5.1 to 6.2 ‰) of mantle range. Geochronology on coexisting zircons suggests several sources (from 200 to 47 Ma) disrupted by basaltic metls (47 ± 0.6 Ma). Gem corundums from Barrington, NSW, also include magmatic sapphires (Ga av. 170 ppm, $\square^{18}O$ 4.6 to 5.8 ‰), but have more Fe (av. 9000 ppm) and less Ti (av. 300 ppm) as chromophores. Zircon dating suggests that gem formation was preceded and overlapped by Cainozoic basaltic melt generation (59–4 Ma). In contrast, a metamorphic sapphire-ruby suite (low Ga, av. 30 ppm) incorporates more Cr into the chromophores (up to 2250 ppm). Fluid inclusions are CO_2-poor, but melt inclusions suggest some alkaline melt interaction. The $\square^{18}O$ values (5.1 to 6.2 ‰) overlap magmatic sapphire values. The formation of rubies may be attributed to interactions at contact zones (*T* 780–940 C) between earlier Permian ultramafic bodies and later alkaline fluid activity. R.A.H.

Models of emerald formation: a new perspective.

J.C. Zwaan. *Gemmologie. Z. Dt. Gemmol. Ges.*, 2007, 56(1-2), 71-4.

The classic model of emerald formation assumes that emeralds found in schist-type deposits are formed by interaction between invading pegmatitic magmas/fluids and pre-existing mafic rock. Colombian emeralds are an exception, hosted by an early Cretaceous black shale limestone; the young Eocene deposits are not related to pegmatites or magmatic fluids. Morteani proposes that these deposits were formed by syn- to post-tectonic reactions during low-grade regional metamorphism. Giuliani, working with schist-like deposits, concluded that emeralds might be formed unconnected with pegmatites, or might be formed near pegmatites but were not formed as a result of single-stage contact metamorphism. The formation of the Sandawana emeralds however cannot be disconnected from magmatic activity. Evidence shows that no single theory can be applied to the formation of schist-type deposits. E.S.

Instruments and Techniques

Measurement of refractive indices with the Gemmeter™: a critical evaluation.

L. Cosnier. *Australian Gemmologist*, 22(12), 2006, 533-8.

Based on infrared reflectivity this new refractometer, which covers a low to high RI range, is shown to be reliable. However comparison with a conventional refractometer shows that the Gemmeter can obtain readings for high RI gems but is less precise for stones with lower RIs. L.J.

A forecast of important techniques in the coming decade.

E. Fritsch. *Gemmologie. Z. Dt. Gemmol. Ges.*, 2007, 56(1-2), 17-20.

The author stresses the continued need for careful observation using 'classical' gemmological methods. Methods which will probably be expanded include UV visible and infrared absorption, Raman scattering and X-ray fluorescence. The emission spectrum is used to help to detect HPHT-treated diamonds; the use of excitation spectra and time resolving luminescence is likely in future to be applied for the separation of natural from treated material. Trace element analysis is certain to be extended and isotopic studies look promising as they are now nearly non-destructive, with SIMS and other ion probes. They have been applied successfully using ^{18}O to determine origin of emeralds. The future gemmologist may not come from the ranks of the earth sciences, but from chemistry and physics. E.S.

Krüss HA10 Hearts and Arrows Loupe.

GAA Instrument Evaluation Committee Report. *Australian Gemmologist*, 23(1), 2007, 29-31.

Krüss Optronics present a simple and easy-to-use instrument that effectively displays the quality of cut found in Tolkowski cut diamonds. L.J.

Synthetics and Simulants

[Inclusions of metal-solvent and color in B-containing monocrystals of artificial diamond.]

A.I. Chepurov, E.I. Zhimulev, I.I. Fedorov and V.M. Sonin. *Proceedings of the Russian Mineralogical Society*, 135(6), 2006, 97-101. (Russian with English abstract.)

Single crystals of type IIb synthetic diamonds, from 0.1 to 2 ct, have been grown with cubo-octahedral habit together with minor faces {110}, {311} and {511}. These crystals are various shades of blue or dark blue depending on the amounts of B in the system; a characteristic feature is a sectorial structure expressed in a non-uniform distribution of colour. Metal inclusions with faceted isometric, lamellar extended inclusions, non-faceted inclusions and microinclusions have been found; they correspond in chemical composition with that of the metal solvent. The IR spectrum of these boron-bearing diamond crystals is presented together with figures showing the dependence of the *a* cell parameter of metallic inclusions on the iron content of the Fe-Ni alloy. R.A.H.

Abstractors

A.M. Clark - A.M.C. R.A. Howie - R.A.H. L. Joyner - L.J.
M. O'Donoghue - M.O'D. E. Stern - E.S

Book Reviews

Pinzgau - Tal der Kristalle und des grünen Feuers.

E. Burgrgsteiner and M. Wachtler, 2007. extraLapis No. 32. Weise, Munich. Pp 99, illus. in colour. ISSN 09458493. Price on application.

Review of the geology, mineralization and mineral species of the Pinzgau area, Salzburg, Austria. Ornamental-quality pink fluorite and fine green titanite (sphene) are among the species likely to be of interest to gemmologists. As always with this series, the standard of production and reproduction of photographs are of the highest order. M.O'D.

Robbing the Sparry Garniture. A 200-Year History of the British Mineral Dealers.

M.P. Cooper, 2007. The Mineralogical Record, Tucson, AZ. 358 pp. Softcover. [No ISBN]. US$49.00.

This is an amazing effort and without doubt has saved, probably at the eleventh hour, a great deal of information that could so easily have been lost. The book is much more than an alphabetical list of dealers (there are far more that might be assumed): Mick Cooper gives us details of their catalogues and illustrates, on many pages, their labels (the content and even the printing style of these often give a clue to the dates when particular specimens are first recovered). Some contemporary dealers have been photographed and reproductions of earlier photographs are plentiful.

While gemmologists will find a number of references to dealers who sold ornamental pieces, they will also enjoy reading about the practitioners of a profession that may appear submerged to many who are more familiar with fashioned artefacts.

The work is a great service to the earth sciences. M.O'D.

Tables of gemstones identification.

R. Dedeyne and I. Quintens, 2007. Glirico (glirico@gemmologie.be), Gent. Pp 309. Hardcover ISBN 9789078768012. Price on application.

Following a brief introduction in which some terms are explained, the remainder of the book presents numerical tables of major constants. There is no central index so, unless the reader already roughly knows whereabouts in the tables the desired species can be found, use of the book is likely to be wasteful of time. As always with tables, the authors have been faced with the question of nomenclature so that obsolete names have crept in as well as the usual fanciful and tedious names for quartz varieties and many others. There are 17 books listed in the bibliography where the GIA's centre of operations is stated to be Los Angeles and *Australian Gemmologist* is named as *Australian Gemmology*. This carelessness is typical of the whole book and the authors have been less than well-served by their advisers. It cannot be recommended (surely this type of book is now obsolete?); a pity because the production is good and the front cover the book's best feature. M.O'D.

Geology of Gem Deposits (short Course Series Volume 37).

L.A. Groat (Ed.) (lgroat@eos.ubc.ca). Mineralogical Association of Canada, Quebec. 288 pp plus 24 colour plates. ISBN 978-0-921294-37-5. US$ 50.00.

Gem deposits are rare because in general the conditions that promote their formation are unusual, and thus worthy of scientific study. Modern geological and analytical techniques have now been applied to gem occurrences in Canada and elsewhere, leading to radical alteration of models and understanding. This volume looks at gemstones from a geological perspective and reviews in ten chapters current concepts on the origins of diamond, ruby, sapphire, emerald and other coloured gems. R.A.H.

Opal, the Phenomenal Gemstone.

Various authors, 2007. extraLapis, English No 10. Lithographie, LLC, East Hampton, CT. 108 pp. ISBN 978 0 970908 0 9. Price on application.

This latest monograph in the welcome extraLapis series carries papers on various aspects of opal, including: Science, history and lore (noted dealers Si and Ann Frazier, who also contributed an opal glossary of terms), Play-of-colour in opal (Max Weibel) , Composite opal (Karl Fischer), Synthetic, colour-enhanced and imitation opal (Michael O' Donoghue), Ethiopia to Indonesia, a sampling of lesser-known opal localities (Gloria Stabler), and Opal

ISSN: 1355-4565

from Mexico (Jürgen Schütz). There is an excellent list of references and a map of world opal localities.

As we have come to expect from this series (and its German counterpart) the colour pictures are beautiful. M.O'D

The World of Fluorescent Minerals.

S. Schneider, 2006. Schiffer Publishing, Atglen, PA. pp 192, illus. in colour. Softcover. ISBN 0 7643 2544 2. US$29.95.

All books on fluorescent minerals need to be fully illustrated in colour and in many examples definition seems to have suffered in the transition, between photograph and reproduction. This very attractive book is an exception; it could serve as a general illustrated guide to minerals even without the fluorescence effects. As well as the photographs there are useful hints for the collector and both dimensions and weights are given for the specimens depicted.

In most cases the same specimen is shown in both LW and SW UV: the arrangement is by country of origin and there is a short list of dealers holding stocks of or specializing in fluorescent minerals: all are in the United States. There is a short bibliography and a list of names and addresses of special interest groups in the United States.

This is an excellent book and most attractively produced. M.O'D.

Namibia, Minerals and Localities. 2nd edn.

L. Von Bezing, R. Bode and S. Jahn, 2007. Bode, Haltern. pp 856, illus. throughout in colour. €111.00.

While the weight of the book may be the first feature to strike the reader, an examination of every opening will quickly indicate that this is one of the world's greatest mineral books, worthily continuing the German tradition of excellence in both text and illustration. In every way this is a splendid book; authoritative text by authors and consultants and some of the most beautiful mineral photographs I have yet seen.

Of course if you are aiming to select a single country which contains the most spectacular mineral specimens, Namibia is one of the best to choose. Gem-quality minerals (tourmaline – it has its own 'Tourmaline gallery') and many others can be found among the photographs. Some of the less common minerals are much better collected for their crystals than for fashioning – look up cuprite, smithsonite, malachite and wulfenite.

The first part of the book describes the history of mineral prospecting and mining in Namibia. Tsumeb, as expected, is comprehensively treated, but there are also the Erongo mountains, the Rössing mountains, the Onganja mine and its copper deposits and, naturally, the pegmatites in the central areas and the story of Luderitz and the diamonds.

This section is followed by an encyclopaedic treatment of the minerals; there are no appendices but the references cover pages 834-38.

This is a breathtaking book; apart from the specimens many photographs give the reader some idea of the country in general. Forget the (reasonable) expense and the weight and buy the book. M.O'D.

Proceedings of the Gemmological Association of Great Britain and Notices

Gem-A Conference and Graduation Ceremony

The 2007 Gem-A Conference was held on Sunday 28 October at the Renaissance London Heathrow Hotel. The theme of the Conference was 'Gems of the Orient: Pearls and Jade', and speakers included Shigeru Akamatsu, George Bosshart, Prof. Dr Henry A. Hanni, Roger Keverne, Chiu Mei Ou Yang, Gaiti Rabbani, Kenneth Scarratt and Elisabeth Strack. A programme of events was arranged to coincide with the Conference, including a private viewing of the Crown Jewels at the Tower of London, visits to the School of Earth Sciences, Kingston University, to view and learn about the equipment used to research gems and minerals, and a Gem Discovery Club specialist evening.

On Monday 29 October the Graduation Ceremony and Presentation of Awards gained in the 2007 examinations was held at Goldsmiths' Hall in the City of London. Chairman of the Gem-A Council, Prof. Alan T. Collins, presided, and David Thomas, Crown Jeweller from 1991 to July 2007, presented the awards.

Ms Chiu Mei Ou Yang of Hong Kong was awarded an Honorary Lifetime Membership in recognition of her substantial contribution to the world of gemmology and to the Association. The award was presented by Gem-A President Alan Jobbins.

The address was given by David Thomas, who stressed to the graduates the importance of their education for the trade and the necessity for continual learning throughout their careers. He concluded by saying; "You can all achieve your dream by dedication, continual learning and belief in yourself. I urge you all to continue your education in this fascinating and historic trade."

The ceremony was followed by a reception for nearly 300 graduates and guests.

Reports of both the Conference and the Graduation Ceremony will be published in the December 2007 issue of *Gems & Jewellery*.

Conference Sponsors and Supporters

The Association is most grateful to the following for their support:

Major sponsors

Marcus McCallum FGA
Room 42-44, New House, 67-68 Hatton Garden, London EC1N 8JY
t: 020 7405 2169
e: info@marcusmccallum.com
w: www.marcusmccallum.com

T.H. March, Insurance Broker
10-12 Ely Place, London EC1N 6RY
t: 020 7405 0009
e: insurance@thmarch.co.uk
w: www.thmarch.co.uk

Sponsors

National Association of Goldsmiths
78a Luke Street, London EC2A 4XG
t: 020 7613 4445
f: 020 7613 4450
e: nag@jewellers-online.org

Supporters

BKT (Rings) Ltd and TJW (Diamonds) Ltd
7 Hatton Garden, London EC1N 8AD.
t: 020 7405 1560/7441/1044
f: 020 7430 0672
e: bkt.tjw@btconnect.com

Maggie Campbell-Pederson
Organic Gems
e: info@maggiecp.com
w: www.maggiecp.com

Marcia Lanyon Limited
PO Box 370, London W6 7NJ.
t: 020 7602 2446

Ruppenthal (UK) Ltd
t: 020 8777 4443
f: 020 8777 2321
e: ruk@ruppenthal.co.uk
w: www.ruppenthal.co.uk

ISSN: 1355-4565

Gem-A Awards

Gem-A Examinations were held worldwide in June 2007. In the Examinations in Gemmology 230 candidates sat for the Diploma Examination of whom 139 qualified, including eight with Distinction and fifteen with Merit. In the Foundation Gemmology Examination, 220 candidates sat of whom 153 qualified. In the Gem Diamond Examination 80 candidates sat of whom 49 qualified, including six with Distinction and seven with Merit.

The Tully Medal is awarded to the candidate who submits the best set of answers in the Gemmology Diploma examination which, in the opinion of the Examiners, are of sufficiently high standard. This year, most unusually, two Tully Medals were awarded. Sophie Louise Wootton of London was awarded the Tully Medal as well as Christie's Prize for Gemmology for the best candidate of the year in the Diploma Examination who derives their main income from activities essentially connected with the jewellery trade. Taisuke Kobayashi of Tokyo, Japan, also received the Tully Medal in addition to the Anderson Bank Prize for the best non-trade candidate of the year in the Diploma in Gemmology.

The Foundation Certificate in Gemmology examination awards, the Anderson Medal for the candidate who submitted the best set of answers which, in the opinion of the Examiners, were of sufficiently high standard, and the Hirsh Foundation Award for the best candidate of the year, were awarded to Holly J. Barker of Johannesburg, South Africa.

The Gem Diamond Diploma examination awards, the Bruton Medal for the candidate who submitted the best set of answers which, in the opinion of the Examiners, were of sufficiently high standard, and the Deeks Diamond Prize for the best candidate of the year, were both awarded to Peter Alexander Jansch of Englefield Green, Surrey. This year the Gem-A Council awarded a special prize for the best set of theory papers in the Gem Diamond Diploma examination, Distinction category. This was awarded to Gregory Peter Hall of Brighton, East Sussex.

The names of the successful candidates are listed below:

EXAMINATIONS IN GEMMOLOGY

Gemmology Diploma

Qualified with Distinction

Guo Xiao Lei, Wuhan, Hubei, P.R. China
Jiang Xin, Wuhan, Hubei, P.R. China
Kobayashi, Taisuke, Tokyo, Japan
Raoult, Francoise, Étables-sur-Mer, France
Sawamura, Tsukasa, Tokyo, Japan
Sekine, Shunji, Tokyo, Japan
Tang Zi Wei, Wuhan, Hubei, P.R. China
Wootton, Sophie Louise, London

Qualified with Merit

Bryl Gaudet, Lou-Pierre, Montreal, Quebec, Canada
Cheng Yuan, Guilin, Guangxi, P.R. China
Cui Xianzhong, London
Di Dongshuang, Wuhan, Hubei, P.R. China
Haokip, Seikholen, Imphal, Manipur, India
Hu, Helen, London
Jain, Apeksha, New Delhi, India
James, Bronwynne, St Albans, Hertfordshire
Li Xiao Lin, Wuhan, Hubei, P.R. China
Machefert, Jean-Michel, Cormeilles-en-Parisis, France
Mo Zurong, Guilin, Guangxi, P.R. China
Sahabunyakul, Saran, Bangkok, Thailand
Smith, Laura Sian, Oxford
Wang Qin, Guilin, Guangxi, P.R. China
Xing Yingying, Wuhan, Hubei, P.R. China

Gem-A Awards

Qualified

Abduriyim, Ahmadjan, Taito-ku, Tokyo, Japan
Adler, Stevan, New York, U.S.A.
Andrianaina Rado, Antananarivo, Madagascar
Avender, Breanne Valeda, Burnaby, British Columbia, Canada
Bove, Bertrand, Vitry-sur-Seine, France
Cao Li Fei, Wuhan, Hubei, P.R. China
Caulton, David, Dore, Sheffield
Chan Che Min, Tsuen Wan, Hong Kong
Chang Hsiao Huei, Westmount, Quebec, Canada
Chauhan, Rakesh, Chandigarh, India
Cheung, Nelly, Tai Koo Shing, Hong Kong
Cheung Ching Ping, Candy, Tseung Kwan, Kowloon, Hong Kong
Chiu Chun-Chieh, Taipei, Taiwan, R.O. China
Corser, Elizabeth, Wellington, Shropshire
Craddock, Natalie, Bridport, Dorset
Cutler, Leticia, Birmingham, West Midlands
Daudin, Mathieu, Paris, France
De Barros, Valere, Maron, France
de Siran de Cavanac, Bérengère, Toulon, France
Dereszewska, Basia, London
Dighton, Anna Louise, Saffron Walden, Essex
Dong Haiyang, Guilin, Guangxi, P.R. China
Doyle, Helen, London
Drummond, Jean, Farnham, Surrey
Faugeroux, Valerie, Lagardelle-sur-Lèze, France
Feng Jing Ling, Shanghai, P.R. China
Ferneyhough, Ella Jane, Birmingham, West Midlands
Fong Yan, William, Tai Po, Hong Kong
Fu Xin, Haidian District, Beijing, P.R. China
Fujii, Yasuhisa, Sinagawa-ku, Tokyo, Japan
Galbraith, Stuart, Bourton-on-the-Water, Gloucestershire
Grimal, Marie, Marseille, France
Guo Qian, Guilin, Guangxi, P.R. China
Han Jie, Coventry, West Midlands
Harrington, Olga, Zurich, Switzerland
Heit, Liesbeth, London
Hsu Chia Jung, Taichung, Taiwan, R.O. China
Hu Xiao Yu, London
Hui Wing Hing, Kowloon, Hong Kong
Iwamoto, Akiko, London
Jin Yan Nan, Wuhan, Hubei, P.R. China
Kim Dong Hui, Daegu, South Korea
Kim Ji Eun, Chungbuk-Do, South Korea
Koundouraki, Evagelia, Athens, Greece
Lam Nga Sheung Hilde, Kowloon, Hong Kong
Lau Tsui Wah, Kowloon Tong, Hong Kong
Lee Cheuk Ming, Kowloon, Hong Kong
Leong Weng Fock, Cedric, Antananarivo, Madagascar
Li Hua, Wuhan, Hubei, P.R. China
Li Zhi, Wuhan, Hubei, P.R. China
Liao Tsai Chun, Taipei, Taiwan, R.O. China
Lilley, Samantha, London
Lin Chun Hsien, Taipei, Taiwan, R.O. China
Lin Li, Guilin, Guangxi, P.R. China
Lin Wanchun, Guilin, Guangxi, P.R. China
Ling Xiao Qing, Shanghai, P.R. China
Liu Zijian, Guilin, Guangxi, P.R. China
Lo, Sunny, Kowloon, Hong Kong
Lo Pui Yin, Shirley, Tai Po, Hong Kong
Lung Wan-Hui, Taipei, Taiwan, R.O. China
Luzuriaga Alvarez, Hugo Vicente, Montreal, Quebec, Canada
McWhirter, Hannah Maeve, Bury St Edmunds, Suffolk
Miller, Me'Shell, North Highlands, California, U.S.A.
Mitchell, Jonathan D., Midland, Texas, U.S.A.
Miyamoto, Kazuhiko, Osaka City, Osaka, Japan
Mok So Yiu, Tsuen Wan, Hong Kong
Munoz-Vasquez, Alejandra C., London
Naing, Sein, Lanmadaw Township, Yangon, Myanmar
Naito, Ayako, Tokyo, Japan
Nakagawa, Yumi, Kitakatsuragi-gun, Nara Pref., Japan
Narudeesombat, Nalin, Bangkok, Thailand
Palmares, Richard P., Sale, Cheshire
Perks, Helen Elizabeth, Telford, Shropshire
Piha, Saara, Helsinki, Finland
Powar, Krishna, Smethwick, West Midlands
Prak, Sam, Toronto, Ontario, Canada
Ranaivoson Hantarinoro, Antananarivo,

Gem-A Awards

Madagascar
Randriamialisoa Tody Harilala, Antananarivo, Madagascar
Ren Lei, Haidian District, Beijing, P.R. China
Rodman, Anna, Sweden
Rossi, Hélène, Besançon, France
Saejoo, Sakrapee, Bangkok, Thailand
Sarraf, Kundan, Lalitpur, Nepal
Shen Jiani, Guilin, Guangxi, P.R. China
Spagnoletti Zeuli, Lavinia, London
Stevenson, Laura Jacqueline, North Vancouver, British Columbia, Canada
Suokko, Teija, Tampere, Finland
Tai Ai-Hwa, Taipei, Taiwan, R.O. China
Takahata, Yoshichika, Takamatsu City, Japan
Tang Jiahui, Guilin, Guangxi, P.R. China
Tanvangi, Pragya, Surat, India
Uchiyama, Mio, Ichikawa City, Chiba Pref., Japan
von Schantz, Casimir, Helsinki, Finland
Voulgaris, Apollon, Mykonos, Greece
Wang Haiyuan, Haidian District, Beijing, P.R.China
Wang Wenqi, Guilin, Guangxi, P.R. China
Wang Yi Xian, Wuhan, Hubei, P.R. China
Watson, Jennifer, Sutton Coldfield, West Midlands
Win, Mo Mo, Yankin Township, Yangon, Myanmar
Wong, Winnie, Tsimshatsui, Kowloon, Hong Kong
Wong Lai Mi, Tseung Kwan O, Hong Kong
Wong Yin Kwan Angela, Tin Shui Wai, New Territories, Hong Kong
Wu, Benson, Oakville, Ontario, Canada
Wu Chiayu, Taipei, Taiwan, R.O. China
Wu Wing Yi, Kowloon, Hong Kong
Yamada, Masashi, Tokyo, Japan
Yamaguchi, Yuko, Osaka, Japan
Yang Jui Lin, Taipei, Taiwan, R.O. China
Yau Wai Yee, Kowloon, Hong Kong
Yeung, Anthea Ka Yee, Hong Kong
Yip Tak Wing, Shatin, Hong Kong
Zhang Duo, Wuhan, Hubei, P.R. China
Zhang Yanyan, Haidian District, Beijing, P.R.China
Zhao Lisha, Guilin, Guangxi, P.R. China
Zheng Lulu, Wuhan, Hubei, P.R. China
ZhuoJun Xu, Shanghai, P.R. China

Gemmology Foundation Certificate

Qualified

Abey, Sara, London
Anastasopoulou, Georgia, Greece
Andersson, Lina, Sundbyberg, Sweden
Andersson, Joel, Lannavaara, Sweden
Andrianaina Rado, Antananarivo, Madagascar
Astrand, Frida, Malmo, Sweden
Au, Anita Suet Ki, Tsimshatsui, Kowloon, Hong Kong
Austen, Katelyn Scarlet, Oldbury, West Midlands
Aye Su Nandar Htay, Yangon, Myanmar
Beer, Robyn M., Rocklin, California, U.S.A.
Bigford, Julie Claire, Malvern Wells, Worcestershire
Brian, Jeremy, Marseille, France
Brichet, Leonore, Vernouillet, France
Bryl Gaudet, Lou-Pierre, Montreal, Quebec, Canada
Burton, Lola Clare, Bournemouth, Dorset
Cane, Deborah, Birmingham, West Midlands
Chan Hing Yip, Ken, Kowloon, Hong Kong
Chan Ka Man, Carmen, Lantau Island, Hong Kong
Chan Wai Sze, Shatin, New Territories, Hong Kong
Chan Yuk Ying, Tsimshatsui, Kowloon, Hong Kong
Chang Hsiao Huei, Westmount, Quebec, Canada
Chapman, Dominic Richard James, Caterham, Surrey
Cheung Fai Har, Candy, Yuen Long, Hong Kong
Cheung Suk Wan, Shatin, New Territories, Hong Kong
Chie, Christine, Heng Fa Chuen, Chai Wan, Hong Kong
Chitty, Warne William, Aspen, Colorado, U.S.A.
Chow Siu Fung, Tsimshatsui, Kowloon, Hong Kong

Gem-A Awards

Chu Fung Yee, Tsimshatsui, Kowloon, Hong Kong
Chung Tsz Bun, Kowloon, Hong Kong
Day, Helen Laura, Wolverhampton, Staffordshire
de Siran de Cavanac, Berengere, Toulon, France
Dereszewska, Basia, London
Dighton, Anna Louise, Saffron Walden, Essex
Duval, Julie, London
Evans, Natalie, London
Evans, Charles I., London
Giertta, Maria, London
Gilli, Claude, Les Pennes Mirabeau, France
Gunnarsson, Camilla, Lannavaara, Sweden
Guy, Nicholas M., Fremington, North Devon
Hall, Christopher Robert, Wednesbury, West Midlands
Hampton, Kate, Mazesycoed, Pontypridd, Wales
Hamren, Elisabeth, Ostersund, Sweden
Han Jie, Coventry, West Midlands
Hansson, Maria, Eslou, Sweden
Harker, Catherine Anne, Birmingham, West Midlands
Hou Xukui, Guilin, Guangxi, P.R. China
Hsu Juiwen, Taiwan, R.O. China
Hu Xiao Yu, London
Hui Yuet Ming, Kowloon, Hong Kong
Huijbrechts, Thomas N., Salisbury, Wiltshire
Iwamoto, Akiko, London
James, Bronwynne, St Albans, Hertfordshire
Jay Wang San, Katherine, Hong Kong
Jeong Eun Ah, Kofu City, Yamanashi Pref., Japan
Kambale, Sonia, Surat, Gujarat, India
Kankkunen, Markus, Tervalmpi, Finland
Kanwar, Kerensa Janet, Renfrew, Scotland
Karkouli, Elpida, Drossia, Greece
Keung Wing Fun, Kowloon, Hong Kong
Kim, Eun Jeong, Gyungnam-Do, South Korea
Kim, Richard, Citrus Heights, California, U.S.A.
Kim, Deok Hyeon, Nam-Gu, Daegu, South Korea
Knutsen, Annmari Ellilia, Oslo, Norway
Kobayashi, Nobue, Taito-ku, Tokyo, Japan
Kok, Hans, DJ Ysselstein, The Netherlands
Kuchard, Monika, London
Kui Nui Reema, Yeong Long, Hong Kong
Lai Siu Kwong, New Territories, Hong Kong
Lam Pui Ling, Shau Kei Wan, Hong Kong
Lam Sau Kwan, Hong Kong
Larsson, Ylva, Lannavaara, Sweden
Lau Ho, Kowloon, Hong Kong
Lee, Sinnie, Kowloon Tong, Hong Kong
Lee Ka Ho, Vincent, Kowloon, Hong Kong
Leong Weng Fock, Cedric, Antananarivo, Madagascar
Leung Ka Yee, Ainsley, Sheung Shui, New Territories, Hong Kong
Li Jingna, Guilin, Guangxi, P.R. China,
Liang Rong, Guilin, Guangxi, P.R. China
Lofberg, Anders, Lannavaara, Sweden
Luzuriaga Alvarez, Hugo Vicente, Montreal, Quebec, Canada
Ma, Hoi Shan, Kowloon, Hong Kong
McWhirter, Euan, London
Man Sai Wing, Kwun Tong, Hong Kong
Marsh, Lynn, Farringdon, Tyne and Wear
Martins Molgard, Silvia, Colombo, Sri Lanka
Mi Zhiwei, Guilin, Guangxi, P.R. China
Mo Ying Lin Marilyn, Kowloon, Hong Kong
Mogridge, Emma Denise, Cornworthy, Devon
Mu Yujing, Shanghai, P.R. China
Narudeesombat, Nalin, Bangkok, Thailand
Ng Wai Hing, Tsuen Wan, New Territories, Hong Kong
Nichol, Camilla, York
O'Hagan, David, Sutton Coldfield, West Midlands
Owen-Jones, Joy, Birmingham, West Midlands
Pan, Ya-Fen, Taiwan, R.O. China
Papapavlou, Despina-Maria, Rhodes, Greece
Park, Seon Hyun, Buk-Gu, Daegu, Korea
Partner, Robert, Cropston, Leicestershire
Patel, Jayeshkumar Ramajibhai, Surat, India
Poon Wing Yan, Tin Shui Wai, New Territories, Hong Kong
Pughe, Marianne, Corbridge, Northumberland
Randriamialisoa Eva Harilala, Antananarivo, Madagascar

Gem-A Awards

Ranorosoa Nadine, Antananarivo, Madagascar
Raoult, Francoise, Étables-sur-Mer, France
Razanadimby, Lalanirina, Antananarivo, Madagascar
Ross, Antonia, Fleet, Hampshire
Rossi, Hélène, Besançon, France
Rufus, Simon, London
Saejoo, Sakrapee, Bangkok, Thailand
Sawyer, Jennifer, Hungerford, Berkshire
Sellors, James, Birmingham, West Midlands
Shah, Krupa, Nairobi, Kenya
Shah, Roshni M., Nairobi, Kenya
Shaw, Heather, Barnsley, Yorkshire
Shum Yau Kuen, Charlotte, Kowloon, Hong Kong
Siegan-Smith, Breige, London
Siriwardena, H.H.D.A.L., Raddolugama, Sri Lanka
Smith, Mark, Richmond, Surrey
So Hoi Ling Beta, New Territories, Hong Kong
Sonoda, Yasuko, Kofu City, Yamanashi Pref., Japan
Spencer, Jason, Birmingham, West Midlands
Tang Jiahui, Guilin, Guangxi, P.R. China
Tang Kai Chung, Yuen Long, New Territories, Hong Kong
Thein Thein Win, Yangon, Myanmar
Toca, Mayte, Antananarivo, Madagascar
Tsuruta, Miho, Onga-gun, Fukuoka Pref., Japan
Ueda, Kenji, Osaka City, Japan
Valerio Sa, Helena, Montreal, Quebec, Canada
van Beek, Ellen, Schoonhoven CB, The Netherlands
Vigneron, Charlotte, Boulogne-Billancourt, France
Vlemmix, J.M.A, Ravenstein AD, The Netherlands
Voyiatzi, Niki, London
Wakabayashi, Takuji, Tokyo, Japan
Wan, Hsiang Hsin, Taipei, Taiwan, R.O. China
Wang, Yinjie, Shanghai, China
Wang Ling, Shanghai, China
Ward, Simon Francis, Leigh-on-Sea, Essex
Watanabe, Yoshiko, Minamitsuru-gun, Yamanashi Pref., Japan
Wong Wing Sze, Hong Kong
Xu Hui, Guilin, Guangxi, P.R. China
Yamada, Mayumi, Kobe City, Hyogo Pref., Japan
Yamaguchi, Yuko, Osaka, Japan
Yeung Siu Sing, Antony, Kowloon, Hong Kong
Yoon, Hee Sung, Seoul, South Korea
Yoshida, Ayana, Tokyo, Japan
Yu, Young Il, Ansan-Si, Gyeongg-Do, Korea
Yu Kwai Sang, Tsuen Wan, New Territories, Hong Kong
Yu Xiubing, Shanghai, P.R. China
Zaleszczyk, Alicja, Birmingham, West Midlands
Zetterblom, Ulrika, Lannavaara, Sweden
Zhang Minghui, Guilin, Guangxi, P.R. China
Zhuang, Zhiyuan, Shanghai, P.R. China

GEM DIAMOND EXAMINATION

Gem Diamond Diploma

Qualified with Distinction

Bell, Lucy Kate, Stirchley, Birmingham, West Midlands
Deeley, Philippa, Etchingham, East Sussex
Jansch, Peter Alexander, Englefield Green, Surrey
Khan Farrukh, Nayer, Washwood Heath, West Midlands
Murray, Helen Claire, Sutton Coldfield, West Midlands
Robichaud, Emilie Gould, London

Qualified with Merit

Beer, Jasmin, Birmingham, West Midlands
Chan Wing Sze, Herleva, Kowloon, Hong Kong
Dong Wei, Wuhan, Hubei, P.R. China
Harker, Catherine Anne, Birmingham, West Midlands
Low, San, Chatham, Kent
Westlake, Ingrid, Chamonix, France
Zhao Xi, Wuhan, Hubei, P.R. China

Gem-A Awards

Qualified

Au Wing Ki, Astor, Happy Valley, Hong Kong
Austen, Katelyn Scarlet, Oldbury, West Midlands
Bao Li, Chaoyangmenwai, Beijing, P.R. China
Boubker, Layla, Hatfield, Hertfordshire
Chan Che-Sheung, Joanna, Hong Kong
Chan Kin Chung, San Po Kong, Kowloon, Hong Kong
Chin Suet Ying, Kwai Chung, New Territories, Hong Kong
Chiu Fong Ting, Siu Hang Tsuen, New Territories, Hong Kong
Dorudi, Roya, London
Georgmas, Emmanuel, Byron, Greece
Harman, Bronwen, Reading, Berkshire
Ho Yue Yau, Tsuen Wan, Hong Kong
Jenkinson, Glenn W., Telford, Shropshire
Jones, Gary, Dudley, West Midlands
Jordan, Steven L., Biggleswade, Bedfordshire
Khaing, Hnin Hnin, London
Ko Yum Sum, Iris, Kowloon, Hong Kong
Lam Shun, Kowloon, Hong Kong
Leno, Petra, Newbury, Berkshire
Leza, Marianna, Ano Glyfada, Greece
Lwin, Pwint Phue, London
Martins, Miki, Burnaby, British Columbia, Canada
Ng Yuk Yu, Shatin, New Territories, Hong Kong
Rice, James, Hull, East Yorkshire
Symes, Evelyn R., Bath, Somerset
Tam Tin Sang, Daniel, Kowloon, Hong Kong
Thomas, David John, Milton Keynes, Buckinghamshire
Wang Gang, Feng Tai District, Beijing, P.R. China
Wang Jiazheng, Wuhan, Hubei, P.R. China
Wang Min, Wuhan, Hubei, P.R. China
Wilson, Naomi, Birmingham, West Midlands
Woolley, Claire Corinna, Cradley Heath, West Midlands
Xie Junjun, Wuhan, Hubei, P.R. China
Xu Hui, Fengtal District, Beijing, P.R. China
Yang Lei, Wuhan, Hubei, P.R. China
Zhao Hang, Wuhan, Hubei, P.R. China

Members' Meetings

London

Annual General Meeting

The Annual General Meeting was held at the National Liberal Club, Whitehall Place, London SW1, on 18 June. Professor Alan Collins chaired the meeting and welcomed members. The Annual Report and Accounts were approved. Sheila Burgoyne and Sally Everitt retired from the Council in rotation and being eligible Sally Everitt was re-elected to the Council. Sheila Burgoyne did not seek re-election. James Riley and Jason Williams had been appointed to serve on the Council since the 2006 AGM and both were elected. Brian Jackson and Gwyn Green retired in rotation from the Members' Audit Committee and, being eligible, were re-elected to the Committee. Hazlems Fenton were re-appointed as auditors for the year.

A special resolution was put to the meeting that the name of the Association be changed to 'The Gemmological Association of Great Britain'. After discussion the name change was put to the vote and was agreed by a large majority.

A presentation by John I Koivula of the GIA, Carlsbad, entitled 'The latest views of the MicroWorld' followed the AGM, a report of which appeared in the August 2007 issue of *Gems & Jewellery*.

Seaman Schepps (1881-1972): America's Court Jeweller

A guided tour of the Seaman Schepps exhibition at the Gilbert Gallery, Somerset House, was held on the afternoon of 18 June, planned to coincide with the Gem-A AGM and talk by John Koivula. The guided tour highlighted the key works of Seaman Schepps, his background, and the historical and social context of his work, as well as the innovative materials he used, unusual settings and originality of designs.

Gem Discovery Club Specialist Evenings

The Gem Club meets every Tuesday evening at the Gem-A London headquarters when Club members have the opportunity to examine a wide variety of stones, and once a month a guest gem or mineral specialist is invited to give a presentation.

The guest in April was Marcus McCallum who talked about stone beads, the recent market explosion, the new stones and cuts coming onto the market, and the methods of treatment. Rui Galopim de Carvalho of Sintra, Portugal, in the UK to speak at the Gem-A Scottish Branch Conference, was the May guest. He gave a presentation on the gemstones used in seventeenth- and eighteenth-century Portuguese jewellery. At the June specialist evening, Club members learnt about the history and characteristics of Lennix synthetic emeralds from guest Roy Huddlestone. Plenty of time was allowed for the participants to examine the large selection of the synthetics that Roy had brought along. The July guest, gem dealer Jason Williams, gave a brief talk on the values and value factors of gemstones before challenging Club members to estimate relative values of a large number of cut and polished gemstones. In August Harry Levy gave an up-date on the treated and synthetic diamonds circulating on the market today. The September specialists, Peter Rome and John Taylor of Charles Mathews (Lapidaries), gave an insight into the art of fine gem cutting by hand. In October, Harold Killingback's subject was asterism in quartz when he demonstrated how light from a laser is affected by the regular array of inclusions in a sphere of star rose quartz. At the Gem Club held at the end of October to coincide with the Gem-A Annual Conference, Jack Ogden gave a presentation entitled 'A Lust for Lustre: 2500 years of the pearl trade from Alexander's armies to the Gem Testing Laboratory'. Jack brought along a selection of pearls for participants to examine.

Midlands Branch

Branch meetings held at the Earth Sciences Building, University of Birmingham, included a presentation on 27 April by Heather McPherson when she asked the question: 'Could you be a valuer?', a talk by Richard Digby on 28 September on 'Cameos and intaglios', and on 26 October organics expert Maggie Campbell Pedersen on 'Gems from life'. The Branch's Summer Supper Party was held on 16 June at Barnt Green.

North East Branch

On 24 May at the Ramada Jarvis Hotel, Wetherby, gem dealer Tracey Jukes spoke on the coloured stone market and on 13 September at the same venue the gems and gem industry of Sri Lanka was the subject of Don Ariyaratna's presentation.

North West Branch

Branch meetings held at YHA Liverpool International, Wapping, Liverpool 1, included on 19 April 'Questions and Answers', a talk by Ian Williams who runs a workshop making hand-made jewellery;

On 17 May Wendy Simkiss spoke on the agate collection of the 15th Earl of Derby, and on 21 June Alan Hodgkinson gave a presentation on opals. The branch AGM was held at YHA Liverpool International when Deanna Brady was re-elected Chairman and Secretary of the Branch.

Scottish Branch

The Scottish Branch Conference was held at the Lovat Hotel, Perth, from 4 to 7 May. Speakers included Dr Emmanuel Fritsch (keynote), Dr David Fisher, Rui Galopim de Carvalho, Henrietta Lidchi and Maggie Campbell Pedersen. As in previous years, the Sunday afternoon was devoted to displays, demonstrations and workshops, and the conference concluded on the Monday with a field trip to 'Ruby Bay' at Elie to hunt for pyrope garnets. (A full report of the event was published in the June 2007 issue of *Gems & Jewellery*.)

Meeting held at the British Geological Survey, Murchison House, West Mains Road, Edinburgh, included a talk by Richard Gardner of Michiko Pearls on 18 June entitled 'The pearl trade today' and on 16 October gem dealer Tracey Jukes spoke on 'Coloured gemstone valuation in the 21st century'. On 11 September the Branch held a joint meeting with the Scottish Mineral and Lapidary Club at their premises in Leith when Memory Stather gave a presentation on gem carving.

Membership

Between 1 April and 31 October 2007, the Council approved the election to membership of the following:

Fellowship and Diamond Membership (FGA DGA)

Cheung Ching Ping, Candy, Tseung Kwan, Kowloon, Hong Kong. 2004/2007
Bill, David Nigel, Burntwood, Staffordshire. 1980/1981
Davis, Jonathan Vincent, Harrow, Middlesex. 1978/1979
Georgmas, Emmanuel, Byron, Greece. 2006/2007
Kahn Farrukh, Nayer, Birmingham, West Midlands. 2006/2007

Fellowship (FGA)

Adler, Stevan, New York, U.S.A. 2007
Amicone, Maria, Quebec, Canada. 2007
Avender, Breanne Valeda, Burnaby, British Columbia, Canada. 2007
Balter, Jonathan, London. 1992
Barbour, Alexandra Frances, Dorchester, Dorset. 2007
Barker, Holly, Johannesburg, South Africa. 2007
Caulton, David, Dore, Sheffield, Yorkshire. 2007
Chang, Hsiao Huei, Westmount, Quebec, Canada. 2007
Chung, Stella Yee Man, Hong Kong. 2007
Corser, Elizabeth, Wellington, Shropshire. 2007
Cropp, Alastair, Milton, Queensland, Australia. 1999
Decourteney, Chris, Poole, Dorset. 2007
de Siran de Cavanac, Bérengère, Toulon, France. 2007
Doyle, Helen, London. 2007
Ellor, Lucy, Farnham, Surrey. 1992
Ferneyhough, Ella, Birmingham, West Midlands. 2007
Frei, Thomas, Pratteln, Switzerland. 2007
Gourlet, Agnes, Paris, France. 2007
Heit, Liesbeth, London. 2007
Hui Yuen-Wah, Hong Kong. 2007
Katayama, Shinko, Colombo, Sri Lanka. 2007
Kemprud, Tanya, Revelstoke, British Columbia, Canada. 2007
Lau, Tsui Wah, Kowloon City, Hong Kong. 2007
Lee, Cheuk Ming, Hong Kong. 2007
Lefebvre, Alburt, Brampton, Ontario, Canada. 2007
Lilley, Samantha, London. 2007
Lo Pui Yin, Shirley, Hong Kong. 2007
Machefert, Jean-Michel, Cormeilles-en-Parisis, France. 2007
Mak Hoi Chuen, Jeff, Hong Kong. 2007
Mak, Kim, Hong Kong. 2006
Manarkattu, Mahesh, Palai, India. 2007
McWhirter, Hannah Maeve, Bury St Edmunds, Suffolk. 2007
Miller, Me'Shell, North Highlands, California, U.S.A. 2007
Mok So Yiu, Tsuen Wan, Hong Kong. 2007
Piha, Saara, Helsinki, Finland. 2007
Rodman, Anna, Lund, Sweden. 2007
Sane, Dipal, Mumbai, India. 1989
Sinagra, Monika, Shanghai, P.R. China. 2007
Suokko, Teija, Tampere, Finland. 2007
Tip Tak Wing, Shatin, Hong Kong. 2007
To Ka Ho, Hong Kong. 1982
Voulgaris, Apollo, Mykonos, Greece. 2007
Wacyk, Carrein Tara, Castelnaudary, France. 2007
Watson, John Richard, Berkhamsted, Hertfordshire. 2007
Wootton, Sophie Louise, London. 2007
Zheng, Zizi, Rochester, New York, U.S.A. 1998
Zotta, Elisa, London. 2007

Diamond Membership (DGA)

Au, Astor Wing Ki, Happy Valley, Hong Kong. 2007
Chung Ka Yee, Anita, Hong Kong. 2007
Freidericos, Nikitas, Athens, Greece. 2007
Harker, Catherine, Birmingham, West Midlands. 2007
Jenkinson, Glenn, Telford, Shropshire. 2007
Kennedy, Martin, Belfast, Northern Ireland. 2007
Lee, Sinnie, Hong Kong. 2007
Leung, Vincent, Toronto, Ontario, Canada. 2007
Netsah, Maayane, Nairobi, Kenya. 2007
Ng Yuk Yu, Shatin, New Territories, Hong Kong. 2007
Ngwe, Ohnmar, London. 2007
Woolley, Claire Corinna, West Midlands. 2007

Associate Membership

Allen, Anne, Dorchester, Dorset
Amrit, Paveet, Northolt, Middlesex
Aung, May Thu, London

Baghdadi, Abeer, Jeddah, Saudi Arabia
Boyle, Katrine, Coatbridge, Lanarkshire
Bright, David, The Hague, The Netherlands
Cable, Kenneth, London
Cane, Mary, London
Carson, Elaine, Hillsborough, Northern Ireland
Carter, Anne Margaret, Wantage, Oxfordshire
Chan Tat Hang, Hong Kong
Chau Lok Yeun Amy, Hong Kong
Chen, Anny, Taipei, Taiwan, R.O. China
Cobley, Samuel Ryan, Forfar, Angus, Scotland
Diamond, Marcia, London
Dolland, Steven, London
Dr Higgins, Maureen, Edinburgh, Scotland
Ewington, Craig, London
Featherstone, Hazel, London
Gits, Pasquinel, Knokke, Belgium
Godden, Angela, Weston, Hertfordshire
Hall, Michael, London
Hamilton, Hunter Ian, Redditch, Worcestershire
Harris, Timothy, Rye, East Sussex
Hoeu, Samnang, London
Hope, Lorraine, London
Hui, Hau Kan, Feltham, Middlesex
Islam, Rezaul, Swansea, Glamorgan, Wales
Kaye, Elaine, Sturminster Newton, Dorset
Khan, Jewell, London
Kumarasinhe, Peter, Crowthorne, Berkshire
Kyaw Thu Min, Yangon, Myanmar
Lau Ka Yan, Hong Kong
Lee Suk Wa, Hong Kong
Lefevre, Andre Francis, Maia, Portugal
Lin Chun-yen, London
Liou Shin-Ling, Egham, Surrey
Lu, Sisi, London
Luk Wai Ho, Hong Kong
Mahdi, Mehiden, London
Manarkattum, Mahesh, Kottayam, India
Manasse, Daniele, Rome, Italy
Maxfield, Melanie, Milverton, Somerset
Mayne, Edwina, London
Meintjes, Vanessa, Hove, East Sussex
Micatkova, Michaela, London
Miller, Susan Catherine, Atlanta, Georgia, U.S.A.
Nasser, Fidaa, Wilrijk, Belgium
Nicolson, Anulak, Bangkok, Thailand
Pask, Amelia, Blenheim, New Zealand
Patel, Indira, London
Patel, Kamlesh Pravinbhat, Ahmedabad, India
Pennino, Monica, Henham, Essex
Qulunbe, Bashe, London
Rasche, Elizabeth, London
Sahabunyakul, Saran, Bangkok, Thailand
Sampieri, Karen, New York, U.S.A.
Santer, Kurt, St Brelade, Jersey, Channel Islands
Shen, Huanqun, Shanghai, P.R. China
Siingwa, Chrispin, Luton, Bedfordshire
Taylor-Warren, Sevenoaks, Kent
Tereszczuk, Stasia-Mae, Little Horwood, Buckinghamshire
Tidey, Alan John, East Farleigh, Kent
Trummer, Eugene, Haywards Heath, West Sussex
Trummer, Joanna, Haywards Heath, West Sussex
Tyler, Linda, Wokingham, Berkshire
Underwood, Antonia, London
Van-Beer, Dreda, Dover, Kent
Vieira, Armindo, London
Waterhouse, Bente, Edenbridge, Kent
Woo, Ka Yin, Hong Kong
Yang Yiwei, London

Transfers

From Fellowship (FGA) to Fellowship and Diamond Membership (FGA DGA)

Bell, Lucy Kate, Birmingham, West Midlands
Blatherwick, Clare, Edinburgh, Scotland
Chan Wing Sze Herleva, Kowloon, Hong Kong
Chan, Mei Fong, Hong Kong
Deeley, Philippa, Etchingham, East Sussex
Dr Lin, Lang-Dong, Taipei, Taiwan
Fisher, Fiona, Jane, Dublin, Ireland
Flower, Caro, Melton Constable, Norfolk
Harman, Bronwen, Reading, Berkshire
Jones, Gary, Dudley, West Midlands
Jordan, Steven, Biggleswade, Bedfordshire
Khan-Farrukh, Birmingham, West Midlands
Larsson, Jacqueline, Amsterdam, The Netherlands
Low, San, Chatham, Kent
Murray, Helen Claire, Sutton Coldfield, West Midlands
North, Sarah, York, North Yorkshire
Robichaud, Emilie Gould, London
Symes, Evelyn R, London
Westlake, Ingrid, Chamonix, France
Zee, Gar Bo Michelle, Hong Kong

From Diamond Membership (DGA) to Fellowship and Diamond Membership (FGA DGA)

Fong Yan, William, Tai Po, Hong Kong
Ko, Cheuk Wah Robin, Hong Kong
Koundouraki, Evagelia, Athens, Greece
Palmares, Richard P, Sale, Cheshire
Perks, Helen Eliazabeth, Telford, Shropshire
Powar, Krishna, Smethwick, West Midlands
Wat, Wing Suet, Hong Kong
Wong Tung Wing, Hong Kong
Wong Yu Lap, Angel, Sha Tin Centre, Hong Kong
Yeung, Anthea Ka, Yee, Hong Kong

From Associate Membership to Fellowship (FGA)

Bowers, Sally Faye, London.
Dereszewska, Basia, London
Dighton, Anna Louise, Saffron Walden, Essex
Drummond, Jean, Farnham, Surrey
Elles, Sarah Louise Jean, London
Fujii, Tasuhisa, Tokyo, Japan
Han, Jie, Coventry, West Midlands
Hu, Xiao, Yu, London
Hug, Samuel, Gosport, Hampshire
Iwamoto, Akiko, London
James, Bronwynne, St Albans, Hertfordshire
Kaneyasu, Yoshimasa, Okayama-Ken, Japan
Khan, Ehtesham, Ullah, Peshawar, Pakistan
Kobayashi, Taisuke, Tokyo, Japan
Learmonth, Bryony, Stafford, Staffordshire
Micatkova, Lubica, London
Mitchell, Jonathan, Midland, Texas, U.S.A.
Miyamoto, Kazuhiko, Osaka, Japan
Naito, Ayako, Tokyo, Japan
Nakagawa, Yumi, Kitakatsuragi-gun, Nara Pref., Japan
Rajbanshi, Niren Man, London
Sahabunyakul, Saran, Bangkok, Thailand
Sawamura, Tsukasa, Tokyo, Japan
Sekine, Shunji, Tokyo, Japan
Sherin, Saira, Peshawar, Pakistan
Takahata, Yoshichicka, Takamatsu City, Japan
Uchiyama, Mio, Japan
von Schantz, Casimir, Helsinki, Finland
Yamada, Masashi, Tokyo, Japan
Yamaguchi, Yuko, Osaka, Japan

Associate Membership to Diamond Membership (DGA)

Bland, Clare, London
Hall, Gregory Peter, Brighton, East Sussex
Li Zhen, London

Subscriptions 2008

It has been agreed that the membership subscription rates will remain unchanged for 2008 at £72.50 for UK members, £80.00 for those in Europe and £85.00 for overseas. Existing Fellows, Diamond and Associate members will be entitled to a £5.00 discount for subscriptions renewed by 31 January 2008.

Gifts

The Association is most grateful to the following for their gifts for research and teaching purposes:

Eisuke Ashida FGA, Kyoto City, Japan, for a monetary donation

Mrs W. Buckingham, Chorleywood, Hertfordshire, for a collection of books in memory of the late William Buckingham FGA

Maggie Campbell Pedersen FGA, London, for a piece of Baltic amber

John Ho Hay Mo FGA, Hong Kong, for a piece of rough johachidolite

Dost Muhammed Khan, Peshawar, Pakistan, for a selection of crystals

Ehtesham Ullah Khan FGA, Peshawar, Pakistan, for a selection of crystals

Nicki Sherriff FGA, Verdun, Quebec, Canada, for two diopside crystals

Thomson Gems, London, for a selection of gemstones

Donations to the 100 Club and Educational Sponsorship will be listed in the next issue of The Journal.

One hundred years of Gemmological Education

In 2008 Gem-A will be celebrating One Hundred Years of Gemmological Education. To ensure that we remain the provider of the highest status gem education through our second century, we have ambitious plans for the expansion and increased accessibility of Gem-A courses worldwide.

This can only be achieved with the support of our Fellows and Members. Our target is one hundred donations of a minimum of £1000 (US$2000) by September 2008.

As a member of the 100 Club, you will play an important role in helping us to achieve our charitable aims. As a patron, you will be honoured with:

- a 100 Club certificate
- an invitation to the Gem Centenary Dinner
- your name on a plaque in the London Headquarters of Gem-A, in our Centenary publication and on our website.

Your contribution will help us to:

- Develop our gem courses and make them more widely available
- Upgrade our in-house facilities for students
- Establish our website as a primary focus for gemmological education and gem information
- Establish a scholarship fund
- Encourage the study of gemmology worldwide through articles and the media
- Make gem education more accessible in developing countries
- Improve ethical and environmental awareness in the gem trade
- Reinstate the Research Diploma for Fellows
- Support for continuous gemmological learning in the gem trade.

Payments may be spread over one year (minimum £83.33 or US$167 per month). Companies and those wishing to make larger contributions or to support specific initiatives, should go to www.gem-a.com/information/noticeBoard.php or contact Olga Gonzalez on +44 (0)20 7404 3334, email olga@gem-a.com.

One hundred years 1908 2008
OF GEMMOLOGICAL EDUCATION

Obituary

David George Kent FGA
1915 – 2007

A tribute by E. Alan Jobbins

David was born in London in 1915, left school at 14 and went to work for Becks, a firm of jewellers in London's Tottenham Court Road, where he stayed for three years. Having gained experience he move to Bravingtons, a large jewellers near King's Cross Station, and spent the rest of his working life there, retiring as a director.

In 1940 he was called up to serve in the Army and joined the Royal Signals Regiment. He spent several years in India as a staff Sergeant responsible for the maintenance of radio communication equipment – which was to serve him well in later life. He was posted to Africa and Germany, and on demobilization decided to learn more of the German language as a follow-up from his final posting. He checked for available courses in *Floodlight* – an educational booklet issued by the then London County Council. Immediately before the entry for 'German' came 'Gemmology'; the subject caught his eye and he was hooked – he never looked back. He studied at Chelsea Polytechnic and in 1948 qualified in the Gemmology Diploma examinations – the same year as Robert Crowningshield, who later became a vice president of the GIA laboratory.

He joined the post-diploma class run by Basil Anderson (the first Director of the London Gem Laboratory) soon after he qualified and this is where I first met him in the early 1950s. He remained a regular attendee until he was in his late 80s. He was a practical examiner for the Gemmology Diploma examination for many years.

David was a very practical man and, helped by his army experience with many types of instruments, was able to devise various ingenious attachments to microscopes and spectroscopes which made observations much easier. In 1993 he was elected a Vice President of the Gemmological Association in recognition of his contribution to the jewellery industry and his considerable help to the Association.

He built up a large collection of gemstones and generously presented his fine suite of colourless stones to Gem-A, other groups of gemstones going to the Victoria and Albert Museum along with historical runs of gemmological journals. He was a great traveller and enjoyed excursions run by Eric Bruton, the celebrated author of *Diamonds*, to gem deposits in Brazil, China, Russia and Thailand. He had gemmological friends around the world, even as far a field as Australia and New Zealand.

The other love of David's life was his bicycle which he only gave up in his 80s. He cycled hundreds of miles around England to visit relatives and gemmological friends. One incident he particularly remembered was a journey to Somerset to see farming friends when he was booked by a country policeman for holding on to a slow moving lorry going uphill. He was rather miffed at this since it was 2 am and he had travelled at night to avoid the traffic and the summer heat. He cycled to work from the suburbs through traffic to central London every day until he retired.

David remained a bachelor all his life. He had few close relatives, his parents and sister having died many years ago. He was like a brother to Mimi, a distant relative, and they shared many years of their retirement together in their sixteenth-floor apartment with magnificent views over the whole of London.

Although not a regular church-goer, David held a very Christian attitude to life and was always ready to help others – particularly young people entering into the jewellery trade. He was a lovely man and great fun to be with, especially when sharing his favourite tipple – a glass of port.

William Charles Buckingham FGA
1921 – 2007

William Buckingham (known in the trade as Billy Buck) started his career in the gem trade in 1937 at the age of sixteen with Jade Dragon Ltd, later to become George Lindley & Co. Ltd. Both he and Mr Lindley served their country gallantly in the Second World War, and rejoined the company after hostilities ceased. Like the late David Kent (see previous page), William attended gemmology classes at the Chelsea Polytechnic and was awarded his Gemmology Diploma in 1948. He took control of and continued running one of the most successful gemstone businesses in London's Hatton Garden after George Lindley died.

William Buckingham served on the Council of the Gemmological Association from 1952 until 1967. In 1988 he very generously donated his fine collection of zircons to the Gemmological Association to mark his retiral after fifty years from George Lindley & Co. He also offered an award to newly-qualified Fellows of the Association who carried out research on the zircons to determine any variation in properties of samples from different localities. Research carried out by the FGAs in the Edinburgh Gemmological Group and their findings were published in *The Journal of Gemmology*, 1993, 23(7), p.387.

William, a proud Normandy veteran, was honoured in death by the draping of his coffin with the Union flag appropriately decked with his campaign medals and flanked by a guard of honour at the Service of Thanksgiving.

Leonard A. Baker

Stanley George Hill FGA
1911 – 2007

Stanley (Stan) Hill was born in Birmingham where he served an apprenticeship as a silversmith. In 1936 was appointed lecturer in metalwork at the Liverpool School of Art. He retired in 1976 but his career as a craftsman and designer continued for many more years. Stan was one of the founders in 1960 of the Bluecoat Display Centre in Liverpool. He had a studio at Bluecoat where he worked regularly until he was nearly 90, hand-crafting jewellery and silverware pieces in a very wearable simple geometrical form.

Stan's interest in geology and gemmology developed in the 1950s and he qualified in the Gemmology Diploma Examinations in 1958. It was the sheer beauty and variety of gemstones that sustained his interest and his creativity in jewellery design.

A staunch member of the North West Branch of the Gemmological Association, Stan would offer help, advice and support to the chairman and the committee. He attended practically every meeting, listening intently to each speaker, and even though some of us thought he had fallen asleep he still managed to ask the most relevant questions. His wish to share his knowledge and enthusiasm for gemstones extended to meetings at his home, where he encouraged everyone to pore over his collection.

Stan's beloved wife Betty died in 2005, but he coped with her loss with great courage. He died peacefully at Arrowe Park Hospital after a short illness.

Richard Hill and Sue Horder (nee Hill)

John L. Pyke FGA
1910 – 2007

John Pyke began his career in the jewellery trade with an apprenticeship at Baker's Jewel Casket in Wigan in 1926. He completed his training in 1931, after graduating with a Distinction in the Gemmology Diploma Examinations. Because of the Depression, the family firm, William Pyke & Sons, founded by his grandfather, could not afford to employ him, but he obtained the position of workshop manager at Coombe Co. Ltd in Rangoon. While in Burma he took the opportunity to travel extensively around the country buying gemstones.

He returned home in 1938 and married Joan the following year, just before war broke out. He volunteered for Wingate's forces, but the army sent him to the Middle East where he was twice mentioned in despatches.

When he was demobbed in 1945 he devoted his considerable energies to rebuilding William

Pyke & Sons, which by that time had no money and very little stock. He ran the company until 1977, but remained Chairman until his death.

He was Chairman of the National Association of Goldsmiths from 1963 to 1968 and later President. During his chairmanship he was greatly involved in the UK's involvement in CIBJO.

John Pyke was a qualified gemmologist with a deep appreciation of all gemstones. He was one of the founder members of the North West Branch of the Gemmological Association which was formed in 1975, later becoming the Branch patron. Said Deanna Brady, Chairman of the North West Branch: "John Pyke often entertained our members with anecdotes about his travels throughout Burma, bringing along his collection of gemstones for all to handle. He was always there, offering continual support to our committee."

John S. Pyke

Prof Akira Chikayama FGA (D.1966), Tokyo, Japan, died on 24 September 2007 at the age of 85.

William Fleming Ferguson FGA (D.1956), Balloch, Strathclyde, Scotland, died in 2007.

Masashi Furuya FGA (D.1976), Yamanashi-ken, Japan, died on 23 October 2007 at the age of 59.

It is with deep regret that we announce the sudden death of Professor Chen Zhonghui of Beijing, P.R. of China, on 6 November 2007. Professor Chen was an Honorary Fellow of the Association and was the examination co-ordinator for China. A full obituary will be published in the next issue of *The Journal*.

Gem-A Events 2008

Saturday 26 and Sunday 27 January	The Materials and Techniques of Ancient Egyptian Jewellery. A special seminar to coincide with the Tutankhamun Exhibition in London. Tutor: JACK OGDEN
Friday 25 January	Midlands Branch. Branch AGM, Bring and Buy, and Team Quiz.
Monday 25 February	Scottish Branch. Techniques of Chinese Jade Carving and the Mughal Terrapin. MARGARET SAX
Friday 29 February	Midlands Branch. Birmingham Silver and the History of the Assay Office. DR SALLY BAGGOTT
Sunday 16 March	Midlands Branch. Practical training day: the use of the microscope.
Tuesday 1 April	Scottish Branch. It's all in the cut. JAMES RILEY
Friday 4 April	Midlands Branch. Fabergé and his workmasters. STEPHEN DALE
Friday 25 April	Midlands Branch. Corundum – natural, treated and synthetic. DOUG GARROD
Friday 2 to Monday 5 May	Scottish Branch Conference, Queen's Hotel, Perth. Speakers will include: George Rossman (keynote), David Callaghan, Alan Hodgkinson, Elisabeth Strack and Stephen Whittaker.
Saturday 25 to Monday 27 October	Special Centenary Conference and Graduation Ceremony.

Contact details

When using e-mail, please give Gem-A as the subject:

London:	Olga Gonzalez on 020 7404 3334; email olga.gonzalez@gem-a.com
Midlands Branch:	Paul Phillips on 02476 758940; email pp.bscfgadga@ntlworld.com
North East Branch:	Mark Houghton on 01904 639761; email sara_e_north@hotmail.com
North West Branch:	Deanna Brady on 0151 648 4266
Scottish Branch:	Catriona McInnes on 0131 667 2199; email scotgem@blueyonder.co.uk
South East Branch:	Veronica Wetten on 020 8577 9074; email veronica@wetten.co.uk
South West Branch:	Richard Slater on 07810 097408; email richard@fellows.co.uk

Gem-A website

For up-to-the-minute information on Gem-A events visit our website at www.gem-a.com

Guide to the preparation of typescripts for publication in The Journal of Gemmology

The Editor is glad to consider original articles shedding new light on subjects of gemmological interest for publication in The Journal. Articles are not normally accepted which have already been published elsewhere in English, and an article is accepted only on the understanding that (1) full information as to any previous publication (whether in English or another language) has been given, (2) it is not under consideration for publication elsewhere and (3) it will not be published elsewhere without the consent of the Editor.

Typescripts Two copies of all papers should be submitted on A4 paper (or USA equivalent) to the Editor. Typescripts should be doubled spaced with margins of at least 25mm. They should be set out in the manner of recent issues of The Journal and in conformity with the information set out below. Papers may be of any length, but long papers of more than 10 000 words (unless capable of division into parts or of exceptional importance) are unlikely to be acceptable, whereas a short paper of 400-500 words may achieve early publication.

The abstract, references, notes, captions and tables should be typed double spaced on separate sheets.

Title page The title should be as brief as is consistent with clear indication of the content of the paper. It should be followed by the names (with initials) of the authors and by their addresses.

Abstract A short abstract of 50-100 words is required.

Key Words Up to six key words indicating the subject matter of the article should be supplied.

Headings In all headings only the first letter and proper names are capitalized.

A This is a first level heading

B This is a second level heading

First and second level headings are ranged left on a separate line.

Third level headings are in italics and are indented within the first line of the text.

Illustrations High resolution digital files, for both colour and black-and-white images, at 300 dpi TIFF or JPEG, and at an optimum size, can be submitted on CD or via email. Vector files (EPS) should, if possible, include fonts. Match proofs are essential when submitting digital files as they represent the colour balance approved by the author(s).

Transparencies, photographs and high quality printouts can also be submitted. It is recommended that authors retain copies of all illustrations because of the risk of loss or damage either during the printing process or in transit.

Diagrams must be of a professional quality and prepared in dense black ink on a good quality surface. Original illustrations will not be returned unless specifically requested.

All illustrations (maps, diagrams and pictures) are numbered consecutively with Arabic numerals and labelled Figure 1, Figure 2, etc. All illustrations are referred to as 'Figures'.

Tables Must be typed double spaced, using few horizontal rules and no vertical rules. They are numbered consecutively with Roman numerals (Table IV, etc.). Titles should be concise, but as independently informative as possible. The approximate position of the Table in the text should be marked in the margin of the typescript.

Notes and References Authors may choose one of two systems:

(1) The Harvard system in which the authors' names (no initials) and dates (and specific pages, only in the case of quotations) are given in the main body of the text, (e.g. Collins, 2001,341). References are listed alphabetically at the end of the paper under the heading References.

(2) The system in which superscript numbers are inserted in the text (e.g. ... to which Collins refers.[3]) and referred to in numerical order at the end of the paper under the heading Notes. Informational notes must be restricted to the minimum; usually the material can be incorporated in the text. If absolutely necessary both systems may be used.

References in both systems should be set out as follows, with double spacing for all lines.

Papers Collins, A.T., 2001. The colour of diamond and how it may be changed. J.Gemm., 27(6), 341-59

Books Balfour, I., 2000. Famous diamonds. 4th edn. Christie's, London. 200pp

Abbreviations for titles of periodicals are those sanctioned by the World List of scientific periodicals 4th edn. The place of publication should always be given when books are referred to.

ISSN: 1355-4565

The Journal of
Gemmology

Volume 30 No. 7/8
July/October 2007

Contents

Cover Picture: Inclusion pattern in a vanadium-bearing tourmaline from Madagascar.
(See Vanadium-bearing gem-quality tourmalines from Madagascar, p.413)

The Gemmological Association of Great Britain
Registered Office: Palladium House, 1-4 Argyll Street, London W1F 7LD

 Designed & Produced by Harley Marketing Communcations UK ISSN: 1355-4565